UNIVERSITÉ DE NEUCHÂTEL

CHYN
Centre d'hydrogéologie
et de géothermie

Fully-integrated hydrological modelling in steep, snow-dominated, geologically complex Alpine terrain

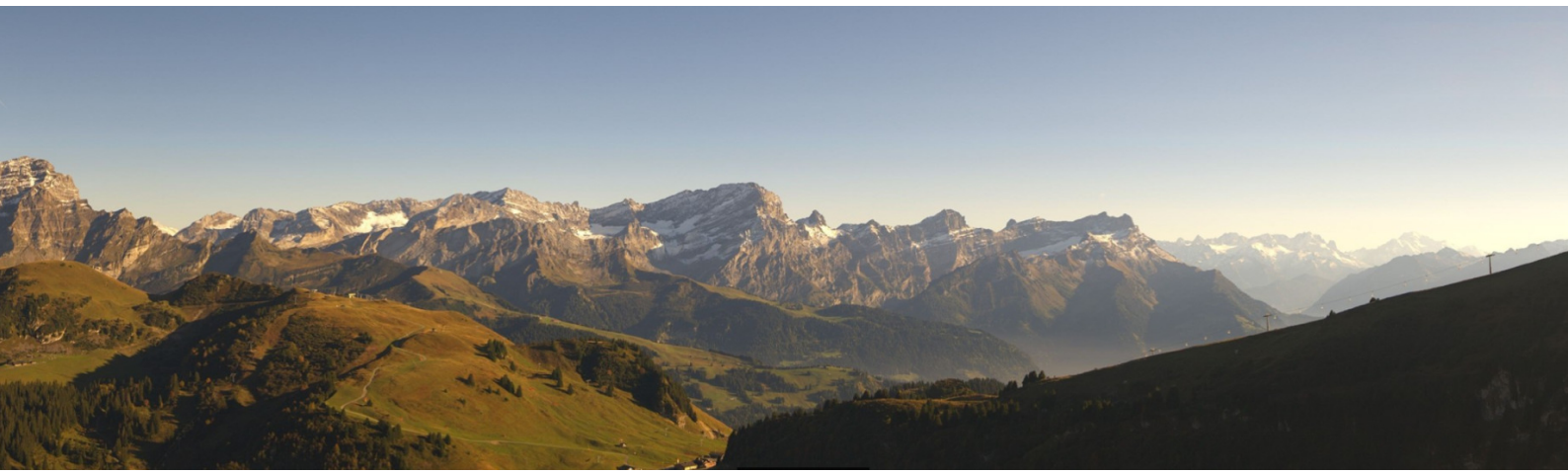

A thesis presented to the Faculty of Science, University of Neuchâtel,
to satisfy the requirements of the degree of Doctor of Sciences by

James M. THORNTON

Defended: **18th May 2020**

Accepted on the recommendation of:

Prof. P. Brunner, University of Neuchâtel, Switzerland (Thesis Director)
Prof. G. Mariéthoz, University of Lausanne, Switzerland (Thesis Co-Director, Rapporteur)
Prof. D. Hunkeler, University of Neuchâtel, Switzerland (Rapporteur)
Prof. R. Therrien, Université Laval, Canada (Rapporteur)
Prof. J.H. Fleckenstein, UFZ, Germany (Rapporteur)

Cover image: *View from Petit-Chamossaire towards the Grand Muveran Massif and Mt. Blanc*
(© Télé Villars-Gryon-Diablerets SA)

UNIVERSITÉ DE NEUCHÂTEL

Faculté des Sciences
Secrétariat-décanat de Faculté
Rue Emile-Argand 11
2000 Neuchâtel – Suisse
Tél : + 41 (0)32 718 21 00
E-mail : secretariat.sciences@unine.ch

IMPRIMATUR POUR THESE DE DOCTORAT

La Faculté des sciences de l'Université de Neuchâtel autorise l'impression de la présente thèse soutenue par

Monsieur James Matthew THORNTON

Titre:

"Fully-integrated hydrological modelling in steep, snow-dominated, geologically complex Alpine terrain"

sur le rapport des membres du jury composé comme suit:

- Prof. Philip Brunner, directeur de thèse, Université de Neuchâtel, Suisse
- Prof. Grégoire Mariéthoz, co-directeur de thèse, Université de Lausanne, Suisse
- Prof. Jan H. Fleckenstein, Helmholtz Center for Environmental Research, Leipzig, Allemagne
- Prof. René Therrien, Université Laval, Québec, Canada
- Prof. Daniel Hunkeler, Université de Neuchâtel, Suisse

Neuchâtel, le 3 juillet 2020

Le Doyen, Prof. P. Felber

P. Fel

Citation: Thornton, J.M. (2020), Fully-integrated hydrological modelling in steep, snow-dominated, geologically complex Alpine terrain, Doctoral Thesis, University of Neuchâtel, Switzerland.

Abstract

The rugged topographic forms and complex geologies that are characteristic of Alpine terrain typically exert a strong influence on catchment-scale hydrological processes. Glaciers, the seasonal snowpack, permafrost, and forests are other integral parts of Alpine environmental systems, and all are currently responding in one way or another to ongoing climatic change. Since a web of process interactions and feedback mechanisms link all system components together, any fairly direct hydrological changes arising from changing snow and ice could be modulated by the response of the broader integrated systems. Yet despite this complex reality, legacy conceptual or "box-type" hydrological models – which employ highly simplified representations of groundwater and other physical processes, and which moreover usually neglect contemporaneous changes in other system components – continue to underpin most predictions of future water availability in the European Alps. The reliability of some of the resultant predictions may therefore be questionable. More sophisticated physically-based codes are available, but also employ simple subsurface representations. At the same time, numerous detailed field investigations have been carried out in alpine catchments, but are rarely extended to numerical modelling exercises.

In this context, the present thesis sought to evaluate the utility of one of the most advanced fully-integrated surface-subsurface flow codes for simulating hydrological dynamics in steep, snow-dominated, and geologically complex Alpine headwaters – under both present and plausible future climate, forest, and permafrost conditions. Surface flows are particularly relevant in such terrain in terms of ecology, flood hazard, and sediment transport, whilst groundwater flow patterns can be strongly influenced by inherently complex three-dimensional (3D) subsurface structures. Furthermore, bi-directional exchanges between these domains can occur frequently, inducing streamflow ephemerality under certain circumstances. In having the capability to simulate all these processes in a coherent, physically-based, and transient fashion, integrated codes theoretically hold great potential for Alpine applications. However, their use in mountainous contexts to date has been predominantly limited to low permeability crystalline catchments of the North American Cordillera.

The development of a model chain incorporating snowpack evolution and integrated surface flow, variably-saturated subsurface flow, and evapotranspiration dynamics was therefore embarked upon. The spatial domain (total area $\sim$37 km^2) was comprised of two adjacent protected headwaters – the Vallon de Nant and Vallon de La Vare – which are located within the renowned Nappe de Morcles (western Swiss Alps). At the outset, very little of the extensive data required to inform such a "data hungry" model was available. To partially remedy this situation,

four shallow groundwater monitoring wells were drilled in late 2016 and instrumented in spring 2017. The resultant groundwater level observations complement meteorological and stream discharge measurements provided by collaborating research groups. A geophysics field campaign was also undertaken with a view to establishing the geometry of the principal alluvial fan aquifer in the study area. The geometries of several other less accessible unconsolidated sedimentary formations thought to host aquifers were estimated by means of a simple geomorphometrical procedure.

With the aid of the GeoModeller software, an accurate, high-resolution, detailed, and spatially extensive 3D model of the bedrock geology was developed. In light of the topographical and geological complexity of the study region, this task was far from straightforward, but was nevertheless ultimately achievable. This contribution thus demonstrates that 3D geological models with appropriate characteristics for hydrogeological applications can be developed in even the most complex settings, and that the lack of such data (at least) should not form an impediment to progressing beyond simple conceptual hydrological models. Alongside the aforementioned unconsolidated aquifer geometries and (very limited) soil data, the geological model informed the subsurface structure of the integrated flow model.

Thereafter, to overcome the lack of any pre-existing third-party gridded meteorological products with the requisite spatio-temporal resolution that such terrain demands, and to determine spatio-temporal patterns of liquid water inputs to the system as accurately as possible, a novel, code-independent, and high resolution (hourly, 25 m) snow simulation, optimisation, and uncertainty framework was proposed. The approach is specifically tailored to the steepness of the study area and the somewhat limited availability of *in situ* meteorological and snow data; two factors which often complicate modelling in mountainous terrain.

Being energy balance-based and additionally accounting for gravitational redistribution, the snow modelling approach extends well beyond that taken in many hydrological models – including otherwise advanced fully-integrated ones – which still mostly rely on index-based snowmelt modelling approaches whose ability to realistically reproduce snow dynamics in complex Alpine terrain is questionable. More specifically, by linking an hybrid physical-statistical energy balance-based snow simulator, implemented in the code WaSiM, with the automatic parameter estimation and uncertainty estimation software PEST, two complementary types of snow observations – namely snow extent maps and snow water equivalent time-series – contributed to the estimation of several important but uncertain parameters.

As part of this process, per-pixel metrics were used to quantify the spatial component of model performance within a multi-variate objective function. As far as is known, this represents the first time unaggregated snow maps derived from Landsat 8 images have been used to calibrate a distributed snow model. Snow dynamics were ultimately reproduced satisfactory, with the residual mismatch probably largely attributable to deficiencies in the meteorological forcing data. Predictive uncertainties and the worth of different observation types were also quantified, and commensurate estimates of firn melt, ice melt, and potential evapotranspiration (ET_p) generated.

The fully-integrated surface-subsurface model was developed using the code HydroGeoSphere (HGS) and partially calibrated, again using PEST, against the streamflow and groundwater level measurements made a several internal locations. Streamflow was reproduced at the main gauging station over an independent 11-month evaluation period (November 2017 – September 2018 inclusive) with a Nash-Sutcliffe Efficiency coefficient of 0.75. The main seasonal signal of the observed groundwater levels could also be broadly replicated, although capturing the observed differences between sites remained elusive, probably due to local scale variability in hydraulic properties. Simulated spatio-temporal patterns of several other important hydrological variables were also visualised to illustrate the model's coherence and the capabilities of such an approach.

Finally, in an attempt to assess the potential magnitude of future hydrological change in such regions and unravel its dominant drivers, the model chain (i.e. WaSiM and HGS) was forced with climate, vegetation, and permafrost scenarios that could be expected under "moderate" warming by approximately the year 2075; this represents the first hydrological climate change impact assessment undertaken using a fully-integrated surface-subsurface model anywhere in the Alps. In the Vallon de Nant catchment, for example, an increase in annual ET_p of approximately 10% and a decline in mean peak winter snow water storage of around 34% (relative to the simulated baseline) are predicted under such a climate. Changes in total annual "snowcover outflow" (i.e. rain plus snowmelt) are projected to be small, however, as reduced summer precipitation is offset by winter increases.

For the entire domain, the combined climate, land cover, and permafrost changes propagate through to an anticipated increase, summed over a three-year simulation period, in actual evapotranspiration (ET_a) of around 44%, and reduction in streamflow of around 10%. Direct climatic changes were found to dominate, with the modulating effect of changes in land cover and permafrost being much more limited by comparison. In conclusion, undertaking similar work more routinely could increase confidence in predictions of the future evolution of alpine hydrology. That said, given the scale of the efforts required to develop and the difficulties associated with

calibrating such models, applications are presently only recommendable in exceptionally important or ecologically sensitive catchments, or else where much of the requisite data already exists.

Keywords: *Alpine hydrology; climate change; snow dynamics; 3D geological modelling; integrated hydrological modelling; automated calibration; permafrost degradation; forest evolution*

Résumé

Les formes topographiques accidentées et les géologies complexes qui caractérisent le terrain alpin exercent généralement une forte influence sur les processus hydrologiques à l'échelle du bassin versant. Les glaciers, le manteau neigeux saisonnier, le pergélisol et les forêts font également partie intégrante des systèmes alpins, et tous réagissent autre aux changements climatiques en cours. Étant donné qu'un réseau d'interactions et de mécanismes de rétroaction relie tous les éléments du système, tout changement hydrologique résultant de la modification de la neige et de la glace pourrait être modulé par la réponse intégrés plus généralement. Pourtant, malgré cette réalité complexe, les modèles hydrologiques conceptuels de de type « boîte » – qui utilisent des représentations très simplifiées des eaux souterraines et des autres processus physiques, et qui, en outre, négligent généralement les changements contemporains des autres composantes du système – continuent à étayer la plupart des prévisions concernant la disponibilité future de l'eau dans les Alpes. La fiabilité de certaines prévisions qui en résultent peut donc être mise en doute. Il existe des codes plus sophistiqués basés sur la physique, mais ils utilisent également des représentations simples du souterrain. De plus, de nombreuses études de terrain détaillées ont été menées dans les bassins versants alpins, mais elles sont rarement allées jusqu'à la modélisation numérique.

Dans ce contexte, la présente thèse a évalué l'utilité de l'un des modèles d'écoulement surface-souterrain entièrement intégrés les plus avancés pour simuler la dynamique hydrologique dans les bassins versants alpins abrupts, dominés par la neige et géologiquement complexes – dans les conditions actuelles et futures plausibles du climat, des forêts et du pergélisol. Les écoulements de surface sont particulièrement importants dans ce type de terrain en termes d'écologie, de risques d'inondation et de transport de sédiments, tandis que les écoulement souterrains peuvent être fortement influencés par des structures souterraines tridimensionnelles (3D) intrinsèquement complexes. En outre, des échanges bidirectionnels entre ces domaines peuvent se produire fréquemment, créant ainsi des cours d'eau éphémères dans certaines circonstances. En ayant la capacité de simuler tous ces processus d'une manière cohérente, transitoire et basée sur la physique, les codes intégrés offrent théoriquement un grand potentiel pour les applications alpines. Toutefois, leur utilisation dans les contextes montagneux s'est jusqu'à présent limitée aux bassins versants cristallins de faible perméabilité de la Cordillère Nord-Américaine.

Le développement d'une chaîne de modèles intégrant l'évolution du manteau neigeux, l'écoulement de surface, l'écoulement souterrain à saturation variable et la dynamique de l'évapotranspiration a donc été entrepris. Le domaine spatial (superficie totale de 37 km^2) était composé de

deux bassins versants adjacents protégés – le Vallon de Nant et le Vallon de La Vare – qui sont situés dans la célèbre Nappe de Morcles (Alpes Suisses occidentales). Au début, très peu des données détaillées étaient disponibles bien qu'elles sont pourtant nécessaires pour alimenter un tel modèle « avide de données ». Pour remédier à cela, quatre puits de surveillance des eaux souterraines peu profondes ont été forés fin 2016 et instrumentés au printemps 2017. Les observations du niveau des eaux souterraines qui en résultent complètent les mesures météorologiques et les mesures du débit des cours d'eau fournies par les groupes de recherche collaborent. Une campagne de géophysique sur le terrain a également été entreprise afin d'établir la géométrie du principal aquifère non consolidés de la zone d'étude, situé dans un cône de déjection. Les géométries de plusieurs autres formations sédimentaires non consolidées moins accessibles contenant des aquifères ont été estimées au moyen d'une procédure géomorphométrique simple.

À l'aide du logiciel GeoModeller, un modèle 3D précis, à haute résolution, détaillé et spatialement étendu de la géologie du substratum rocheux a été développé. Compte tenu de la complexité topographique et géologique de la région étudiée, cette tâche était loin d'être simple, mais elle était néanmoins réalisable. Cette contribution démontre que des modèles géologiques 3D présentant des caractéristiques appropriées pour des applications hydrogéologiques peuvent être développés même dans les contextes les plus complexes. En plus, le manque de ces données ne devrait pas constituer un obstacle à la progression au-delà de simples modèles hydrologiques conceptuels. Outre les géométries des aquifères non consolidés et les données sur les sols (très limitées), le modèle géologique a permis d'établir la structure souterraine du modèle d'écoulement intégré.

Par la suite, afin de pallier l'absence de produits météorologiques tiers préexistants avec la résolution spatio-temporelle requise pour un tel terrain et de déterminer les données spatio-temporelles représentant les apports d'eau liquide dans le système aussi précisément que possible, un nouveau cadre de simulation, d'optimisation et d'incertitude de la neige à haute résolution (à l'heure, 25 m), indépendant du modèle, a été proposé. L'approche est spécifiquement adaptée à la pente de la zone d'étude et à la disponibilité limitée des données météorologiques et nivologiques *in situ* ; deux facteurs qui compliquent souvent le travail en terrain montagneux.

L'approche de modélisation de la neige, basée sur le bilan énergétique et tenant compte de la redistribution gravitationnelle, va bien au-delà de celle de nombreux modèles hydrologiques, y compris des modèles avancés entièrement intégrés. Ces modèles reposent encore principalement sur des approches de modélisation de la fonte des neiges basées sur des indices, dont la capacité à reproduire de manière réaliste la dynamique de la neige en terrain alpin complexe est limitée. Plus spécifiquement, en reliant un simulateur de neige hybride (physique–statistique)

basé sur le bilan énergétique, implémenté dans le code WaSiM, avec le logiciel d'estimation automatique des paramètres et d'estimation de l'incertitude PEST, deux types complémentaires d'observations de la neige – à savoir les cartes d'étendue de neige et les séries chronologiques d'équivalent en eau de la neige – ont contribué à l'estimation de plusieurs paramètres importants.

Dans le cadre de ce processus, des mesures par pixel ont été utilisées pour quantifier la composante spatiale de la performance du modèle dans une fonction objectif multivariable. Pour autant que l'on sache, c'est la première fois que des cartes de neige non agrégées dérivées d'images Landsat 8 ont été utilisées pour calibrer un modèle de neige distribué. La dynamique de la neige a finalement été reproduite de manière satisfaisante, la disparité restant étant probablement en grande partie attribuable aux données de forçage météorologique. Les incertitudes prédictives et la valeur des différents types d'observation ont également été quantifiées, et des estimations de la fonte du névé, de la fonte de glace et de l'évapotranspiration potentielle (ET_p) ont été générées.

Le modèle surface-souterrain intégré a été développé avec le code HydroGeoSphere (HGS) et partiellement calibré, toujours à l'aide de PEST, par rapport au débit du cours d'eau et aux mesures du niveau des eaux souterraines. Le débit a été reproduit à la station principale sur une période d'évaluation indépendante de 11 mois (novembre 2017 – septembre 2018 inclus) avec un coefficient d'efficacité Nash-Sutcliffe de 0,75. Le principal signal saisonnier des niveaux d'eau souterraine observés a été également généralement reproduit, bien que capturer les différences observées entre les sites soit restée hors d'atteinte, probablement en raison de la variabilité des propriétés hydrauliques à l'échelle locale. Des données spatio-temporelles simulées de plusieurs autres variables hydrologiques importantes ont également été visualisées pour illustrer la cohérence du modèle et les capacités d'une telle approche.

Enfin, avec le but d'évaluer l'ampleur potentielle du changement hydrologique futur dans ces régions et d'en dégager les facteurs dominants, la chaîne de modèles (WaSiM et HGS) a été forcée avec des scénarios changement de climat, de végétation et de pergélisol projetés en cas de réchauffement « modéré » d'ici 2075 environ ; il s'agit de la première évaluation de l'impact du changement climatique hydrologique entreprise à l'aide d'un modèle surface-souterrain intégré dans les Alpes. Dans le bassin hydrographique du Vallon de Nant, par exemple, une augmentation de l'ET_p annuelle d'environ 10 % et une diminution du pic moyen de stockage d'eau sous forme de neige en hiver d'environ 34 % (par rapport à la base de référence simulée) sont prévues dans un tel climat. Les changements dans les apports d'eau liquide dans le système (pluie plus la fonte des neiges) annuels sont cependant prévus d'être faibles, car la réduction des précipitations estivales est compensée par l'augmentation des précipitations hivernales.

Pour l'ensemble du domaine, les changements combinés du climat, de la couverture terrestre et du pergélisol devraient entrainer une augmentation, sur une période de simulation de trois ans, de l'évapotranspiration réelle (ET_a) d'environ 44 %, et une réduction du débit des cours d'eau d'environ 10 %. Les changements climatiques directs se sont avérés dominants, l'effet modulateur des changements de la couverture terrestre et du pergélisol étant beaucoup plus limité en comparaison. En conclusion, le fait d'entreprendre des travaux similaires plus régulièrement pourrait accroître la confiance dans les prévisions de l'évolution future de l'hydrologie alpine. Cela dit, étant donné l'ampleur des efforts nécessaires pour développer et les difficultés associées à la calibration de tels modèles, les applications ne sont actuellement recommandées que dans les bassins versants exceptionnellement importants ou écologiquement sensibles, ou encore là où une grande partie des données requises existent déjà.

Mots-clés: *Hydrologie en milieu alpin; changement climatique; dynamique de la neige; modélisation géologique en 3D; modélisation hydrologique intégrée; calibration automatisé; dégradation du permafrost; évolution des forêts*

Acknowledgements

This highly interdisciplinary thesis was financed by the Swiss National Science Foundation. In addition to that pivotal support, many individuals and organisations have made valuable contributions to its accomplishment; the kind assistance provided by each of them is hereby gratefully acknowledged. Above all, I thank Philip Brunner and Grégoire Mariéthoz for the trust they placed in me to proceed independently for the most part, the expert guidance they provided when necessary, and the pleasant working atmosphere they fostered. It has been a privilege to work with you both. I am likewise grateful to all those who assisted me with fieldwork, namely Roberto Costa, Laurent Marguet, Jeremy Zimmermann, Simone Hintze, Violaine Ponsin, Aliénor von Roten, Marie Vallat, and Leanne Phelps. The meteorological and streamflow data provided by Anthony Michelon, Natalie Ceperley, and Åsa Horgby assumed an important role in the project, whilst Raphaël Vallat contributed a thermal image. Swisstopo and MeteoSwiss together provided a substantial proportion of the data used, and open source software (namely R and QGIS) was used heavily. Celia Trunz provided a helpful introduction to the GeoModeller software, and Tristan Brauchli was involved as a co-author of one paper. Members of the Spatial Ecology, High Mountain Geomorphology, and Applied and Environmental Geophysics groups at the Université de Lausanne gave generously of their time and expertise at various stages; I thank especially Daniel Scherrer for simulating future forest scenarios, Olivier Brönnimann for helping to process various climatic data, and Nic Deluigi for providing permafrost distribution maps. Emily Voytek, Niklas Linde, and Ludovic Baron enabled the geophysics campaign and associated work to be realised. René Therrien invited me to conduct a short but fruitful research visit to his group at Université Laval, Canada, whilst Steve Berg and his colleagues at Aquanty Inc. also freely shared their considerable knowledge. Marie Arnoux helped to improve the French résumé. More generally, it has been a pleasure to work alongside many colleagues, friends, and members of administrative staff at the Centre d'Hydrogéologie et de Géothermie and the broader Université de Neuchâtel over the past four years, including Claire Carlier, with whom I shared an office. I appreciate the commitment of the experts who have agreed to join the evaluation committee, and finally extend my deepest thanks to my family and Sonia for their support.

Table of Contents

List of Figures

List of Tables

Preface – Global context

As the global population and living standards have increased, so too has the pressure exerted upon many of earth's natural environments and their associated ecosystems (Sage, 2019). Whilst some of the attendant environmental problems, such as sustained deforestation in tropical regions (Martínez-Ramos et al., 2016; Conte et al., 2019), are now longstanding, others have only assumed enhanced prominence more recently – the increasingly ubiquitous pollution of the environment by plastics (Lavers and Bond, 2017; Peeken et al., 2018) being one such example. However, even such undoubtedly profound "classical" environmental issues are becoming increasingly overshadowed as the multitude of complex challenges related to anthropogenic climate change become ever more apparent (Dow and Downing, 2016).

Atmospheric greenhouse gas concentrations continue to rise; the globally averaged concentration of CO_2, for instance, reached 407.8 parts per million (ppm) in 2018 – yet another instrumental record (WMO, 2019). The resultant shifts in radiative forcing are now clearly affecting near-surface air temperatures. Indeed, 2019 was declared the second warmest year since records began, just behind 2016 (when strong El Niño conditions prevailed) (Copernicus, 2020). Moreover, via a series of processes interactions and feedback mechanisms, climate change effects are now cascading widely across the earth system.

Advances in observational technologies have permitted various manifestations of environmental change be monitored with high accuracy over recent decades. For instance, a compilation of satellite measurements established that the Greenland ice sheet is losing mass at a rate seven times faster than it was during the 1990s (The IMBIE Team, 2019). Ocean temperature measurements, meanwhile, confirm substantial heat uptake; global mean temperatures were successively warmer in each of the three years to 2019 (Cheng et al., 2020). According to precision satellite altimetry, the combination of continental ice loss and thermal expansion of ocean water have raised mean sea levels by approximately 7 cm over the past 25 years, and the rate of increase is accelerating (Nerem et al., 2018). Since around 600 million people currently live in low-lying coastal regions (McGranahan et al., 2007), the consequences of continued sea-level rise in terms of coastal flood risk are obvious (Buchanan et al., 2016; Rahmstorf, 2017).

Elsewhere, permafrost in northern regions is thawing (Biskaborn et al., 2019) and – in certain cases – more rapidly than was previously expected, contributing further to carbon emissions (Turetsky et al., 2020). Abrupt land subsidence is contributing to this effect, and represents one of many positive feedback mechanisms, whereby initial perturbations are amplified, that are either known or hypothesised to operate within the earth system. Such feedback mechanisms may

ultimately lead to "tipping points", i.e. states beyond which far reaching, uncontrollable, and potentially irreversible consequences could occur, being surpassed. Indeed, somewhat alarmingly, Lenton et al. (2019) recently suggested that the chances of this happening with respect to several major possible tipping points have increased appreciably of late. Numerous spectacular, highly-specialised ecosystems (both aquatic and terrestrial) are likewise gravely threatened. An especially high-profile example is the Great Barrier Reef, situated off the coast of Queensland, Australia, whose corals have suffered repeated bleaching in recent years due to exceptionally warm ocean temperatures (Ainsworth et al., 2016; Hughes et al., 2018).

Potential associations between climate change and dangerous, damaging extreme weather events such as floods, droughts, tropical cyclones, and forest fires are also coming under enhanced scrutiny. In the immediate aftermath of such events, the question as to whether already-realised climate change had any discernible impact on their probabilities of occurrence (i.e. frequencies) or magnitudes (i.e. intensities) often arises. However, in light of the inherent complexity of the earth system, plus the inconvenience that extreme events are by very definition rare (and so systematic data pertaining to them is naturally limited), definitively answering such questions is far from straightforward (IPCC, 2012). Nevertheless, using a simulation-based approach called probabilistic event attribution, Otto et al. (2018) suggested that climate change had made rainfall events such as that which caused damaging flooding across northern Britain in December 2015 almost 60% more likely than under counterfactual, pre-industrial climatic conditions. Comparable conclusions have been drawn with respect to an increased likelihood of drought in California, United States, for instance (Diffenbaugh et al., 2015). That said, ongoing methodological debates (Jézéquel et al., 2018) and the occasional emergence of completely contradictory conclusions (cf. Cheng et al., 2016 regarding Californian drought) indicate that the field of extreme event attribution remains nascent.

Looking to the future, a substantial "gap" has been identified between current and projected future greenhouse gas emissions on the one hand, and the greatly reduced levels that would be required in order to limit the increase in global mean temperature to "well below" 2°C (relative to pre-industrial levels, as enshrined in the Paris agreement) on the other (UN Environment Programme, 2019). Moreover, whilst constraining global warming to such a range may avert many of the most catastrophic foreseeable impacts of climate change, it does not represent any kind of "safe" level *per se*. It must furthermore be highlighted that a good deal of future earth system change is already "committed", i.e. is impending, as slowly responding components such as the ice sheets and oceans will take considerable time to reach their new equilibria following the stabilisation of radiative forcing (Abram et al., 2019).

This very brief summary of the global situation hopefully conveys that the scientific evidence now forms a strong and diverse foundation upon which drastic and rapid reductions in global greenhouse gas emissions can be advocated. It could even perhaps be argued that something of a shift away from fundamental scientific endeavour towards market-driven, technological, and political solutions is due. After all, the trajectory of future anthropogenic emissions is unknown, and so any scientific projections must be qualified by considerable (and irreducible) epistemic uncertainties. Yet whilst such practical solutions must undoubtedly assume a central role in both reducing greenhouse gas emissions and developing the resiliency necessary for "living with" inevitable climate change, and indeed investments and efforts in these areas are already well underway, an imperative role for scientific investigation equally remains. Satisfactorily reproducing observations pertaining the salient physical processes in a computational sense is, in fact, a prerequisite to making reliable future predictions, even if it is not always described so explicitly as such.

For example, even if a given future emissions scenario could be assumed with full certainty, alternative climate models give inconsistent indications of the extent to which local conditions will be affected. Climate modelling efforts must therefore be sustained. Furthermore, and of more direct relevance to this thesis, even if future local climatic conditions could be assumed with certainty, in complex systems especially, even the direction of change of a particular variable or variables of interest, such as the availability of water resources, is often unclear. The resultant "cascade of uncertainty" (Wilby and Dessai, 2010) can severely hamper planning and mitigation efforts.

In summary, despite the attendant uncertainties, many critical scientific questions concerned with the unravelling of environmental complexity remain to be answered. With effort, many answers can reasonably be expected to be obtained. The present thesis proceeds in this direction with specific regards to an important but rapidly changing type of environment that has (deliberately) not yet been introduced – that of rugged, mid-latitude mountains.

Abram, N. et al. (2019). Framing and Context of the Report. *IPCC Special Report on the Ocean and Cryosphere in a Changing Climate*. Ed. by H.-O. Pörtner et al.

Ainsworth, T. D., Heron, S. F., Ortiz, J. C., Mumby, P. J., Grech, A., Ogawa, D., Eakin, C. M., and Leggat, W. (2016). Climate change disables coral bleaching protection on the Great Barrier Reef. *Science* 352, 338–342.

Biskaborn, B. K. et al. (2019). Permafrost is warming at a global scale. *Nature Communications* 10, 264.

Buchanan, M. K., Kopp, R. E., Oppenheimer, M., and Tebaldi, C. (2016). Allowances for evolving coastal flood risk under uncertain local sea-level rise. *Climatic Change* 137, 347–362.

Cheng, L. et al. (2020). Record-Setting Ocean Warmth Continued in 2019. 37, 137–142.

Cheng, L., Hoerling, M., Aghakouchak, A., Livneh, B., Quan, X. W., and Eischeid, J. (2016). How has human-induced climate change affected California drought risk? *Journal of Climate* 29, 111–120.

Conte, L., Renner, M., Brando, P., Oliveira dos Santos, C., Silvério, D., Kolle, O., Trumbore, S. E., and Kleidon, A. (2019). Effects of tropical deforestation on surface energy balance partitioning in southeastern Amazonia estimated from maximum convective power. *Geophysical Research Letters* 46, 4396–4403.

Copernicus (2020). *2019 was the second warmest year and the last five years were the warmest on record*. URL: https://climate.copernicus.eu/copernicus-2019-was-second-warmest-year-and-last-five-years-were-warmest-record.

Diffenbaugh, N. S., Swain, D. L., Touma, D., and Lubchenco, J. (2015). Anthropogenic warming has increased drought risk in California. *Proceedings of the National Academy of Sciences of the United States of America* 112, 3931–3936.

Dow, K. and Downing, T. E. (2016). *The Atlas of climate change: mapping the world's greatest challenge*. Univ of California Press.

Hughes, T. P., Kerry, J. T., and Simpson, T. (2018). Large-scale bleaching of corals on the Great Barrier Reef. *Ecology* 99, 501.

IPCC (2012). *Managing the Risks of Extreme Events and Disasters to Advance Climate Change Adaptation.* Ed. by C. Field et al. Cambridge: Cambridge University Press, p. 582.

Jézéquel, A., Dépoues, V., Guillemot, H., Trolliet, M., Vanderlinden, J. P., and Yiou, P. (2018). Behind the veil of extreme event attribution. *Climatic Change* 149, 367–383.

Lavers, J. L. and Bond, A. L. (2017). Exceptional and rapid accumulation of anthropogenic debris on one of the world's most remote and pristine islands. *Proceedings of the National Academy of Sciences of the United States of America* 114, 6052–6055.

Lenton, T. M., Rockström, J., Gaffney, O., Rahmstorf, S., Richardson, K., Steffen, W., and Schellnhuber, H. J. (2019). Climate tipping points - too risky to bet against. *Nature* 575, 593–595.

Martínez-Ramos, M., Ortiz-Rodríguez, I. A., Piñero, D., Dirzo, R., and Sarukhán, J. (2016). Anthropogenic disturbances jeopardize biodiversity conservation within tropical rainforest reserves. *Proceedings of the National Academy of Sciences of the United States of America* 113, 5323–5328.

McGranahan, G., Balk, D., and Anderson, B. (2007). The rising tide: Assessing the risks of climate change and human settlements in low elevation coastal zones. *Environment and Urbanization* 19, 17–37.

Nerem, R. S., Beckley, B. D., Fasullo, J. T., Hamlington, B. D., Masters, D., and Mitchum, G. T. (2018). Climate-change–driven accelerated sea-level rise detected in the altimeter era. *Proceedings of the National Academy of Sciences of the United States of America* 115, 2022–2025.

Otto, F. E., Van Der Wiel, K., Van Oldenborgh, G. J., Philip, S., Kew, S. F., Uhe, P., and Cullen, H. (2018). Climate change increases the probability of heavy rains in Northern England/Southern Scotland like those of storm Desmond - A real-time event attribution revisited. *Environmental Research Letters* 13.

Peeken, I., Primpke, S., Beyer, B., Gütermann, J., Katlein, C., Krumpen, T., Bergmann, M., Hehemann, L., and Gerdts, G. (2018). Arctic sea ice is an important temporal sink and means of transport for microplastic. *Nature Communications* 9.

Rahmstorf, S. (2017). Rising hazard of storm-surge flooding. *Proceedings of the National Academy of Sciences of the United States of America* 114, 11806–11808.

Sage, R. F. (2019). Global Change Biology: A Primer. *Global Change Biology*, 3–31.

The IMBIE Team (2019). Mass balance of the Greenland Ice Sheet from 1992 to 2018. *Nature*.

Turetsky, M. R. et al. (2020). Carbon release through abrupt permafrost thaw. *Nature Geoscience* 13, 138–143.

UN Environment Programme (2019). *Emissions Gap Report 2019*. Tech. rep.

Wilby, R. L. and Dessai, S. (2010). Robust adaptation to climate change. *Weather* 65, 180–185.

WMO (2019). *WMO Greenhouse Gas Bulletin (GHG Bulletin) - No. 15: The State of Greenhouse Gases in the Atmosphere Based on Global Observations through 2018*. Tech. rep. Geneva: World Meteorological Organization, p. 8.

1 | Introduction

Photograph: *The dry upper section of L'Avançon de Nant in October 2018, looking south towards the Lion d'Argentine*

"Research on mountain water resources must become more integrative by linking relevant disciplines"

(Viviroli et al., 2011)

1.1 General motivation

1.1.1 The importance of mountain hydrology

Runoff from mountainous regions has long held considerable importance for human societies. Indeed, an estimated 1.6 billion people – over 20% of the global population – currently live in areas that receive water originating from high mountains (Immerzeel et al., 2020). On the European continent, meanwhile, 40% of all fresh water is thought to derive from the Alps. In addition to supporting aquatic and riparian ecosystems (e.g. Brown et al., 2015), mountainous water resources are typically exploited for various purposes including drinking water provision, crop irrigation, hydropower production, and use in the tourism industry (EEA, 2009). They can consequently be considered a valuable "ecosystem service"; that is, a service provided by nature that benefits human societies (Grêt-Regamey et al., 2012).

The importance of mountains as "water towers" (Viviroli et al., 2007) stems from the orographic enhancement of precipitation they induce (Napoli et al., 2019), and their capacity to temporally store water on seasonal and longer timescales – most notably in the form of snow and ice – before subsequently releasing it. Mountainous streams thus typically exhibit not only higher specific discharge (i.e. discharge per unit catchment area) than lowland watercourses in the same climatic region (Horton et al., 2006), but are also characterised by favourable temporal flow distributions. These effects are often sufficient to maintain streamflow through hotter and perhaps also dryer summer and autumn periods (Barnett et al., 2005).

However, the mountain cryosphere is highly sensitive to warming air temperatures, and is accordingly undergoing profound change (Hock et al., 2019; Huss et al., 2017). Predominantly negative impacts on water security, water quality, and tourism and recreation are now being reported from mountainous regions around the globe (Hock et al., 2019). Water resources emanating from major mountain chains such as the Hindu Kush Himalaya (Asia) and the Andes (South America), upon which large populations are heavily reliant, are thought to be especially threatened (Quincey et al., 2017; Vuille et al., 2018; Pritchard, 2019). Furthermore, via a series of interactions and feedback mechanisms, hydrology (not only surface water, but also ground-

water) in turn exerts a strong influence on other mountainous system components, especially vegetation – which is itself rapidly changing with climate (e.g. Anderson et al., 2020).

This thesis intends to investigate the feasibility of a prospective means by which predictions of the hydrological impacts of possible future climate change might be improved in complex mountainous catchments, such as those found in the European Alps. Such predictions are urgently required by environmental managers as a basis for decision making, but are complicated by various factors including complex subsurface geologies, highly heterogeneous snow patterns, and intricate evapotranspiration dynamics.

In closure of this section, a brief semantic note is appropriate. In what follows, the term "alpine" refers to steep, rugged, high elevation terrain in which snow and ice exert a strong influence on the hydrological regime. This is a somewhat broader definition than using the term to merely denote the "alpine" zone in a typical elevational profile, i.e. the area located above the upper limit of trees (the "sub-alpine" zone) but below the sparsely vegetated "nival" zone. Capitalised, the term ("Alpine") relates specifically to the European Alps.

1.1.2 Climate change in the European Alps

1.1.2.1 Observed changes and their impacts

Recent summer mean temperatures across the European continent have been unprecedented in the context of at least the last two millennia (Luterbacher et al., 2016). The extreme heatwave of 2003, which caused approximately 70,000 additional deaths (Robine et al., 2008), stands out as a particularly devastating episode. More detailed assessments of past change tend to be presented at only national levels. Being centrally located, predominantly mountainous (80% if the delineation proposed by Körner et al., 2017 is used), and, furthermore, the country within which the study area of this thesis is located, Switzerland provides an appropriate case.

Remarkably, the Swiss annual mean air temperature has already increased by approximately 2.1°C since 1864 (MeteoSwiss, 2019). Recent analyses such as that by Begert and Frei (2018), which go beyond simply averaging several long station records, are important in ensuring that such figures are nationally representative. A particularly striking aspect of the record is that the most pronounced warming has occurred since the 1980s. In fact, nine out of the 10 warmest years have been during the 21st Century (CH2018, 2018).

As has already been mentioned, the present thesis is primarily concerned with the Alpine part of the country. Figure 1.1, which differentiates historical warming trends on spatial, seasonal, and

longer term temporal bases, is therefore particularly instructive. Considering the period 1961-2017, for instance, reveals that extremely pronounced warming has occurred across practically the entire country during spring (MAM) and summer (JJA), with a more moderate trend in evidence during autumn (SON) and winter (DJF). Moreover, autumn and winter trends during this period are statistically insignificant across much of the more mountainous southern portion.

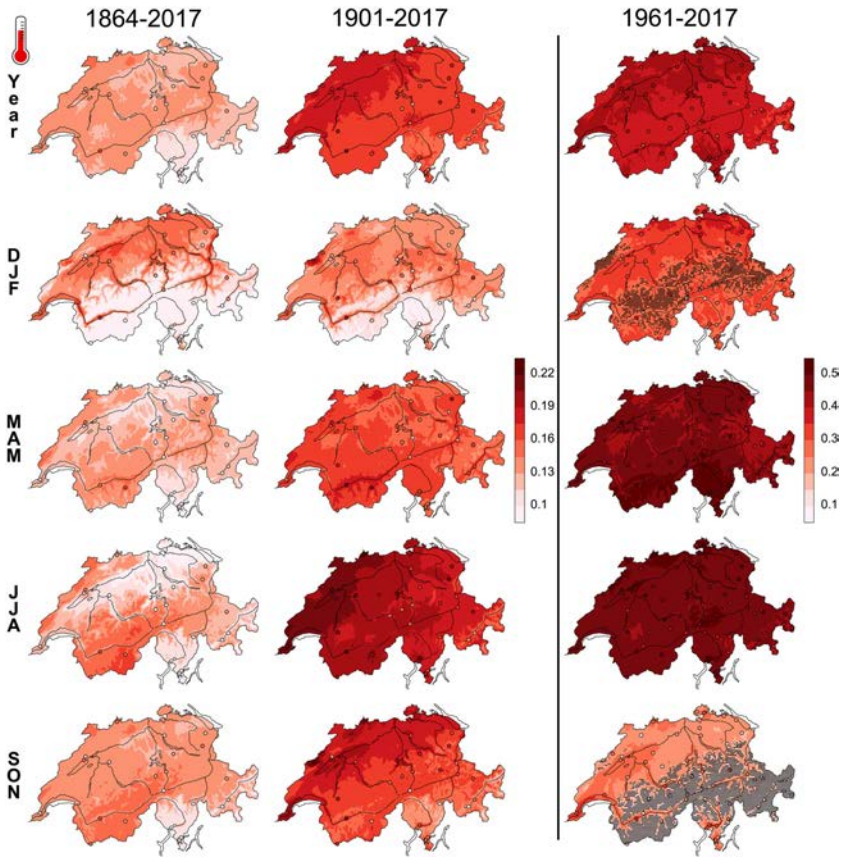

Figure 1.1: Linear trends in annual and seasonal mean temperature across Switzerland (°C per decade). Source: Isotta et al. (2019).

Changes in annual or seasonal mean temperatures also imply shifts across the entire temperature probability distribution. Impacts on the extremes (or "tails") could be particularly strong. For example, returning briefly to the continental level, Christidis et al. (2015) suggest that the probability of extremely hot summers across Europe has increased drastically of late.

The mountain cryosphere is generally highly sensitive to warming conditions, which is to say that relatively small temperature increases can induce large and rapid responses (Finger et al., 2011). Given the warming that has already occurred, it is unsurprising that a plethora of studies

chronicling Alpine glacial retreat, snow cover declines, and permafrost degradation have been compiled (Beniston et al., 2018). Of the aforementioned, the rapid mass loss and retreat of the glaciers represents the most visible and incontrovertible indication of climate change.

Figure 1.2 presents the specific mass balance trends of seven selected glaciers, all of which are now clearly strongly negative. To remove the influence of the dynamic response of individual glaciers that can occasionally slightly complicate the interpretation of such figures, Vincent et al. (2017) estimated the so-called "point mass balance" of six glaciers across the Alps. By doing so, their common, climate-driven variably could be isolated. Their results indicated that substantial widespread mass loss occurred between 2003 and 2013, averaging 16 m water equivalent from each glacier. Such findings reinforce those of earlier studies that involved remote sensing and longitudinal analyses of digital elevation models (e.g. Paul et al., 2004; Paul and Haeberli, 2008; Fischer, Huss, et al., 2015).

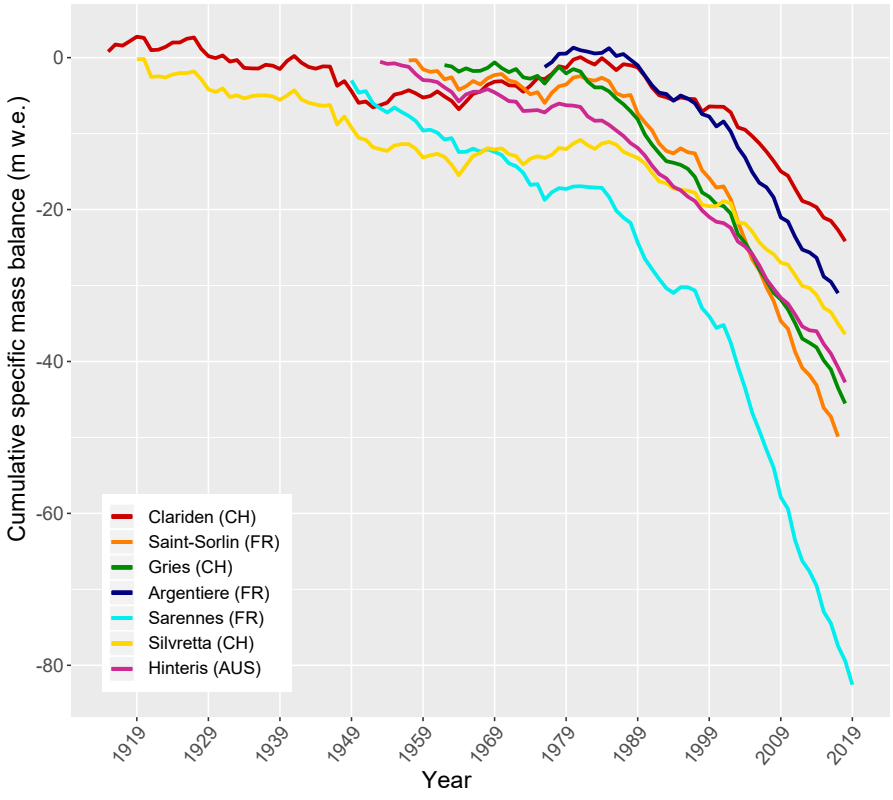

Figure 1.2: Cumulative specific mass balance of selected glaciers in the European Alps since the start of their respective measurements, in metres water equivalent (m w.e.). Original figure, generated using data from (WGMS, 2019).

Further statistics underline the rapidity with which such changes can occur. For instance, in the hydrological year 2016/17, as a result of meagre winter snowfall and a hot subsequent summer, Swiss glaciers lost approximately 3% of their entire volume (Huss et al., 2018). The following year, despite considerable snowfall at higher elevations, summer heatwave conditions inferior only to 2003 resulted in a further 2.5% reduction – equivalent to approximately 1.4 bn cubic meters of ice (SCNAT, 2018).

Seasonal snowmelt traditionally constitutes the dominant annual runoff signal in the Alps (Beniston, 2012). Since snow accumulation exhibits considerable inter-annual variability, snow trend detection can be challenging. Nevertheless, reliable evidence for a decline in the solid to liquid precipitation ratio (Marty and Meister, 2012), as well as an increase in the frequency and intensity of melt episodes (Klein et al., 2016), has now emerged. Declining snow cover duration and depth trends are consequently apparent at specific measurement stations (ibid.) and, importantly, have been corroborated by more extensive investigations. Marty, Tilg, et al. (2017), for instance, examined Snow Water Equivalent (SWE) – a variable which has more direct hydrological relevance than snow depth or duration – and reported declines across the Alps, especially in spring (Figure 1.3).

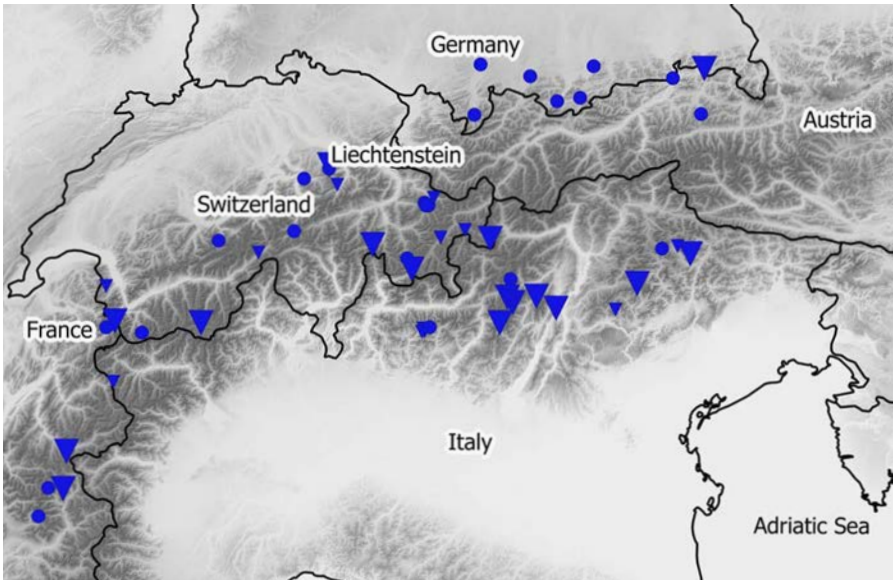

Figure 1.3: Geographical distribution of the 45 year trend for 1 April SWE (1868-2012) across the European Alps. Blue specifies a negative trend (all stations). Large triangles indicate significant trends ($p < 0.05$) and small triangles indicate weakly significant trends ($p < 0.2$). Circles represent stations with no significant trend ($p \geq 0.2$). Source: Marty, Tilg, et al. (2017). © American Meteorological Society. Used with permission.

Theoretically, these observed trends in the glaciers and snowpack could be partly associated with precipitation changes. Yet as Figure 1.4 demonstrates, past changes in annual and seasonal precipitation across Switzerland have been fairly modest – certainly much more so than for temperature – and, almost everywhere, cannot be considered statistically significant. Hence, the strong cryospheric responses can be chiefly ascribed to temperature increases. Precipitation trends do emerge from long-term Swiss meteorological station records if one focusses on heavy precipitation metrics, however (Scherrer et al., 2016).

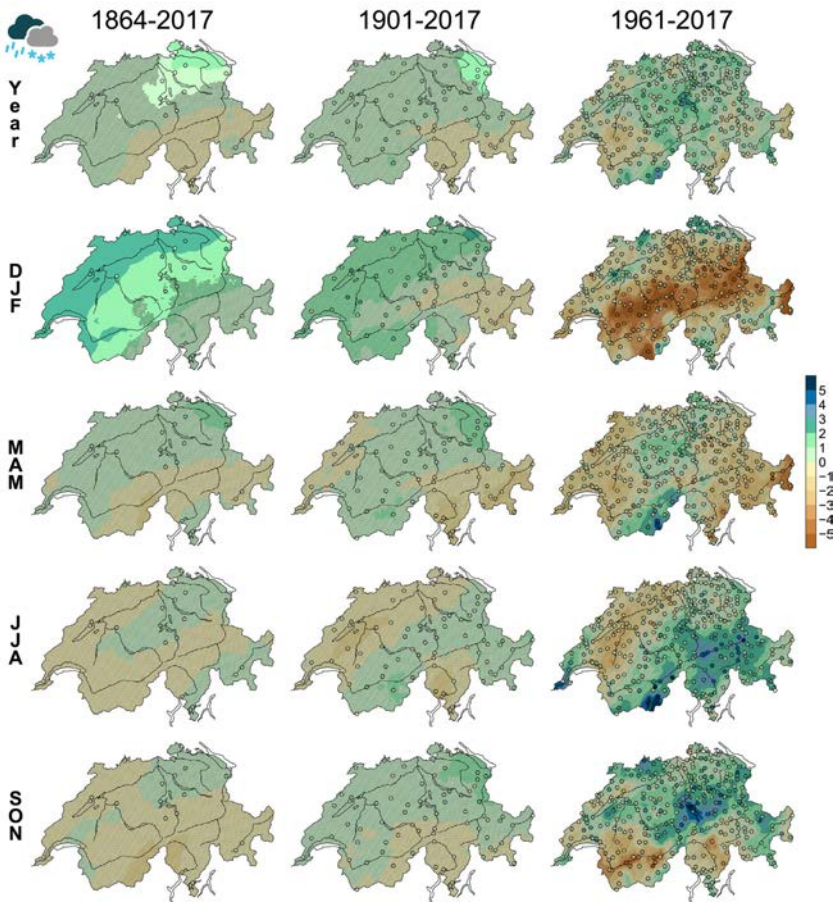

Figure 1.4: Decadal percentage change in annual and seasonal precipitation across Switzerland relative to the 1981-2010 reference period. The extensive stippling highlights areas where the trends are statistically insignificant. Source: Isotta et al. (2019).

Possible trends in other variables such as global radiation, relative humidity, and wind speed have received much less attention. That said, Sanchez-Lorenzo et al. (2017) reported a significant increase in global radiation, strongest in spring, across Europe between 1983 and 2010.

Moving on to consider observed hydrological impacts, many heavily glacierised catchments exhibit significant increasing annual streamflow trends which, being strongest in summer, can confidently be attributed to enhanced ice melt (Pellicciotti et al., 2010). Annual streamflow increases arising from consistently negative glacier mass balance obviously cannot continue indefinitely, however. On the contrary, once a certain critical volume of ice is surpassed, meltwater generation will decline monotonically (even if it continues to exceed the annual inputs for some time). Catchment properties (notably elevation) and other local conditions determine the "position" of a given catchment along this trajectory. For example, according to the recent global modelling study of Huss and Hock (2018), the Rhône catchment as a whole has probably already reached "peak water".

Streamflow trends are generally less conspicuous at lower elevations, where snowmelt influences are more pronounced (Stewart, 2009). Nonetheless, and in accordance with the expected impacts of warming conditions (e.g. a shift towards a greater proportion of liquid precipitation and earlier snow melt), Birsan et al. (2005) reported that a general tendency towards increased winter and spring runoff in Swiss catchments that was most apparent at higher elevations. The potential for ice and snowmelt trends to have competing influences (i.e. for decreasing snowmelt contributions to be (temporarily) compensated for by increasing ice melt ones), especially in summer, is another reason why streamflow trend detection and attribution can be difficult in certain catchments. In summary, winter low flows in the Alps are generally increasing, whilst summer flow trends are generally negative, apart from in heavily glaciated catchments (Stahl et al., 2010). Annual discharge trends are least negative in high elevation catchments (Michel et al., 2020). Incidentally, no corresponding studies are known to have evaluated Alpine groundwater level trends; if sufficient measurements exist, this could represent an attractive avenue for future research.

The frequency of rain-on-snow events, which can cause major floods in alpine areas, also appears to have increased (Beniston and Stoffel, 2016). It has likewise proven possible to associate past air temperature increases with elevated fluvial sediment transport (Costa et al., 2018), although climatically-independent anthropogenic factors also come into play (Lane et al., 2019). Furthermore, due to the continued inflow of cold snow and ice melt, increases in the water temperature of Alpine streams and rivers are clearly dampened in comparison with their lower elevation counterparts, but this effect is expected to diminish in coming years (Michel et al., 2020). Finally, as foreseen (Theurillat and Guisan, 2001), additional components of alpine environmental systems and their associated ecosystems such as plant species compositions (Rixen et al., 2018), vegetation more generally (Rogora et al., 2018), and permafrost (Noetzli and Phillips, 2019) are

also undergoing change, and/or are expected to increasingly do so in future. Although some of these changes may have minimal indirect hydrological impacts, others are likely to be more consequential; the latter are discussed further in due course.

1.1.2.2 Projected future changes

In order to make future predictions of a range of climatic variables, General Circulation Models (also referred to as Global Climate Models; in either case GCMs) are routinely employed in conjunction with a small number of (non-equiprobable) scenarios that represent possible courses of global socio-economic development. Whilst these scenarios were previously defined purely according to assumed greenhouse gas (GHG) emissions ("emissions scenarios"), the current version explicitly refer to the atmospheric GHG concentrations expected to result from each ("Representative Concentration Pathways", or RPCs; van Vuuren et al., 2011).

Since the lateral resolution of GCMs is low (typically on the order of hundreds of kilometres), downscaling must usually be undertaken to provide projections that are meaningful for assessing climate change impacts on relatively local scales, especially in regions with heavily accentuated topography such as the Alps. This process is increasingly being undertaken dynamically, by coupling GCMs with more finely discretised Regional Climate Models (RCMs) (even if statistical techniques must generally still be relied upon to produce extremely localised information). Due to contrasting process conceptualisations and implementations, the projections made by different GCM-RCM combinations under a given socio-economic scenario often exhibit much variability. For this reason, they are generally deployed in combination (i.e. as an ensemble) where possible.

Focussing on a moderate emissions scenario (namely A1B, the standard reference at the time; Nakicenovic et al., 2000), Gobiet et al. (2014) presented a fairly thorough overview of climate change projections across the Alpine region. Above all, the contribution clearly conveys the complexity of the matter, which is related to both the nature of the climate system and the capabilities of the current generation of climate models. Indeed, although dependent on the variable and future period in question, alternative model outputs frequently have a wide spread, and do not always even consistently agree on the sign (i.e. direction) of expected future change. Despite this, certain broad statements can be made with reasonable confidence.

Foremost amongst these is the very strong likelihood of continued near-surface air temperature increases – a signature present in all the models assessed by (ibid.) – with an acceleration likely in the second half of the 21st century also probable. Even in this case, however, the spread

amongst ensemble members was not negligible. In addition, and interestingly, the authors observed that the projected rates of future warming are actually slower than historically observed ones. They posit that whilst this could simply be an effect of natural variability, it may equally indicate that the models have a certain propensity towards systematic underestimation of temperature trends. A particularly important open question regarding mountainous temperatures is whether or not warming might be augmented at higher elevations; an effect known as elevation dependant warming (EDW; Pepin et al., 2015). Zubler et al. (2014) suggested that may indeed be the case in the Alps, although Hock et al. (2019) caution that such suggestions should be treated with care – the processes implicated are highly complex and, in some instances, the opposite situation (i.e. reduced warming rates with increasing elevation) seems to occur.

Precipitation volumes are expected to increase in winter and decrease in summer. However, it must be emphasised that the attendant uncertainties are much more substantial than those accompanying temperature projections (Gobiet et al., 2014; Zubler et al., 2014). Fischer, Keller, et al. (2015) analysed future precipitation projections for Switzerland in detail, concluding that the envisaged summer drying is likely to be brought about by a reduction in the number of days with precipitation. In mountainous parts, a decline in large scale frontal (as opposed to small scale convective) summer rainfall is anticipated. Extreme precipitation projections have also been assessed. Rajczak et al. (2013), for instance, advise that extreme event intensities are likely to increase in most parts of the Alps, especially during autumn. Whilst even more uncertain, potential future shifts in global radiation and relative humidity are thought likely to track precipitation changes, with reductions in global radiation and increases in relative humidity likely to accompany increasing precipitation (and vice versa).

Recently, a new set of climate projections for Switzerland have been released (CH2018, 2018). Whilst these projections, which are collectively known as CH2018, are broadly concordant with the expectations outlined above, one distinguishing feature is that they are fully transient. In other words, the meteorological data generated by each RCP-CGM-RCM model "chain" and then statistically downscaled (onto both a 2 km resolution grid and existing station locations) follow completely independent trajectories over both the past and future periods (ibid.). In this sense, they provide many alternative time-series of possible future "weather". In applications able to make use of such extensive information, limitations associated with the previous approach whereby historical meteorological observations were simply modified by change factors derived from the future climate simulations – such as the assumption that event frequencies will remain invariant – can be overcome. Chapter 5 does make use of the CH2018 scenarios, albeit not the full richness of their transient information.

Predictive modelling exercises have already proceeded to assess the possible impacts of such projected climate changes on the Alpine cryosphere. For example, Jouvet and Huss (2019) simulated the future evolution of the iconic Great Aletsch glacier – presently the longest in the Alps. Amongst other aspects, this study reveals the extent to which the glacier is in disequilibrium with even the present climate. At the larger scale of the entire chain, Zekollari et al. (2019) applied a novel glacier evolution simulation framework that accounted for ice flow processes. Their results indicate that, relative to 2017, volumetric reductions of approximately 50% can be expected by 2050. Over this time horizon, the specific RCP followed is anticipated to have little effect on outcomes, but becomes more important by the end of the 21st Century; approximately one third of the present ice volume will remain if the most optimistic RCP 2.6 scenario is tracked, but ice is projected to have largely disappeared if the extreme "worst case" (i.e. but certainly not necessarily most probable; Hausfather and Peters, 2020) pathway, RCP 8.5, materialises. Finally, in terms of snow, the physically-based simulations of Marty, Schlögl, et al. (2017) indicate that unless a strong intervention scenario (akin to RCP 2.6) is followed, mean reductions in regional depths of around 50% are probable by as early as 2050, with substantial attendant changes in the duration of seasonal snow cover and in snowline elevations (decreases and increases, respectively).

As Section 1.2.2 explains in greater detail, in order to propagate such climatic and subsequent cryopsheric changes through to their likely impacts upon water resources, and thereby deliver the predictions that are required by water managers and other stakeholders as a basis for planning and/or mitigation decisions (Reynard et al., 2014), some form of hydrological modelling must be undertaken. However, developing models which have explanatory as opposed to merely descriptive power in such terrain is often far from straightforward. For now, it can simply be mentioned that many so-called hydrological climate change impact assessments (HCCIAs) account for changes in future snow and ice, an intermediate step, in a similar manner to those examples given above.

1.1.3 Modelling mountain hydrology: the ultimate challenge!

Several rather fundamental challenges are commonly encountered when undertaking hydrological investigations in mountainous regions. Firstly, alpine catchments have highly distinctive physical characteristics, and play host to a large number of diverse processes. In addition, being driven by pronounced elevational and in many cases also geological gradients on the one hand, and strong inter-annual, seasonal, and diurnal fluctuations on the other, the majority of these processes exhibit considerable spatio-temporal variability.

Another, perhaps underappreciated factor is that the assortment of potentially important hydrological processes can span a considerable vertical range, from the snowpack to deep groundwater, leaving them to traditionally remain the preserve of specialised but separate communities of academics and practitioners. Complexity levels are especially high in areas where bedrock geologies are "unconventional"; e.g. where complex arrangements of calcareous sediments are present (Chen and Goldscheider, 2014; Filippini et al., 2018). As a result of the very orogenic processes that led to their formation, such complex geologies are more likely to be encountered in Alpine regions than elsewhere.

Consequently, steep slopes replete with dynamic waterfalls, torrents, and streams, heterogeneous snow patterns and melt rates, complex subsurface architectures in both the bedrock and unconsolidated sediments, and diverse land cover are all characteristic features of Alpine terrain. Moreover, unsaturated subsurface zones can be very thick (e.g. Bonat et al., 2020), and vertical hydraulic gradients large (Manning and Caine, 2007). In truly karstic and other similar settings, topographically "closed" basins (i.e. basins without surface outflows) may also be present, forcing groundwater flow across topographic divides.

This complexity is compounded by the fact that access difficulties, inhospitable conditions for both fieldwork and instrumentation, and in certain cases legislative protections can all severely limit the ease with which environmental data can be obtained in alpine areas. For example, meteorological station density typically decreases markedly with increasing elevation (Minder et al., 2010; Härer, 2017); a situation that, coupled with the pronounced spatial variability in physical phenomena alluded to above, affects the spatial representativeness of the observations that can be made. Thus, even historical meteorological conditions away from measurement stations (i.e. spatial fields), which form a key input to most hydrological modelling exercises, often remains highly uncertain (Tobin et al., 2011). Similarly, it is becoming increasingly apparent that in many types of headwater systems, a substantial proportion of total basin outflow may actually pass beneath the stream gauging infrastructure in place (Carlier et al., 2018; Staudinger et al., 2019), or else otherwise bypass surface measurement points. This essentially amounts to another measurement challenge with important modelling implications.

In the worst case, perhaps a consequence of their lower population densities and apparent immediate economic importance compared to lowland areas (e.g. in terms of agricultural production), the collection, compilation, or generation of spatial environmental datasets corresponding to mountainous regions can be entirely overlooked, even in highly developed countries such as Switzerland. Figure 1.5, for instance, reveals that the more mountainous southern portion of the country is not covered by existing detailed hydrogeological maps. Similarly, in the Canton of

Vaud (within which the study area of this thesis is located; see Section 1.4.3), detailed soil maps are only available for the lower elevation regions. Aside from where tunnelling and other infrastructure projects have been carried out, the dearth of information in mountain environments is, unsurprisingly, particularly acute with respect to the subsurface – this environment being arguably the most challenging of all to access and measure (Gabrielli et al., 2012).

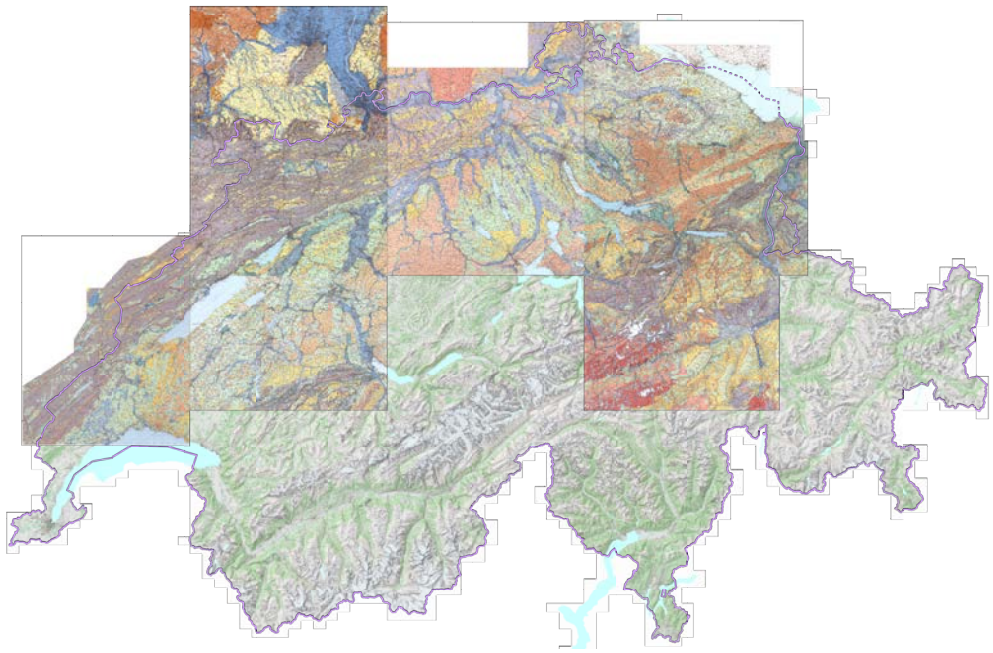

Figure 1.5: The extent of detailed (1:100,000) hydrogeological mapping in Switzerland (as of March 2020). The mountainous southern part of the country is almost entirely neglected. Source: Swiss Federal Office of the Environment (FOEN).

In consequence of this unique combination of system complexity and data paucity, and notwithstanding recent efforts that are discussed shortly, understanding of the functioning of mountainous catchments generally remains limited (Penna et al., 2016). This is problematic because both sound conceptual understanding and informative data are prerequisites for the development of powerful numerical representations (i.e. those with robust predictive capabilities). As it is, modelling mountain hydrology can duly be fraught with difficulty (Strasser and Kunstmann, 2013), with Klemeš (1990) even going so far as to describe it as "the ultimate challenge"!

Although major advancements have been made in the intervening period, including the maturation of satellite remote sensing (Dong, 2018; Nolin, 2010), the emergence of various gridded meteorological datasets (e.g. Efthymiadis et al., 2006; Isotta et al., 2014; Panziera et al., 2018), and the wider availability of improved hydrological models (to be discussed at length shortly),

the general assertion of Klemeš arguably remains highly applicable today, bestowing an attractive allure on this important discipline. Having established the overriding motivation and context of this thesis, the subsequent sections proceed, with reference to the literature, to critically discuss the current status of the broad field of alpine hydrology. A number of research gaps that this thesis hopes to help to close are then identified.

1.2 The status quo and regards in which it should be improved

Current research with regards to the prediction of alpine hydrological system responses to climate change is lacking in perhaps two main areas. Firstly, detailed field based investigations often focus on only short spatial scales, and are vary rarely accompanied by any form of numerical modelling. Secondly, the simulations that are undertaken to explore possible climate change impacts are associated with several important constraints; one being the continued reliance on simplistic conceptual models, and another being the general disregard of potential indirect climate change impacts upon hydrology, arising for example from forest expansion. These research gaps are explained and justified more thoroughly in the following subsections. Certain additional and somewhat more specific issues, including the lack appropriate 3D geological models of mountainous regions, the continued use of simple snow modelling approaches, and suchlike have also impeded progress. Issues of nature issues are only touched upon briefly in this general introduction, but are considered at greater length in the chapters which respectively concern them.

1.2.1 Field-based investigations

1.2.1.1 Overview of aims, methods, and insights gleaned

Field investigations in alpine catchments have long placed strong emphasis on snow and ice (Elder et al., 1991; Bales and Harrington, 1995; Jansson et al., 2003), and research along these lines remains very active (e.g. Grünewald et al., 2014; Bilish et al., 2019). Gradually, such studies have begun to be augmented by field campaigns and monitoring exercises which have taken a more holistic perspective of the functioning of alpine hydrological systems, especially as regards the role of groundwater. At the most local of scales, Bayard et al. (2005) measured the influence of frozen soils on snowmelt partitioning in 5 m^2 hillslope plots, finding a very high proportion of meltwater to infiltrate under frost-free conditions. Using a karstic cave as a

natural lysimeter, Meeks and Hunkeler (2015) observed that soils can impede deep snowmelt percolation.

It has also been identified that various unconsolidated sedimentary features often present in alpine terrain (primarily above the vegetation limit) have the potential to host aquifers. Several recent field investigations have therefore sought to elucidate the geometries (i.e. thicknesses) of such features, their subsurface storage capacities (i.e. porosities), the ease with which groundwater can flow within them (i.e. their saturated hydraulic conductivities), as well as the specific pathways and mechanisms by which it does so. Proglacial moraines (Langston et al., 2011; Lehmann-Horn et al., 2011; McClymont et al., 2012; Magnusson et al., 2014; Pourrier et al., 2014; Kobierska et al., 2015), talus slopes (Clow et al., 2003; Muir et al., 2011), and rock glaciers (Winkler et al., 2016; Harrington et al., 2018) have all been studied to these ends. Additionally, the hydrological behaviour of certain combinations of unconsolidated features, notably talus-moraine (Roy and Hayashi, 2009) and talus-meadow complexes (McClymont et al., 2010), has also recieved attention.

Environmental constraints generally preclude the invasive installation of subsurface monitoring equipment in alpine environments. As a result, most of the aforementioned studies relied on geophysical techniques, including seismic refraction, ground penetrating radar (GPR), and electrical resistivity tomography (ERT) surveys. Such approaches are non-invasive, and furthermore provide reasonably extensive spatially-distributed information (typically on the order of tens or hundreds of metres). Due to their complementarity, the deployment of different techniques in combination has proven particularly fruitful (e.g. McClymont et al., 2011). These studies have provided some of the first relatively large scale (or "field-effective") estimates of key hydraulic properties of unconsolidated aquifer features (Langston et al., 2013; Magnusson et al., 2014).

Other studies have relied on alternative methods to gain an appreciation of spatio-temporal hydrological dynamics in a broader sense, including at catchment scale. Although the fundamentals of such methods are more established (even bordering on the traditional/classical), for the reasons discussed above their their effective application requires additional thought in alpine terrain and conditions; a certain creativity and flexibility to make the appropriate modifications is has therefore often been called for. Investigations with the intention to measure or estimate the various components of catchment water balances fall squarely within this category, with the study of Hood et al. (2006) representing an early influential example. Two more recent studies – one focussing upon the Lake O'Hara catchment in the Canadian Rockies, and the other the Vallon de Réchy in the Swiss Alps – have applied such an approach at catchment scale (Hood and Hayashi, 2015; Cochand, Christe, et al., 2019). Both began with detailed snow survey to

quantify distributed snow water storage (or Snow Water Equivalent; SWE) at approximately the peak accumulation of the winters in question. In the case of Cochand, Christe, et al. (2019), this was achieved using an airbourne LiDAR survey). The researchers then proceeded to attempt to quantify the extent to which the subsequent melt water is temporarily stored as groundwater, and ultimately contributes to streamflow later in the year. The results of Cochand, Christe, et al. (ibid.), for instance, suggested that 45% of snow storage was temporarily stored as groundwater.

Taking a comparatively broad "systems view", but this time with the intention of determining the influence of subsurface structure on groundwater flow pathways in a karstic environment beneath and adjacent to a retreating glacier (the Glacier de Tsanfleuron, Switzerland), Gremaud et al. (2009) employed artificial tracers extensively. Amongst other outcomes, their results indicated that variability in glacial meltwater production discernibly influences subsurface flow. Natural tracers (e.g. hydrochemistry, stable water isotopes) have also been widely used; the primary objective here usually being to separate alpine streamflow hydrographs into their various constituent "source" components (Collins and Young, 1981; Liu et al., 2004; Cowie et al., 2017; Zhang et al., 2018). The contributions of Lauber et al. (2014), Floriancic et al. (2018), and Bonat et al. (2020) represent additional examples of fieldwork-oriented studies which have put fairly classical hydrogeological techniques to use in order to characterise the internal dynamics of Alpine catchments in a fairly comprehensive or holistic fashion. Floriancic et al. (2018), for instance, utilised numerous different methods, including hydrograph recession analyses, to explore the spatial variability in groundwater storage depletion during dry period in a headwater in southeastern Switzerland.

In certain locations, the installation of groundwater monitoring networks was evidently feasible. Based on noble gas concentrations and multiple isotopic signatures measured in waters sampled from a series of observation wells drilled in unconsolidated sediments (as well as surface water bodies) in the Olympic Valley catchment, Sierra Nevada (California, United States), Singleton and Moran (2010) were able to infer that seasonal recharge from the lower slopes dominates the replenishment of the alluvial aquifer. Analyses of pure hydrometric measurements from monitoring networks in more pre-Alpine regions, meanwhile, have elucidated the complex relationships between components such as snowmelt, topography, soil moisture, subsurface stormflow, and surface water-groundwater interactions (Smith et al., 2014; Penna et al., 2015; Rinderer et al., 2016; Zuecco et al., 2019). More exceptionally, boreholes have even been drilled in mountainous bedrock, with the resultant data yielding further insights. For example, based on noble gas data from numerous bedrock wells in Handcart Gulch – an alpine watershed in Colorado, United States – Manning and Caine (2007) posited that seasonal water table

fluctuations exceeding 50 m occur in the upper reaches.

The substantial knowledge advancements arising from such studies are frequently encapsulated and communicated in the form of conceptual diagrams, or conceptual models – an example of which is presented in Figure 1.6 (see the other studies cited for further examples). As a point of clarification, such conceptual models should perhaps rather be referred to "perceptual" models, so as to avoid confusion with numerical models with a "conceptual" flavour (Beven, 2011).

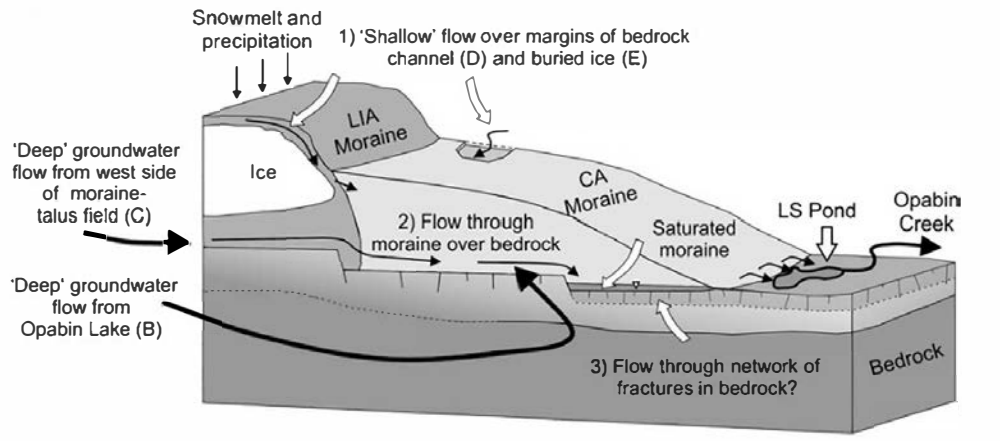

Figure 1.6: Schematic diagram of inferred subsurface structures and hydrological processes occurring within and beneath an unconsolidated moraine in the Lake O'Hara catchment, Canadian Rockies. Thin black arrows show hypothesised groundwater flow paths, whilst white arrows point to different components of the groundwater flow system. Here, the bedrock is conceptualised as being essentially impermeable, with the interface between unconsolidated sediments and bedrock therefore becoming a key determinant of system behaviour. Such an assumption is less applicable in karstified and heavily weathered or fractured crystalline settings, however. Source: McClymont et al. (2011).

More generally speaking, these dedicated field studies unequivocally demonstrated that, despite their characteristically steep slopes and limited soil and vegetation cover, high-elevation catchments categorically do not act as impermeable "Teflon" basins, as had been supposed by some (Williams et al., 2015).

Rather, the strong interactions between surface and groundwaters that many studies evidence underlines the difficulty (and perhaps even futility) of seeking to label or track water according to its sources, or alternatively distinguish distinct "event" and "pre-event" components; snow and ice melt often feeds torrents that flow over steep bedrock outcrops as surface water, subsequently infiltrate into and recharge talus slopes, alluvial fan, or other unconsolidated aquifers

thereby "becoming" groundwater, before eventually re-emerging into the stream network as surface water, whereupon further surface-surface exchanges might occur. Tracer-based hydrograph separation approaches often require that rather strong assumptions be made (e.g. that a small number of distinct end-member sources such as rain, snowmelt, and/or groundwater exist, and mix conservatively; Cowie et al., 2017 and references therein), and should therefore be interpreted very cautiously.

Spatio-temporal variability in the isotopic composition of snowmelt (Schmieder et al., 2016) and rainfall (Fischer et al., 2017) represent additional confounding factors in isotope hydrograph separation studies. For instance, according to which of several distributed rain collectors was taken to represent catchment average conditions (traditionally only one site is used)The former, for instance, Fischer et al. (ibid.) reported differences in estimated "pre-event" streamflow contributions of up to 60% in a small pre-Alpine Swiss catchment. Alternatively, various purely data (and more specifically filter)-based hydrogrpah deconvolution approaches may be applied to measured streamflow time-series, although the sensitivity of the results to the choice of method can be high (Partington et al., 2012). Incidentally, hydrograph separation is not straightforward using model-based approaches either (Weiler et al., 2018).

For further discussion of the topics mentioned above, several recent review articles including those of Klaus and McDonnell (2013), Frenierre and Mark (2014), Vincent et al. (2019), Jones et al. (2019), and Markovich et al. (2019) may be consulted.

1.2.1.2 Limitations

In addition to the challenges posed to hydrograph separation methods summarised above, one major drawback of many previous field-based alpine hydrology studies is the rather limited spatial scales that have been considered. The applies especially to those geophysics-based studies which, due to practical constraints, generally only considered individual landscape features on a fairly individualistic or "stand-alone" basis. Consequently, the combined hydrological behaviour of all such landscape elements within a headwater catchment, including the extent to which they ultimately contribute to stream discharge, remains substantially less well known. This scale issue is admittedly less relevant to some of the other approaches mentioned, although the data provided in those cases tends to be more of a more general nature, and hence perhaps open to alternative interpretations.

Field-based investigations have also overwhelmingly been concerned with better understanding the systems under present-day conditions. The perceptual models developed are seldom

extended to any sort of numerical simulations, and hardly ever to those which, in seeking to robustly reproduce internal dynamics, are comparably detailed, spatially distributed, and comprehensive (e.g. include both surface water and groundwater). Numerical simulations are necessary to make inferences away from measurements locations under present-day conditions, and even more importantly are recognised – being the only real alternative to simple extrapolation – as crucial to the generation of predictions under modified climate or land cover condition. As such, previous field studies have generally been greatly lacking in these respects. Comprehensive numerical modelling would additionally represents a means by which the hydrological behaviour of alpine catchment systems – including how their multitudinous components like streams, aquifers, lakes, and suchlike, behave in combination to influence streamflow regimes at the catchment outlet under both present and possible future conditions – might be more confidently established. The very few instances in which such numerical modelling has been undertaken with a view to augmenting insights derived from field measurements alone, in terms of either testing competing hypotheses (Kurylyk and Hayashi, 2017; Pauritsch et al., 2017) or exploring future scenarios (Rogger et al., 2017), allude to the considerable benefits that following such an approach more routinely might bring.

Overall, applications of numerical models in mountainous terrain – the vast majority of which are concerned with predicting climate change impacts upon streamflows (see the next section) – have arguably become detached from the latest process insights gleaned through dedicated, often multi-method field campaigns like those discussed in this section. Whilst the spatial and temporal scales on which future predictions are required are important considerations, certain limitations associated with the most commonly used types of models also contribute to this divergence.

1.2.2 Hydrological climate change impact assessments

In contrast to most studies discussed hitherto, the very intention of HCCIAs is to generate quantitative predictions of the future evolution of water resources. Given the importance of alpine hydrology (Section 1.1.1) and the rapidity with which key components of alpine hydrological systems are changing (Section 1.1.2.1), it is unsurprisingly that the number of HCCIAs in alpine settings has grown to become extremely substantial, the studies of Horton et al. (2006), Schaefli et al. (2007), Laghari et al. (2012), Rahman et al. (2013), Wagner et al. (2017), and Jenicek et al. (2018) representing just a few examples. A fairly standard experimental structure is generally followed, as illustrated in Figure 1.7, which was taken from Addor et al. (2014) – a particularly comprehensive example.

To summarise, downscaled GCM-RCM outputs corresponding to a number of alternative emissions (or greenhouse gas concentration) scenarios usually form the starting point. Before proceeding further, any biases in these climate model outputs must be identified (by making the appropriate comparisons with *in situ* observations over a common historical period) and corrected. Precipitation outputs tend to be particularly afflicted by biases. Statistical techniques such as quantile mapping are often applied to make the necessary rectifications. Then, under the established "delta change" approach, change factors, which may be both spatially and seasonally variable, must be identified by comparing model outputs over a historical baseline period with those corresponding to one or more future periods of equal duration. Hydrological model input data corresponding to the future may then be generated by applying the derived change factors (additively in the case of temperature, or multiplicatively in the case of precipitation) to historical meteorological observations. Alternatively, if fully transient scenarios are available and their use is desired, the necessary future "weather" time-series, defined either directly at existing station locations or on a relatively fine resolution grid, would essentially already exist.

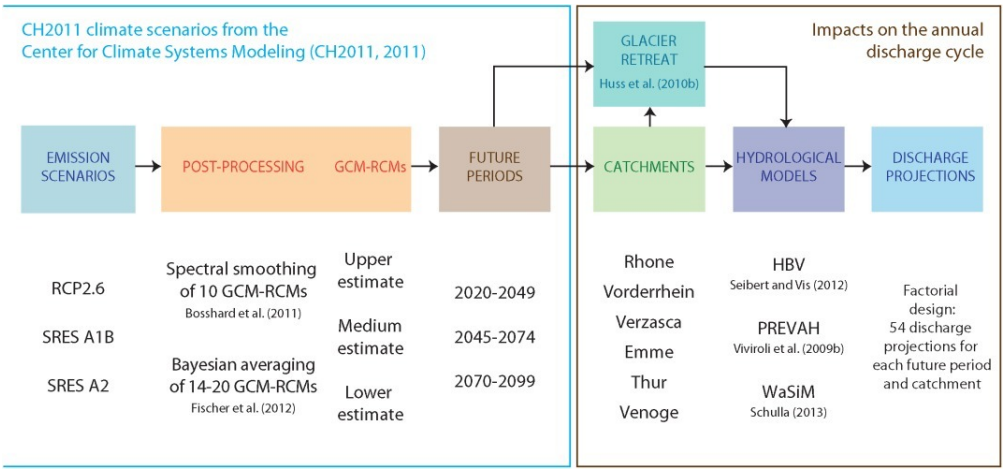

Figure 1.7: Flowchart illustrating the typical experimental design for assessments of climate change impacts upon alpine stream discharge and their associated uncertainties. Source: Addor et al. (2014).

In either case, the next phase involves developing and calibrating one or more hydrological models using historical historical observations. Thereafter, the calibrated hydrological model(s) can be forced with the time-series pertaining to the emissions scenario/GCM-RCM/future time period combinations of interest, and finally the resultant future streamflow simulations compared with their historical baselines. It is thus apparent that alongside the climate models, hydrological models represent key components of the simulation chain.

1.2.2.1 Conceptual hydrological models

Simple conceptual or "box-type" hydrological models, in which presupposed storage and flow components are represented via a series of reservoirs and fluxes, continue to dominate such assessments, especially in the European Alps (e.g. Andrianaki et al., 2019). HBV (Lindström et al., 1997), PREVAH (Viviroli et al., 2009), SWAT (Arnold et al., 2012) are perhaps the most frequently employed codes, although similar ones such as SEHR-ECO (Schaefli et al., 2014) are also available. Figure 1.8 shows the general structure of such models. Depending on the particular code selected, configurations may be spatially lumped (as shown), partially distributed (which is often achieved using elevation bands in mountainous terrain), or fully distributed. In the latter two instances, the various compartments are essentially replicated for each spatial aggregation unit.

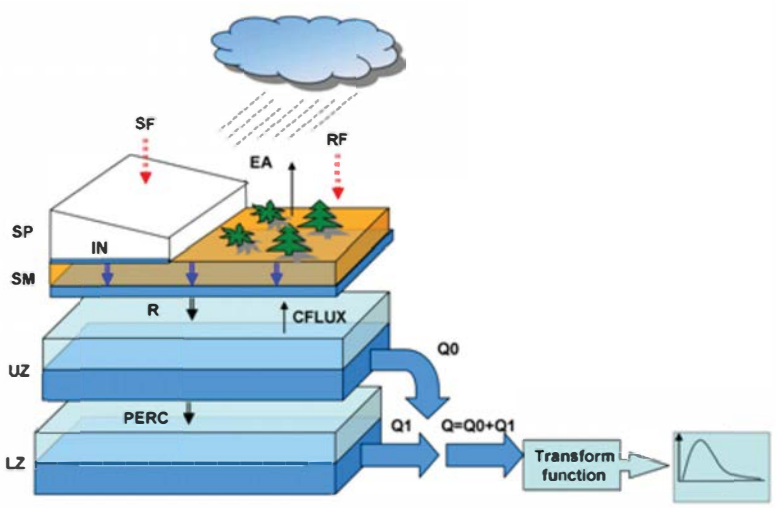

Figure 1.8: Illustration of the simplified structure of conceptual "box-type" hydrological models, in this case a spatially lumped application of HBV. The contrast with the complex conceptual diagram shown in Figure 1.6 is striking. Source: Shrestha et al. (2009).

Such models are associated with important benefits in the context of HCCIAs. Firstly, their data requirements are fairly modest, which is convenient given the generally limited availability of data in alpine areas; time-series of air temperature, precipitation, and potential evapotranspiration (ET_p) usually suffice in addition to those of measured streamflow (required for calibration). Another major attraction is their high computational efficiency, which facilitates the consistent simulation of long (i.e. climatically relevant) periods over large regions (even entire countries) (Kling, 2006; Brunner et al., 2019), frequently in conjunction with multiple RCP-GCM-RCM

combinations. This efficiency further enables Monte Carlo-based parameter sensitivity, estimation, and uncertainty quantification frameworks, which require a substantial number (typically thousands) of individual model executions, to be applied (Finger et al., 2011; Dobler and Pappenberger, 2013).

Consequently, using conceptual hydrological models, it is often possible to place any projected future hydrological changes simulated within their broader context – not only in terms of natural (or "internal") climate variability but also with respect to future emissions uncertainty, climate model spread, and hydrological model parameter uncertainty. For example, Addor et al. (2014) propagated the various uncertainties through the simulation chain, and could ultimately quantitatively attribute the contribution of each source to the overall uncertainty associated with future discharge predictions.

Furthermore, as befits their frequent use in Alpine HCCIAs, such codes generally offer representation of glacier and snow processes, mostly commonly via empirical melt formulations.

In indicating earlier and diminished future spring peak flows, elevated winter baseflows, reduced glacial melt contributions, and stronger rainfall signals, the results of such studies tend to be fairly consistent with logical expectations (and hence one another) in terms of future streamflow predictions. Of course, more extreme climate scenarios are associated with more pronounced projected changes, and local catchment characteristics such as elevation also exert a strong influence on simulated outcomes. As an example, Figure 1.9 shows projected future changes in the discharge of the River Rhône near its inflow to Lac Léman.

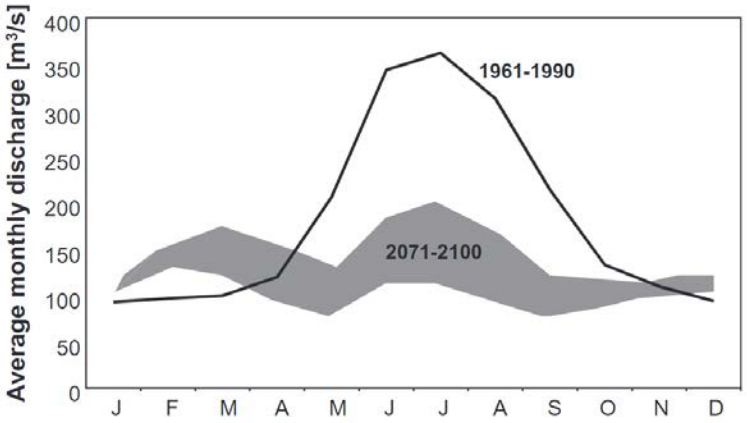

Figure 1.9: Historical (1961-1990) and predicted future (2071-2100) monthly discharge of the Rhône river close to its mouth in the Lac Léman near Montreux, Switzerland under the IPCC's A2 emissions scenario. Source: Beniston (2012).

Despite these benefits, conceptual models are also associated with a number of drawbacks which stem from the model parameters lacking physical meaning, the model structures often lacking spatial explicitness, and the persistent use of streamflow measurements alone as calibration targets.

More specifically, using such codes, it is not straightforward to constrain parameter values to plausible ranges (as is theoretically possible with more physically-based approaches; Loague and VanderKwaak, 2004). Meanwhile, streamflow measurements at catchment outlets are great integrators of variability, and so provides little insight into internal catchment processes. This situation places considerable emphasis on the calibration process to reproduce observations (Krause et al., 2005), but simultanously leaves much scope for overfitting (Avanzi et al., 2020) and/or equifinality – whereby many alternative parameter sets produce comparably good fits with limited observations (Beven, 2006; see also Ebel and Loague, 2006).

In other words, parameters may be free to assume values which serve to compensate for deficiencies elsewhere in the modelling process such that streamflow measurements are replicated well, but not necessarily via internally consistent and hydrologically plausible mechanisms. This essentially equates to getting the right answers, but for the wrong reasons (Kirchner, 2006). Should models indeed be little more than "mathematical marionettes, dancing to the tune of observed data" (ibid.), making physical inferences on the basis of the results could be fraught with danger.

Yet that is precisely what is done in HCCIAs; the empirical relationships arrived at through calibration over a historical period are assumed to hold into the future, despite future forcing conditions likely exceeding those contained in the calibration period. Ultimately, the reliability of future streamflow predictions made using conceptual hydrological models may be questionable (Duethmann et al., 2020). As something of an aside, it may conceptual model applications are also interpreted in physical terms in studies with other aims (e.g. Staudinger et al., 2017), the conclusions of which should likewise be considered with some caution.

Crucially, diagnosing such problematic situations can be extremely challenging. It is even arguable that the risk of inadvertently optimising to "wrong" or misinterpreted data is elevated when using conceptual models. For instance, measured streamflow is routinely assumed to correspond to the entire terrestrial outflow of a given catchment. However, under certain circumstances, a substantial proportion may flow beneath or otherwise somehow bypass the gauging station (Staudinger et al., 2019). Should this subsurface outflow component be ignored, the principle of mass conservation would require some compensatory effects be introduced, conceivably raising evapotranspiration rates to unduly high levels. Goswami and O'Connor (2010)

describe such a case. After initial calibration, a (mass-conservative) conceptual model was found to perform well on a distinctly non-conservative lowland karstic catchment in Ireland. It was eventually discovered that this situation arose through a certain parameter being unrealistically curtailed by the calibration process. This is also an all too rare example of model "failure" being openly discussed. Without independent data and more complex model structures able to utilise it, rigorous testing may be impossible and such issues can easily remain obscured.

Integrating observed spatial patters with spatially distributed conceptual models provides more opportunities for identifying possible overfitting and reducing equifinality (Grayson and Blöschl, 2001). For example, Parajka et al. (2007) considered two cases – only streamflow data, and streamflow plus snow pattern data – calibrating semi-distributed conceptual models of many Austrian catchments. It was generally not possible to maintain such good streamflow fits when the snow observations were also included in the objective function as those attained when fitting to only streamflow data, indicating that overfitting would have occurred without the introduction of the additional data.

However, despite the promise of such approaches and the vastly increased availability spatially distributed data, the use of fully distributed conceptual models in HCCIAs is still not routine. As such, the sharp terrain and geology-driven variability in catchment properties and physical processes that are characteristic of alpine terrain might be somewhat overlooked. Distributed models are also imperative when seeking to assess the indirect hydrological impacts of land cover change – an inherently spatial phenomenon – in addition to direct climatic impacts (see Section 1.2.3).

Attention has also been drawn to the the considerable emphasis placed on the Nash-Sutcliffe Efficiency criterion (NSE; Nash and Sutcliffe, 1970) when assessing the goodness-of-fit of simulated to observed hydrographs. This almost ubiquitous metric is in fact merely one of several possible alternatives. More specifically it has been argued that this measure, which places particular emphasis to higher flow quantiles, is not discriminatory enough given the strong seasonal flow regimes of alpine catchments (Schaefli and Gupta, 2007). Due to this characteristic and parameter equifinality, it is considered relatively straightforward to reproduce observed alpine streamflow series very well according to the NSE criterion using conceptual models, but – as already highlighted – doing so provides no guarantee of internal hydrological consistency or predictive robustness (Klemeš, 1990; Schaefli, 2016). The limited inter-comparability of NSE statistics between different applications in contrasting environments has also recently been re-emphasised (Seibert et al., 2018).

Furthermore, although geological influences are hardly ever discussed in the context of traditional HCCIAs – the bedrock type is usually only described cursorily along with other study area characteristics and then never mentioned again, it should be clearly stated that the representation groundwater processes in conceptual models is rather weak. As Staudinger et al. (2019) note, most bucket-type models conceptualise groundwater using one or more simple linear reservoirs. Even in spatially distributed configurations, information on the distribution of subsurface properties is at best captured only implicit, and lateral subsurface flows are rarely accounted for (Bierkens et al., 2015). Such models are thus evidently incapable of incorporating 3D geological information, should it exist.

In turn any geological influences on hydrological processes more broadly may be somewhat overlooked. This is important because as Section 1.1.3 has already alluded to, good reasons exist as to why which the subsurface environment should be paid particular attention when simulating Alpine hydrology (or in other words why groundwater processes are likely to be important). Most obviously, large hydraulic gradients exist. Also, as a result of the very tectonic processes that led to mountain formation, pronounced topography and geological complexity go hand-in-hand. It is known that this complexity in bedrock geology can strongly influence groundwater processes (and by extension overall catchment function) not only in calcareous Alpine environments like that considered in this thesis – where flow pathways may be somewhat independent of the surface topography – but in other mountainous geological settings too (Manning and Caine, 2007; Gleeson and Manning, 2008; Kosugi et al., 2011; Welch and Allen, 2014).

Some conceptual codes also suffer constraints of a more technical nature. For instance, HBV is limited to a daily time-step, which renders it incapable of reproducing any diurnal fluctuations (e.g. in snow melt or evapotranspiration), as well as accurately characterising the temporal distribution of sub-daily rainfall events (e.g. intense but short-lived convective storms). Moreover, and in contrast to PREVAH which can now be run on a gridded basis (Speich et al., 2015), HBV still cannot be applied in a fully distributed sense. In such regards, whilst it is true that all hydrological models have certain strengths and weaknesses (Hrachowitz and Clark, 2017), some are undoubtedly more capable than others.

Finally, most conceptual models employ empirical, index-based snow and ice melt modelling approaches whose capacity to satisfactorily reproduce complex alpine snow dynamics is questionable, above all in smaller and/or more rugged catchments. Again, these heavily empirical approaches may be less reliable than physically-based algorithms under strongly modified climatic conditions (Warscher et al., 2013). To conclude this section, it may be fairly contended that across the discipline of hydrological modelling in general, simple conceptual models continue

to benefit from a certain legacy attachment despite the subsequent emergence and continued development of alternative, perhaps better-suited tools (Addor and Melsen, 2019).

1.2.2.2 More physically-based models

Codes with a stronger physical basis can theoretically be parameterised more easily on the basis of field measurements, are explicitly spatial (thereby allowing land cover change to be considered), and are more likely to perform well under modified climatic condition. Indeed, they are often found to outperform simpler models in comparison exercises. As an initial example, Moeck et al. (2018) investigated the capabilities of several classes of model to estimate groundwater recharge in a Swiss pre-Alpine headwater in simple 1D configurations. Whilst all models performed similarly over the calibration period, predictions made using the more complex physically-based models were associated with with lower predictive uncertainty limits those made using a lumped parameter "bucket" model over a contrasting independent validation period. However, more physically-based models have been applied much less extensively in HCCIAs than their conceptual counterparts.

Traditional 3D groundwater codes like FEFLOW (Diersch, 2013) and MODFLOW (Harbaugh, 2005) are one class of established physically-based tool. A few early 3D groundwater modelling studies were conducted in mountainous terrain (Forster and Smith, 1988; Flerchinger et al., 1996), and their successors still occasionally emerge (e.g. Doyle et al., 2015). However, because climate impact assessments are primarily concerned with the extent to which subsurface geology and flows influence the broader hydrological system, that such models simulate only groundwater flow is an obvious detraction; surface water flows are important in steep mountainous terrain from ecological, flood risk, and sediment transport perspectives (Turowski et al., 2009; Datry et al., 2014; Micheletti and Lane, 2016; Leigh et al., 2016). Moreover, separate models are usually required to the generate recharge estimates which form groundwater model inputs. It is nevertheless slightly surprising that few (if any) studies in which purely groundwater models have been applied to assess climate change impacts on subsurface flows in alpine catchments seem to have been undertaken.

Predominantly physically-based gridded hydrological models have proven more popular. Indeed, WaSiM (Schulla, 2017), TOPKAPI-ETH (Ragettli et al., 2014), and WEB-DHM-S (Shrestha et al., 2015) were all developed for mountainous applications and accordingly offer far more comprehensive and reliable treatments of the salient processes than conceptual models – although their data requirements are elevated and set-up more involved. WaSiM is fairly typical of such codes. It first solves the water balance on a cell-by-cell basis – via either a vertical (1D)

TOPMODEL-like or Richards' equation treatment of the unsaturated zone – before applying terrain-derived routing functions to generate streamflow hydrographs at specified points along the predefined stream network. Computational requirements are more substantial than those of conceptual models, but generally remain manageable. A good example of an application of such a model for Alpine HCCIA is provided by Fatichi et al. (2015).

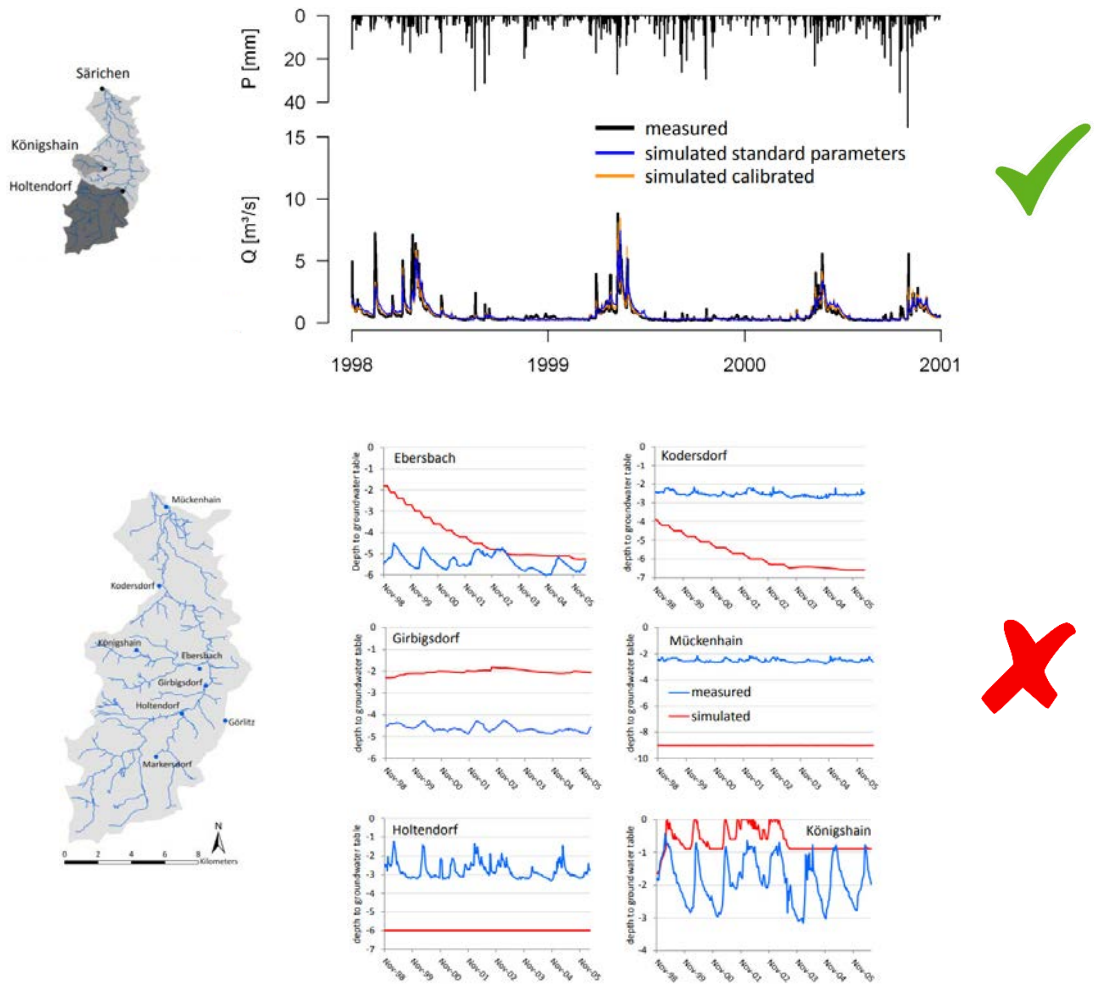

Figure 1.10: Example of a comparison between observed streamflows and groundwater levels and their counterparts simulated using WaSiM. This figure illustrates that even using sophisticated, physically-based, and spatially distributed hydrological models, it can still be possible to satisfactorily reproduce streamflow observations at the catchment outlet (in this case at Särichen; NSE = 0.74) whilst simultaneously failing to reproduce internal dynamics; in this case groundwater levels. Source: Gädeke et al. (2014).

Such codes are affected by some of the same limitations as their simpler counterparts, however, especially with regards to the subsurface. In WaSiM, for instance, although a 2D lateral groundwater module is available, a simple conceptual bucket representation of groundwater is most commonly applied (but see Kraller et al. (2012) who extended the more sophisticated option using a neural network to better account for a karstic network). WaSiM's user manual consequently recommends that coupling with an external groundwater model be undertaken wherever groundwater is expected to play an important role (Schulla, 2017). As previously discussed, this can this can generally be expected to be the case in Alpine catchments. TOPKAPI-ETH similarly employs a grid-based topographic representation before the subsurface is discretised into (only) three layers. The uppermost two represent the "shallow and deep soil horizons", and are treated as non-linear reservoirs. The bottom layer, meanwhile, is present to account for "slow flow components" (through fractured bedrock, for example), and is treated as a linear reservoir (Fatichi et al., 2015). Because the corresponding subsurface parameters are generally not varied spatially, applications of these models also risk overlooking local geological influences.

In essence, such models do not necessarily represent all components of the hydrological system with a comparable degree of sophistication. In turn, it may remain possible to reproduce streamflow observations whilst simultaneously failing to capture observations related to other aspects. Figure 1.10, for instance, illustrates that Gädeke et al. (2014) were able to obtain satisfactory streamflow fits even using "standard" parameters, but were unable to reproduce observed groundwater levels at internally distributed locations very satisfactorily. Once again, this case emphasises that confronting models with different types of and/or spatially-distributed observations is crucial to the identification of such situations.

In addition, at least until fairly recently, even these codes – which have a strong mountain focus – continued to employ simple empirical snow and ice melt modelling approaches. To improve WaSiM in this respect, Warscher et al. (2013) implemented an energy balance scheme. Extremely complex physically-based, multi-layer snowpack models are also beginning to be applied more frequently in broader hydrological contexts. The Cold Regions Hydrology Model (CRHM), which is partially distributed (employing the concept of Hydrological Response Units; HRUs), is a prominent example of such a model; DeBeer and Pomeroy (2017) present an example application of this code to a small instrumented research catchment in Canada. A fully distributed alternative, Alpine3D (Lehning et al., 2006), has now been coupled with the conceptual, semi-distributed, travel time-based hydrological response model StreamFlow to likewise extend a sophisticated representation of snow processes through to the estimation of stream discharge (Gallice et al., 2016; Brauchli et al., 2017). Wever et al. (2017) made further progress

by "inserting" a 1D Richards' equation scheme between Alpine3D and StreamFlow in order to better represent soil moisture dynamics. That said, possibly on account of their higher computational demands, these approaches have been used only infrequently in HCCIAs to date (but see e.g. Bavay et al., 2013). It is also worth mentioning at this juncture that even the most advanced snow models, like Alpine3D, firstly do not yet account for all potentially important processes, such as the gravitational redistribution from extremely steep slopes, and secondly can only ever be expected to perform as well as the meteorological data with which they are forced permits (Förster et al., 2014).

Overall, whilst more physically-based models incorporate much more advanced snow and surface hydrology schemes that conceptual models, their streamflow simulation capacities generally remain underpinned by simplified subsurface representations of only shallow soil water dynamics, made via basic buckets and routing schemes. This level of complexity may suffice in certain settings, such as where soils mantle relatively impermeable bedrock, and few substantial permeable unconsolidated deposits are present. Elsewhere, including in the terrain under consideration in the present thesis, this is less likely to be the case.

1.2.2.3 Summary

The review presented thus far had demonstrated that, in the context of extremely steep, topographically complex, snow dominated, and geologically complex Alpine systems (i.e. precisely where reliable CCHIAs are most urgently needed), all well established modelling approaches are associated with important limitations or omissions. In the worst cases, these limitations may undermine the reliability of the predictions made using them. After describing one further specific drawback associated with the "status quo", an emerging class of hydrological model that could potentially ameliorate this situation is introduced.

1.2.3 Indirect climate change effects

In addition to the cryospheric changes discussed extensively in Section 1.1.2, ongoing climatic change is expected to induce responses in other components too; indeed, some such changes are already underway. For instance, permafrost will inevitably (continue to) degrade (Evans et al., 2018; Walvoord and Kurylyk, 2016), while it is anticipated that forests will increasingly colonise higher slopes (Goulden and Bales, 2014). Thanks in no small part to dedicated field efforts, and as Figure 1.11 illustrates, various links between such components have been established, and it is increasingly clear that alpine environmental systems are comprised of a complex web of

(often non-linear) process interactions and feedback mechanisms (Henne et al., 2018). Because many of these individual components are somehow involved in the hydrological cycle, any fairly "direct" hydrological changes due to climate change (e.g. through rapid cryospheric changes) have the potential to be modulated – either enhanced or diminished – by the broader response of of the integrated system as a whole (Wang et al., 2018). However, HCCIAs have largely ignored this possibility to date.

More specifically, the various processes and interactions involved act on highly contrasting spatio-temporal scales, and many are furthermore likely to be rather subtle, non-intuitive, and/or induce opposing effects. For example, the global synthesis presented by Fan et al. (2017) revealed the co-dependency of soil moisture patterns and vegetation characteristics (i.e. both aspects influence each other) across a range of biotic and abiotic conditions. Similarly, forest development depends not only on climatic conditions but also on future soil development, avalanche activity (Zurbriggen et al., 2014), and land use decisions (the latter of which is of course external to the natural environmental system).

Introducing climate change further compounds the complexity. For example, predicting future evapotranspiration rates is complicated by their joint dependency on vegetation characteristics, climatic conditions (i.e. the atmospheric demand for moisture), and near-surface moisture availability. Although it is generally assumed that actual evapotranspiration (ET_a) from mountainous areas will increase under a warmer climate owing to elevated atmospheric demand (Huntington and Niswonger, 2012), possible decreases associated with soil moisture deficits – whereby atmospheric demand cannot be met – cannot be ruled out, especially at lower elevations during summer (Calanca et al., 2006).

Not altogether dissimilarly, as permafrost degrades, rates of infiltration/groundwater recharge in high-elevation areas could be expected to increase, leading to more groundwater storage and higher groundwater tables. However, should forests concomitantly colonise the higher slopes, provided the system is not moisture limited, rates of ET_a could also be augmented which, in isolation, would lower water tables. Questions related to Which of these competing effects will outweigh the other and under what circumstances (i.e. the influence of catchment properties) remain very much open.

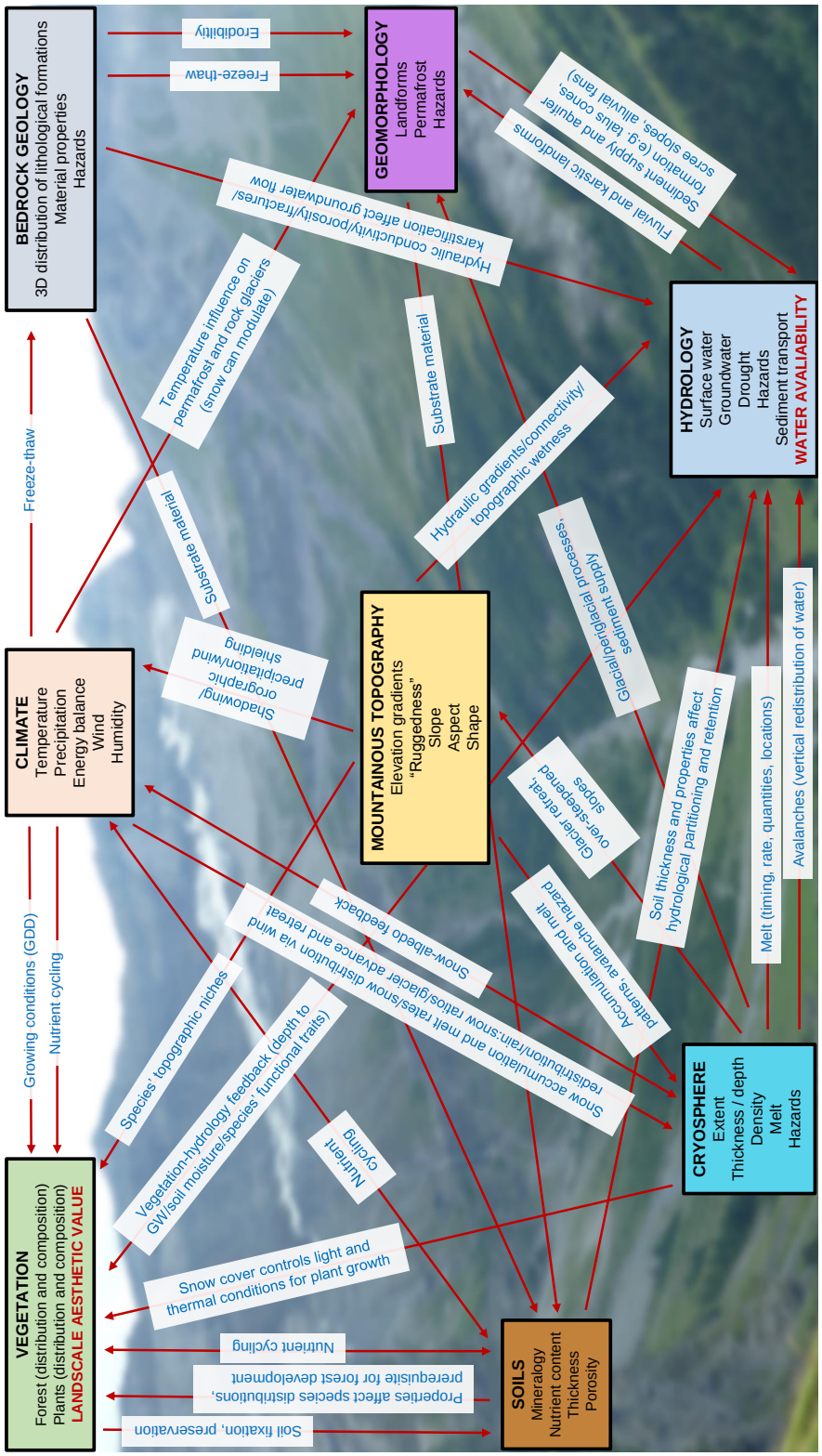

Figure 1.11: Schematic diagram showing some of the interactions and feedback mechanisms that are known to operate between different components of alpine environmental systems (original figure).

The partitioning of meltwater at the land surface could likewise be affected by subtle changes. Barnett et al. (2008), for instance, envisage a negative (i.e. self-regulatory) feedback mechanism whereby earlier snowmelt could lead liquid water being generated preponderantly during a period of the year when evaporative demand remains fairly low. As such, despite diminished future snowpack volumes, snowmelt infiltration and recharge could, counterintuitively, increase. Should snow (rather paradoxically at first glance, but for similar reasons) also more slowly under future warmer conditions (Musselman et al., 2017), this effect could be further reinforced. Faced with such complexity, more detailed local studies, as well as investigations which transcend traditional disciplinary boundaries, have been called for (Viviroli et al., 2011). The potential value of "hyphenated hydrology" has similarly been espoused (McCurley and Jawitz, 2017).

Unfortunately, as already stated, indirect changes are rarely considered in HCCIAs, leaving the hydrological impacts of vegetation and permafrost highly uncertain (Rogger et al., 2017; Maxwell, 2020). Many of the limitations associated with traditional conceptual models especially (e.g. their lack of physical basis and the fact that they are not always spatially distributed) have severely impeded their capability to respond to such questions. Put simply, they hardly begin to address the complex interactions and feedback mechanism that could be implicated in overall hydrological system change. Ultimately, some systems are just too complex to be described in a highly parsimonious way (Ebel and Loague, 2006), and so more sophisticated models are now required (Fatichi et al., 2016).

Some progress towards a more comprehensive representation is being made. For example, Speich et al. (2020) coupled a spatially-distributed conceptual hydrological model with a dynamic vegetation models, thereby offering some prospect of representing the important bi-directional feedbacks involved, albeit within the constraints of conceptual hydrological framework for the time being. Tague and Grant (2009) and Godsey et al. (2014), meanwhile, applied the distributed process-based model RHESSys to several different catchments in the western United States in an attempt to diagnose interactions between snowmelt, subsurface drainage characteristics, and streamflow under warming conditions, whilst Rasouli et al. (2019), applied the CRHM to investigate the relative importance of concomitant climate, vegetation, and soil changes in three further watersheds in the North American Cordillera. Finally, Mastrotheodoros et al. (2020) recently simulated the entire Alps using an ecohydrological model in order to study the "drought paradox" hypothesis – the concept that at higher elevations at least, evapotranspiration rates might actually increase during hot and dry conditions. This model did not include groundwater, however.

To more fully realise the goal generating reliable predictions of the overall fate of alpine hydrological systems to ongoing climate change, such approaches must arguably be extended even further to – as far as is practicable – incorporate the representation of snow, surface water, groundwater, and vegetation/*ET* dynamics in a more explicit and integrated fashion.

1.3 What additional insights could fully-integrated models provide?

An important initial step towards accounting for both surface and groundwater within a single framework was made by Arnold et al. (1993), who added a groundwater component to an existing catchment-scale surface water model. However, only with the subsequent advent of models like ParFlow-CLM (Maxwell and Miller, 2005), HydroGeoSphere (HGS; Aquanty Inc., 2016), MIKE SHE (Graham and Butts, 2005), CATHY (Camporese et al., 2010), and GEOtop (Endrizzi et al., 2014), which more tightly integrate the representation of surface and variably-saturated subsurface flow, can the "blueprint" for a comprehensive and internally coherent physically-based description of the catchment hydrology envisioned by Freeze and Harlan (1969) truly said to have been realised (Simmons et al., 2020). Ever growing computational efficiency and the careful engineering of codes able to take advantage of it (e.g. through parallelisation) have driven recent advancements.

Such "continuum" models are based on non-linear partial differential equations (PDEs). As Figure 1.12 illustrates, they simulate most potentially important processes, and do so according to established physical principles in a spatio-temporally explicit (i.e. 3D, transient) manner. Fully-integrated codes typically solve some formulation of the shallow water equations for 2D surface flow and Richards' equation for 3D variably-saturated subsurface flow simultaneously in a globally implicit fashion (Maxwell et al., 2014; Kollet et al., 2017). Coupling between these domains is achieved using either the Continuity of Pressure (COP) or the first-order exchange coefficient (FOEC) approach (Liggett et al., 2012). Either way, the dynamic bi-directional exchange between the surface and subsurface domains (including groundwater emergence) can occur freely, and all simulated fluxes (including surface water-groundwater exchanges) can generally be extracted arbitrarily at points in time and space within the simulation domain. The approach taken by integrated models therefore contrasts markedly with even that of comparatively sophisticated physically-based distributed hydrological models like WaSiM.

More significant differences between integrated codes emerge with respect to the discretisation approaches and numerical techniques they employ. Perhaps the most important distinction is whether they require a structured (i.e. rectangular) grid (and thereby employ finite-difference schemes), or rather whether they support unstructured meshes (which facilitate finite-element or finite-volume methods). Indeed, in Chapter 5, HGS was elected for use primarily because it supports unstructured grids (partially unstructured in this case); complex natural geometries to be described more accurately and efficiently in this way than is possible with structured meshing approaches, although it may be noted that "terrain following" transformations have been developed to improve the topographic representation in ParFlow, which uses a structured mesh (Maxwell, 2013). HGS also offers several potential options with respect to karstified formations; the subsurface can either be treated as an equivalent porous media at the elemental scale, as having dual permeability or porosity, and/or as being discretely fractured (see also Hartmann et al., 2014).

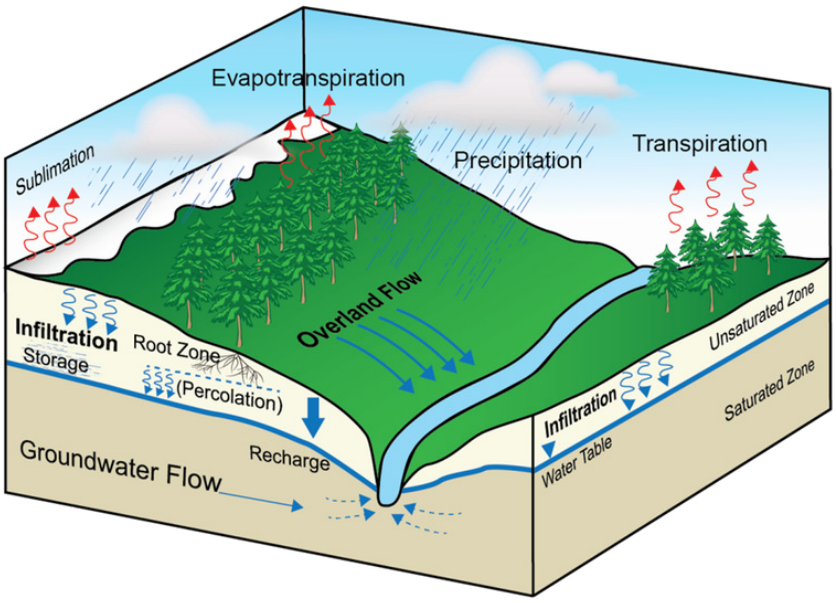

Figure 1.12: Illustration of the broad range of hydrological processes fully-integrated surface-subsurface flow models such as HydroGeoSphere simulate in a physically-based and spatio-temporally explicit fashion. Despite the somewhat simplified representation shown here, spatial variability in (2D) surface and (3D) subsurface properties can be fully represented. Source: IIHR-Hydroscience & Engineering, University of Iowa.

As with other types of physically-based models, any predictions made under changed climate conditions are likely to be more reliable than those made using more empirical approaches

(Fatichi et al., 2016; Paniconi and Putti, 2015). Another generic but important benefit of integrated models is that in simulating so many hydrological variables explicitly in space and time, and provided any potential incommensurability or other technical challenges can be overcome, they offer enormous potential to be integrated with (or to "synthesise") a wide variety both traditional and more novel types of observational data, including spatial pattern data (Grayson and Blöschl, 2001; Mendiguren et al., 2017; Schilling, Cook, et al., 2019). As such, multi-objective calibration and evaluation frameworks can, in principle, be easily devised and implemented, which in turn has the potential to reduce equifinality and improve system understanding.

Degrading integrated models to facilitate comparisons between full complexity and simplified versions, meanwhile, can reveal what an appropriate level of abstraction might for a given system, problem, or set of predictions required; this task, of determining optimal model complexity for a given application, is currently a major objective across many branches of the earth and environmental sciences. Furthermore, even if not all conceivable feedback are yet included in integrated models – representation of the fully coupled co-evolution of vegetation or geomorphological dynamics (Partington et al., 2017) with hydrology, for instance, still remain in prospect – in at least fully representing the feedbacks between groundwater and surface water (besides other aspects), they can be considered perhaps the most promising tools with which the hydrological impacts of indirect climate change effects discussed in Section 1.1.3 can start to be explored.

Many early integrated modelling studies simulated highly simplified and spatially-limited synthetic domains with a view to better understanding the fundamental physics, i.e. removing the potential for the causal mechanism(s) of interest to be obscured by real-word complexity (Atchley and Maxwell, 2011; Brunner et al., 2012; Irvine et al., 2012). Such work remains ongoing (e.g. Carlier et al., 2019). However, shorn of the real-word complexity or "uniqueness of place" (Beven, 2000), it is far from guaranteed that the combinations of model structures and effective parameters employed in such numerical experiments, and hence the insights gleaned, are transferable to the "messy" hydrological realities of actual catchments where management decisions are required.

Gradually, a shift towards more realistic and larger scale applications has occurred. Simulations of real-world 2D cross sections (Schilling et al., 2014) and individual aquifers can be considered intermediate "staging posts" along this path. The contributions of Jones et al. (2008) and Kollet and Maxwell (2008) can lay claim to being amongst the first to apply fully-integrated surface-subsurface models at catchment scale to real systems. Since then, many applications in contrasting environmental settings and at more extensive spatial scales have been presented

Sulis et al. (2011), Hwang et al. (2018), Jaros et al. (2019), and Condon et al. (2020). Such models can potentially help to unravel the types of complex responses arising from non-linear feedbacks and interactions under change that were discussed in Section 1.2.3. As Section 5.1 explains more fully, integrated models hold particular potential in mountainous terrain.

However, integrated models are not without their own limitations. Their data requirements are extremely high, and new users must embark upon a steep learning curve (Brunner and Simmons, 2012). Computational expense is likewise considerable, with model execution times of days to weeks being far from uncommon (Miller et al., 2018). In addition, despite their physical basis, many parameters cannot practically be measured, or alternatively cannot be measured at model commensurate scales; the upshot of which is that they also usually require calibration. (James et al., 2010). Extending this reasoning further, it has even been contended that such models are, in fact, nothing more than complex conceptual models, lumped at the elemental scale (Beven, 1989).

Other have retorted by advocating that the paradigm of calibration should be embraced more fully even with process-based models (Mendoza et al., 2015). Nevertheless, in practical terms, long execution times at present impinge significantly upon the applicability of automated parameter estimation and uncertainty analysis tools, which require many model runs (von Gunten et al., 2014; Foster and Maxwell, 2019). Ala-aho et al. (2017) highlighted that whilst integrated models have helped improve understanding of runoff generation processes, their "high data requirements and difficulties in model calibration are typically assumed to preclude their use in catchment-scale studies".

Highly simplified configurations excepted, execution times could likewise limit the extent to which any projected future changes might be contextualised with regards to natural variability. Finally, possibly due to many integrated codes having their origins in the groundwater modelling community, relatively simplistic temperature-index snow modelling approaches are taken (e.g. Cochand, Therrien, et al., 2019). In its incarnation as ParFlow.CLM (i.e. having been coupled to the Common Land Model (CLM), which does employ an energy balance snowmelt scheme), ParFlow is exempt from this criticism.

Such factors have undoubtedly held back applications of integrated models at catchment scale in complex mountainous terrain to date. As Section 5.1 reveals, most have been confined to crystalline and other relatively low permeability catchments located in the west of the North American continent, which are highly contrasting in character to the geologically younger, more rugged, and more calcareous terrain under consideration here. In addition, previous studies made

many expedient assumptions. Assumptions of this nature are completely understandable in synthetic studies. Gleeson and Manning (2008), for example, deliberately neglected numerous features of real mountains systems in their HGS models, including transience and spatial variability in meteorological forcing, the accumulation and ablation of the seasonal snowpack, glacier dynamics, the presence of permeable surficial geology and soils, heterogeneity in bedrock, and evapotranspiration processes precisely to avoid obscuring the very relationships that they wished to scrutinise. On the other hand, when such assumptions (even if somewhat less severe) are made in studies that seek to be more realistic and representative of real environments, they may be less defensible; again, see Section 5.1 for further details. Incidentally, apart from the study of Gleeson and Manning (ibid.), HGS does not yet appear to have been applied in mountainous terrain of any sort.

In fact, there have been no known applications of any fully-integrated hydrological models in steep, rugged, and extremely geological complex Alpine headwaters. The present thesis therefore attempts to take an initial step in this direction. Despite their real or perceived limitations, the various potential benefits of integrated models (both in general and more specifically in complex mountainous terrain, and all the more so with respect to their more simplistic, commonly used counterparts) justify considering their utility in such settings. With that in mind, and considering the themes that have emerged in this critical review of the current state of research on alpine hydrology, the aims and objectives of the thesis were established.

1.4 The present thesis

1.4.1 Aims and objectives

This thesis aims **to reproduce the entire hydrological cycle of an Alpine headwater, from the snowpack to deep groundwater circulation, in a physically-based, integrated, spatially explicit, and transient fashion over a recent historical period**, and **to make hydrological impact predictions under plausible future climate, vegetation, and permafrost conditions**. The research undertaken to address these aims revolves around five important and open research questions, which are as follows:

1. Is it possible to develop three-dimensional (3D) models of bedrock geology that are appropriate for subsequent numerical groundwater and/or integrated surface-subsurface flow modelling in even the most complex sedimentary Alpine settings?

2. How might different types of complementary snow observations be incorporated with physically-based, spatially distributed snow models in order to improve and quantify the uncertainty associated with simulations of snow dynamics in rugged and comparatively data-sparse Alpine terrain?

3. To what extent can the geometries of potential unconsolidated Quaternary aquifers be estimated in a non-invasive and cost-effective fashion across entire moderately-sized, inaccessible Alpine headwater catchments?

4. Can fully-integrated surface-subsurface hydrological models that include (even) more of the known complexity than previous efforts (e.g. with respect to subsurface geometries and snow dynamics) be developed, calibrated, and applied to reproduce spatio-temporal hydrological dynamics in complex headwaters under present climatic, land cover, and permafrost conditions? and;

5. What insights can applying such models under a plausible future climatic, land cover, and permafrost scenario yield with respect to the magnitude and importance of possible drivers of future hydrological change?

Answering these questions can be considered the objectives of this thesis. Ultimately, it is hoped that some conclusions regarding the utility of fully-integrated models in simulating hydrological dynamics in extremely complex Alpine terrain can be drawn.

1.4.2 Workflow and structure

Figure 1.13 illustrates the high-level workflow that was designed and implemented with these objectives in mind.

The remainder of the thesis is structured as follows: In **Chapter 2**, the development of high-resolution, accurate, and spatially extensive 3D models of bedrock geology in extremely complex Alpine terrain is presented. Thereafter, **Chapter 3** proposes a novel approach to the incorporation of contrasting types of snow observations in the optimisation of a sophisticated, high-resolution distributed snow model. In **Chapter 4**, meanwhile, further work that was undertaken to refine the subsurface structure – this time with regards to potential unconsolidated Quaternary aquifers – is described. As such, together, these chapters deal with the advancements needed to establish or improve the structure and forcing of integrated models in alpine terrain. That said, the advancements made in **Chapters 2** and **3** in particular have value in their own right, i.e. in the respective disciplines of structural/hydrogeology and snow hydrology more broadly.

Chapter 5, which describes the development of the sophisticated integrated model and its application to quantify the overall hydrological functioning of the study catchment under both recent and plausible future climate, vegetation, and permafrost in overall Alpine hydrological system functioning, represents the culmination of the thesis. Finally, overall conclusions are drawn and recommendations for future research made in **Chapter 6**.

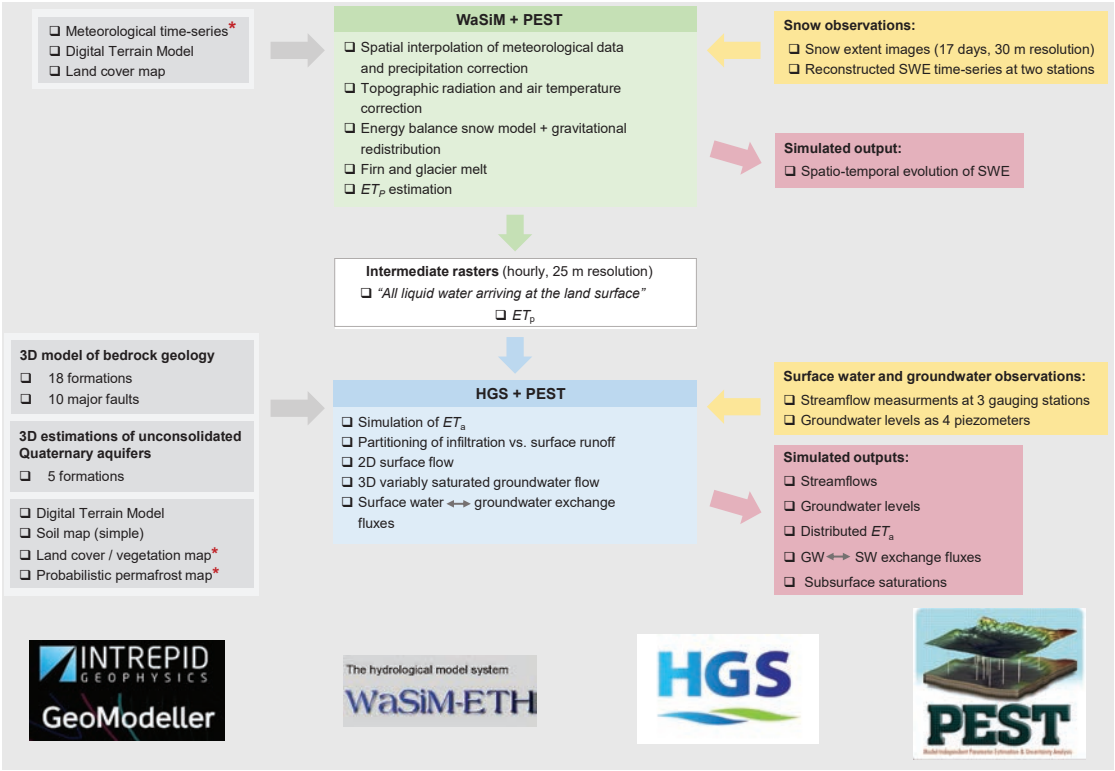

Figure 1.13: The experimental design of the thesis. The red asterisks indicate elements for which both present and plausible future scenarios were considered.

The workflow has strong credentials for describing many processes that are known or anticipated to hold hydrological importance in such terrain in a spatially distributed, transient, and predominantly physically-based fashion. More specifically, an energy balance-based simulation of snow dynamics that incorporates mass-conservative vertical redistribution from steep slopes is undertaken, alongside the representation of 2D surface flow, 3D variably-saturated subsurface flow (including the influence of 3D geological structures according to a specifically developed model), and evapotranspiration (ET_a) – all at high spatio-temporal resolution. Numerous outputs can be extracted at any point of the simulation domain in time and space, which opens up considerable opportunities for internally evaluating the proposed mathematical description.

More specifically, by using WaSiM initially, it was possible to overcome the challenges that: i) high-resolution spatio-temporal forcing data (including estimates of ET_p) that overlap in time the field observations that were made were required to force the integrated surface-subsurface simulator (HGS), but no third party products were available, and that HGS moreover did not offer any meteorological "pre-processing" capability to generate such data, and ii) that the snow modelling approach offered by HGS is presently fairly rudimentary, involving a temperature-index scheme in which snow densities are fixed and temporally invariant, sublimation parameterised as a constant, and snow redistribution processes are unaccounted for (Schilling, Park, et al., 2019). Such a simplistic snow modelling approach is unlikely to be capable of satisfactorily reproducing snow dynamics, and hence the arrival of melt water at the land surface, in complex alpine terrain.

Conversely, using HGS for the remainder of the workflow enables important limitations associated with WaSiM to be circumvented, including the facts that i) it does not support the representation of 3D groundwater flow, and ii) does not describe surface water and groundwater interactions in a fully-integrated fashion. (Note: the one-way coupling is justified by the fact that any feedbacks from hydrology to snow are of minor importance).

In this way, the experimental design sought to leverage the benefits of these two types of models whilst simultaneously mitigating against their respective limitations. The hydrological modelling philosophy employed here thus extends well beyond simply capturing precipitation-runoff relationships, but rather aims to represent the spatio-temporal variability of the salient physical processes, and the fluxes they induce, as comprehensively as possible.

1.4.3 A brief introduction to the study area

A single study area of approximately 37 km^2 is focussed upon throughout. The region is comprised of two adjacent headwaters, and is situated in the *Haute Alpes Calcaires* (western Swiss Alps) (Figure 1.14). The choice of study site was dictated by the larger project, entitled IntegrAlp – *"Integrating spatial predictions of vegetation, soils, geomorphology, and hydrology for improved assessment of ecosystem services under climate change"* – within the framework of which the research was conducted.

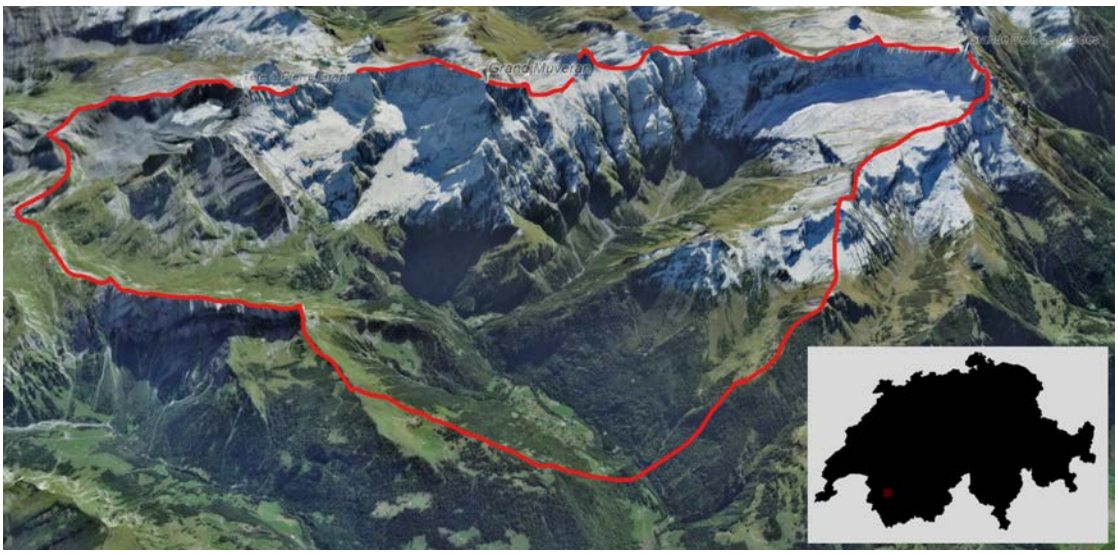

Figure 1.14: A view across the study catchment, whose extent is delimited by the red line, looking to the south-east. Source: Swiss Federal Office of Topography. The inset shows the catchment's situation within Switzerland. Click here to explore!

The bedrock geology of the area is extremely complex, slopes are steep, and snow exerts a major influence on the hydrological regime. Apart from some grazing of the alpine pastures in summer, the region remains in a highly natural, even pristine state, making it rare in the context of the Alps. On one hand, this is highly attractive, since physical processes can be investigated without any consideration having to be made for potential anthropogenic impacts. In this instance, however, it also meant that no long-term systematic hydro-meteorological measurements were available upon the commencement of this research in 2016. As such, the task of developing a rather comprehensive and notoriously data hungry hydrological model, and one that moreover intended to avoid making "convenient" simplifying assumptions where they may not be justifiable, was a daunting one. More practically speaking, it was imperative that field activities began as quickly as possible, and that the project proceeded in a simultaneous "measure and model" fashion. The study area's physical characteristics are described more thoroughly in due course.

1.4.4 Status of related publications

A version of Chapter 2 has been published in the journal *Scientific Data*, and a version of Chapter 3 has been submitted to *Water Resources Research*. Two additional manuscripts developed from Chapter 5 are currently in preparation. It is less probable that material from this introductory chapter and Chapter 4 will be prepared for separate publication, although this remains to be

confirmed. If they do proceed, these contributions will take the form of a review paper and an original research article, respectively.

References

Addor, N. and Melsen, L. A. (2019). Legacy, rather than adequacy, drives the selection of hydrological models. *Water Resources Research* 55, 378–390.

Addor, N., Rössler, O., Köplin, N., Huss, M., Weingartner, R., and Seibert, J. (2014). Robust changes and sources of uncertainty in the projected hydrological regimes of Swiss catchments. *Water Resources Research* 50, 7541–7562.

Ala-aho, P., Soulsby, C., Wang, H., and Tetzlaff, D. (2017). Integrated surface-subsurface model to investigate the role of groundwater in headwater catchment runoff generation: A minimalist approach to parameterisation. *Journal of Hydrology* 547, 664–677.

Anderson, K., Fawcett, D., Cugulliere, A., Benford, S., Jones, D., and Leng, R. (2020). Vegetation expansion in the subnival Hindu Kush Himalaya. *Global Change Biology* 26, 1608–1625.

Andrianaki, M., Shrestha, J., Kobierska, F., Nikolaidis, N. P., and Bernasconi, S. M. (2019). Assessment of SWAT spatial and temporal transferability for a high-altitude glacierized catchment. *Hydrology and Earth System Sciences* 23, 3219–3232.

Aquanty Inc. (2016). *HydroGeoSphere User Manual*. Tech. rep.

Arnold, J. G., Allen, P. M., and Bernhardt, G. (1993). A comprehensive surface-groundwater flow model. *Journal of Hydrology* 142, 47–69.

Arnold, J. G. et al. (2012). SWAT: Model use, calibration, and validation. *Biological Systems Engineering: Papers and Publications* 406.

Atchley, A. L. and Maxwell, R. M. (2011). Influences of subsurface heterogeneity and vegetation cover on soil moisture, surface temperature and evapotranspiration at hillslope scales. *Hydrogeology Journal* 19, 289–305.

Avanzi, F., Maurer, T., Glaser, S. D., Bales, R. C., and Conklin, M. H. (2020). Information content of spatially distributed ground-based measurements for hydrologic-parameter calibration in mixed rain-snow mountain headwaters. *Journal of Hydrology* 582, 124478.

Bales, R. C. and Harrington, R. F. (1995). Recent progress in snow hydrology. *Reviews of Geophysics* 33, 1011–1020.

Barnett, T. P., Adam, J. C., and Lettenmaier, D. P. (2005). Potential impacts of a warming climate on water availability in snow-dominated regions. *Nature* 438, 303–309.

Barnett, T. P. et al. (2008). Human-induced changes in the hydrology of the western United States. *Science* 319, 1080–1083.

Bavay, M., Grünewald, T., and Lehning, M. (2013). Response of snow cover and runoff to climate change in high Alpine catchments of Eastern Switzerland. *Advances in Water Resources* 55, 4–16.

Bayard, D., Stähli, M., Parriaux, A., and Flühler, H. (2005). The influence of seasonally frozen soil on the snowmelt runoff at two Alpine sites in southern Switzerland. *Journal of Hydrology* 309, 66–84.

Begert, M. and Frei, C. (2018). Long-term area-mean temperature series for SwitzerlandâCombining homogenized station data and high resolution grid data. *International Journal of Climatology* 38, 2792–2807.

Beniston, M. (2012). Impacts of climatic change on water and associated economic activities in the Swiss Alps. *Journal of Hydrology* 412-413, 291–296.

Beniston, M. and Stoffel, M. (2016). Rain-on-snow events, floods and climate change in the Alps: Events may increase with warming up to 4°C and decrease thereafter. *Science of the Total Environment* 571, 228–236.

Beniston, M. et al. (2018). The European mountain cryosphere: a review of its current state, trends, and future challenges. *The Cryosphere* 12, 759–794.

Beven, K. J. (1989). Changing ideas in hydrology - the case of physically-based models. *Journal of Hydrology* 105, 157–172.

Beven, K. J. (2000). Uniqueness of place and process representations in hydrological modelling. *Hydrology and Earth System Sciences* 4, 203–213.

Beven, K. J. (2006). A manifesto for the equifinality thesis. *Journal of Hydrology* 320, 18–36.

Beven, K. J. (2011). *Rainfall-runoff modelling: The primer*. John Wiley & Sons.

Bierkens, M. F. et al. (2015). Hyper-resolution global hydrological modelling: What is next?: "Everywhere and locally relevant" M. F. P. Bierkens et al. Invited Commentary. *Hydrological Processes* 29, 310–320.

Bilish, S. P., Callow, J. N., McGrath, G. S., and McGowan, H. A. (2019). Spatial controls on the distribution and dynamics of a marginal snowpack in the Australian Alps. *Hydrological Processes* 33, 1739–1755.

Birsan, M.-V., Molnar, P., Burlando, P., and Pfaundler, M. (2005). Streamflow trends in Switzerland. *Journal of Hydrology* 314, 312–329.

Bonat, M., Lucianetti, G., Mastrorillo, L., Viaroli, S., and Mazza, R. (2020). The role of alpine valley fill deposits for groundwater storage (Dolomites, Italy). *Grundwasser* 25, 3–14.

Brauchli, T., Trujillo, E., Huwald, H., and Lehning, M. (2017). Influence of slope-scale snowmelt on catchment response simulated with the Alpine3D model. *Water Resources Research* 53, 10723–10739.

Brown, L. E., Dickson, N. E., Carrivick, J. L., and Füreder, L. (2015). Alpine river ecosystem response to glacial and anthropogenic flow pulses. *Freshwater Science* 34, 1201–1215.

Brunner, M. I., Björnsen Gurung, A., Zappa, M., Zekollari, H., Farinotti, D., and Stähli, M. (2019). Present and future water scarcity in Switzerland: Potential for alleviation through reservoirs and lakes. *Science of the Total Environment* 666, 1033–1047.

Brunner, P., Doherty, J., and Simmons, C. T. (2012). Uncertainty assessment and implications for data acquisition in support of integrated hydrologic models. *Water Resources Research* 48, 1–18.

Brunner, P. and Simmons, C. T. (2012). A fully integrated physically based hydrogeological model. *Ground Water* 50, 170–176.

Calanca, P., Roesch, A., Jasper, K., and Wild, M. (2006). Global warming and the summertime evapotranspiration regime of the Alpine region. *Climatic Change* 79, 65–78.

Camporese, M., Paniconi, C., Putti, M., and Orlandini, S. (2010). Surface-subsurface flow modeling with path-based runoff routing, boundary condition-based coupling, and assimilation of multisource observation data. *Water Resources Research* 46.

Carlier, C., Wirth, S. B., Cochand, F., Hunkeler, D., and Brunner, P. (2018). Geology controls streamflow dynamics. *Journal of Hydrology* 566, 756–769.

Carlier, C., Wirth, S. B., Cochand, F., Hunkeler, D., and Brunner, P. (2019). Exploring geological and topographical controls on low flows with hydrogeological models. *Groundwater* 57, 48–62.

CH2018 (2018). *CH2018 – Climate Scenarios for Switzerland: Technical Report*. Tech. rep. Zurich, p. 271.

Chen, Z. and Goldscheider, N. (2014). Modeling spatially and temporally varied hydraulic behavior of a folded karst system with dominant conduit drainage at catchment scale, Hochifen-Gottesacker, Alps. *Journal of Hydrology* 514, 41–52.

Christidis, N., Jones, G. S., and Stott, P. A. (2015). Dramatically increasing chance of extremely hot summers since the 2003 European heatwave. *Nature Climate Change* 5, 46–50.

Clow, D. W., Schrott, L., Webb, R., Campbell, D. H., Torizzo, A., and Dornblaser, M. (2003). Ground Water Occurrence and Contributions to Streamflow in an Alpine Catchment, Colorado Front Range. *GroundWater* 41, 937–950.

Cochand, F., Therrien, R., and Lemieux, J. M. (2019). Integrated hydrological modeling of climate change impacts in a snow-influenced catchment. *Groundwater* 57, 3–20.

Cochand, M., Christe, P., Ornstein, P., and Hunkeler, D. (2019). Groundwater storage in high Alpine catchments and its contribution to streamflow. *Water Resources Research* 55, 2613–2630.

Collins, D. N. and Young, G. J. (1981). Meltwater hydrology and hydrochemistry in snow- and ice-covered mountain catchments. *Nordic Hydrology* 12, 319–334.

Condon, L. E., Atchley, A. L., and Maxwell, R. M. (2020). Evapotranspiration depletes groundwater under warming over the contiguous United States. *Nature communications* 11, 873.

Costa, A., Molnar, P., Stutenbecker, L., Bakker, M., Silva, T. A., Schlunegger, F., Lane, S. N., Loizeau, J.-L., and Girardclos, S. (2018). Temperature signal in suspended sediment export from an Alpine catchment. *Hydrology and Earth System Sciences* 22, 509–528.

Cowie, R. M., Knowles, J. F., Dailey, K. R., Williams, M. W., Mills, T. J., and Molotch, N. P. (2017). Sources of streamflow along a headwater catchment elevational gradient. *Journal of Hydrology* 549, 163–178.

Datry, T., Larned, S. T., and Tockner, K. (2014). Intermittent rivers: a challenge for freshwater ecology. *BioScience* 64, 229–235.

DeBeer, C. M. and Pomeroy, J. W. (2017). Influence of snowpack and melt energy heterogeneity on snow cover depletion and snowmelt runoff simulation in a cold mountain environment. *Journal of Hydrology* 553, 199–213.

Diersch, H.-J. G. (2013). *FEFLOW finite element modeling of flow, mass and heat transport in porous and fractured media*. Springer Science & Business Media.

Dobler, C. and Pappenberger, F. (2013). Global sensitivity analyses for a complex hydrological model applied in an alpine watershed. *Hydrological Processes* 27, 3922–3940.

Dong, C. (2018). Remote sensing, hydrological modeling and in situ observations in snow cover research: A review. *Journal of Hydrology* 561, 573–583.

Doyle, J. M., Gleeson, T., Manning, A. H., and Mayer, K. U. (2015). Using noble gas tracers to constrain a groundwater flow model with recharge elevations: A novel approach for mountainous terrain. *Water Resources Research* 51, 8094–8113.

Duethmann, D., Blöschl, G., and Parajka, J. (2020). Why does a conceptual hydrological model fail to predict discharge changes in response to climate change? *Hydrology and Earth System Sciences Discussions*, 1–28.

Ebel, B. A. and Loague, K. (2006). Physics-based hydrologic-response simulation: Seeing through the fog of equifinality. *Hydrological Processes* 20, 2887–2900.

EEA (2009). *Regional climate change and adaptation – The Alps facing the challenge of changing water resources*. Tech. rep. 8, pp. 1–143.

Efthymiadis, D., Jones, P. D., Briffa, K. R., Auer, I., Böhm, R., Schöner, W., Frei, C., and Schmidli, J. (2006). Construction of a 10-min-gridded precipitation data set for the Greater Alpine Region for 1800-2003. *Journal of Geophysical Research Atmospheres* 111, 1–22.

Elder, K., Dozier, J., and Michaelsen, J. (1991). Snow accumulation and distribution in an Alpine Watershed. *Water Resources Research* 27, 1541–1552.

Endrizzi, S., Gruber, S., Dall'Amico, M., and Rigon, R. (2014). GEOtop 2.0: Simulating the combined energy and water balance at and below the land surface accounting for soil freezing, snow cover and terrain effects. *Geoscientific Model Development* 7, 2831–2857.

Evans, S. G., Ge, S., Voss, C. I., and Molotch, N. P. (2018). The role of frozen soil in groundwater discharge predictions for warming alpine watersheds. *Water Resources Research* 54, 1599–1615.

Fan, Y., Miguez-Macho, G., Jobbágy, E. G., Jackson, R. B., and Otero-Casal, C. (2017). Hydrologic regulation of plant rooting depth. *Proceedings of the National Academy of Sciences of the United States of America* 114, 10572–10577.

Fatichi, S., Rimkus, S., Burlando, P., Bordoy, R., and Molnar, P. (2015). High-resolution distributed analysis of climate and anthropogenic changes on the hydrology of an Alpine catchment. *Journal of Hydrology* 525, 362–382.

Fatichi, S. et al. (2016). An overview of current applications, challenges, and future trends in distributed process-based models in hydrology. *Journal of Hydrology* 537, 45–60.

Filippini, M. et al. (2018). Differentiated spring behavior under changing hydrological conditions in an alpine karst aquifer. *Journal of Hydrology* 556, 572–584.

Finger, D., Pellicciotti, F., Konz, M., Rimkus, S., and Burlando, P. (2011). The value of glacier mass balance, satellite snow cover images, and hourly discharge for improving the performance of a physically based distributed hydrological model. *Water Resources Research* 47, 1–14.

Fischer, A. M., Keller, D. E., Liniger, M. A., Rajczak, J., Schär, C., and Appenzeller, C. (2015). Projected changes in precipitation intensity and frequency in Switzerland: A multi-model perspective. *International Journal of Climatology* 35, 3204–3219.

Fischer, B. M., van Meerveld, H. J., and Seibert, J. (2017). Spatial variability in the isotopic composition of rainfall in a small headwater catchment and its effect on hydrograph separation. *Journal of Hydrology* 547, 755–769.

Fischer, M., Huss, M., and Hoelzle, M. (2015). Surface elevation and mass changes of all Swiss glaciers 1980-2010. *Cryosphere* 9, 525–540.

Flerchinger, G. N., Shang, S., and Finnie, J. I. (1996). Simulating three-dimensional ground water response in a small mountainous watershed. *Water Resources Bulletin* 32, 1081–1088.

Floriancic, M. G., van Meerveld, I., Smoorenburg, M., Margreth, M., Naef, F., Kirchner, J. W., and Molnar, P. (2018). Spatio-temporal variability in contributions to low flows in the high Alpine Poschiavino catchment. *Hydrological Processes* 32, 3938–3953.

Forster, C. and Smith, L. (1988). Groundwater flow systems in mountainous terrain: 2. Controlling factors. *Water Resources Research* 24, 1011–1023.

Förster, K., Meon, G., Marke, T., and Strasser, U. (2014). Effect of meteorological forcing and snow model complexity on hydrological simulations in the Sieber catchment (Harz Mountains, Germany). *Hydrology and Earth System Sciences* 18, 4703–4720.

Foster, L. M. and Maxwell, R. M. (2019). Sensitivity analysis of hydraulic conductivity and Manning's n parameters lead to new method to scale effective hydraulic conductivity across model resolutions. *Hydrological Processes* 33, 332–349.

Freeze, R. and Harlan, R. (1969). Blueprint for a physically-based, digitally-simulated hydrologic response model. *Journal of Hydrology* 9, 237–258.

Frenierre, J. L. and Mark, B. G. (2014). A review of methods for estimating the contribution of glacial meltwater to total watershed discharge. *Progress in Physical Geography* 38, 173–200.

Gabrielli, C. P., McDonnell, J. J., and Jarvis, W. T. (2012). The role of bedrock groundwater in rainfall-runoff response at hillslope and catchment scales. *Journal of Hydrology* 450-451, 117–133.

Gädeke, A., Koch, H., Pohle, I., and Grünewald, U. (2014). Comparing WaSiM-ETH to HBV-light in climate change impact assessments – Advantages and disadvantages. *WaSiM User Conference*. Munich.

Gallice, A., Bavay, M., Brauchli, T., Comola, F., Lehning, M., and Huwald, H. (2016). StreamFlow 1.0: An extension to the spatially distributed snow model Alpine3D for hydrological modelling and deterministic stream temperature prediction. *Geoscientific Model Development* 9, 4491–4519.

Gleeson, T. and Manning, A. H. (2008). Regional groundwater flow in mountainous terrain: Three-dimensional simulations of topographic and hydrogeologic controls. *Water Resources Research* 44.

Gobiet, A., Kotlarski, S., Beniston, M., Heinrich, G., Rajczak, J., and Stoffel, M. (2014). 21st century climate change in the European Alps - A review. *Science of The Total Environment* 493, 1138–1151.

Godsey, S. E., Kirchner, J. W., and Tague, C. L. (2014). Effects of changes in winter snowpacks on summer low flows: Case studies in the Sierra Nevada, California, USA. *Hydrological Processes* 28, 5048–5064.

Goswami, M. and O'Connor, K. M. (2010). A "monster" that made the SMAR conceptual model "right for the wrong reasons". *Hydrological Sciences Journal* 55, 913–927.

Goulden, M. L. and Bales, R. C. (2014). Mountain runoff vulnerability to increased evapotranspiration with vegetation expansion. *Proceedings of the National Academy of Sciences* 111, 14071–14075.

Graham, D. and Butts, M. B. (2005). Flexible, integrated watershed modelling with MIKE SHE. *Watershed Models*. Ed. by V. Singh and D. Frevert. CRC Press. Chap. 10, pp. 245–272.

Grayson, R. B. and Blöschl, G. (2001). *Spatial patterns in catchment hydrology: Observations and modelling*. Cambridge: Cambridge University Press.

Gremaud, V., Goldscheider, N., Savoy, L., Favre, G., and Masson, H. (2009). Geological structure, recharge processes and underground drainage of a glacierised karst aquifer system, Tsanfleuron-Sanetsch, Swiss Alps. *Hydrogeology Journal* 17, 1833–1848.

Grêt-Regamey, A., Brunner, S. H., and Kienast, F. (2012). Mountain Ecosystem Services: Who Cares? *Mountain Research and Development* 32, S23–S34.

Grünewald, T., Bühler, Y., and Lehning, M. (2014). Elevation dependency of mountain snow depth. *The Cryosphere* 8, 2381–2394.

Harbaugh Arlen, W. (2005). MODFLOW-2005 , The U.S. Geological Survey Modular Ground-Water Model – the Ground-Water Flow Process. *U.S. Geological Survey Techniques and Methods*, 253.

Härer, S. (2017). Making use of local remote sensing measurements for improving snow cover products over different scales. PhD thesis. Ludwig-Maximilians-Universität München, p. 133.

Harrington, J. S., Mozil, A., Hayashi, M., and Bentley, L. R. (2018). Groundwater flow and storage processes in an inactive rock glacier. *Hydrological Processes* 32, 3070–3088.

Hartmann, A., Goldscheider, N., Wagener, T., Lange, J., and Weiler, M. (2014). Karst water resources in a changing world: Review of hydrological modeling approaches. *Reviews of Geophysics* 52, 218–242.

Hausfather, Z. and Peters, G. P. (2020). Emissions - the 'business as usual' story is misleading. *Nature* 577, 618–620.

Henne, P. D. et al. (2018). An empirical perspective for understanding climate change impacts in Switzerland. *Regional Environmental Change* 18, 205–221.

Hock, R. et al. (2019). High Mountain Areas. *IPCC Special Report on the Ocean and Cryosphere in a Changing Climate*. Ed. by H.-O. Pörtner et al. Chap. 2.

Hood, J. L. and Hayashi, M. (2015). Characterization of snowmelt flux and groundwater storage in an alpine headwater basin. *Journal of Hydrology* 521, 482–497.

Hood, J. L., Roy, J. W., and Hayashi, M. (2006). Importance of groundwater in the water balance of an alpine headwater lake. *Geophysical Research Letters* 33, 1–5.

Horton, P., Schaefli, B., Mezghani, A., Hingray, B., and Musy, A. (2006). Assessment of climate-change impacts on alpine discharge regimes with climate model uncertainty. *Hydrological Processes* 20, 2091–2109.

Hrachowitz, M. and Clark, M. P. (2017). HESS Opinions: The complementary merits of competing modelling philosophies in hydrology. *Hydrology and Earth System Sciences* 21, 3953–3973.

Huntington, J. L. and Niswonger, R. G. (2012). Role of surface-water and groundwater interactions on projected summertime streamflow in snow dominated regions: An integrated modeling approach. *Water Resources Research* 48.

Huss, M., Bauder, A., Marty, C., and Nötzli, J. (2018). *Neige, glace et pergélisol 2016/17*. Tech. rep. Swiss Alpine Club.

Huss, M. and Hock, R. (2018). Global-scale hydrological response to future glacier mass loss. *Nature Climate Change* 8, 135–140.

Huss, M. et al. (2017). Toward mountains without permanent snow and ice. *Earth's Future* 5, 418–435.

Hwang, H. T., Park, Y. J., Sudicky, E. A., Berg, S. J., McLaughlin, R., and Jones, J. P. (2018). Understanding the water balance paradox in the Athabasca River Basin, Canada. *Hydrological Processes* 32, 729–746.

Immerzeel, W. W. et al. (2020). Importance and vulnerability of the world's water towers. *Nature* 577, 364–369.

Irvine, D. J., Brunner, P., Franssen, H. J. H., and Simmons, C. T. (2012). Heterogeneous or homogeneous? Implications of simplifying heterogeneous streambeds in models of losing streams. *Journal of Hydrology* 424-425, 16–23.

Isotta, F. A., Begert, M., and Frei, C. (2019). Long-Term Consistent Monthly Temperature and Precipitation Grid Data Sets for Switzerland Over the Past 150 Years. *Journal of Geophysical Research: Atmospheres* 124, 3783–3799.

Isotta, F. A. et al. (2014). The climate of daily precipitation in the Alps: Development and analysis of a high-resolution grid dataset from pan-Alpine rain-gauge data. *International Journal of Climatology* 34, 1657–1675.

James, A. L., McDonnell, J. J., Tromp-Van Meerveld, I., and Peters, N. E. (2010). Gypsies in the palace: Experimentalist's view on the use of 3-D physics-based simulation of hillslope hydrological response. *Hydrological Processes* 24, 3878–3893.

Jansson, P., Hock, R., and Schneider, T. (2003). The concept of glacier storage: A review. *Journal of Hydrology* 282, 116–129.

Jaros, A., Rossi, P. M., Ronkanen, A. K., and Kløve, B. (2019). Parameterisation of an integrated groundwater-surface water model for hydrological analysis of boreal aapa mire wetlands. *Journal of Hydrology* 575, 175–191.

Jenicek, M., Seibert, J., and Staudinger, M. (2018). Modeling of future changes in seasonal snowpack and impacts on summer low flows in Alpine catchments. *Water Resources Research* 54, 538–556.

Jones, D. B., Harrison, S., Anderson, K., and Whalley, W. B. (2019). Rock glaciers and mountain hydrology: A review. *Earth-Science Reviews* 193, 66–90.

Jones, J. P., Sudicky, E. A., and McLaren, R. G. (2008). Application of a fully-integrated surface-subsurface flow model at the watershed-scale: A case study. *Water Resources Research* 44, 1–13.

Jouvet, G. and Huss, M. (2019). Future retreat of Great Aletsch Glacier. *Journal of Glaciology*, 1–4.

Kirchner, J. W. (2006). Getting the right answers for the right reasons: Linking measurements, analyses, and models to advance the science of hydrology. *Water Resources Research* 42.

Klaus, J. and McDonnell, J. (2013). Hydrograph separation using stable isotopes: Review and evaluation. *Journal of Hydrology* 505, 47–64.

Klein, G., Vitasse, Y., Rixen, C., Marty, C., and Rebetez, M. (2016). Shorter snow cover duration since 1970 in the Swiss Alps due to earlier snowmelt more than to later snow onset. *Climatic Change* 139, 637–649.

Klemeš, V. (1990). The modelling of mountain hydrology: the ultimate challenge. *Hydrology of Mountainous Areas (Proceedings of the Strbské Pleso Workshop, Czechoslovakia, June 1988)*, 29–44.

Kling, H. (2006). Spatio-temporal modelling of the water balance of Austria. PhD thesis. University of Natural Resources and Applied Life Sciences Vienna.

Kobierska, F., Jonas, T., Kirchner, J. W., and Bernasconi, S. M. (2015). Linking baseflow separation and groundwater storage dynamics in an alpine basin (Dammagletscher, Switzerland). *Hydrology and Earth System Sciences* 19, 3681–3693.

Kollet, S. J. and Maxwell, R. M. (2008). Capturing the influence of groundwater dynamics on land surface processes using an integrated, distributed watershed model. *Water Resources Research* 44, 1–18.

Kollet, S. et al. (2017). The integrated hydrologic model intercomparison project, IH-MIP2: A second set of benchmark results to diagnose integrated hydrology and feedbacks. *Water Resources Research* 53, 867–890.

Körner, C., Jetz, W., Paulsen, J., Payne, D., Rudmann-Maurer, K., and M. Spehn, E. (2017). A global inventory of mountains for bio-geographical applications. *Alpine Botany* 127.

Kosugi, K., Fujimoto, M., Katsura, S., Kato, H., Sando, Y., and Mizuyama, T. (2011). Localized bedrock aquifer distribution explains discharge from a headwater catchment. *Water Resources Research* 47.

Kraller, G., Warscher, M., Kunstmann, H., Vogl, S., Marke, T., and Strasser, U. (2012). Water balance estimation in high Alpine terrain by combining distributed modeling and a neural network approach (Berchtesgaden Alps, Germany). *Hydrology and Earth System Sciences* 16, 1969–1990.

Krause, P., Boyle, D. P., and Bäse, F. (2005). Comparison of different efficiency criteria for hydrological model assessment. *Advances in Geosciences* 5, 89–97.

Kurylyk, B. L. and Hayashi, M. (2017). Inferring hydraulic properties of alpine aquifers from the propagation of diurnal snowmelt signals. *Water Resources Research* 53, 4271–4285.

Laghari, A. N., Vanham, D., and Rauch, W. (2012). To what extent does climate change result in a shift in Alpine hydrology? A case study in the Austrian Alps. *Hydrological Sciences Journal* 57, 103–117.

Lane, S. N., Bakker, M., Costa, A., Girardclos, S., Loizeau, J.-L., Molnar, P., Silva, T., Stutenbecker, L., and Schlunegger, F. (2019). Making stratigraphy in the Anthropocene: climate change impacts and economic conditions controlling the supply of sediment to Lake Geneva. *Scientific Reports* 9, 8904.

Langston, G., Bentley, L. R., Hayashi, M., Mcclymont, A., and Pidlisecky, A. (2011). Internal structure and hydrological functions of an alpine proglacial moraine. *Hydrological Processes* 25, 2967–2982.

Langston, G., Hayashi, M., and Roy, J. W. (2013). Quantifying groundwater-surface water interactions in a proglacial moraine using heat and solute tracers. *Water Resources Research* 49, 5411–5426.

Lauber, U., Kotyla, P., Morche, D., and Goldscheider, N. (2014). Hydrogeology of an Alpine rockfall aquifer system and its role in flood attenuation and maintaining baseflow. *Hydrology and Earth System Sciences* 18, 4437–4452.

Lehmann-Horn, J. A., Walbrecker, J. O., Hertrich, M., Langston, G., McClymont, A. F., and Green, A. G. (2011). Imaging groundwater beneath a rugged proglacial moraine. *Geophysics* 76.

Lehning, M., Völksch Ingo, I., Gustafsson, D., Nguyen, T. A., Stähli, M., and Zappa, M. (2006). ALPINE3D: A detailed model of mountain surface processes and its application to snow hydrology. *Hydrological Processes*. Vol. 20. (10), pp. 2111–2128.

Leigh, C., Boulton, A. J., Courtwright, J. L., Fritz, K., May, C. L., Walker, R. H., and Datry, T. (2016). Ecological research and management of intermittent rivers: an historical review and future directions. *Freshwater Biology* 61, 1181–1199.

Liggett, J. E., Werner, A. D., and Simmons, C. T. (2012). Influence of the first-order exchange coefficient on simulation of coupled surface-subsurface flow. *Journal of Hydrology* 414-415, 503–515.

Lindström, G., Johansson, B., Persson, M., Gardelin, M., and Bergström, S. (1997). Development and test of the distributed HBV-96 hydrological model. *Journal of Hydrology* 201, 272–288.

Liu, F., Williams, M. W., and Caine, N. (2004). Source waters and flow paths in an alpine catchment, Colorado Front Range, United States. *Water Resources Research* 40, 1–16.

Loague, K. and VanderKwaak, J. E. (2004). Physics-based hydrologic response simulation: Platinum bridge, 1958 Edsel, or useful tool. *Hydrological Processes* 18, 2949–2956.

Luterbacher, J. et al. (2016). European summer temperatures since Roman times. *Environmental Research Letters* 11, 024001.

Magnusson, J., Gustafsson, D., Hüsler, F., and Jonas, T. (2014). Assimilation of point SWE data into a distributed snow cover model comparing two contrasting methods. *Water Resources Research* 50, 7816–7835.

Manning, A. H. and Caine, J. S. (2007). Groundwater noble gas, age, and temperature signatures in an Alpine watershed: Valuable tools in conceptual model development. *Water Resources Research* 43.

Markovich, K. H., Manning, A. H., Condon, L. E., and McIntosh, J. C. (2019). MountainâBlock Recharge: A Review of Current Understanding. *Water Resources Research* 55, 8278–8304.

Marty, C. and Meister, R. (2012). Long-term snow and weather observations at Weissfluhjoch and its relation to other high-altitude observatories in the Alps. *Theoretical and Applied Climatology* 110, 573–583.

Marty, C., Schlögl, S., Bavay, M., and Lehning, M. (2017). How much can we save? Impact of different emission scenarios on future snow cover in the Alps. *Cryosphere* 11, 517–529.

Marty, C., Tilg, A.-M., and Jonas, T. (2017). Recent evidence of large-scale receding Snow Water Equivalents in the European Alps. *Journal of Hydrometeorology* 18, 1021–1031.

Mastrotheodoros, T. et al. (2020). More green and less blue water in the Alps during warmer summers. *Nature Climate Change* 10, 155–161.

Maxwell, R. M. (2013). A terrain-following grid transform and preconditioner for parallel, large-scale, integrated hydrologic modeling. *Advances in Water Resources* 53, 109–117.

Maxwell, R. M. (2020). Water colour and climate. *Nature Climate Change* 10, 102–103.

Maxwell, R. M. and Miller, N. L. (2005). Development of a coupled land surface and groundwater model. *Journal of Hydrometeorology* 6, 233–247.

Maxwell, R. M. et al. (2014). Surface-subsurface model intercomparison: A first set of benchmark results to diagnose integrated hydrology and feedbacks. *Water Resources Research* 50, 1531–1549.

McClymont, A. F., Hayashi, M., Bentley, L. R., and Liard, J. (2012). Locating and characterising groundwater storage areas within an alpine watershed using time-lapse gravity, GPR and seismic refraction methods. *Hydrological Processes* 26, 1792–1804.

McClymont, A. F., Hayashi, M., Bentley, L. R., Muir, D., and Ernst, E. (2010). Groundwater flow and storage within an alpine meadow-talus complex. *Hydrology and Earth System Sciences* 14, 859–872.

McClymont, A. F., Roy, J. W., Hayashi, M., Bentley, L. R., Maurer, H., and Langston, G. (2011). Investigating groundwater flow paths within proglacial moraine using multiple geophysical methods. *Journal of Hydrology* 399, 57–69.

McCurley, K. L. and Jawitz, J. W. (2017). Hyphenated hydrology: Interdisciplinary evolution of water resource science. *Water Resources Research* 53, 2972–2982.

Meeks, J. and Hunkeler, D. (2015). Snowmelt infiltration and storage within a karstic environment, Vers Chez le Brandt, Switzerland. *Journal of Hydrology* 529, 11–21.

Mendiguren, G., Koch, J., and Stisen, S. (2017). Spatial pattern evaluation of a calibrated national hydrological model - A remote-sensing-based diagnostic approach. *Hydrology and Earth System Sciences* 21, 5987–6005.

Mendoza, P. A., Clark, M. P., Barlage, M., Rajagopalan, B., Samaniego, L., Abramowitz, G., and Gupta, H. (2015). Are we unnecessarily constraining the agility of complex process-based models? *Water Resources Research* 51, 716–728.

MeteoSwiss (2019). *Climate Change in Switzerland*. URL: https://www.meteoswiss.admin.ch/home/climate/climate-change-in-switzerland.html.

Michel, A., Brauchli, T., Lehning, M., Schaefli, B., and Huwald, H. (2020). Stream temperature and discharge evolution in Switzerland over the last 50 years: annual and seasonal behaviour. *Hydrology and Earth System Sciences* 24, 115–142.

Micheletti, N. and Lane, S. N. (2016). Water yield and sediment export in small, partially glaciated Alpine watersheds in a warming climate. *Water Resources Research* 52, 4924–4943.

Miller, K. L., Berg, S. J., Davison, J. H., Sudicky, E. A., and Forsyth, P. A. (2018). Efficient uncertainty quantification in fully-integrated surface and subsurface hydrologic simulations. *Advances in Water Resources* 111, 381–394.

Minder, J. R., Mote, P. W., and Lundquist, J. D. (2010). Surface temperature lapse rates over complex terrain: Lessons from the Cascade Mountains. *Journal of Geophysical Research Atmospheres* 115, 1–13.

Moeck, C., von Freyberg, J., and Schirmer, M. (2018). Groundwater recharge predictions in contrasted climate: The effect of model complexity and calibration period on recharge rates. *Environmental Modelling and Software* 103, 74–89.

Muir, D. L., Hayashi, M., and Mcclymont, A. F. (2011). Hydrological storage and transmission characteristics of an alpine talus. *Hydrological Processes* 25, 2954–2966.

Musselman, K. N., Clark, M. P., Liu, C., Ikeda, K., and Rasmussen, R. (2017). Slower snowmelt in a warmer world. *Nature Climate Change* 7, 214–219.

Nakicenovic, N., Alcamo, J., Grubler, A., Riahi, K., Roehrl, R. A., Rogner, H.-H., and Victor, N. (2000). *Special report on emissions scenarios (SRES), a special report of Working Group III of the intergovernmental panel on climate change*. Cambridge University Press.

Napoli, A., Crespi, A., Ragone, F., Maugeri, M., and Pasquero, C. (2019). Variability of orographic enhancement of precipitation in the Alpine region. *Scientific Reports*, 1–8.

Nash, J. E. and Sutcliffe, J. V. (1970). River flow forecasting through conceptual models part IâA discussion of principles. *Journal of Hydrology* 10, 282–290.

Noetzli, J. and Phillips, M. (2019). *Mountain permafrost hydrology - Hydro-CH2018 Project.* Tech. rep. Bern, Switzerland: WSL Institute for Snow and Avalanche Research SLF, p. 18.

Nolin, A. W. (2010). Recent advances in remote sensing of seasonal snow. *Journal of Glaciology* 56, 1141–1150.

Paniconi, C. and Putti, M. (2015). Physically based modeling in catchment hydrology at 50: Survey and outlook. *Water Resources Research* 51, 7090–7129.

Panziera, L., Gabella, M., Germann, U., and Martius, O. (2018). A 12-year radar-based climatology of daily and sub-daily extreme precipitation over the Swiss Alps. *International Journal of Climatology* 38, 3749–3769.

Parajka, J., Merz, R., and Blöschl, G. (2007). Uncertainty and multiple objective calibration in regional water balance modelling: Case study in 320 Austrian catchments. *Hydrological Processes* 21, 435–446.

Partington, D., Brunner, P., Simmons, C., Werner, A., Therrien, R., Maier, H., and Dandy, G. (2012). Evaluation of outputs from automated baseflow separation methods against simulated baseflow from a physically based, surface water-groundwater flow model. *Journal of Hydrology* 458-459, 28–39.

Partington, D., Therrien, R., Simmons, C. T., and Brunner, P. (2017). Blueprint for a coupled model of sedimentology, hydrology, and hydrogeology in streambeds. *Reviews of Geophysics* 55, 287–309.

Paul, F. and Haeberli, W. (2008). Spatial variability of glacier elevation changes in the Swiss Alps obtained from two digital elevation models. *Geophysical Research Letters* 35, 1–5.

Paul, F., Kääb, A., Maisch, M., Kellenberger, T., and Haeberli, W. (2004). Rapid disintegration of Alpine glaciers observed with satellite data. *Geophysical Research Letters* 31, 12–15.

Pauritsch, M., Wagner, T., Winkler, G., and Birk, S. (2017). Investigating groundwater flow components in an Alpine relict rock glacier (Austria) using a numerical model. *Hydrogeology Journal* 25, 371–383.

Pellicciotti, F., Bauder, A., and Parola, M. (2010). Effect of glaciers on streamflow trends in the Swiss Alps. *Water Resources Research* 46, 1–16.

Penna, D., van Meerveld, H. J., Zuecco, G., Dalla Fontana, G., and Borga, M. (2016). Hydrological response of an Alpine catchment to rainfall and snowmelt events. *Journal of Hydrology* 537, 382–397.

Penna, D., Mantese, N., Hopp, L., Dalla Fontana, G., and Borga, M. (2015). Spatio-temporal variability of piezometric response on two steep alpine hillslopes. *Hydrological Processes* 29, 198–211.

Pepin, N. et al. (2015). Elevation-dependent warming in mountain regions of the world. *Nature Climate Change* 5, 424–430.

Pourrier, J., Jourde, H., Kinnard, C., Gascoin, S., and Monnier, S. (2014). Glacier meltwater flow paths and storage in a geomorphologically complex glacial foreland: The case of the Tapado glacier, dry Andes of Chile (30°S). *Journal of Hydrology* 519, 1068–1083.

Pritchard, H. D. (2019). Asia's shrinking glaciers protect large populations from drought stress. *Nature* 569, 649–654.

Quincey, D., Klaar, M., Haines, D., Lovett, J., Pariyar, B., Gurung, G., Brown, L., Watson, C., England, M., and Evans, B. (2017). The changing water cycle: the need for an integrated assessment of the

resilience to changes in water supply in High-Mountain Asia. *Wiley Interdisciplinary Reviews: Water* 5, e1258.

Ragettli, S., Cortés, G., Mcphee, J., and Pellicciotti, F. (2014). An evaluation of approaches for modelling hydrological processes in high-elevation, glacierized Andean watersheds. *Hydrological Processes* 28, 5674–5695.

Rahman, K., Maringanti, C., Beniston, M., Widmer, F., Abbaspour, K., and Lehmann, A. (2013). Streamflow modeling in a highly managed mountainous glacier watershed using SWAT: The upper Rhone River watershed case in Switzerland. *Water Resources Management* 27, 323–339.

Rajczak, J., Pall, P., and Schär, C. (2013). Projections of extreme precipitation events in regional climate simulations for Europe and the Alpine Region. *Journal of Geophysical Research: Atmospheres* 118, 3610–3626.

Rasouli, K., Pomeroy, J. W., and Whitfield, P. H. (2019). Are the effects of vegetation and soil changes as important as climatechange impacts on hydrological processes. *Hydrology and Earth System Sciences Discussions*, 1–33.

Reynard, E. et al. (2014). Interdisciplinary assessment of complex regional water systems and their future evolution: how socioeconomic drivers can matter more than climate. *Wiley Interdisciplinary Reviews: Water* 1, 413–426.

Rinderer, M., van Meerveld, I., Stähli, M., and Seibert, J. (2016). Is groundwater response timing in a pre-alpine catchment controlled more by topography or by rainfall? *Hydrological Processes* 30, 1036–1051.

Rixen, C., Winkler, M., Bardy-durchhalter, M., Barni, E., Bjorkman, A. D., and Breiner, F. T. (2018). Accelerated increase in plant species richness on mountain summits is linked to warming. *Nature* 556, 231–234.

Robine, J. M., Cheung, S. L. K., Le Roy, S., Van Oyen, H., Griffiths, C., Michel, J. P., and Herrmann, F. R. (2008). Death toll exceeded 70,000 in Europe during the summer of 2003. *Comptes Rendus - Biologies* 331, 171–178.

Rogger, M., Chirico, G. B., Hausmann, H., Krainer, K., Brückl, E., Stadler, P., and Blöschl, G. (2017). Impact of mountain permafrost on flow path and runoff response in a high alpine catchment. *Water Resources Research* 53, 1288–1308.

Rogora, M. et al. (2018). Assessment of climate change effects on mountain ecosystems through a cross-site analysis in the Alps and Apennines. *Science of the Total Environment* 624, 1429–1442.

Roy, J. W. and Hayashi, M. (2009). Multiple, distinct groundwater flow systems of a single moraine-talus feature in an alpine watershed. *Journal of Hydrology* 373, 139–150.

Sanchez-Lorenzo, A., Enriquez-Alonso, A., Wild, M., Trentmann, J., Vicente-Serrano, S. M., Sanchez-Romero, A., Posselt, R., and Hakuba, M. Z. (2017). Trends in downward surface solar radiation from satellites and ground observations over Europe during 1983â2010. *Remote Sensing of Environment* 189, 108–117.

Schaefli, B., Nicótina, L., Imfeld, C., Da Ronco, P., Bertuzzo, E., and Rinaldo, A. (2014). SEHR-ECHO v1.0: A spatially explicit hydrologic response model for ecohydrologic applications. *Geoscientific Model Development* 7, 2733–2746.

Schaefli, B. (2016). Snow hydrology signatures for model identification within a limits-of-acceptability approach. *Hydrological Processes* 30, 4019–4035.

Schaefli, B. and Gupta, H. V. (2007). Do Nash values have value? *Hydrological Processes* 21, 2075–2080.

Schaefli, B., Hingray, B., and Musy, A. (2007). Climate change and hydropower production in the Swiss Alps: Quantification of potential impacts and related modelling uncertainties. *Hydrology and Earth System Sciences* 11, 1191–1205.

Scherrer, S. C., Fischer, E. M., Posselt, R., Liniger, M. A., Croci-Maspoli, M., and Knutti, R. (2016). Emerging trends in heavy precipitation and hot temperature extremes in Switzerland. *Journal of Geophysical Research: Atmospheres* 121, 2626–2637.

Schilling, O. S., Doherty, J., Kinzelbach, W., Wang, H., Yang, P. N., and Brunner, P. (2014). Using tree ring data as a proxy for transpiration to reduce predictive uncertainty of a model simulating groundwater-surface water-vegetation interactions. *Journal of Hydrology* 519, 2258–2271.

Schilling, O. S., Cook, P. G., and Brunner, P. (2019). Beyond classical observations in hydrogeology: the advantages of including exchange flux, temperature, tracer concentration, residence time, and soil moisture Observations in groundwater model calibration. *Reviews of Geophysics* 57, 146–182.

Schilling, O. S., Park, Y. J., Therrien, R., and Nagare, R. M. (2019). Integrated surface and subsurface hydrological modeling with snowmelt and pore water freeze–thaw. *Groundwater* 57, 63–74.

Schmieder, J., Hanzer, F., Marke, T., Garvelmann, J., Warscher, M., Kunstmann, H., and Strasser, U. (2016). The importance of snowmelt spatiotemporal variability for isotope-based hydrograph separation in a high-elevation catchment. *Hydrology and Earth System Sciences* 20, 5015–5033.

Schulla, J. (2017). *WaSiM (Water balance Simulation Model) Model Description*. Tech. rep. Zürich: Hydrology Software Consulting J. Schulla, p. 332.

SCNAT (2018). *GLAMOS 1881-2018, The Swiss Glaciers 1880-2016/17*.

Seibert, J., Vis, M. J., Lewis, E., and van Meerveld, H. J. (2018). Upper and lower benchmarks in hydrological modelling. *Hydrological Processes* 32, 1120–1125.

Shrestha, D. L., Kayastha, N., and Solomatine, D. P. (2009). A novel approach to parameter uncertainty analysis of hydrological models using neural networks. *Hydrology and Earth System Sciences* 13, 1235–1248.

Shrestha, M., Koike, T., Hirabayashi, Y., Xue, Y., Wang, L., Rasul, G., and Ahmad, B. (2015). Integrated simulation of snow and glacier melt in water and energy balance-based, distributed hydrological modeling framework at Hunza River Basin of Pakistan Karakoram region. *Journal of Geophysical Research: Atmospheres* 120, 4889–4919.

Simmons, C. T., Brunner, P., Therrien, R., and Sudicky, E. A. (2020). Commemorating the 50th anniversary of the Freeze and Harlan (1969) Blueprint for a physically-based, digitally-simulated hydrologic response model. *Journal of Hydrology* 584, 124309.

Singleton, M. J. and Moran, J. E. (2010). Dissolved noble gas and isotopic tracers reveal vulnerability of groundwater in a small, high-elevation catchment to predicted climate changes. *Water Resources Research* 46.

Smith, R. S., Moore, R. D., Weiler, M., and Jost, G. (2014). Spatial controls on groundwater response dynamics in a snowmelt-dominated montane catchment. *Hydrology and Earth System Sciences* 18, 1835–1856.

Speich, M. J. R., Zappa, M., Scherstjanoi, M., and Lischke, H. (2020). FORests and HYdrology under Climate Change in Switzerland v1.0: a spatially distributed model combining hydrology and forest dynamics. *Geoscientific Model Development* 13, 537–564.

Speich, M. J., Bernhard, L., Teuling, A. J., and Zappa, M. (2015). Application of bivariate mapping for hydrological classification and analysis of temporal change and scale effects in Switzerland. *Journal of Hydrology* 523, 804–821.

Stahl, K., Hisdal, H., Hannaford, J., Tallaksen, L. M., Van Lanen, H. A., Sauquet, E., Demuth, S., Fendekova, M., and JÌodar, J. (2010). Streamflow trends in Europe: Evidence from a dataset of near-natural catchments. *Hydrology and Earth System Sciences* 14, 2367–2382.

Staudinger, M., Stoelzle, M., Cochand, F., Seibert, J., Weiler, M., and Hunkeler, D. (2019). Your work is my boundary condition!: Challenges and approaches for a closer collaboration between hydrologists and hydrogeologists. *Journal of Hydrology* 571, 235–243.

Staudinger, M., Stoelzle, M., Seeger, S., Seibert, J., Weiler, M., and Stahl, K. (2017). Catchment water storage variation with elevation. *Hydrological Processes* 31, 2000–2015.

Stewart, I. T. (2009). Changes in snowpack and snowmelt runoff for key mountain regions. *Hydrological Processes* 23, 78–94.

Strasser, U. and Kunstmann, H. (2013). Tackling complexity in modelling mountain hydrology: Where do we stand, where do we go? *IAHS-AISH Proceedings and Reports* 360, 3–12.

Sulis, M., Paniconi, C., Rivard, C., Harvey, R., and Chaumont, D. (2011). Assessment of climate change impacts at the catchment scale with a detailed hydrological model of surface-subsurface interactions and comparison with a land surface model. *Water Resources Research* 47, 1–22.

Tague, C. and Grant, G. E. (2009). Groundwater dynamics mediate low-flow response to global warming in snow-dominated alpine regions. *Water Resources Research* 45, 1–12.

Theurillat, J.-P. and Guisan, A. (2001). Potential impact of climate change on vegetation in the European Alps: A review. *Climatic Change* 50, 77–109.

Tobin, C., Nicotina, L., Parlange, M. B., Berne, A., and Rinaldo, A. (2011). Improved interpolation of meteorological forcings for hydrologic applications in a Swiss Alpine region. *Journal of Hydrology* 401, 77–89.

Turowski, J. M., Yager, E. M., Badoux, A., Rickenmann, D., and Molnar, P. (2009). The impact of exceptional events on erosion, bedload transport and channel stability in a step-pool channel. *Earth Surface Processes and Landforms* 34, 1661–1673.

Van Vuuren, D. P., Edmonds, J. A., Kainuma, M., Riahi, K., and Weyant, J. (2011). A special issue on the RCPs. *Climatic Change* 109, 1–4.

Vincent, A., Violette, S., and Aðalgeirsdóttir, G. (2019). Groundwater in catchments headed by temperate glaciers: A review. *Earth-Science Reviews* 188, 59–76.

Vincent, C., Fischer, A., Mayer, C., Bauder, A., Galos, S. P., Funk, M., Thibert, E., Six, D., Braun, L., and Huss, M. (2017). Common climatic signal from glaciers in the European Alps over the last 50 years. *Geophysical Research Letters* 44, 1376–1383.

Viviroli, D., Dürr, H. H., Messerli, B., Meybeck, M., and Weingartner, R. (2007). Mountains of the world, water towers for humanity: Typology, mapping, and global significance. *Water Resources Research* 43, 1–13.

Viviroli, D., Zappa, M., Gurtz, J., and Weingartner, R. (2009). An introduction to the hydrological modelling system PREVAH and its pre- and post-processing-tools. *Environmental Modelling & Software* 24, 1209–1222.

Viviroli, D. et al. (2011). Climate change and mountain water resources: overview and recommendations for research, management and policy. *Hydrology and Earth System Sciences* 15, 471–504.

Von Gunten, D., Wöhling, T., Haslauer, C., Merchán, D., Causapé, J., and Cirpka, O. A. (2014). Efficient calibration of a distributed pde-based hydrological model using grid coarsening. *Journal of Hydrology* 519, 3290–3304.

Vuille, M. et al. (2018). Rapid decline of snow and ice in the tropical Andes – Impacts, uncertainties and challenges ahead. *Earth-Science Reviews* 176, 195–213.

Wagner, T., Themeßl, M., Schüppel, A., Gobiet, A., Stigler, H., and Birk, S. (2017). Impacts of climate change on stream flow and hydro power generation in the Alpine region. *Environmental Earth Sciences* 76, 4.

Walvoord, M. A. and Kurylyk, B. L. (2016). Hydrologic impacts of thawing permafrost – a review. *Vadose Zone Journal* 15, 0.

Wang, H., Tetzlaff, D., and Soulsby, C. (2018). Modelling the effects of land cover and climate change on soil water partitioning in a boreal headwater catchment. *Journal of Hydrology* 558, 520–531.

Warscher, M., Strasser, U., Kraller, G., Marke, T., Franz, H., and Kunstmann, H. (2013). Performance of complex snow cover descriptions in a distributed hydrological model system: A case study for the high Alpine terrain of the Berchtesgaden Alps. *Water Resources Research* 49, 2619–2637.

Weiler, M., Seibert, J., and Stahl, K. (2018). Magic components-why quantifying rain, snowmelt, and icemelt in river discharge is not easy. *Hydrological Processes* 32, 160–166.

Welch, L. A. and Allen, D. M. (2014). Hydraulic conductivity characteristics in mountains and implications for conceptualizing bedrock groundwater flow. *Hydrogeology Journal* 22, 1003–1026.

Wever, N., Comola, F., Bavay, M., and Lehning, M. (2017). Simulating the influence of snow surface processes on soil moisture dynamics and streamflow generation in an alpine catchment. *Hydrology and Earth System Sciences* 21, 4053–4071.

WGMS (2019). *Fluctuations of Glaciers Database*. URL: http://dx.doi.org/10.5904/wgms-fog-2019-12.

Williams, M. W., Hood, E., Molotch, N. P., Caine, N., Cowie, R., and Liu, F. (2015). The 'teflon basin' myth: hydrology and hydrochemistry of a seasonally snow-covered catchment. *Plant Ecology and Diversity* 8, 639–661.

Winkler, G., Wagner, T., Pauritsch, M., Birk, S., Kellerer-Pirklbauer, A., Benischke, R., Leis, A., Morawetz, R., Schreilechner, M. G., and Hergarten, S. (2016). Identification and assessment of groundwater flow and storage components of the relict Schöneben Rock Glacier, Niedere Tauern Range, Eastern Alps (Austria). *Hydrogeology Journal* 24, 937–953.

Zekollari, H., Huss, M., and Farinotti, D. (2019). Modelling the future evolution of glaciers in the European Alps under the EURO-CORDEX RCM ensemble. *The Cryosphere* 13, 1125–1146.

Zhang, Q., Knowles, J. F., Barnes, R. T., Cowie, R. M., Rock, N., and Williams, M. W. (2018). Surface and subsurface water contributions to streamflow from a mesoscale watershed in complex mountain terrain. *Hydrological Processes*.

Zubler, E. M., Fischer, A. M., Liniger, M. A., Croci-Maspoli, M., Scherrer, S. C., and Appenzeller, C. (2014). Localized climate change scenarios of mean temperature and precipitation over Switzerland. *Climatic Change* 125, 237–252.

Zuecco, G., Rinderer, M., Penna, D., Borga, M., and van Meerveld, H. (2019). Quantification of subsurface hydrologic connectivity in four headwater catchments using graph theory. *Science of The Total Environment* 646, 1265–1280.

Zurbriggen, N., Nabel, J. E., Teich, M., Bebi, P., and Lischke, H. (2014). Explicit avalanche-forest feedback simulations improve the performance of a coupled avalanche-forest model. *Ecological Complexity* 17, 56–66.

2 | Developing a 3D model of bedrock geology in a topographically and structurally complex Alpine region

A version of this chapter has been published as:

Thornton, J. M., Mariethoz, G., and Brunner, P. (2018). A 3D geological model of a structurally complex alpine region as a basis for interdisciplinary research. *Scientific Data* 5, 1–20. doi: 10.1038/sdata.2018.238

Photograph: *The famous folds in the Cretaceous strata of the Petite Dent de Morcles*

"A general problem with the modelling of flow in mountainous regions arises from the geometric complexity of the system"

(Gárfias, 2009)

Abstract

Across a substantial proportion of the European Alps, sedimentary sequences comprised predominantly of limestones, shales, and marls have been folded and faulted into complex geometrical arrangements. Due to the strong contrasts in hydraulic properties throughout these sequences, the geometries can strongly influence hydrological processes. 3D geological models can improve conceptual understanding of subsurface flow pathways in such systems and form a basis for subsequent numerical flow simulations. However, they must be detailed enough to represent hydrologically important features, and spatially extensive enough to capture subsurface connections. Additionally, their resolution must enable the reproduction of thin or complex geometries. Despite the availability of appropriate input data and increasingly capable software, meeting these demands remains challenging. In this context, a dataset characterising subsurface geometries of formations comprising a section of the Nappe de Morcles – a large recumbent fold in the Swiss Alps – was developed using the GeoModeller software. The locations of the interfaces between lithological formations and their spatial orientations were firstly extracted from existing sources. Then, using state-of-the-art algorithms, the interfaces were interpolated. Finally, an iterative process of evaluation and re-interpolation was undertaken. The geology was concluded to have been satisfactorily reproduced; modelled interfaces correspond well with input data, and the estimated volumes beyond these locations seem geologically plausible. The resultant model represents 18 distinct formations, and covers an area of 9.6×13.4 km. The data are provided in a raw voxel format (10 m resolution) and as surfaces for visualisation in open-source software. As far as is known, this model is the most detailed such model of a section of the Alps yet presented. Going forward, it will contribute to the parameterisation of physically-based numerical simulations integrating snow dynamics, surface-water flow, groundwater flow, and evapotranspiration to assess the holistic response of alpine hydrological systems to climatic change. Overall, this contribution demonstrates the potential that now exists develop complex geological models in support of contemporary Alpine research, adding value to traditional geological information in the process.

2.1 Introduction

Three-dimensional (3D) geological models are digital representations of subsurface formations and their associated features. Recently, the appreciation of their utility to several disciplines has grown, and software tools enabling their construction have proliferated (Jones et al., 2009). In earth sciences and engineering, they have, *inter alia*, contributed to the development of improved earthquake location catalogues (Béthoux et al., 2016) and informed excavation and tunnelling projects (Bistacchi et al., 2008; Vanneschi et al., 2014). They are also supporting ongoing radioactive waste storage site assessments (Mont Terri Project, n.d.). In hydrogeology, meanwhile, they have facilitated groundwater resource estimates (Hassen et al., 2016), enabled the characterisation of karst aquifer geometries, flow pathways, and catchment areas (Jeannin et al., 2013; Ballesteros et al., 2015; Malard et al., 2015; Turk et al., 2015), and provided a basis for numerical modelling related to geothermal energy prospection (Guglielmetti et al., 2013).

In tectonically and topographically complex sedimentary settings like the European Alps, 3D models must be generally detailed, high-resolution, and accurate in order to be suitable for their intended application(s). The term detailed refers to the representation of certain characteristic features which, here, would include folds, faults, and spatially-variable formation thicknesses. Developing a model with high spatial resolution, meanwhile, might involve employing a fine (e.g. cell size $\leqslant$10 m) Digital Terrain Model (DTM) to define the topographic surface, and/or using a sufficient density of georeferenced points to closely replicate the shapes of observed geological features. When exporting a model onto a grid or mesh, care must be exercised to ensure that the resolution is commensurate with the modelled features, especially thin layers or complex shapes. Finally, a model can be considered accurate if the estimated formations and associated features are close to their true positions (although the true positions may be impossible to establish perfectly).

Approximately 30% of the Alps are composed of carbonate rocks, the majority of which are karstified (i.e. discrete conduit networks have developed via dissolution) (Goldscheider, 2005). However, these rocks are not uniform in their chemico-mineralogical composition, and hence their degree of karstification. Moreover, they are commonly interspersed with lower permeability layers, such as marls and shales, as illustrated by Figure 2.1a. The entire sequences have been folded, fractured, and faulted into complex geometrical arrangements by tectonic forces. Since well-karstified limestones are several orders of magnitude more permeable than marls and shales, the contrasts in hydraulic conductivity within these sequences can be considerable. Where so, the stratigraphic geometry exerts a profound influence on groundwater flow patterns

(Jeannin et al., 2013). For example, in a karstified limestone aquifer overlying a marly aquiclude, flow would typically be concentrated just above the interface, its direction corresponding to that of the maximum dip, i.e. flow would be broadly parallel to the strata (and so highly anisotropic) (Figure 2.1b). It follows that in folded settings, anticlines – assuming normal orientation – typically act as regional groundwater divides, with synclines conversely representing locations of accumulation (Goldscheider and Andreo, 2007). Faults can also have a notable influence (Herold et al., 2000); on one hand they may act as preferential pathway permitting flow across the strata, including enabling formations that would otherwise be considered aquicludes to be bypassed, but on the other, their offsets can disconnect aquifers.

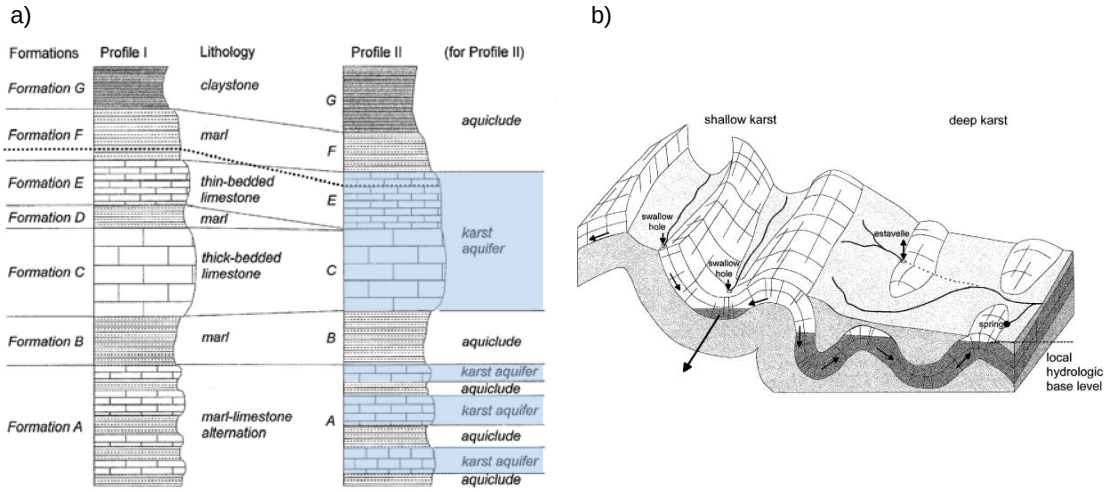

Figure 2.1: An illustration of the combined stratigraphic and geometrical influence on groundwater flow in calcareous Alpine regions: a) the typical sequence of limestones, shales, and marls, and b) the influence of aquitard geometry on regional groundwater flow patterns in such terrain. Source: Goldscheider and Andreo (2007).

As such, considering 3D geology is crucial when conceptualising and seeking to simulate groundwater flow in these environments (e.g. Ofterdinger et al., 2014). 3D geological models are considerably more powerful with respect to the development, visualisation, and communication of geological understanding than traditional 2D maps and cross-sections. They also provide a direct foundation for subsequent (3D) numerical flow modelling. However, for applications in topographically complex and potentially karstified limestone terrain, geological models must meet several criteria. Firstly, subsurface features that can affect flow must be accurately characterised. Secondly, to provide a realistic overall depiction, the topographic surface must be represented at high resolution. Finally, models must be spatially extensive enough to capture any proven or hypothesised subsurface connections; such connections can function over distances of

up to several kilometres, and are capable of importing or exporting water across topographical boundaries.

Despite the improving capabilities of 3D modelling software and a large body of existing geological data pertaining to the Alps, these combined requirements (for geological models to be detailed, high- resolution, accurate, and spatially-extensive) continue to represent substantial technical and computational challenges to model development. One important reason for this is that the available software packages are oriented towards basin analysis for the oil industry, and hence are poorly suited to the representation of the complex geological structures that are prevalent in alpine areas (Guerin et al., 2015). It is therefore unsurprising that, irrespective of intended application, few such geological models exist in the Alps; those that do are generally very large in scale, and therefore limited in detail (Schreiber et al., 2010; Sue et al., 2010; Vouillamoz et al., 2012), although there are exceptions in this regard (Zanchi et al., 2009).

Furthermore, and datasets that are developed are rarely made available as to the broad, interdisciplinary community who could potentially benefit from them. As such, lack of 3D geological data in such regions may be posited as one important factor that is hampering movement away from highly conceptual hydrological modelling approaches towards more advanced ones with a view to better understanding the hydrological functioning of complex alpine catchments under both present and plausible future conditions; certainly a choice of 3D groundwater and integrated-surface subsurface codes that are capable of ingesting 3D geological information are now at the ready, as was explained in Chapter 1.

In this context, a novel dataset characterising a section of a well-studied nappe fold in the Swiss Alps is presented. No 3D geological model of this complex region previously existed, and it was unclear at the outset whether developing an appropriate model was even feasible. Alongside information from various other disciplines, the outcome is taken forward in subsequent chapters to inform a catchment scale, integrated hydrological model. Various other ongoing or future interdisciplinary environmental investigations could also benefit from the development.

2.2 Methods

2.2.1 Study area

2.2.1.1 Geological context

The Nappe de Morcles is a renowned example of a tectonic nappe fold. It has an amplitude exceeding 10 km and possesses a prominent inverse limb whose stratigraphy is completely reversed. It is the lowest of several such tectonic entities that strike to the SW–NE and together comprise the Helvetic Nappes (Figure 2.2). The nappe sits above a region of autochthonous and parautochthonous material which, in turn, overlies the crystalline Aiguilles Rouges massif. It is composed primarily of calcareous shelf sediments (i.e. limestones, marls, shales, and sandstones) of Jurrassic to Paleogene age.

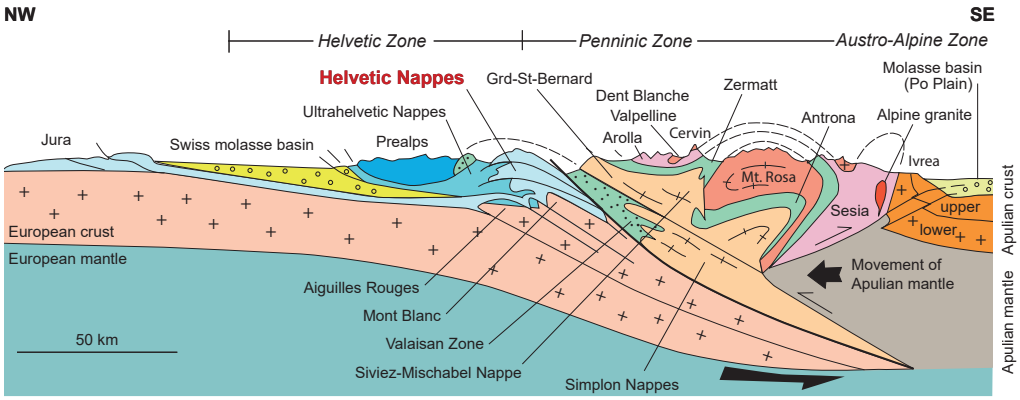

Figure 2.2: A profile through the European Alps showing the situation of the Helvetic Nappes. The Nappe de Morcles, which is the focus of this work, is the lowermost of the three nappes. Source: modified after Renard et al. (2015), © Dunod, 2015.

A series of notable works established and refined knowledge of the nappe's structure (Argand, 1916; Lugeon and Argand, 1937; Lugeon, 1940; Badoux, 1971; Badoux, 1972; Ramsay, 1981; Badoux and Gabus, 1991; Escher et al., 1993; Pfiffner, 1993). In summary, the main fold axis plunges 27° on average towards the NE (Badoux, 1991). Several secondary folds are superimposed upon the main structure, forming a characteristic "oak leaf" pattern. Faults of potential hydrological relevance in the focus region are generally oriented E-W, although their extents are limited. No relevant thrust surfaces are present in this zone. The region remains an important focus for nappe fold formation studies (Bauville et al., 2013; von Tscharner et al., 2016).

2.2.1.2 General characteristics of the focus area

The geological model domain was centred on two adjoining headwater catchments in the western Swiss Alps – the Vallon de Nant and the Vallon de la Vare – that had already been identified as the focus for subsequent hydrological model development. These valleys lie within the north-western section of the Nappe de Morcles (Figure 2.3). More specifically, the Vallon de Nant has been incised from the inverse zone of the nappe, whilst the Vallon de La Vare lies in the frontal zone. For reasons that shall be explained shortly, the focus area was extended to the southeast to include La Sarvaz spring.

The elevation range within the focus area is considerable (around 2,500 m), and precipitation abundant (annual average $\sim$1600 mm·yr^{-1} in the lowest reaches, increasing with elevation). Low winter temperatures result in a significant proportion of the annual precipitation falling as snow (Dutoit, 1983), and small glaciers are able to persist at relatively low elevations in the uppermost parts. Considerable diversity is encountered with respect to vegetation, geomorphology, and hydrology. The area has remained practically untouched by anthropogenic activity; indeed, the Vallon de Nant has been a natural reserve since 1969. Overall, the area represents an ideal "natural laboratory" for research across the environmental sciences (von Däniken et al., 2014).

The first stage of the geological model development involved establishing the spatial domains (see Figure 2.3). Formations belonging to the other Helvetic Nappes or the Ultrahelvetic zone were excluded from the model to keep the degree of complexity manageable.

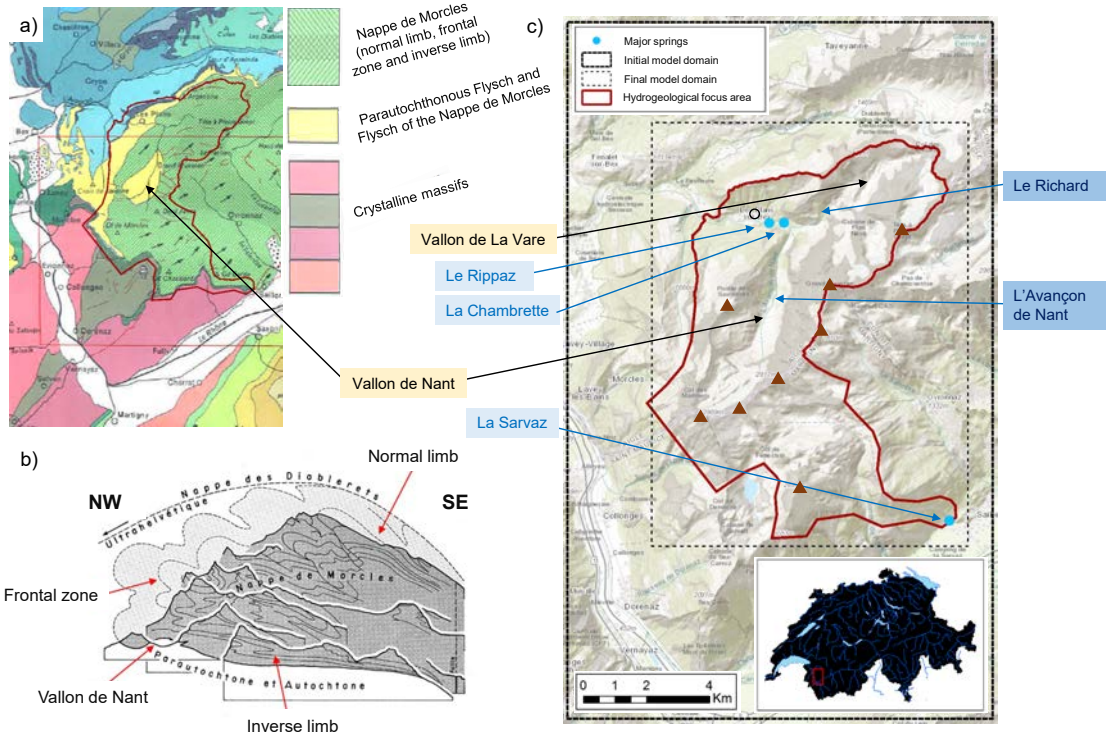

Figure 2.3: Geological overview of the study area, including: a) A tectonic sketch indicating the general geological situation (reproduced from Badoux, 1971, non-digital version, © Source: Swiss Federal Office of Topography, 1971), b) An illustrative cross-section through the Nappe de Morcles showing its pre-erosion structure, including secondary folds, and the present topographic arrangement (reproduced from Badoux, 1971, © Source: Swiss Federal Office of Topography, 1971), and c) The "original" and "final" geological model domains that were defined, major springs locations, and the area of hydrogeological interest (the so-called "focus area") (original figure). Selected mountain peaks are also marked (brown triangles); starting from the north and proceeding clockwise, these are: Tête à Pierre Grept (2,904 m), Grand Muveran (3,051 m), Petit Muveran (2,810 m), Grand Chavalard (2,899 m), Dent Favre (2,917 m), Grand Dent de Morcles (2,969 m), Petit Dent de Morcles (2,929 m) and Point des Savolaires (2,294 m). Finally, the village of Les Plans-sur-Bex (hollow black circle) is also indicated.

2.2.1.3 Stratigraphy and initial hydrogeological inferences

A sketch of the stratigraphy in the area of the Vallon de Nant, modified after Badoux (1991) (Figure 2.4), provides a useful introduction to the regional geology. (Note that this diagram does not include all the formations that were eventually modelled; for that, consult Table 2.2).

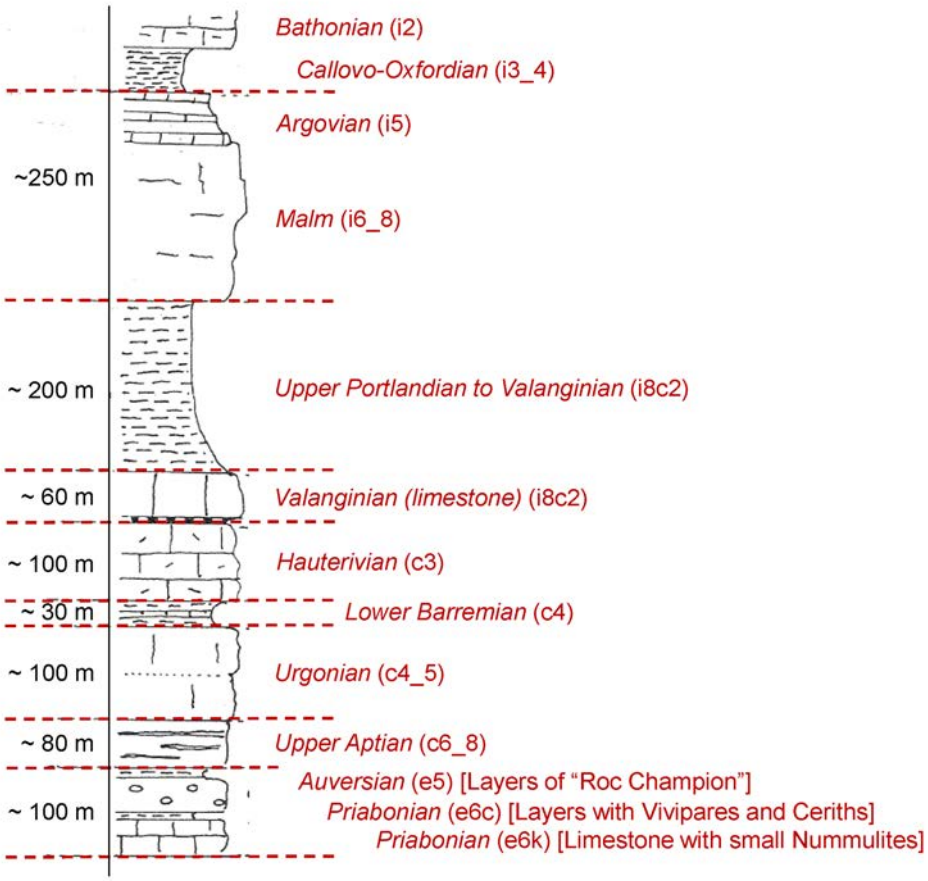

Figure 2.4: Sketch of the stratigraphy in the region of the Vallon de Nant. This figure is modified after Badoux (1991). Note that the sequence is represented as it is observed in this section of the nappe, i.e. is inverted, with the oldest formations above the younger ones.

The 1:25,000 scale geological maps of "Morcles" (Badoux, 1971) and "Les Diablerets" (Badoux and Gabus, 1991) represented the primary sources of detailed geological information, however. The lithological descriptions provided in the accompanying explanatory notes enabled the likely hydrogeological importance of certain formations to be established. Previous studies conducted on neighbouring or nearby tectonic units where equivalent formations are encountered (Goldscheider, 2005; Gremaud et al., 2009) further elucidated the probable hydrostratigraphy.

Few hydrological or hydrogeological investigations have previously been conducted in the study area. The karstic spring of La Chambrette, which emerges above the northern bank of L'Avançon de Nant near the village of Les Plans-sur-Bex, was, however, the subject of an early artificial tracer test (Lugeon and Gagnebin, 1928). This experiment demonstrated the existence of a hydrological connection between the closed basin of "La Varre" and the spring. Since these two locations are separated by the Lower Barremian – a formation that should, as mentioned above – be rather impermeable according to its lithology, it was proposed that a fault of some description must enable flow to traverse it. Today, the spring is exploited by Romande Energie SA.

Another spring, Le Rippaz, is no longer karstic by the time it emerges rather diffusely from Quaternary moraines, a little downstream from La Chambrette on the opposite (southern) bank of L'Avançon. Currently, it is being developed to augment the water supply of a neighbouring commune (Municipalite d'Ollon, 2014; Municipalite d'Ollon, 2015). An associated tracer test confirmed that the formations of the Lower Cretaceous near Pointe des Savolaires constitute the main karstic aquifer. This system could thus be thought of as a chain of aquifers – first karstic and then unconsolidated gravel – which together dampen the variability of spring discharge to snowmelt and rainfall inputs. Finally, as mentioned earlier, the focus area was extended several kilometres to the southeast to include La Sarvaz; another, higher discharge karstic spring that emerges near the village of Saillon, Valais. This decision was taken because, according to initial understanding of the geological structure and likely favourable hydraulic properties – specifically of the Malm – some the precipitation falling on the southern and eastern ridges of the Vallon de Nant may ultimately drain to this location, rather than via L'Avançon de Nant. Additionally, the discharge of La Sarvaz has been monitored for several years, providing observations that could prove useful during hydrological model development.

One aspect of the regional geology that remains somewhat unclear is the extent to which the various theoretically karstfiable formations are actually karstified at this site. The only known speleological exploration in the region returned an inventory of only six small caves (Perrin, 1993), although this exploration was neither systematic nor exhaustive. The walls of the Urgonian limestone near Pointe des Savolaires were reported to be the only limestones pure enough to contain cavities of speleological interest (ibid.). However, while the presence of caves is an unambiguous indicator of karstification, the inverse is not true; an absence (or non-discovery) of explorable caves certainly does not necessarily indicate an absence of hydrologically meaningful karstification, since conduits much smaller than humanly accessible can still transport significant volumes of water extremely rapidly. Nevertheless, it should be remembered that flowing water is required for conduit development; if a theoretically karstifiable limestone has been disconnected

from recharge or circulation by low permeability layers, it may remain little karstified.

Although the conclusions of this speleological prospection broadly concord with hydrogeological expectations drawn from the lithological descriptions, they do highlight the issue of chemio-mineralogical purity, and more specifically the possibility that the degree of karstification in this study area may not be as high as elsewhere in the Helevetic zone. In any case, a benefit of the approach taken – of only estimating formation geometries initially – is that in contrast to the methodology followed by other authors (Ballesteros et al., 2015; Turk et al., 2015), there is no need to definitively categorise each formation as being either an aquifer or aquiclude initially; reality is certainly not this binary. Rather, the intention is to vary and hopefully constrain parameters corresponding to the hydraulic properties of the various formations during subsequent numerical model calibration.

Finally, aquifers are not confined to bedrock formations, of course. Glacio-fluvial and other sediments (e.g. talus cones) fill the valley floors. It is expected that the recharge of these units (where permeable) is dominated by spring snowmelt, with drainage subsequently taking place over the course of the late spring, summer, and autumn via a number of springs and ephemeral "seeps". The geological model presented herein does not include these unconsolidated formations, focussing instead on the more voluminous bedrock. That said, geoelectrical surveys will be undertaken shortly with a view to representing the geometry and heterogeneity of unconsolidated material properties in the integrated hydrological model.

2.2.1.4 Surface hydrology and its possible association with bedrock geology

The surface hydrology of the Vallon de Nant is characterised by the eponymous Nants; the torrents that course down its steep slopes. They are located principally to the south and east, and have a highly variable flow that responds rapidly to rainfall and snow and ice melt. The most important are the Nant des Têtes and the Torrent des Martinets, which together constitute the majority of the discharge of L'Avançon. The torrents are also responsible for a great deal of sediment transport; these deposits accumulate to form a large alluvial fan in the middle section of the valley. The annual hydrological regime of L'Avançon de Nant may be classified as nivo-glacial (Aschwanden and Weingartner, 1985); that is to say, it has a mixed snow and ice-dominated response with a discharge peak in early summer corresponding to melt of the snowpack, variable discharges from one year to another, diurnal cycles superimposed on the hydrograph due to ice melt, and groundwater contributions which maintain baseflow.

Surface water is noticeably scarcer in the upper part of the Vallon de La Vare than the Vallon de Nant, although a small stream – Le Richard – does develop and joins L'Avançon downstream of Pont de Nant. This contrast between the two valleys can probably be explained by differences in their position in the nappe. Specifically, the Vallon de Nant is underlain by low-permeability flysch, which limits groundwater exportation and permits the existence of a relatively long section of permanent stream (it is only ephemeral in the upper section in dry, cold autumn and winter periods, when the groundwater level in this upper section has fallen such that it can no longer contribute to streamflow). The presence of a clay-rich layer of glacial till at some intermediate depth between the surface and bedrock interface may also contribute to this behaviour, although this hypothesis remains to be tested by geophysics. In contrast, the Vallon de La Vare lies in the inverse zone, and thus the impermeable flysch is oriented approximately vertically away to the north, near L'Argentine. Hence, the bedrock beneath the valley floor is composed of the more permeable limestones of the Lower Cretaceous. One aim of the 3D model is to help visualise and better understood such influences. Additionally, having two somewhat geologically contrasting catchments adjacent to one another provides the opportunity to explore the specific influences of geology on hydrology whilst other factors, including climate, remain fairly constant.

2.2.2 Input data

A wealth of geological information pertaining to the European Alps exists, having been developed over decades of dedicated study by committed regional experts. Presently, this information exists primarily in the form of two-dimensional (2D) maps and cross-sectional diagrams. Despite observational advances in most other fields of the geosciences, the field mapping techniques and concepts underpinning the production of such structural geology datasets have changed little in over a century (Coe et al., 2010). As such, their quality remains similar to more contemporary outputs. Moreover, the prevalence of observable features such as stratigraphic interfaces, faults, and folds mean that such datasets are typically more accurate in mountainous regions than in settings where the bedrock is more obscured by unconsolidated deposits (Zanchi et al., 2009). Indeed, the deep incision made by the Vallon de Nant into the inverse limb of the nappe can be thought of as a kind of "window" into its interior – a visible cross-section. Certainly, the availability of appropriate geological data should rarely be a limiting factor for the development of 3D models in the Alps, although the arguable under-exploitation of the existing body of information means it might have been hitherto.

As already mentioned, thanks to its reputation as a classic example of a first-order nappe and intriguing attendant complexity, the structural geology of the region has a long history of being

studied and mapped. At this juncture, it is worth briefly highlighting the effort that the production of the maps, cross-sections, and associated explanatory notes that comprise the current Geological Atlas of Switzerland in this region entailed. In the introductory remarks to his illustrated text *Tectonics of the Morcles Nappe between Rhône and Lizerne*, Badoux states that the work undertaken prior to the publication of the second edition maps took 8 years! (Badoux, 1972). By this time, under the tutelage of Lugeon, he had already developed a great passion for, and expertise on, the geology of the Vaud Alps. These maps remain the highest resolution, most current geological dataset of the Swiss Confederation in this region.

As Table 2.1 indicates, input data for the model were derived from three primary sources: i) a Digital Terrain Model (DTM), ii) surface geological maps, and iii) vertical geological cross-sectional diagrams.

2.2.3 Workflow

Having gained an appreciation of the study area and identified and sourced appropriate input data pertaining to it, several sequential steps were followed in order to develop the geological model (Figure 2.5). In summary, data extracted from existing geological maps and vertical cross-sections were compiled along with a digital terrain model (DTM) in the GeoModeller software environment (Intrepid Geophysics, 2013). GeoModeller is a commercial platform developed by the BRGM (French Geological Survey) and Intrepid Geophysics; for further information, see Calcagno et al. (2008) and Guillen et al. (2008). It facilitates the estimation of continuous geological models that respect all available data indicating the locations of interfaces between different lithological formations, the spatial orientations of these formations, and any faults present in the domain. Certain geological rules are also taken into account. The following sections describe each phase in more detail.

Data type	Name	Author / owner	Key characteristics	Format
Digital Terrain Model (DTM)	swissALTI^{3D}	swisstopo	2 m native spatial resolution, vertical uncertainty ± 0.5 m < 2000 m, $\pm 1 - 3$ m > 2000 m	Raster (.asc)
Surface geological maps	GeoCover (Sheet 58 "Morcles")	swisstopo	1:25,000, shows formation interfaces, orientations (dip and dip direction), and faults	Vector (.shp) (pre-digitised from paper maps)
	GeoCover (Sheet 88 "Les Diablerets")	swisstopo	1:25,000, shows formation interfaces, orientations (dip and dip direction), and faults	Vector (.shp) (pre-digitised from paper maps)
Vertical geological cross-sections	Explanatory booklet of Sheet 58 "Morcles"	Badoux (1971) (swisstopo)	Series of "stacked" cross-sections showing interpreted formation interfaces (start and end points un-georeferenced)	Images in .pdf document
	Explanatory booklet of Sheet 88 "Les Diablerets"	Badoux and Gabus (1991) (swisstopo)	Series of "stacked" cross-sections showing interpreted formation interfaces (start and end points georeferenced)	Images in .pdf document

Table 2.1: Input datasets for the development of the geological model. The lack of anthropogenic exploitation of the remote and protected study area means that no boreholes extending to the bedrock existed.

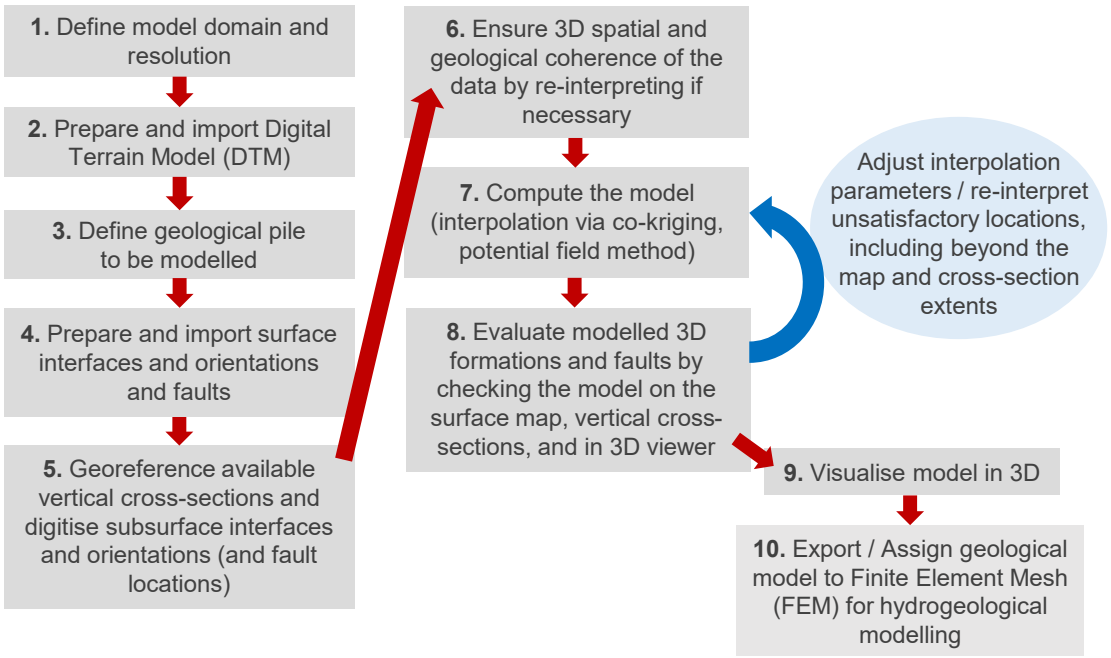

Figure 2.5: The workflow followed to develop the 3D geological model. Steps 7 and 8 involved an iterative process of comparing the model to the input data on both the surface and vertical sections, adjusting the interpolation parameters and/or the input data density, re-computing the model, and re-comparing with the input data.

2.2.3.1 Defining the model domain and resolution

Studying the regional geology and hydrogeology enabled the initial and final domains for the geological model development to be established (Figure 2.3). The initial model domain was slightly larger than the final one to ensure that all data that could potentially inform the geological model in the smaller focus area were included in the estimation. In light of the complex topography and prior knowledge of the presence of geometrically complex and thin units, it was decided that the model development should proceed at a resolution of 10 m.

2.2.3.2 Preparing and importing the Digital Terrain Model

The swissALTI^{3D} digital terrain model (DTM) is a raster dataset with a horizontal cell resolution of 2 m. It represents the land surface without vegetation or buildings (swisstopo). The vertical uncertainties associated with the product, quoted in Table 2.1, are more than low enough for the application at hand. For the purpose of model development, the dataset was resampled to 10 m. This resampling served to smooth out high-frequency noise (i.e. small-scale topographic features) and reduce the computational burden. The resultant dataset was imported into

GeoModeller (Figure 2.6). It forms the upper surface of the geological model.

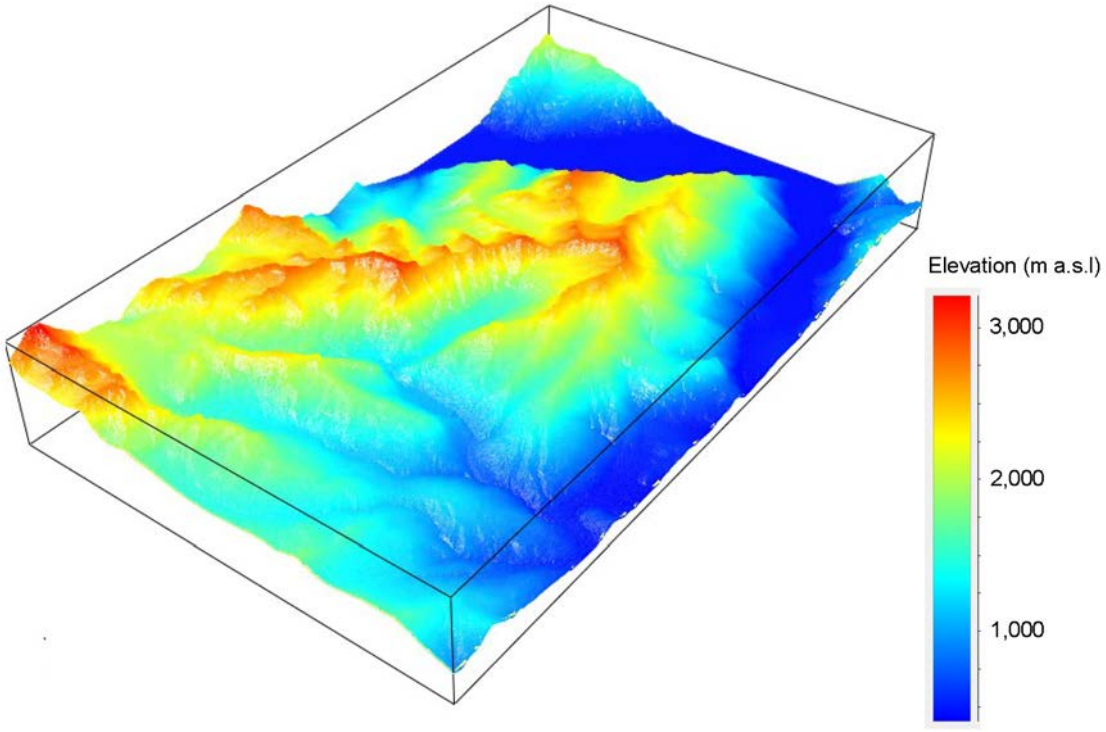

Figure 2.6: Topographic surface of the geological model. This surface was defined according to the resampled incoming Digital Elevation Model (DTM) (10 m resolution), and visualised in the GeoModeller interface. Here, the view is towards the southeast.

2.2.3.3 Establishing the "geological pile"

The term geological pile refers to the sequence of lithological formations to be modelled. Since the domain extends over two separate geological map sheets, each having a slightly different formation classification scheme, some reconciliation was required to arrive at a single sequence. In the end, the sequence modelled was extremely similar to that of the Morcles map sheet. Given the potential multi-disciplinary applications of the dataset, maintaining a classification that closely resembled that of the map legends was considered preferable to grouping any formations *a priori*. Of course, should further simplification be required for a particular end use, the formations represented in the output dataset can be grouped later.

2.2.3.4 Preparing and importing surface interface data, orientation data, and faults

Two types of surficial geological data from the relevant map sheets (Badoux, 1971; Badoux and Gabus, 1991) were obtained in digital format (Figure 2.7). These were: i) polylines formed by joined points indicating the locations of the interfaces between the formations of the geological pile which outcrop at the surface (also known as "contacts"), and ii) point features describing the orientation of these formations at certain locations on the surface (also known as "structural data"). Where necessary, interface polylines were reattributed to match the formations defined in the geological pile. Whilst taking care to maintain their shapes, they were also simplified to reduce the number of vertices. This spatial data processing was conducted using the open source software QGIS. The processed polylines were then imported into GeoModeller. Given the complexity and number of interface shapes in the study region, this approach was more efficient than the more common practice of importing a pre-georeferenced image of a geological map into GeoModeller and then manually digitising the surface formation interfaces in that software environment. In locations where it was clear that a given boundary was continuous beneath the Quaternary cover (and hence was not actually defined) but the location of the boundary could be easily estimated, additional points were inserted. In certain other locations, bedrock interfaces completely obscured by the surficial cover could not be estimated. The consequent data gaps represent a source of uncertainty in the final model (which proposes continuous boundaries as a result of the interpolation).

The orientation points were attributed to formations of the geological pile by means of spatial intersection. Some surface orientation data points that fell between vertical cross-sections in the heavily folded frontal zone had to be discarded because at these locations, the polarities/younging directions (i.e. whether normal or overturned) could not be confidently determined.

Faults with offsets that were believed large enough to potentially disconnect aquifers, numbering 10 in total, were explicitly represented. Firstly, their surface extents were digitised and imported into GeoModeller. The trace of only one of these faults appeared on a vertical cross-section; the shape of this one was therefore be digitised in the vertical plane also. The remainder were assumed to be vertical in the absence of any other orientation information. Finally, since all faults are shown by the existing geological maps to be finite, which is to say that they do not extend across the entire domain, it was necessary to estimate an "ellipsoid of influence" for each. Faults with more limited offsets, which are not represented, could still be responsible for

preferential hydrological flow pathways; an effect that could be represented in any subsequent hydrogeological modelling by prescribing discrete fractures, or by treating the corresponding volumes as having dual permeability.

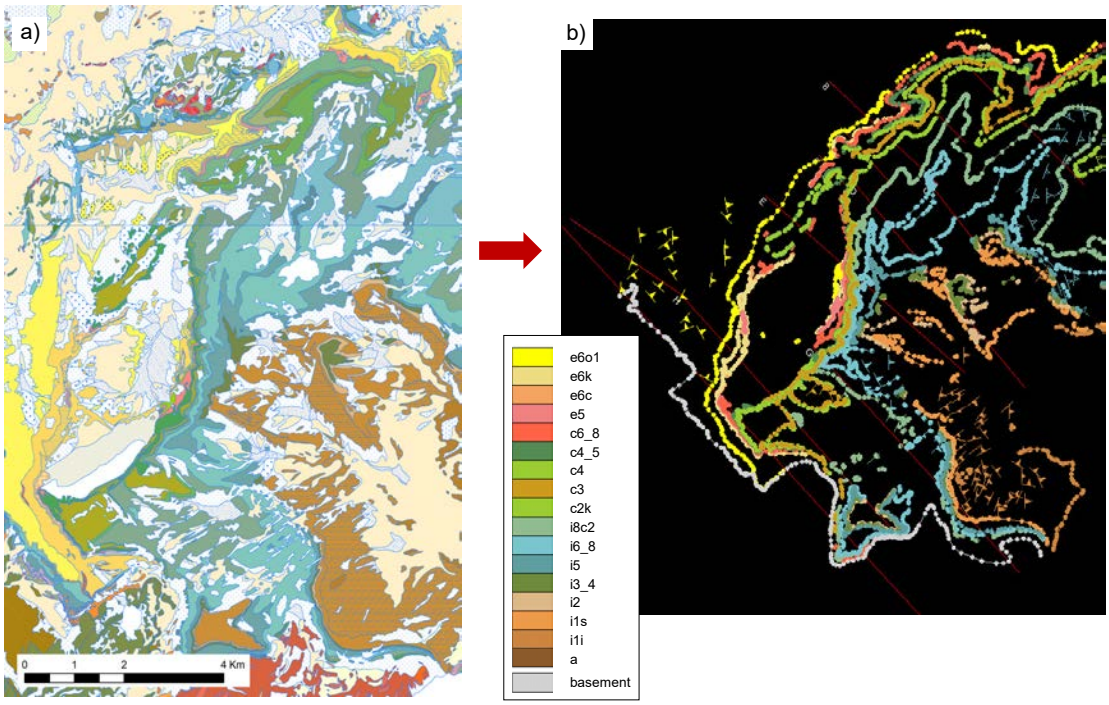

Figure 2.7: Extraction of the surface geological input data. Georeferenced point features (formation interface locations and marked structural data) a) extracted from the surface map (Badoux, 1971; Badoux and Gabus, 1991, Source: © Swiss Federal Office of Topography, 1971, 1991) and b) imported into the GeoModeller interface. The legend refers to the coding of the formations of the stratigraphic pile. Circles indicate interface points, and arrows indicate orientations. Note that since the DTM had already been imported, these points were in fact located in 3D and not only 2D space (i.e. they could be associated with a z-value).

2.2.3.5 Georeferencing vertical cross-sections, and digitising subsurface interfaces and orientations

The "stacked" vertical cross-sections (Badoux, 1971; Badoux and Gabus, 1991) (Figure 2.8a) provide interpretations of the subsurface structures. Including such information in the estimation of model was crucial because the non-stationarity of the domain, which arises due to the pronounced folding and faulting, precludes the straightforward extrapolation of surface observations into the subsurface. Prior to being imported into GeoModeller, the diagrams were cropped and the cross-section start and end locations georeferenced (Figure 2.8b). For each cross-section,

the correspondence between the topographic surface profiles in the GeoModeller environment (i.e. the profile of the DTM between the georeferenced cross-section start and end points) and the representation of the topography on the georeferenced diagram was assessed (refer to the red line in Figure 2.8c). The close matches observed provided confidence that both the georeferencing of the cross-section diagrams and the original representation of the topography along the sections were satisfactory. The lengthy task of manually digitising the subsurface formation interfaces illustrated on the cross-sections, and their associated orientations, was then undertaken. In this process, the interface surfaces were assumed orthogonal to the section plane, i.e. the dip direction is parallel to the section, with dip angles estimated at regular intervals along each interface according to the angles formed with the horizontal plane. Due to the plunge of the axis of the main nappe structure, the subsurface dip and dip directions resulting from this assumption may not be entirely correct in all instances. However, the approach taken was the only practical way in which some subsurface orientation data could be included, which in turn was absolutely necessary to successfully model the region. This assumption is not expected to have any implications for the utility of the model for hydrological and other environmental applications. In total, 11 cross-sections distributed throughout the domain contributed to the model.

Following the completion of Steps 4 and 5, the surface and subsurface interface and orientation points could be visualised in 3D and their consistency with one another verified and, where necessarily, improved (Step 6). Figure 2.9 shows the final arrangement of digitised formation interfaces (both surface and subsurface) that were taken into account in the computation of the model.

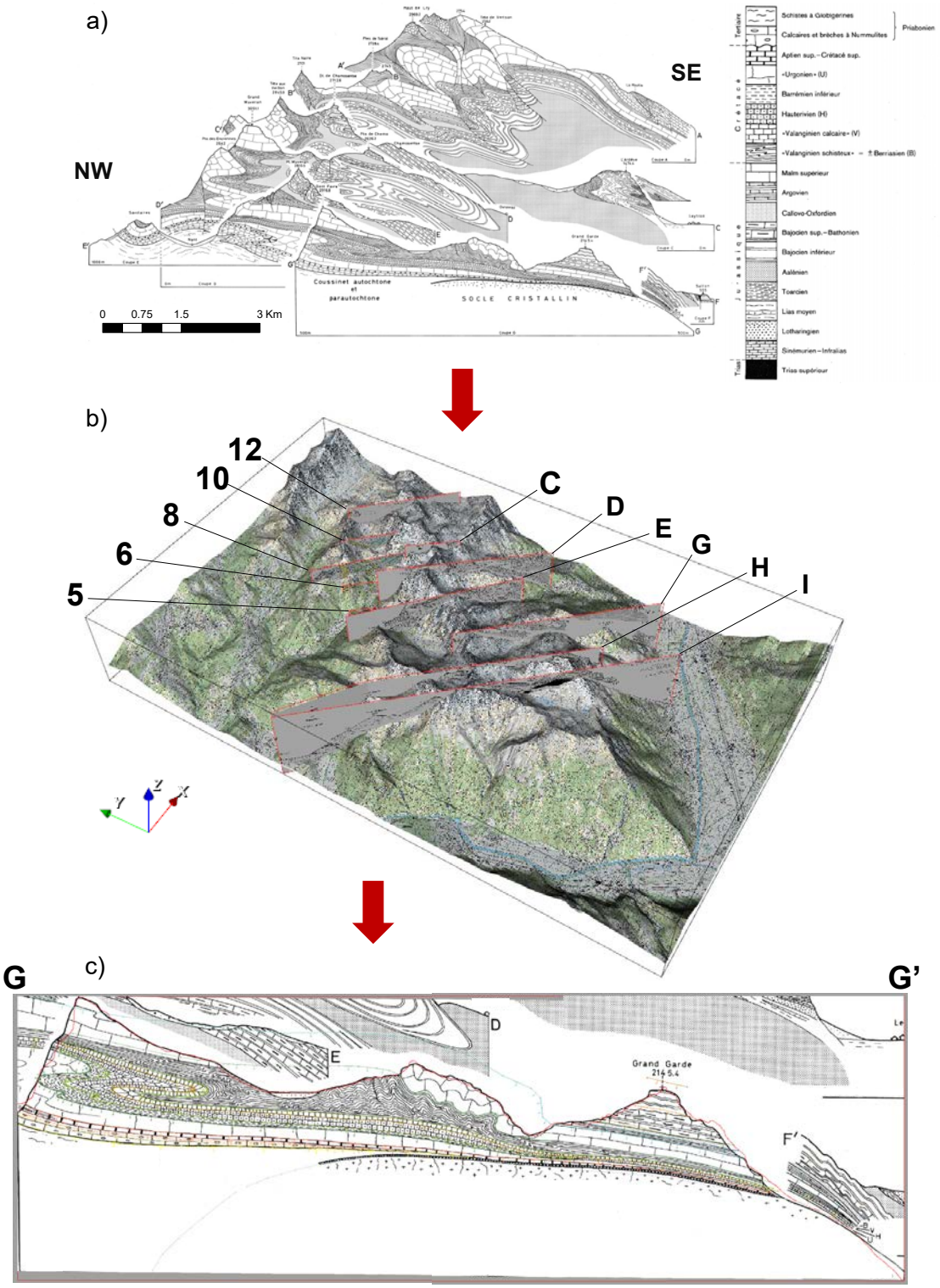
a)
SE
NW
0 0.75 1.5 3 Km
Coussinet autochtone et parautochtone
SOCLE CRISTALLIN
Schistes à Globigérines
Calcaires et brèches à Nummulites
Priabonien
Aptien sup.–Crétacé sup.
Urgonien (U)
Barrémien inférieur
Hauterivien (H)
Valanginien calcaire (V)
Valanginien schisteux = ± Berriasien (B)
Malm supérieur
Argovien
Callovo-Oxfordien
Bajocien sup.–Bathonien
Bajocien inférieur
Aalénien
Toarcien
Lias moyen
Lotharingien
Sinémurien–Infralias
Trias supérieur
b)
12
10
8
6
5
C
D
E
G
H
I
c)
G
G'
D
E
Grand Garde
2145.4
F'

Figure 2.8 (previous page): Steps undertaken to process the subsurface geological data. a) Incoming vertical cross-sections. Note that only C-I (i.e. those from the Morcles map sheet) are shown in this panel (Badoux, 1971, Source: © Swiss Federal Office of Topography, 1971), although Sections 2-12 (from the Diablerets map sheet; Badoux and Gabus, 1991, Source: © Swiss Federal Office of Topography, 1991) were also used in the model development, b) All 11 cross sections, having been georeferenced, visualised in the 3D viewer of GeoModeller, and c) An example of a georeferenced cross section (GG') visualised in the 2D viewer of GeoModeller, with subsurface interface and orientation data points digitised according to the locations and dips of the various interfaces shown (coloured lines and arrows, respectively). Once these sections were viewed, it was also ensured that the topographic surface illustrated on the diagram closely matched that derived from the DTM along the same profile (red line); a close match, as seen in this example, indicates sound georeferencing. Furthermore, since the DTM has been developed using modern technology (LiDAR and photogrammetry) and is therefore of high quality, a close match also indicates an accurate representation of the topographic surface in the original figure.

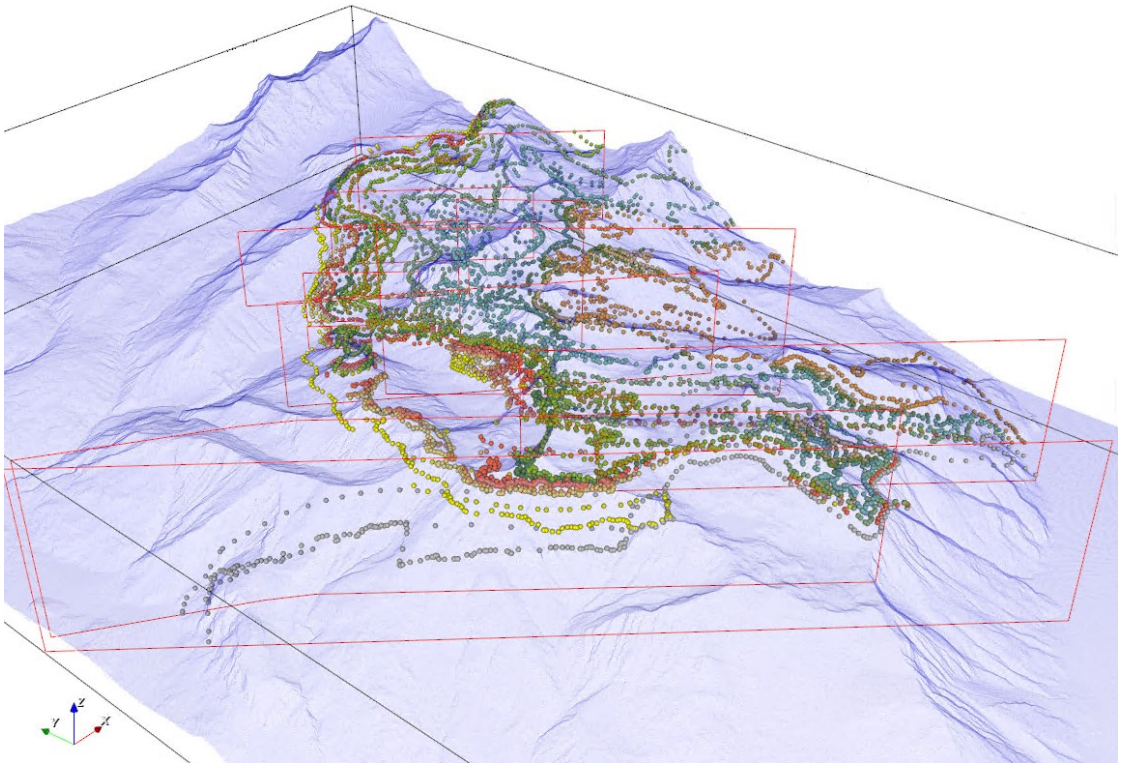

Figure 2.9: All digitised geological formation interfaces, derived from both the surface maps and vertical cross-sections, visualised in 3D with a semi-transparent topographic surface. To avoid cluttering, only interface data points are shown, although orientations were also visualised and checked in the same fashion. Here, the view is towards the north-east.

2.2.3.6 Computing the model

In contrast to more traditional "explicit" or "surface-based" approaches, which essentially involve users generating geological surfaces or volumes based directly on the available data, GeoModeller takes an "implicit approach" to model estimation. Such an approach relies on algorithms that integrate observed data with geological interpretation. The particular theory and algorithms that are employed have been comprehensively described and exemplified elsewhere (Calcagno et al., 2008; McInerney and Guillen, 2005; Chilès et al., 2004), but to summarise: formation interface and orientation data are co-kriged to produce a 3D scalar field, or potential field (Lajaunie et al., 1997). Equipotential iso-surfaces with certain reference values represent formation interfaces, whilst the gradients of the scalar function describe their orientations. Several potential fields can be combined in the same model to, for instance, reconstruct complex erosive and/or onlap relationships between geological series (which are simply groups of individual formations). Faults can be represented by inserting discontinuities into the potential field. Once computed, the surfaces or volumes are visualised by means of a marching cube methodology (Lorensen and Cline, 1987).

The key benefits of taking an implicit approach are that certain conditions of geological validity (e.g. the prohibition of overlapping interfaces) are directly enforced (Caumon et al., 2009), and that interface contact and orientation data can be considered simultaneously in the estimation of a continuous model (Maxelon et al., 2009). Another positive feature is that a given model can be updated relatively quickly following the addition of new data. In this case, several "competing" models could be generated efficiently using slightly different subsets of the data, alternative interpretations of the relationship between formations in the geological pile, and varied parameter values. Drawbacks of the implicit approach include its relatively high memory usage, and the limited opportunity that exists for users to manually adjust individual modelled surfaces to match their expectations or expert knowledge.

The first stage of computing the model involved testing how the relations between the series (which are simply groups of formations) of the geological pile might best be represented. According to the legend of the Morcles map, erosive relationships exist between the Jurassic and the Cretaceous series, and also between the Cretaceous and Tertiary series. In early iterations these series were indeed treated separately with "Erode" relations, such that one or more would take precedence and cut over the others (depending on which were defined as "Erode" and which remained "Onlap", as well as their relative positions in the pile). However, this prevented data from the upper or lower formation of one series from constraining formations in the next series,

leading to some cross-cutting situations that were deemed unrealistic. Because the interfaces of all formations seem to generally follow one another, with few if any instances of formations within the modelled series having been completely eroded, it was eventually decided to treat all formations as part of a single series.

The only further inputs necessary to compute a model are the values of three (isotropic) interpolation parameters: the range, the nugget effect of geological interface data, and the nugget effect of geological orientation data. The range represents the spherical distance beyond a given location at which data points will have no influence on the model. The nugget effect parameters represent the variance between the values of observed data points that is not explained by separation distance, but could rather reflect measurement error or stochasticity (i.e. "noise"). Here, it can be thought of as the mismatch permitted between model and data.

As part of an iterative computation and re-evaluation process, the adjustable parameters were systematically varied until a satisfactory balance between a smooth model and model that honoured the data was obtained. In practical terms, this was achieved by visually comparing the input data and the modelled interfaces on both surface and vertical sections. The final parameter values arrived at are:

- Range: 2,000 m
- Nugget effect on geological interface data: 0.00001 (arbitrary unit of the potential field)
- Nugget effect on geological orientation data: 0.1 (arbitrary unit of the potential field)

2.3 Results

2.3.1 Evaluating the model

The most relevant approach to evaluating the model was visually assessing how well lithological formation interfaces defined by the input data compared with the modelled interfaces – both on surface and on the vertical cross-sections. Comparisons of the input data and final modelled interfaces on the surface section and four randomly selected vertical cross-sections are therefore shown in Figure 2.10. The close matches obtained indicate that the interpolation algorithm can reproduce the structures defined in the input data. If one then assumes that the original geological interpretation presented in the maps (i.e. the input data itself) is reasonable, one may suggest that the new 3D model is also geologically plausible. Taking slices through the domain

between cross-section locations, and visualising the estimated volumes of individual formations with their corresponding input points, reinforced this assessment.

Although the number of input data points observations is high, given the inaccessibility of the subsurface, they are still unlikely to be sufficient to constrain a unique model (Maxelon et al., 2009). For this reason, no data were explicitly withheld to provide independent evaluation data; keeping any observations aside would inevitably have had an adverse impact on the final model.

The resultant dataset (Figure 2.11) represents 18 formations, including their associated folds and selected major faults, and covers a horizontal area of 9.6×13.4 km.

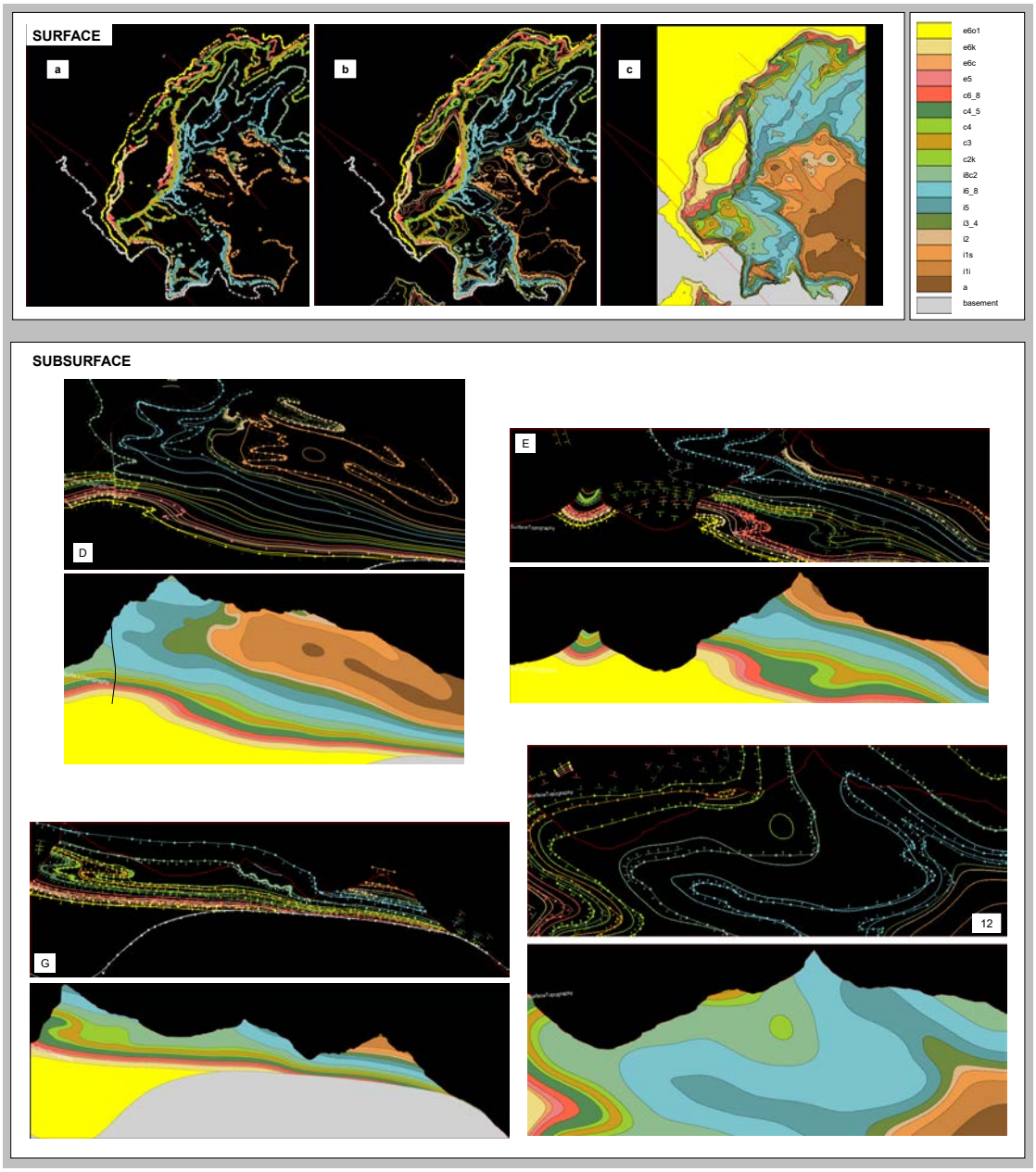

Figure 2.10: Comparison of input interface data points and modelled interfaces. The thin lines with circles and arrows correspond to the input data extracted from the surface maps (surface section), or digitised directly from the formation interfaces illustrated on the cross-section diagrams (vertical sections). Specifically, the circles represent interface data points and arrows represent orientation data points. Input orientation data points are not shown on the surface section in the interests of clarity. The thicker, continuous lines correspond to the modelled surfaces. For the surface, the data points alone (a) and then data points with the interpolated interfaces underneath (b) are shown separately. The final filled volumes are also shown for all sections (Panel c shows this for the surface section). Vertical cross-section letters follow the convention of the original inputs. In Section D, one of the faults that has been modelled is visible. Two disconnected circles (spheres in 3D) are visible; these are model artefacts, and are discussed in due course.

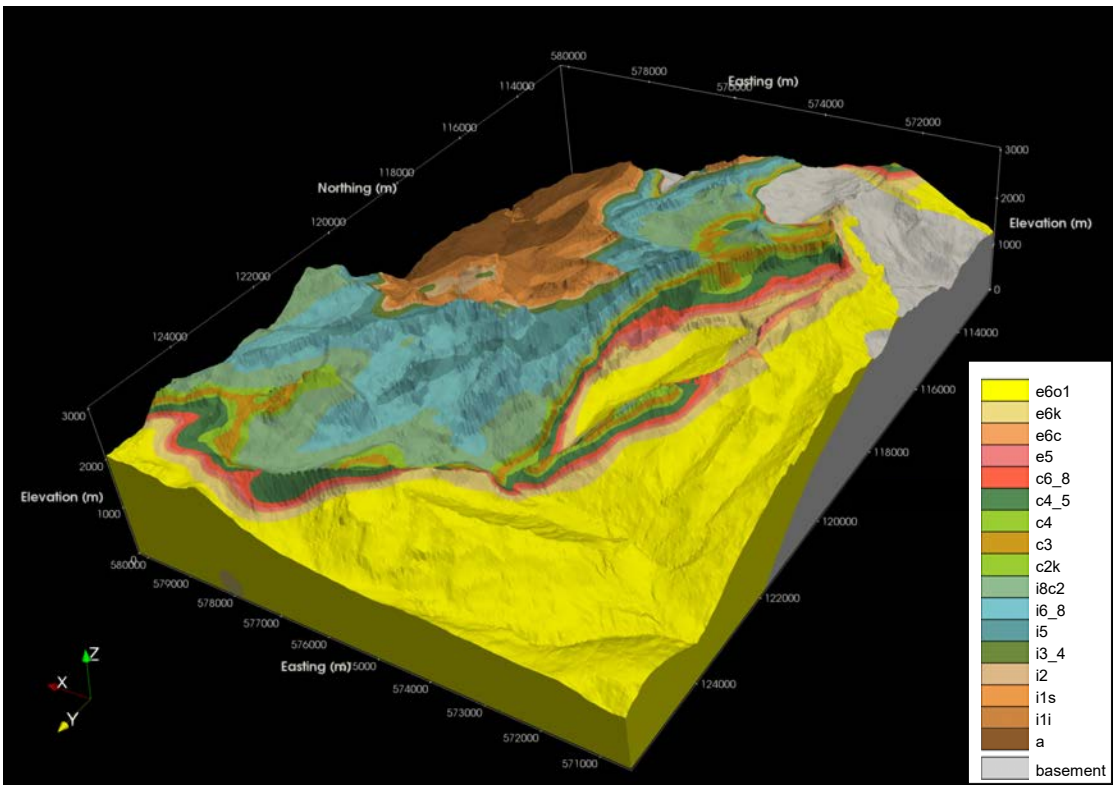

Figure 2.11: Illustration of the final coherent 3D model of bedrock geology, looking towards the south-west. This figure was produced in ParaView. Coordinates are given in the CH1903 / LV03 system. The formation codes correspond broadly to those of the legend of the 58 Morcles sheet (Badoux, 1971), although the geological pile was slightly modified to reconcile it with the Diablerets sheet. Some colours were slightly adjusted to increase visual impact. In the western part of the domain, the stratigraphy is overturned, i.e. geologically older units are found above younger ones. Quaternary cover is not included in the model. Formations of the Ultrahelvetic zone are not included in the model, and thus the presence of "e6o1" (bright yellow) in the extreme north-west of the figure is not reflective of the real geology in this region (as indicated in Figure 2.3a). Similarly, the model is less well constrained in the extreme east of the domain (i.e. towards the centre of the nappe), which is away from the main area of interest.

A further visual comparison was made between a panoramic sketch of the geology of the eastern side of the Vallon de Nant ("Planche II" of Badoux, 1972) and a roughly equivalent view produced in the modelled environment, again with satisfactory results (Figure 2.12).

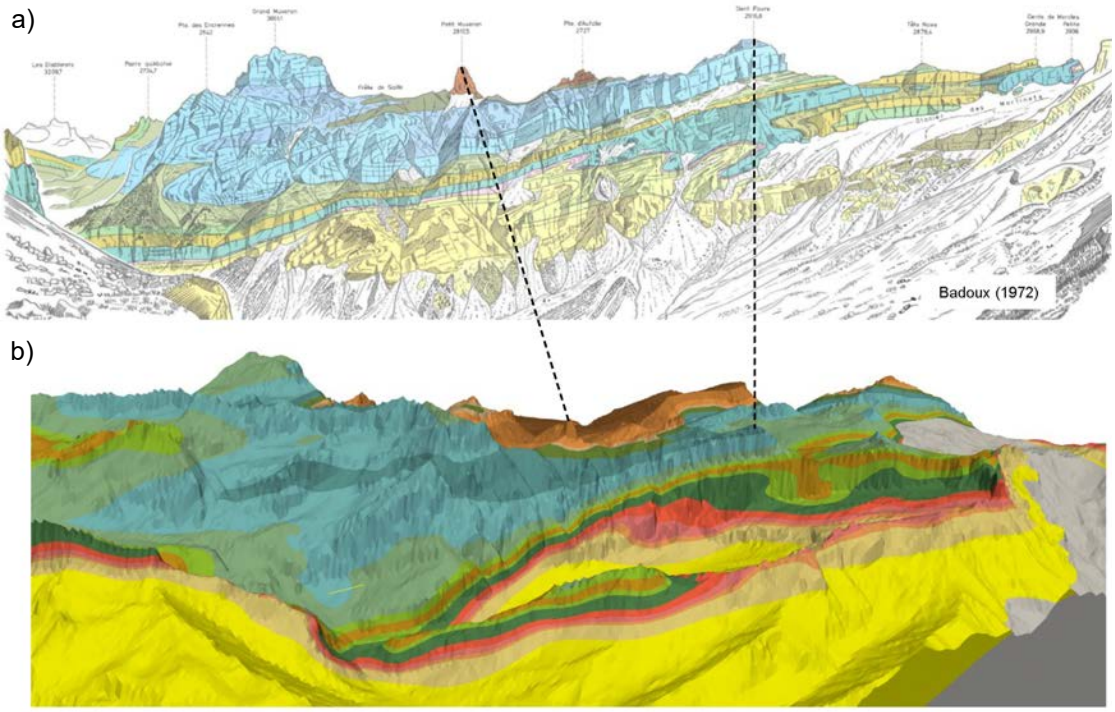

Figure 2.12: Comparison between: a) a geological sketch of the eastern wall of the Vallon de Nant and, b) a similar view generated within the modelled environment. The upper illustration was produced by Badoux (1972), whilst the lower was generated by The Author in Paraview.

2.3.2 Exporting the model

The model was exported in a regular voxel format at both 10 m and 50 m resolution. In this format, to reduce data volumes, the position of each voxel is given implicitly. In principle, the voxel model can be used directly for hydrogeological modelling. However, this would be rather inefficient with respect to the number of nodes and elements required. More contemporary practice would be to separately generate a finite element mesh of variable resolution, which allows appropriate representation of important features whilst minimising the total number of nodes, and then assign geological codes to each element in this mesh according to the geological model via a spatial query. Following this, based on knowledge of the lithology, one may attribute reasonable initial estimates of the values of parameters describing physical properties throughout the domain. Such meshes could be comprised of layered prisms or, as are beginning to emerge, fully-unstructured tetrahedra. Various possibilities exist for refining or optimising the arrangement of elements according to surface or subsurface features, although this topic lies beyond the scope of the present article. 3D shapes were also exported for visualisation. More

specifically, the formation interface surfaces may be loaded as polygonal meshes in ParaView (Ayachit, 2015); an open source 3D visualisation software. In this environment, layers can be visualised or hidden at the user's behest, and interacted with virtually. Finally, the GeoModeller project containing the model was saved in its native format.

The model data are provided in a generic voxel format at two different resolutions: 10 m and 50 m (regular cubic cells) ("Generic voxel format") (see the online repository). The lithological code is listed for each cell. For ease of processing, no refinement of the vertical resolution has been made near the topographic surface in either case. The 10 m resolution voxel model is also provided in a modified voxel format that can be loaded into the freely-available visualisation software SGeMS (Remy et al., 2009) ("SGeMS voxel format"). In addition, formation interface surface were prepared in a format that can be visualised in ParaView ("Surfaces for ParaView"). Finally, the entire GeoModeller project is provided in its native format; this can be viewed by readers with a GeoModeller licence ("Native GeoModeller Project"). Instructions for visualising the data are provided in Appendix A. In the SGeMS format, the lithological formations are represented by the codes listed in Table 2.2.

Code	Formation	Stage	Description
0	"Out" / air		Above topographic surface
10	Basement	Metamorphic	Crystalline massifs
11	a	Aalenian	Dark clayey shales
12	i1i	Lower Bajocian	Alternating marly shales and siliceous limestones
13	i1s	Upper Bajocian	Siliceous limestones
14	i2	Bathonian	Limestones and dark shale
15	i3_4	Callovo-Oxfordian	Shaley marls
16	i5	Argovian	Grey bedded limestones
17	i6_8	Upper Malm	Compact limestones
18	i8c2	Upper Portlandian to Valanginian	Alternating marls and clayey limestones
19	c2k	Valanginian	Predominantly dense limestones
20	c3	Hauterivian	Siliceous limestones
21	c4	Lower Barremian	Alternating marls and limestones
22	c4_5	Urgonian	Light-coloured, dense limestone
23	c6_8	Upper Albian–Cenomanian	Sandy shales and limestones
24	e5	Auversian	Layers of "Roc Champion"
25	e6c	Priabonian	Layers with Vivipares and Ceriths
26	e6k	Priabonian	Limestone with small Nummulites
27	e6o1	Upper Eocene to Lower Oligocene	Parautochthonous Flysch

Table 2.2: Numerical codes assigned to each geological formation for visualisation in SGeMS. The corresponding geological map codes, stratigraphic stages, and lithological descriptions (translated from French) are also provided.

2.4 Discussion

The interpolation approach employed to develop the 3D model is based on co-kriging. For this reason, the density of data points may have some effect on the model. Whilst the relatively high-density surface points were extracted directly from the (pre-digitised) map data, and were therefore rather treated as rather "fixed" (although the density of vertices on relatively straight surface interfaces was increased so these features were not unduly de-weighted), the subsurface points had to be digitised manually from the cross-sectional diagrams. The density at which these points were inserted was at the discretion of the model developer, and was therefore somewhat arbitrary. This inevitably introduced a degree of subjectivity into the modelling process. On the other hand, it also provided a degree of flexibly to vary the extent to which data con-

strain the model regionally. For instance, where uncertainty in the position of an interface was considered lower (e.g. near an observable interface at the surface), the density of points could be increased. Furthermore, where the precise location of the interface was unknown in a particular region but the orientations could be inferred from adjacent layers, subsurface orientation data points could be inserted independently of interface data. Finally, as mentioned above, some additional interface points were even inserted onto the surface section where it was clear that a given boundary was continuous but was simply not marked on the map as a result of being obscured by Quaternary deposits. Accounting for these aspects, rather than simply computing the model based only on the available data, enabled us to produce a model that both honoured the data and could be deemed geologically plausible.

The resultant model is deterministic. In this regard, it may be noted firstly that the number of outcrops present in the highly eroded, mountainous study area mean that the geological structures are relatively easy to observe. Therefore, although the area is geologically complex, and the existing data (which formed the inputs) are naturally associated with some uncertainty (the vertical cross-sections naturally more than the surface data), this data uncertainty is arguably less pronounced than in other geological settings where bedrock outcrops are less conspicuous. The series of vertical cross-sections is also very dense. As such, it seems unlikely that attempting to refine the field data or geological interpretation, as expressed in the existing surface mapping or vertical cross-sections, would yield major improvements in the output.

Nevertheless, in future work, it would be possible to assess the uncertainty associated with the deterministic geometrical representation to be assessed by generating multiple realisations of the model. This could be achieved by perturbing the parameter values within a probabilistic framework. That said, it may be suggested that the high data density leaves little scope for model variability during the interpolation stage. Furthermore, before embarking on such a task, the relative magnitudes of various uncertainties that could arise throughout a wider modelling chain should be contemplated. For example, in the forthcoming hydrogeological application, the uncertainty in the hydraulic conductivities of the various formations is likely to be much more substantial that the uncertainty in their geometrical structures. Exploring the capability of high resolution LiDAR terrain data to improve the input interface locations represents another potential research avenue.

A number of challenges were encountered during the development process. Consequently, the final dataset is associated with some limitations. These limitations could motivate further improvements in 3D geological modelling algorithms in general, or the present model in particular. They are as follows:

- The polarity (normal/overturned) of some surface orientation points in the frontal zone was not clear. In the horizontal plane, these points were located between vertical cross-sections. Given the extreme folding in the region, their polarities could not be easily confirmed. These points were omitted.

- The subsurface orientation data derived from the vertical cross-sections were taken as if there is no plunge (i.e. as if the cross-sections are perfectly orthogonal to the main fold). In reality, the plunge angle is spatially variable, and the true dip and dip direction at any given location are dependent on the plunge angle and as well as the geometry of any secondary folds in those locations. Making the assumption of orthogonality was thus the only practical way in which subsurface orientations could be assigned, which in turn was important for successfully modelling this structurally complex region. Given its intended application(s), this assumption is not expected to have a major impact on the model.

- In addition to the data prescribed, the implicit approach taken by GeoModeller inherently considers "geological concepts" when constraining the output. Whilst some of these constrains are highly beneficial (e.g. overlapping or "leaking" geological layers are not permitted), others, such as a tendency towards regularity in formation thickness throughout the domain, were more troublesome. This is because the thickness of some formations, most notably "i6_8", does change drastically over short distances in the study area. Consequently, some interpolation artefacts such as disconnected "spheres" are present in areas of the model where the gradient in the potential field changes rapidly, particularly near the apices of sharp folds. In such a structurally complex environment, and with a large observation dataset, slightly improved results could have perhaps been obtained by assigning a greater weight to the observations and giving less freedom to the geostatistical interpolation.

- When computing the model, the same range value was used for both the interface data and the orientation data. In GeoModeller, it is not possible to specify a different nugget parameter for, say, the interface data according to whether it was derived from the surface maps or the vertical cross-sections. In other words, it is only possible to make a distinction between the interface and orientation data when assigning range and nugget effect values, which are global parameters. This was unfortunate here because, being directly observable, the surface data points are much less uncertain than subsurface contacts, which are highly dependent on interpretation. Hence, all observations of a certain type carried an equal weight in the model.

- Quaternary cover is excluded from the present model. The only direct available data pertaining to the unconsolidated Quaternary deposits are a series of shallow boreholes near the source of Le Rippaz, and reveal it to be highly heterogeneous. The Quaternary fill in the Vallon de Nant itself is likely to be a complex mixture of material having glacial, fluvial, and colluvial origins. Reconstructing Quaternary cover in such environments is challenging in its own right. However, it is likely to be necessary for reliable hydrogeological flow simulations. For this reason, some attempt at estimating the volumes at least is made in Chapter 4. In future work, these volumes could be populated with more realistic representations of heterogeneous hydraulic properties using stochastic geostatistical simulation approaches, such as Multiple Point Statistics.

2.5 Conclusion

No 3D geological model the study region – which is now the focus of a concerted interdisciplinary research effort – had been published or otherwise made available at the outset of this work. Whilst the development of a model with the requisite characteristics for hydrogeological and other applications was both technically challenging and time consuming, this data gap has now been addressed.

The modelled formation interfaces correspond well with the location of these interfaces according to the input data, both at the surface and on available vertical cross-sections. Assuming the geological interpretation presented in the original maps and cross-sections is reasonable, the close matches obtained provide confidence that modelled representation of the geology also acceptable; a view that was upheld by additional comparisons with interpretive sketches.

In the sense that no new primary data has been collected, this work could be considered a data augmentation exercise. The model thus demonstrates the considerable potential that exists to add value to existing geological data. The resultant model amounts to more than the sum of its inputs, however; via the combination of the various input datasets and the process of geostatistical interpolation, it provides insight over the entire domain, ultimately forming an unprecedented geometrical description of the geological formations of the western and northern section of the Nappe de Morcles. In fact, the model presented probably represents the most comprehensive and detailed geological model of a section of the European Alps yet presented.

In contrast to certain previous publications which describe the development of 3D geological models only superficially, here, a detailed, step-by-step process has been presented. This should

assist future researchers and practitioners in developing complex 3D geological models in future. Again in contrast to most previous instances, the data generated here are made freely-available, and care has been taken to ensure that they can be visualised in open source software. A range of applications across the earth and environmental sciences are likely to benefit if such work is conducted more consistently.

Going forward, the geological model will be employed alongside various other datasets to parameterise physically-based, numerical simulations that integrate snow dynamics, surface water flow, groundwater flow, and evapotranspiration. These simulations intend to better elucidate the overall response of mountain hydrological systems to ongoing climatic change. Finally, having been developed with the stringent requirements of hydrological applications in mind, the model should also be suitable for a range of other applications, including rockfall hazard modelling, sediment provenance identification, hydrochemical data interpretation, and pedogenic studies.

Contribution statement

I (The Author) conducted the vast majority of the work, including sourcing and preparing the input datasets, generating and evaluating the model, preparing the figures, and writing the manuscript. Professor G. Mariethoz advised on data processing and participated in the finalisation of the manuscript. Professor P. Brunner contributed the initial idea that a 3D geological model could be useful to the broader research, and also participated in the finalisation of the manuscript.

Data citation

Thornton, J. M., Mariethoz, G. Brunner, P. (2018). https://doi.org/10.6084/m9.figshare.c.4130759.v1

Acknowledgments and code availability

The work was conducted as part of the IntegrAlp project, funded by the Swiss National Science Foundation. Discussions with Professors. J.-L. Epard and A. Parriaux are gratefully acknowledged.

GeoModeller is a proprietary software licensable from Intrepid Geophysics (see https://www.intrepid-geophysics.com/ig/index.php?page=geomodeller); v.3.3.0 was used in this work. The open source GIS software QGIS (https://qgis.org/en/site/) was used for much of the data handling and processing.

References

Argand, E. (1916). Sur l'arc des Alpes occidentales. *Eclogae Geologicae Helvetiae* 45.

Aschwanden, H. and Weingartner, R. (1985). Die Abflussregimes der Schweiz. *Publikation Gewässerkunde Geographisches Institut der Universität Bern* 65.

Ayachit, U. (2015). *The ParaView Guide: A Parallel Visualization Application*. Kitware, Inc., USA.

Badoux, H. (1971). *Carte et notice explicative, Feuille 1305 - Dt. de Morcles, Atlas géologique de la Suisse (1:25,000)*. Tech. rep.

Badoux, H. (1972). *Tectonique de la nappe de Morcles entre Rhône et Lizerne, Matériaux pour La carte Géologique de la Suisse*. Kümmerly & Frey.

Badoux, H. (1991). Géologie simplifiée de la région de Morcles - Les Diablerets - Vallon de Nant. *La Thomasia: Jardin alpin de Pont de Nant 1891-1991*. Lausanne: Musées et jardins botaniques cantonaux, Lausanne. Chap. 2.

Badoux, H. and Gabus, J. H. (1991). *Carte et notice explicative, Feuille 1285 - Les Diablerets, Atlas géologique de la Suisse (1:25,000)*. Tech. rep.

Ballesteros, D., Malard, A., Jeannin, P. Y., Jiménez-Sánchez, M., García-Sansegundo, J., Meléndez-Asensio, M., and Sendra, G. (2015). KARSYS hydrogeological 3D modeling of alpine karst aquifers developed in geologically complex areas: Picos de Europa National Park (Spain). *Environmental Earth Sciences* 74, 7699–7714.

Bauville, A., Epard, J.-L., and Schmalholz, S. M. (2013). A simple thermo-mechanical shear model applied to the Morcles fold nappe (Western Alps). *Tectonophysics* 583, 76–87.

Béthoux, N., Theunissen, T., Beslier, M.-O., Font, Y., Thouvenot, F., Dessa, J.-X., Simon, S., Courrioux, G., and Guillen, A. (2016). Earthquake relocation using a 3D a-priori geological velocity model from the western Alps to Corsica: Implication for seismic hazard. *Tectonophysics* 670, 82–100.

Bistacchi, A., Massironi, M., Dal Piaz, G. V., Dal Piaz, G., Monopoli, B., Schiavo, A., and Toffolon, G. (2008). 3D fold and fault reconstruction with an uncertainty model: An example from an Alpine tunnel case study. *Computers and Geosciences* 34, 351–372.

Calcagno, P., Chilès, J. P., Courrioux, G., and Guillen, A. (2008). Geological modelling from field data and geological knowledge. Part I. Modelling method coupling 3D potential-field interpolation and geological rules. *Physics of the Earth and Planetary Interiors* 171, 147–157.

Caumon, G., Collon-Drouaillet, P., Le Carlier De Veslud, C., Viseur, S., and Sausse, J. (2009). Surface-based 3D modeling of geological structures. *Mathematical Geosciences* 41, 927–945.

Chilès, J. P., Aug, C., Guillen, A., and Lees, T. (2004). Modelling the geometry of geological units and its uncertainty in 3D from structural data : The potential-field method. *Orebody Modeling and Strategic Mine Planning - Spectrum 14*, 22–24.

Coe, A. L., Argles, T. W., Rothery, D. A., and Spicer, R. A. (2010). *Geological Field Techniques*. Ed. by A. L. Coe. 1st Editio. Wiley-Blackwell.

Dutoit, A. (1983). Dutoit, Annelise. La végétation de l'étage subalpin du vallon de Nant. *Section protection de la nature et des sites et conservation de la faune du Canton de Vaud.*

Escher, A., Masson, H., and Steck, A. (1993). Nappe geometry in the Western Swiss Alps. *Journal of Structural Geology* 15, 501–509.

Gárfias, J. (2009). Groundwater in mountain regions. *Groundwater Volume I*. Ed. by L. Silveira and E. J. Usunoff. Oxford: EOLSS Publishers / UNESCO. Chap. 8, pp. 195–217.

Goldscheider, N. (2005). Fold structure and underground drainage pattern in the alpine karst system Hochifen-Gottesacker. *Eclogae Geologicae Helvetiae* 98, 1–17.

Goldscheider, N. and Andreo, B. (2007). The geological and geomorphological framework. *Methods in Karst Hydrogeology*. Ed. by N. Goldscheider and D. Drew. London: CRC Press. Chap. 2, pp. 9–23.

Gremaud, V., Goldscheider, N., Savoy, L., Favre, G., and Masson, H. (2009). Geological structure, recharge processes and underground drainage of a glacierised karst aquifer system, Tsanfleuron-Sanetsch, Swiss Alps. *Hydrogeology Journal* 17, 1833–1848.

Guerin, A., Nguyen, L., Abellán, A., Carrea, D., Derron, M. H., and Jaboyedoff, M. (2015). Common problems encountered in 3D mapping of geological contacts using high-resolution terrain and image data. *European Journal of Remote Sensing* 48, 661–672.

Guglielmetti, L., Comina, C., Abdelfettah, Y., Schill, E., and Mandrone, G. (2013). Integration of 3D geological modeling and gravity surveys for geothermal prospection in an Alpine region. *Tectonophysics* 608, 1025–1036.

Guillen, A., Calcagno, P., Courrioux, G., Joly, A., and Ledru, P. (2008). Geological modelling from field data and geological knowledge. Part II. Modelling validation using gravity and magnetic data inversion. *Physics of the Earth and Planetary Interiors* 171, 158–169.

Hassen, I., Gibson, H., Hamzaoui-Azaza, F., Negro, F., Rachid, K., and Bouhlila, R. (2016). 3D geological modeling of the Kasserine Aquifer System, Central Tunisia: New insights into aquifer-geometry and interconnections for a better assessment of groundwater resources. *Journal of Hydrology* 539, 223–236.

Herold, T., Jordan, P., and Zwahlen, F. (2000). The influence of tectonic structures on karst flow patterns in karstified limestones and aquitards in the Jura Mountains, Switzerland. *Eclogae Geologicae Helvetiae* 93, 349–362.

Intrepid Geophysics (2013). *3D GeoModeller Reference*.

Jeannin, P. Y., Eichenberger, U., Sinreich, M., Vouillamoz, J., Malard, A., and Weber, E. (2013). KARSYS: A pragmatic approach to karst hydrogeological system conceptualisation. Assessment of groundwater reserves and resources in Switzerland. *Environmental Earth Sciences* 69, 999–1013.

Jones, R. R., McCaffrey, K. J., Clegg, P., Wilson, R. W., Holliman, N. S., Holdsworth, R. E., Imber, J., and Waggott, S. (2009). Integration of regional to outcrop digital data: 3D visualisation of multi-scale geological models. *Computers and Geosciences* 35, 4–18.

Lajaunie, C., Courrioux, G., and Manuel, L. (1997). Foliation fields and 3D cartography in geology: Principles of a method based on potential interpolation. *Mathematical Geology* 29, 571–584.

Lorensen, W. E. and Cline, H. E. (1987). Marching cubes: A high resolution 3D surface construction algorithm. *Proceedings of the 14th annual conference on Computer graphics and interactive techniques - SIGGRAPH '87*. Vol. 21. (4). New York, USA: ACM Press, pp. 163–169.

Lugeon, M. (1940). *Notice explicative, Feuille 19 - Les Diablerets, Atlas géologique de la Suisse (1:25,000)*. Tech. rep.

Lugeon, M. and Argand, E. (1937). *Notice explicative, Feuille 485 Saxon – Morcles, Atlas géologique de la Suisse (1:25,000)*. Tech. rep.

Lugeon, M. and Gagnebin, E. (1928). L'origine des sources de la Chambrette aux Plans sur Bex (Alpes Vaudoises). *Bulletin de la Société vaudoise des Sciences* 56.

Malard, A., Jeannin, P.-Y., Vouillamoz, J., and Weber, E. (2015). An integrated approach for catchment delineation and conduit-network modeling in karst aquifers: application to a site in the Swiss tabular Jura. *Hydrogeology Journal* 23, 1341–1357.

Maxelon, M., Renard, P., Courrioux, G., Brändli, M., and Mancktelow, N. (2009). A workflow to facilitate three-dimensional geometrical modelling of complex poly-deformed geological units. *Computers and Geosciences* 35, 644–658.

McInerney, P. and Guillen, A. (2005). Building 3D geological models directly from the data? A new approach applied to Broken Hill, Australia. *Digital Mapping Techniques '05*, 119–130.

Mont Terri Project (n.d.). *3D geological model*. URL: https://www.mont-terri.ch/en/geology%20/3D-geological-model.html.

Municipalite d'Ollon (2014). *PREAVIS MUNICIPAL n° 2014 / 08: Acquisition de la parcelle n° 4434 au lieu-dit "La Rippaz" sur le territoire de la Commune de Bex*. Tech. rep.

Municipalite d'Ollon (2015). *PREAVIS MUNICIPAL n° 2015/09: Recaptage des sources de La Rippaz*. Tech. rep.

Ofterdinger, U. S., Renard, P., and Loew, S. (2014). Hydraulic subsurface measurements and hydrodynamic modelling as indicators for groundwater flow systems in the Rotondo granite, Central Alps (Switzerland). *Hydrological Processes* 28, 255–278.

Perrin, J. (1993). Prospection dans le Vallon de Nant (Bex). *Le Trou (Bulletin du Groupe Spéléo Lausanne)* 56, 40–45.

Pfiffner, O. A. (1993). The structure of the Helvetic nappes and its relation to the mechanical stratigraphy. *Journal of Structural Geology* 15, 511–521.

Ramsay, J. G. (1981). Tectonics of the Helvetic Nappes. *Geological Society, London, Special Publications* 9, 293–309.

Remy, N., Boucher, A., and Wu, J. (2009). *Applied Geostatistics with SGeMS: A User's Guide*. Cambridge: Cambridge University Press.

Renard, M., Lagabrielle, Y., Martin, E., and Saint-Sauveur, M. R. (2015). *Eléments de Géologie*. Ed. by Dunod. Dunod, p. 1152.

Schreiber, D., Lardeaux, J. M., Martelet, G., Courrioux, G., and Guillen, A. (2010). 3-D modelling of Alpine Mohos in Southwestern Alps. *Geophysical Journal International* 180, 961–975.

Sue, C., Calcagno, P., Courrioux, G., Tricart, P., Frechet, J., and Thouvenot, F. (2010). Relationships between inherited crustal structures and seismicity in the western Alps inferred from 3D structural modeling. *Bulletin de la Societe Geologique de France* 181, 583–590.

Thornton, J. M., Mariethoz, G., and Brunner, P. (2018). A 3D geological model of a structurally complex alpine region as a basis for interdisciplinary research. *Scientific Data* 5, 1–20.

Turk, J., Malard, A., Jeannin, P. Y., Petrič, M., Gabrovšek, F., Ravbar, N., Vouillamoz, J., Slabe, T., and Sordet, V. (2015). Hydrogeological characterization of groundwater storage and drainage in an alpine karst aquifer (the Kanin massif, Julian Alps). *Hydrological Processes* 29, 1986–1998.

Vanneschi, C., Salvini, R., Massa, G., Riccucci, S., and Borsani, A. (2014). Geological 3D modeling for excavation activity in an underground marble quarry in the Apuan Alps (Italy). *Computers & Geosciences* 69, 41–54.

Von Däniken, I., Guisan, A., and Lane, S. (2014). RechAlp.vd: Une nouvelle plateforme UNIL de support pour la recherche transdisciplinaire dans les Alpes vaudoises. *Bulletin de la Société vaudoise des Sciences* 94, 175–178.

Von Tscharner, M., Schmalholz, S., and Epard, J.-L. (2016). 3-D numerical models of viscous flow applied to fold nappes and the Rawil depression in the Helvetic nappe system (western Switzerland). *Journal of Structural Geology* 86, 32–46.

Vouillamoz, N., Sue, C., Champagnac, J. D., and Calcagno, P. (2012). 3D cartographic modeling of the Alpine arc. *Tectonophysics* 579, 131–143.

Zanchi, A., Francesca, S., Stefano, Z., Simone, S., and Graziano, G. (2009). 3D reconstruction of complex geological bodies: Examples from the Alps. *Computers and Geosciences* 35, 49–69.

3 | Efficient multi-objective calibration and uncertainty analysis of distributed snow simulations in rugged alpine terrain

A version of this chapter was recently submitted to *Water Resources Research* for consideration as:

Thornton, J.M., Mariethoz, G., Brauchli, T.J., and Brunner, P. (2020). Efficient multi-objective calibration and uncertainty analysis of distributed snow simulations in rugged alpine terrain.

Photograph: *Heterogeneous remaining snow cover in the upper reaches of the Vallon de Nant, late June 2016*

"Index approaches...are not suitable tools to produce reasonable results for snow cover development in complex Alpine terrain"

(Warscher et al., 2013)

Abstract

In steep and rugged mountainous terrain, robust simulations of snow accumulation and ablation are crucial to many hydrological and ecological applications. However, apart from in highly instrumented research catchments, meteorological data are usually limited, and so driving spatial fields highly uncertain. In addition, potentially important snow redistribution processes cannot presently be simulated across entire catchments using physical algorithms. It is therefore often appropriate for several empirical parameters to be introduced into otherwise physically-based snow models. Here, with a view towards ultimately generating gridded representations of snowmelt dynamics that are as accurate as possible, a novel approach to the calibration of a high-resolution energy balance-based snow model that additionally accounts for gravitational snow redistribution, implemented in the code WaSiM, is presented. Aided by specialist software (PEST), several important but uncertain parameters were estimated using an efficient, gradient-based method with respect to two complementary types of snow observations – snow extent maps derived from Landsat 8 images, and snow water equivalent (SWE) time-series reconstructed at two contrasting locations. Assessed on a per-pixel basis over 17 days that encompass practically the full range of possible snow cover conditions, snow patterns were reproduced with a mean accuracy of 85%. The spatial performance metrics obtained compared favourably with those previously reported, whilst the temporal evolution of SWE at the stations was also satisfactorily simulated. Subsequent uncertainty and data worth analyses revealed that: i) the propensity for model predictions to be erroneous was substantially reduced by the calibration process, ii) pre-calibration uncertainty was largely associated with two parameters that were introduced to modify the longwave component of the energy balance, but this uncertainty was greatly diminished by calibration, and iii) a lower elevation SWE time-series was particularly valuable, despite the comparatively small number of observations at this site. Commensurate firn melt, ice melt, liquid precipitation, and potential evapotranspiration datasets were also produced. This is thought to be the first instance in which snow maps derived from Landsat 8 imagery have been included in the calibration of a distributed snow model of any sort. In summary, contemporary snow models, observation technologies, and inverse approaches can now be combined to both constrain and quantify the uncertainty associated with simulations of alpine snow dynamics.

3.1 Introduction

Meltwater derived from the seasonal snowpack currently dominates both the annual groundwater recharge and cumulative streamflow of many mid-elevation temperate mountainous catchments. At higher elevations, the progressive ablation of firn and glacier ice throughout summer periods represent important additional sources of liquid water to the terrestrial hydrosphere. Globally, these snow and ice-derived meltwaters directly sustain millions of people (Pritchard, 2019) and constitute an ecosystem service of enormous value (Sturm et al., 2017). However, hydrological regimes which have historically been heavily influenced by snow and ice are likely to be greatly affected by warming temperatures (Barnett et al., 2005; Viviroli et al., 2011), with summer low flow magnitudes thought to be particularly vulnerable (Jenicek et al., 2016; Dierauer et al., 2018). Indeed, a wealth of evidence attesting the widespread decline of the glaciers and other hydrologically-relevant components of the mountain cryosphere now exists (Klein et al., 2016; Huss et al., 2017; Beniston et al., 2018; Bolch et al., 2012; Bormann et al., 2018; Vuille et al., 2018), and the consequential impacts on stream discharges are increasingly detectable (Casassa et al., 2009; Micheletti and Lane, 2016; Lane and Nienow, 2019). Accordingly, predictions of the impacts of future climatic change on the quantity and timing of mountain runoff remain in high demand, and the substantial body of literature in which hydrological models are applied to make such predictions continues to be augmented (e.g. Fatichi et al., 2015; Huss and Hock, 2018). In addition, the hydrological significance of rain-on-snow events, convective thunderstorms, and more sustained episodes of frontal rainfall in alpine terrain – especially in terms of flood, debris flow, and landslide hazard (Papathoma-Köhle et al., 2011; Rössler et al., 2014; Leonarduzzi et al., 2017) – requires that liquid precipitation patterns also not be overlooked. The same applies to potential evaporative losses which – whilst often comparatively overlooked – can also represent an important component of the alpine water balance (Herrnegger et al., 2012; Mutzner et al., 2015; Cochand et al., 2019).

After calibrating hydrological models against stream discharge measurements alone, even independent discharge observations can often be reproduced well whilst internal spatial dynamics – including those pertaining to the snowpack – remain poorly represented (Duethmann et al., 2014; Shrestha et al., 2014). Such situations arise due to a lack of information on internal system functioning in discharge data, coupled with the considerable freedom that traditional calibration approaches offer. However, a good understanding of, and ability to reproduce computationally, the spatio-temporal dynamics of all potentially important hydrological processes – and thereby obtain the "right answers" via hydrologically plausible mechanisms (Kirchner,

2006) – is a prerequisite to the subsequent generation of reliable future predictions. Assessing simulated patterns of model state variables against spatially distributed observations can provide a more stringent test of model capabilities, and is therefore a means by which the internal consistency of hydrological models can be enhanced. With specific regards to temperate mountain regions, following the early contributions of Grayson, Blöschl and colleagues (Blöschl et al., 1991; Grayson and Blöschl, 2001; Grayson et al., 2002), significant advancements in the incorporation of spatially distributed snow observations, derived primarily from satellite images, have been made in both model calibration and evaluation. For example, Finger et al. (2011) used Monte Carlo simulations to assess the value of including snow cover images alongside glacier mass balance and discharge measurements in the multi-objective performance of a distributed hydrological model of the snow and ice-dominated Rhonegletscher catchment in Switzerland, finding a combination of snow cover and discharge data to be optimal. Duethmann et al. (2014) also employed a Monte Carlo approach, this time in an attempt to quantify the relationship between the information content and the number of snow cover images included in the calibration of a model covering several mountainous catchments in central Asia. In a comparison of two alternative strategies for the simulation of hydrological processes the high-elevation Andes, Ragettli et al. (2014) likewise incorporated snow cover data, although in this case for purely evaluative purposes. More recently, as part of an investigation into the mechanisms responsible for marked increases in suspended sediment concentrations that were observed in the upper Rhône in the 1980s, Costa et al. (2018) calibrated a simple snow model using distributed snow observations. Finally, additional studies have employed distributed snow images not as evaluation criteria but rather as model input (Berezowski et al., 2015; Wulf et al., 2016).

Whilst the aforementioned examples attest to the considerable progress that has been made lately, many common modelling approaches are associated with certain limitations that may affect their capability to generate reliable estimates of snow dynamics, and by extension accurate patterns of the arrival of meltwater at the land surface, in moderately-sized, topographically complex headwater catchments. Yet simulating snowpack dynamics in such catchments as accurately as possible is crucial to provide suitable inputs to the detailed, physically-based, spatially distributed hydrological models that are increasingly being applied with a view to better understanding often nuanced aspects of alpine hydrological systems in a fairly holistic sense, including their responses to external change (e.g. Tague and Grant, 2009; Kurylyk and Hayashi, 2017). The number and spatio-temporal variability of controls and processes influencing snow dynamics in rugged terrain (Clark et al., 2011) pose a substantial challenge, however.

The first important limitation is that despite the now widespread availability of relevant spatial data, spatially lumped (e.g. Wagner et al., 2017) or only partially distributed (Duethmann et al., 2014; Staudinger et al., 2017) hydrological models, which cannot represent heterogeneity on scales below the aggregation unit, continue to be frequently applied. Although such lumped models have their uses, integrating them with distributed observations is complicated; comparisons of catchment (or some other aerially) averaged snow covered area (SCA) must be resorted to (Ragettli et al., 2014), or else spatial variability somehow reimposed afterwards (Parajka and Blöschl, 2008). Moreover, snow patterns are of utmost importance many non-hydrological applications, including the prediction of vegetation species distributions (Randin et al., 2015) and winter tourism (Grünewald et al., 2010).

Secondly, irrespective of spatial discretisation, most previous hydrological modelling studies that have incorporated distributed snow observations relied on snow products from the Moderate Resolution Imaging Spectroradiometer (MODIS) (Clark et al., 2006; Duethmann et al., 2014; Ragettli et al., 2014; Engel et al., 2017; Costa et al., 2018). The 500 m pixel resolution at which binary (snow or no-snow) and/or snow covered fraction (f_{SCA}) data is available (Rittger et al., 2013) is simply too coarse for certain applications. For instance, both Ragettli et al. (2014) and Hanzer et al. (2016) report difficulties in capturing the complex snow patterns (e.g. small patches and snow-free ridges) that are commonly observed in rugged terrain using MODIS imagery. Consequently, the information content of these data with respect to relatively fine scale processes that can nevertheless substantially alter the internal hydrological functioning of steep mountain catchments is limited. Much higher resolution (30 m) snow maps can be derived from Landsat imagery, but thus far have only been applied for model corroboration or evaluation as opposed to calibration. Additionally, with the notable exceptions of Hanzer et al. (ibid.) and Wayand et al. (2018), only a small number of images have previously been considered (Bernhardt et al., 2012; Warscher et al., 2013; Schöber et al., 2010).

Thirdly, empirical temperature and other index-based methods for estimating snow (and ice) melt rates (Hock, 2003) remain standard (Ragettli and Pellicciotti, 2012; Addor et al., 2014; Etter et al., 2017), despite their capability to satisfactorily reproducing snow dynamics in complex alpine terrain being questionable (Warscher et al., 2013). Provided additional meteorological data are available, more sophisticated energy balance approaches (both full physics, multiple snow-layer configurations and simplified versions) have been advocated (Magnusson et al., 2015; Meeks et al., 2017). One particular attraction of distributed energy balance snow models in steep, complex terrain is that they explicitly represent all the fluxes that influence melt, as well as their pronounced spatio-temporal variability. Another benefit is that, in requiring reduced

calibration, energy balance models are likely to perform reliably under forcing conditions that exceed the range of historical observations – as is typically the case in climate change impact assessments (Mas et al., 2018) – than their simpler counterparts. Indeed, the most sophisticated full physics, multi-layered snow models such as Alpine3D (Lehning et al., 2006) can now be coupled with simple conceptual hydrological schemes (Gallice et al., 2016) to simulate snow dynamics across, and runoff from, entire catchments. That said, simulating wind and gravitational redistribution processes at these scales using physical algorithms remains computationally prohibitive (Mott and Lehning, 2010; Musselman et al., 2015; Brauchli et al., 2017). This poses a particular headache in very steep terrain, where accounting for gravitational snow redistribution especially is indispensable for hydrologically realistic simulations of the evolution of snow water equivalent (SWE) and meltwater patterns (Bernhardt et al., 2012; Kerr et al., 2013; Sommer et al., 2015); *in extremis*, failure to do so can lead to undesirable model artifacts ("snow towers"; Freudiger et al., 2017). Fortunately, a variety of pragmatic empirical correction methods and algorithms have emerged to enable such processes to be accounted for (Bernhardt et al., 2012; Vögeli et al., 2016; Marshall et al., 2019).

A more fundamental challenge associated with modelling mountain hydrological systems is that the meteorological inputs are often extremely poorly constrained. Due to wind-induced gauge undercatch, precipitation measurements tend to be systematically underestimated (Pan et al., 2016; Kochendorfer, Rasmussen, et al., 2017); this bias is most pronounced when the precipitation phase is solid (i.e. snow), and with increasing wind speed. Moreover, even in comparatively well-instrumented regions like the European Alps, meteorological station density decreases substantially with elevation (Pepin et al., 2015). When combined with the high degree of variably that characterises mountain meteorology (Mott et al., 2014), the upshot that even if the original ground measurements could be made perfectly, the resultant interpolated spatial fields would still be associated with considerable uncertainty. Both assessments of the error characteristics of common instruments (see e.g. the WMO-SPICE project; Kochendorfer, Nitu, et al., 2017) and careful investigations into spatial interpolation methods (Tobin et al., 2011) have been pursued to address this challenge. "Inverse" methods, whereby distributed models and snow observations are somehow integrated to estimate various important but uncertain parameters, are also beginning to be applied to overcome forcing data deficiencies.

For instance, in a snow model analysis that included both MODIS and Landsat-derived snow observations for evaluation, Engel et al. (2017) reported modifying a "snow correction factor" was required to compensate for biased measurements of winter precipitation and thereby improve fits. Shrestha et al. (2014), meanwhile, actually calibrated a distributed, multi-layer water and

energy balance model (WEB-DHM-S) to minimise the cumulative error in snow cover patterns (again according to MODIS) and discharge simulations; in so doing, an elevation dependent snowfall correction factor was optimised. A particular novelty of that study was that the correspondence between simulated and observed patterns was expressed at the pixel level. The same model was subsequently applied by Naseer et al. (2019), who – instead of applying traditional linear, elevation-dependent lapse rates for the spatial interpolation of meteorological data, which may break down in complex terrain – attempted to integrate 3D temperature profiles derived from climate model reanalysis data. There was no spatial component to the calibration undertaken in this study, however.

Finally, uncertainty quantification should ideally form a central pillar of all environmental modelling exercises. Whilst some previous studies have directly addressed uncertainty in SWE reconstructions (Franz et al., 2010; He et al., 2011; Slater et al., 2013; Meeks et al., 2017), this has predominately been undertaken only at discrete station locations (i.e. not using distributed models). In relation to this, it must be emphasised that as the sophistication, scale, and resolution a given "forward" model increases, the efficiency of any calibration and uncertainty quantification algorithms becomes a crucial consideration; even despite ever-increasing computational power, "brute force" approaches involving thousands of Monte Carlo simulations still quickly become impractical.

In this context, and with the intention of generating the most accurate representation of spatio-temporal "liquid water input" to a rugged and relatively data-poor Alpine catchment, this study proposes a novel, model-independent framework for the integration of high-resolution snow observations and distributed snowpack simulations. Initially, a fully-distributed energy balance-based snow model that additionally represents gravitational redistribution is established at high spatio-temporal resolution (25 m, hourly) using WaSiM (Schulla, 2017). An objective function incorporating both high-resolution snow cover maps derived from satellite imagery and reconstructed SWE time-series at two locations is then developed and minimised using an efficient, iterative calibration algorithm in order to estimate the values of parameters describing important snow-related processes. Via the inclusion of high-resolution distributed snow observations, SWE time-series, and a model that accounts for gravitational redistribution, this approach can be considered an extension of that presented by Shrestha et al. (2014) that is applicable to steeper, more rugged catchments. As far as is known, Landsat-derived snow cover images have never been previously used in the calibration of any distributed snow model. That the spatial fit metrics are computed for a much larger catalogue of images than previous studies, and that the uncertainty associated with selected key predictions (including the contribution of different parameters

and groups of observations to its reduction) can be elucidated are further distinguishing features of this study. Through the application of a dynamic glacier model and additional algorithms, commensurate spatio-temporal datasets of firn and ice melt, liquid precipitation, and potential evapotranspiration (ET_p) were also produced to inform a subsequent fully-integrated surface-subsurface hydrological model. The methodology holds considerable potential for improving representations of alpine snow dynamics that are required by several related disciplines.

3.2 Study area

The study area is slightly reduced from that of Chapter 2, being now comprised of only the two adjacent headwater catchments (the Vallon de Nant the Vallon de La Vare) and an immediately downstream area, covering a total area of 36.7 km^2 (Figure 3.1).

The elevational range is considerable, extending from 950 to over 3,050 m above sea level (a.s.l.). The topography is accordingly extremely steep in places (mean = 35°), and is rugged. Lower parts of the catchment are forested. At the Last Glacial Maximum, only the highest peaks protruded above the ice (Bini et al., 2009). An array of Quaternary unconsolidated sedimentary features overly the complex Mesozoic bedrock. These unconsolidated features have glacial, fluvial, and mass movement origins, and several of them are believed to act as aquifers.

Approximately 45% of annual precipitation falls as snow. Given the topographic steepness, gravitational snow redistribution occurs frequently, as evidenced by snow-free slopes and cliffs in the winter months. The photographs presented in Figure 3.2, meanwhile, which were taken in the Vallon de Nant on the 31 January 2018 following a period of exceptional snowfall (Bründl et al., 2019) illustrate the considerable snow redistribution that can occur under more extreme conditions. Intense summer thunderstorms are a further noteworthy feature of the area's meteorological regime. The surficial hydrology of the Vallon de Nant is characterised by its eponymous Nants – temporary torrents whose discharge responds rapidly to rain and snowmelt. Additionally, being shaded by surrounding cliffs, several small glaciers persist at relatively low elevations in the north-facing upper reaches of both sub-catchments.

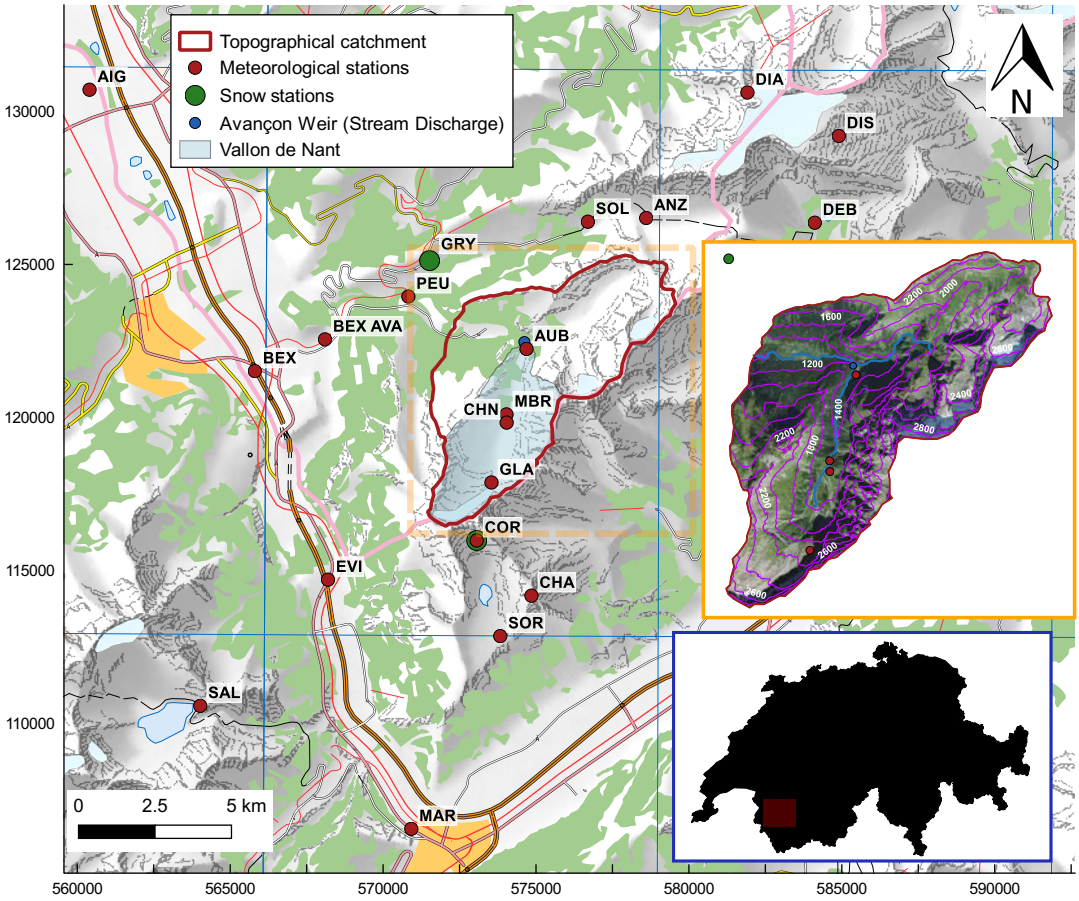

Figure 3.1: The study catchment and locations of measurement stations that provided data to the present study. The precipitation data at the SOR station were ultimately removed from input dataset as the measured totals seemed too low compared with nearby stations at similar elevations. Background data © swisstopo.

The Vallon de Nant has been a designated Natural Reserve since 1969 and the Vallon de La Vare also remains in a highly natural state, making the study area rather unusual in the context of the European Alps. Reflecting this, several recent environmental investigations have focussed upon the area, including those of Vittoz et al. (2009), Grand et al. (2016), Lane et al. (2016), Benoit et al. (2018), and Giaccone et al. (2019).

Figure 3.2: Evidence of pronounced avalanche activity in the Vallon de Nant following extreme snowfall in early 2018 (photographs taken 31 January 2018). If such redistribution are not accounted in models of snowpack dynamics, simulated meltwater patterns are likely to be unrealistic.

3.3 Data availability and processing

3.3.1 Meteorological forcing

The model requires gridded estimates of incoming shortwave radiation, precipitation, relative humidity, sunshine duration, air temperature, vapour pressure, and wind speed. No third-party meteorological datasets with the desired spatial and temporal resolution and/or crossing over in time with the available field measurements, the earliest of which began in 2016, existed at the outset. The forcing datasets for the present study were therefore developed from meteorological station measurements (Figure 3.1; Supplementary Table B.1).

Most of the stations belong to the official networks of MeteoSwiss and the WSL Institute for Snow and Avalanche Research (SLF), and are located several kilometres from the study catchment and, crucially, at lower elevations. At these stations, hourly sums for precipitation and hourly means for all other variables were downloaded from IDAWEB – the online data portal of MeteoSwiss (MeteoSwiss, n.d.) – the hydrological years 2015-2018 (i.e. 1 October 2014 to 30 September 2018).

These data were complemented by observations from stations belonging to a local network operated by the University of Lausanne (S. Hiscox, *pers. comm.*; Michelon et al. (2017) and subsequent updates via personal communication), several of which are located within the study catchment itself. Wang et al. (2018), amongst other studies, demonstrate the value of such "local" meteorological data to simulation exercises in mountainous terrain. That said, and unsurprisingly given the harsh environment and limited access (especially in winter), the local stations had a higher proportion of missing data than the nationally-operated ones. Fairly intensive processing and quality assurance efforts were therefore required.

Irrespective of the station operator, precipitation data from unheated gauges were not considered. Also, the precipitation data at SOR were eventually removed from the input dataset as the measured totals were deemed unrepresentative (too low compared with nearby stations at a similar elevations; Brauchli et al., 2018).

The processed time-series were then plotted and inspected interactively using niVis (SLF, n.d.[b]); the hourly time-series themselves are presented in the supplementary material, whilst the temporal coverage between stations and overall missing data percentages for each variable over the four-year simulation period are shown in Supplementary Figures B.1 and B.2.

The simulation period was limited to the four hydrological years 2015-2018 by a lack of reliable local meteorological and discharge data prior to this. Although relatively short, the simulation period contains a reasonable diversity of snow conditions, including both relatively snow-rich and snow-poor winters.

As already discussed, obtaining accurate spatial fields of meteorological variables in mountainous regions remains challenging. This situation has two direct implications for modelling. Firstly, precipitation measurements made using traditional instruments must be corrected for wind-induced undercatch and other factors that cause a systematic bias towards underestimation. Different corrections were applied depending on the the incident precipitation phase using Equations 3.1 and 3.2 (Schulla, 2017):

$$P_{corr} = P(snoa \cdot WS + snob) \quad TA < rstt \tag{3.1}$$

$$P_{corr} = P(liqa \cdot WS + liqb) \quad TA > rstt \tag{3.2}$$

where P is measured precipitation (mm), P_{corr} is corrected precipitation (mm), *snoa* (-) and *snob* (-) are global correction factors for solid precipitation, *liqa* (-) and *liqb* (-) are global correction factors for solid precipitation, *WS* is wind speed ($m \cdot s^{-1}$), and *rstt* is the rain-snow threshold temperature (°C).

The rain-snow threshold temperature, here denoted by *rstt*, is not a constant deterministic value, but instead varies in time and space (Jennings et al., 2018). As such, this parameter was optimised, alongside several others (see Section 3.4.2), through calibration. The magnitude of precipitation underestimation is likewise highly uncertain, although solid precipitation measurements are almost certainly more affected than liquid precipitation ones. For this reason, both *snob* and *snoa* were also calibrated, whilst *liqa* and *liqb* were assigned the fixed values of 0.01 and 1.02, respectively. It must be mentioned that neither the solid nor liquid precipitation error characteristics were known at individual stations and/or for individual events, which precluded any more targeted corrections.

The second implication is that the choice of spatial interpolation algorithms must be carefully considered. For example, given the pronounced and complex topography, both spatial and elevation dependencies in the various meteorological variables should ideally be accounted for. A 25 m resolution digital terrain model (DTM) (Swisstopo, n.d.) formed the model grid. Then, for each variable, an appropriate algorithm was applied to interpolate all available station measurements of that variable at each time-step. To account for their strong elevation dependence, air temperature, wind speed, relative humidity, and vapour pressure measurements were interpo-

lated using Elevation Dependant Regression (EDR). In the case of air temperature, the potential for variability in the linear relationships across elevation bands, including full temperature inversions, was permitted. For precipitation, meanwhile, a linear combination of Inverse Distance Weighting (IDW) and EDR was applied, the ratio of which, *idwedr*, was also subjected to calibration. In this way, a certain balance between spatial patterns and (spatially constant) elevational dependence in the measurements was achieved. Since incoming shortwave radiation and sunshine duration demonstrate more limited elevation dependence, they were interpolated more straightforwardly using IDW. Whenever IDW was applied, the maximum search radius was set such that no stations were excluded.

This approach differs from that taken in certain other studies in which either predefined or calibrated constant linear temperature-elevation gradients or elevation-precipitation gradients have been applied. For example, Brauchli et al. (2017) distributed corrected single station precipitation measurements across their study catchment by applying a constant lapse rate of 2 %/100 m. This and other studies (e.g. Naseer et al., 2019) suggest that in complex terrain, such constant lapse rates may be unrealistic. Avoiding the use of such constant gradients can therefore be considered a broadly positive feature of the methodology taken here, since it ultimately retains more of the spatial and temporal structure of the local meteorological measurements to be retained.

That said, with such an approach, the temporal coverage or "cross-over" between the underlying station data (shown in Supplementary Figures B.1 and B.2) becomes important because for a given meteorological variable and time-step, only stations returning observations of that variable at that time-step contribute to the resultant spatial field. In other words, no temporal gap filling or interpolation is undertaken, with each time-step being independent from the last. Consequently, uncertainty in the interpolated spatial fields is not constant but rather varies as a function of both the number and location of stations providing measurements of a given variable at a given time-step.

Finally, the interpolated hourly temperature and radiation grids were corrected to account for topographic shading effects using the scheme of Oke (1987). An empirical temperature factor involved in this step, *radc*, was also calibrated. All the aforementioned steps were all undertaken using the distributed model WaSiM (Schulla, 2017).

3.3.2 Snow observations

Two complementary types of observed snow data were developed to constrain the model; i) binary observed snow extent maps derived from Landsat 8 imagery, and ii) SWE time-series

at station locations. The imagery provides complete spatial coverage but only for temporal "snapshots" and moreover does not provide direct information on snowpack water storage. The time-series conversely provide high-frequency, temporally continuous information on SWE, but only at two discrete locations.

17 Landsat 8 scenes which were captured within the period of meteorological data availability (i.e. the hydrological years 2015-2018) and were cloud-free over the study area were prepared. For each, the Normalised Difference Snow Index (NDSI; Dozier, 1989) of every pixel was firstly calculated according to Equation 3.3.

$$NDSI_{L8} = \frac{B_3 - B_6}{B_3 + B_6} \tag{3.3}$$

where B_3 and B_6 are Bands 3 (0.525-0.600 µm) and 6 (1.560-1.660 µm) of a given Landsat 8 image, respectively.

The reflectance signatures of water bodies can give rise to NDSI values that, in image histograms, lie close to or even obscure the boundary between snow and non-snow-covered pixels (which have higher and lower NDSI values, respectively). Therefore, to prevent the signal from the large lakes present in the Landsat scenes having an adverse affect on the image classification, the lake extents were simply masked out.

Preliminary snow extent delineations were then made by applying a threshold corresponding approximately to the minima separating the two (usually) distinctive regions in the image histograms, i.e. one mass of pixels with lower NDSI values which can be confidently be classified as no-snow, and a second mass of pixels of higher NDSI values which clearly correspond to snow-covered areas. The resultant binary maps were then overlain upon the corresponding True Colour Composite (TCC) images and visual comparisons made. Following this, the thresholds for each image in turn were manually refined until satisfactory final classifications were reached. As part of this process, the sensitivity of the derived snow extents the threshold (varied within a plausible range) was qualitatively assessed. Figure 3.3 illustrates the main steps involved. The final thresholds varied somewhat between images – see Härer et al., 2018 for a dedicated exploration of NDSI threshold choice. Whilst the manual approach to threshold identification employed here was feasible for this fairly small image catalogue of images, generating accurate snow maps for a larger collection of images would require a more automated procedure.

Finally, to facilitate their integration in the automated calibration process, the maps were re-projected to the CH1903 system (EPSG: 21781), clipped to the study catchment, and down-

scaled from their native 30 m resolution to align with the 25 m resolution model grid using the nearest neighbour approach. The full catalogue of observed snow extents, which together encompasses practically the full range of possible snow cover conditions, is shown in Figure 3.4. Supplementary Figure B.4, meanwhile, provides comparisons of all TCC images and delineated observed snow extents (alongside their corresponding final simulated outputs).

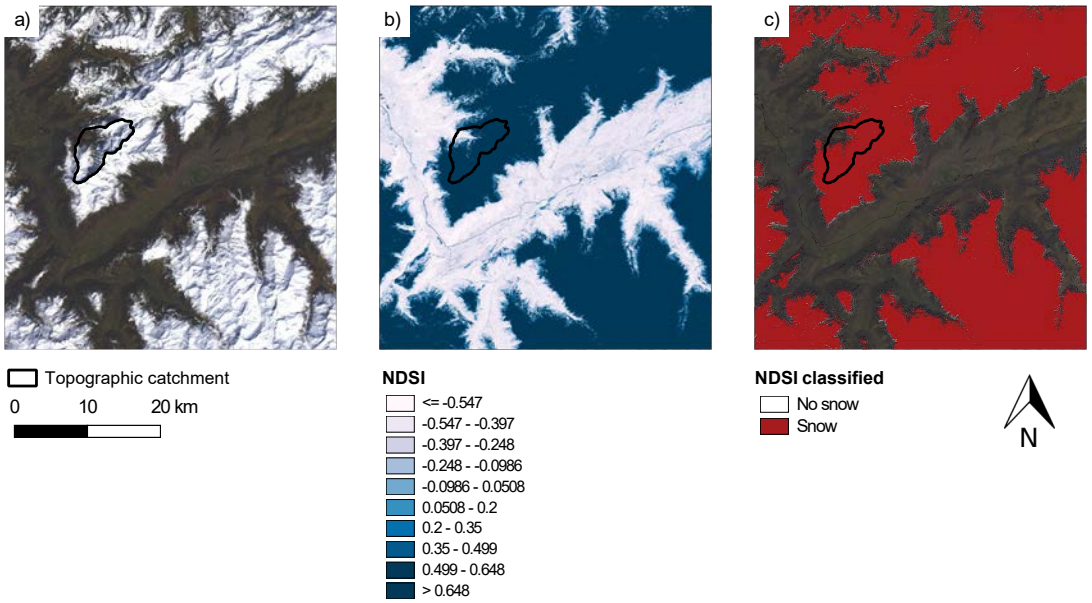

Figure 3.3: Illustration of the process followed to generate the binary snow extent maps, taking the 8 April 2015 as an example: a) True Colour Composite, b) calculated NDSI raster, and c) final binary observed extent developed by identifying and applying a threshold to (b). Each image in the observed catalogue was individually inspected and classified in this fashion.

Besides the more general issues of cloud cover and temporal gaps between satellite overpasses, dark forest canopies and areas of shadow constitute the main challenges associated with using the NDSI to map snow extents in steep mountainous terrain (Wang et al., 2015). Regarding the present study, whilst a small number of snow-covered pixels under dark forest and in heavily shaded snow-covered terrain may have been misclassified as snow-free, the maps generally compare very well the TCC images. Moreover, the sensitivity assessment of the classified snow extents to plausible thresholds mentioned above found it to be small. As such, the maps can be taken to represent snow extents with a reasonably high degree of accuracy, especially in the more open upper regions of the catchment where snow patterns are of most interest.

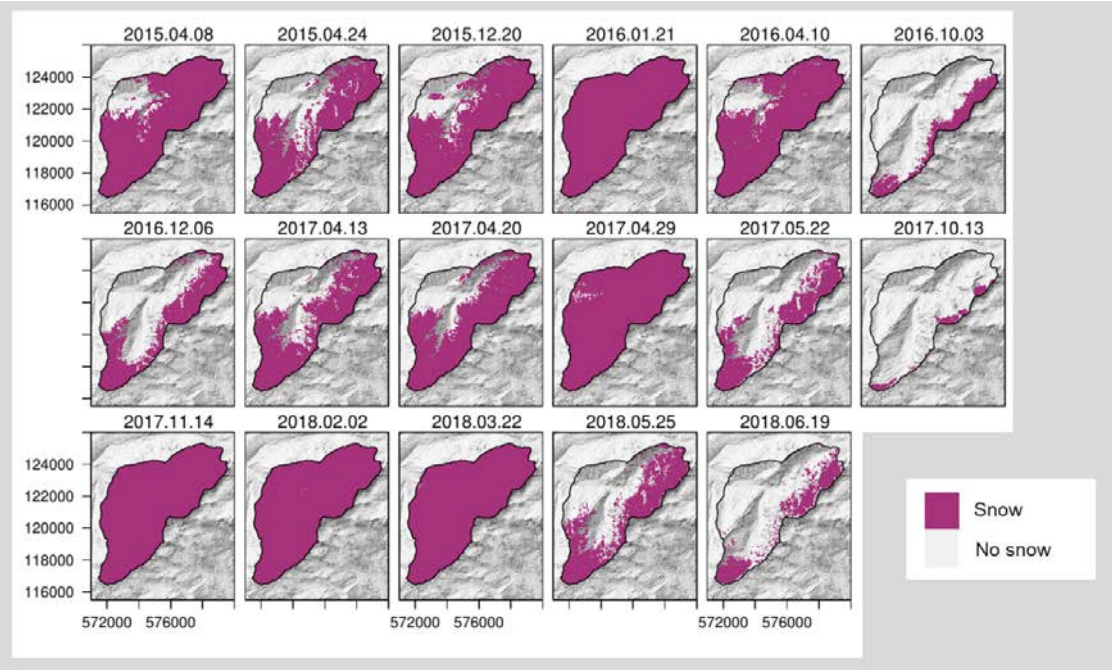

Figure 3.4: The complete catalogue of 30-metre resolution observed snow extent maps that was compiled. The date of each image is indicated above the respective pane. Coordinates are given in the CH1903 system throughout.

With a view to informing the model with more direct information on snow water storage, time-series of SWE were also reconstructed at two contrasting station locations using different methods according to data availability. As the single layer snow model configuration employed only provides total snow water storage (as opposed to full information on the interrelation between snowpack density, depth, and SWE), SWE reconstructions were also required to enable direct comparisons with the model outputs.

The two stations providing regular snow measurements over the period in question were located just outside the study catchment, with each lying towards one extreme of its elevational range (see Figure 3.1). These data were again obtained from the MeteoSwiss data portal. The high elevation station, Grand Cor (COR; Elevation: 2,602 m), belongs to the SLF's Intercantonal Measurement and Information System (IMIS) (SLF, n.d.[a]). These stations do not measure solid precipitation directly, but instead record snow height and several other variables that can be used to drive the 1D physically-based, multi-layer model SNOWPACK (Lehning et al., 2002), which also underpins the distributed model Alpine3D. An hourly time-series of the evolution of SWE at COR over the entire four year simulation period was constructed in this fashion.

The second, lower elevation station is located in Gryon (GRY; Elevation: 1,146 m). Unlike at COR, only (manual) daily snow height measurements are made here, making it impossible to apply SNOWPACK. The empirical model of Jonas et al. (2009), which was constructed from a large sample of snow observations from the Swiss Alps and enables the estimation of snow density as a function of geographic region, month of the year, and elevation, was therefore applied. Parameters corresponding to the elevation band <1,400 m were applied, along with the "Region 1" offset were applied; these being applicable to the site. The resultant densities were then multiplied by measured snow heights to give SWE at daily intervals.

As such, neither of the "observed" SWE time-series, which are presented alongside their simulated counterparts from the final model in Figure 3.6, are actually direct measurements. In order to utilise these data model calibration, the simulation domain was extended slightly.

3.3.3 Stream discharge

A concrete weir gauging station located at the outlet of the Vallon de Nant sub-catchment (E: 574,620, N: 122,462) provides high-frequency streamflow estimates from spring 2016, from which hourly mean flows were calculated for (brief) use later in this work. The empirical stage-discharge relationship (i.e. rating curve) underpinning the data was developed by salt dilution gauging (Ceperley et al., 2018). Despite the regular cross-section, these data are somewhat uncertain, especially at flow extremes (at low flows, this is due to shifting channel configurations immediately upstream of the weir).

3.4 Numerical modelling and calibration

3.4.1 Simulating snow accumulation, redistribution, and melt

Like for the precipitation correction and meteorological data interpolation, WaSiM (Schulla, 2017) was selected to form the foundation of the snow modelling approach. This decision was made following a review and some testing of possible alternatives, including Alpine3D which – although a strong contender – does not account for gravitational snow redistribution or glacial dynamics. Snow accumulation, redistribution, and melt were calculated at an hourly time-step on the 25 m model grid. To achieve this, the precipitation phase was first estimated for each pixel and time-step by according to the interpolated air temperature and a transitional range

within which both solid and precipitation can occur (Equation 3.4).

$$S_{frac} = \frac{rstt + T_{trans-TA}}{2 \cdot T_{trans}} \; for \; (rstt - T_{trans}) < TA < (rstt + T_{trans}) \tag{3.4}$$

where S_{frac} is the fraction of the total precipitation that is snow (0-1), *TA* is the air temperature (°C), *rstt* is the rain-snow threshold temperature, and T_{trans} is half of the rain-snow transition temperature range (°C).

T_{trans} was fixed to 1°C (i.e. the total transition range was 2°C), whilst *rstt* took the same (calibrated) value as that applied to distinguish precipitation phase in the earlier correction phase (Equation 3.1). Snowmelt was then calculated by solving the surface energy balance for the energy available for melt following the approach of Warscher et al. (2013). In this scheme, the snowpack is treated as a single homogeneous layer beneath the surface, for which the energy balance is computed using Equation 3.5.

$$Q + H + E + A + G + M_{ae} = 0 \tag{3.5}$$

where Q is the shortwave and longwave radiation balance, H is the sensible heat flux, E is the latent heat flux, A is the advective energy supplied by solid or liquid precipitation, G is the soil heat flux (which is small compared to other fluxes and was set here to 2 $W \cdot m^{-2}$, and M_{ae} is the energy potentially available for melting during a given time-step.

Melting and non-melting conditions were distinguished according to *rstt*. When the energy balance is positive (i.e. $M_{ae} > 0$) and air temperature favourable, melt (M) can occur. Finally, M is expressed in mm of water by introducing the latent heat of fusion, c_i (Equation 3.6).

$$M = \frac{M_{ae} \cdot dt}{c_i} \tag{3.6}$$

Sublimation, which can amount to an important component of the alpine water balance (Strasser et al., 2008), is explicitly modelled in this approach. Two additional scaling parameters, *lwin* and *lwout*, could be modified their default values of one in order to fine tune the incoming and outgoing longwave components of the energy balance, respectively; in this way, potential errors in both albedo and cloudiness could be accounted for. Here, both were subjected to calibration, albeit within relatively narrow bounds (see Table 3.1).

Gravitational redistribution was additionally simulated using a mass-conservative algorithm that is underpinned by a topographic analysis. It was implemented in WaSiM by Warscher et al. (2013). Several steps are involved; along with the previously introduced approaches, these are

comprehensively described by both Warscher et al. (ibid.) and Schulla (2017). Here, merely the main parameters are discussed. Two of these represent the critical local slope limits; *mids* controls the lower inclination limit for gravitational slides, whilst *mads* is the upper inclination angle above which all incoming snow is immediately transported downslope. Since these slope angles are dependent on the model grid scale, they cannot easily be transferred from previous studies, and were therefore included as calibration targets. Following the advice of Schulla (ibid.), two further parameters related to the gravitational redistribution were also calibrated. *frss* is the fraction of the snowpack at a given time-step that can form a slide. Its value should usually be set to some small fraction of the current snow storage in a cell, typically on the order of 1% (although this is time-step dependent). *scmd* is an upper depositional mass limit (mm) for snow flows. Whilst such an approach is capable of estimating plausible snow redistribution patterns, it must be emphasised that the specific timing of avalanches cannot be predicted in such a fashion (Warscher et al., 2013).

Warscher et al. (ibid.) also proposed a simple algorithm designed to account for the redistribution of snow by wind. More recently still, methods seeking to improve WaSiM's representation of the interaction between snow and coniferous forest canopies have been published (Förster et al., 2018). However, neither of these sets of algorithms were included in the final model of this study; including wind algorithm actually resulted in poorer model fits to the observations (see later discussion), whilst the WaSiM release containing the extensions of Förster et al. (ibid.) came to late for them to be thoroughly evaluated.

3.4.2 Multi-objective calibration

As already mentioned, although the model has an energy balance core, several empirical parameters (11 in total) required estimating. Table 3.1 lists these parameters along with the upper and lower bounds that were assigned to each on the basis of prior knowledge. Raleigh et al. (2016) showed that behind temperature and precipitation, longwave radiation measurements most strongly affect energy balance snow simulations results, and moreover noted that longwave measurements are uncommon in high elevation terrain; such considerations justify including parameters related to longwave radiation in the calibration. For numerical reasons, all parameters were log transformed, hence why the lower bounds of three parameters which would ordinarily have been zero were marginally higher than that. The final estimated values are also listed to prevent the later duplication of a similar table.

Parameter	Description	Lower Bound	Upper Bound	Estimated value
rstt	Snow-rain temperature threshold (°C)	0.0000001	3.5	0.0266
snoa	Snow precipitation correction (-)	0.0000001	0.15	0.0283
snob	Snow precipitation correction (-)	1.45	1.45	1.4500
radc	Factor for temperature correction (-), $radc \cdot (-1.6.... + 1.6)$, in the radiation correction module	0.1	8.0	0.1731
mads	Maximum slope for snow deposition (°)	45.0	75.0	73.5269
scmd	Upper deposition limit for gravitational redistribution (mm)	0.0000001	10.0	1.1497
mids	Minimum slope for gravitational slides (°)	20.0	48.0	43.3811
frss	Fraction of snowpack that forms the slide (0-1)	0.001	0.05	0.0076
idwedr	Relative weight of IDW to EDR in the interpolation of precipitation (0-1)	0.05	0.85	0.05
lwin	Correction factor for incoming long wave radiation for fine tuning the energy balance (accounting for errors in cloudiness and albedo)	0.7	1.3	1.2167
lwou	Correction factor for incoming long wave radiation for fine tuning the energy balance (accounting for errors in cloudiness and albedo)	0.7	1.3	1.1920

Table 3.1: WaSiM model parameters that were subject to calibration. The final estimated parameter values are also reported here to prevent the later duplication of a very similar table.

A novel, multi-objective calibration approach that incorporated both the spatial snow extents and the reconstructed SWE time-series was then developed. For each of the 17 days on which an observed extent map had been produced, the spatial component of the overall goodness-of-fit for each model iteration was quantified as follows:

1. The simulated SWE maps at the end of the days for which observed maps were available were extracted and clipped to the extent of the study catchment.

2. Pixels in the simulated SWE maps were reclassified to either snow or no-snow using a 5 mm exceedance threshold (i.e. pixels with SWE > 5 mm were classified as snow covered).

3. All pixels were binned into one of the quadrants of the contingency matrix shown in Table 3.2 according to whether snow presence/absence had been correctly simulated in comparison with the observed maps or not.

4. Three related performance metrics were calculated after Aronica et al. (2002) using Equations 3.7 to 3.9.

	Observed snow	**Observed no snow**
Simulated snow	a	b
Simulated no snow	c	d

Table 3.2: Contingency matrix used for the per pixel classification of distributed snow model outputs.

$$F_1 = \frac{\sum_{i=1}^{n} a + \sum_{i=1}^{n} d}{n} \tag{3.7}$$

$$F_2 = \frac{\sum_{i=1}^{n} a}{\sum_{i=1}^{n} a + \sum_{i=1}^{n} b + \sum_{i=1}^{n} c} \tag{3.8}$$

$$F_3 = \frac{\sum_{i=1}^{n} a - \sum_{i=1}^{n} b}{\sum_{i=1}^{n} a + \sum_{i=1}^{n} b + \sum_{i=1}^{n} c} \tag{3.9}$$

where a, b and c are the quadrants of the contingency matrix (Table 3.2), and n is the total number of pixels.

F_1 corresponds to the overall proportion of correctly simulated pixels. F_2 and F_3 typically result in lower scores since they expressly discount pixels that are snow free in both simulations and observations; on many days this quadrant can be heavily populated, snow-free pixels at lower elevations being relatively easy to reproduce (Warscher et al., 2013). In each case, a perfect fit between simulations and observations would return a value of one. Therefore, for each model iteration, the squared residuals between the three F-statistics obtained and one was calculated. Model performance with respect to the observed SWE time-series was quantified according to the squared residuals of simulated and observed values at each time-step.

In constructing a single multi-objective function that could be minimised and thus produce the best overall fit according to both types of observations, weights had to be assigned to each individual squared residual. The aim of this (subjective) process was to ensure that each observation

had a certain "visibility" in the calibration process, whilst an appropriate balance between the two data types was also achieved. The hierarchical weighting scheme illustrated in Figure 3.5 was ultimately settled upon.

In summary, the spatial data were weighted slightly more heavily than the time-series (60:40), thereby ensuring that both types had a strong influence but with the spatial patterns being slightly dominant (the spatial pattern calibration being a key novelty). To reflect their more stringent nature, F_2 and F_3 values were double weighted with respect to F_1 values. Finally, to account for the disparity in measurement frequency at the snow stations – hourly at COR but only daily at GRY – observations at the latter were assigned weights 24 times higher than those at the former to ensure parity. The objective function (OF) is expressed in Equation 3.10.

$$\begin{aligned} OF = \sum_{i=1}^{17}[wF_1(1-F_1)^2] + \sum_{i=1}^{17}[wF_2(1-F_2)^2] + \sum_{i=1}^{17}[wF_3(1-F_3)^2] \\ + \sum_{i=1}^{35063}[wCOR(COR.SWE_{sim} - COR.SWE_{obs})^2] \\ + \sum_{i=1}^{1461}[wGRY(GWR.SWE_{sim} - GWR.SWE_{obs})^2] \end{aligned} \tag{3.10}$$

where wF_1,wF_2, wF_3, *wCOR*, and *wGRY* are the relative weights that were assigned to each observation belonging to the different observation groups, as illustrated in Figure 3.5, i.e. 0.706, 1.412, 1.412, 0.0057 and 0.01368%, respectively, F_1, F_2, and F_3 are the fit statistics calculated for each of the 17 pairs of images according to Equations 3.7 to 3.9, and $COR.SWE_{sim}$, and $COR.SWE_{obs}$, $GRY.SWE_{sim}$, and $GRY.SWE_{obs}$ are the observed and simulated SWE values at each time time-step at the COR and GRY stations, respectively.

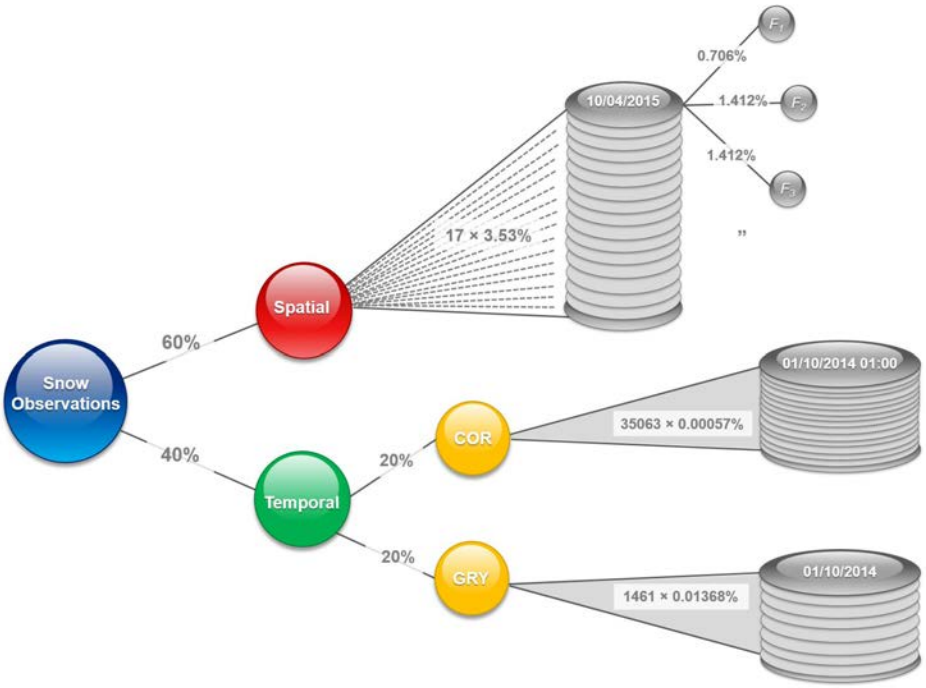

Figure 3.5: Diagram illustrating the weights, expressed as percentages (%) of the total, that were assigned to each individual snow "observation". For each observed snow extent map, the three F-statistics (with each being given a value of one) were treated as individual observations. In total, there were 51 (17×3) distinct spatial "observations", 35,063 (hourly) SWE observations spanning the four-year simulation period at COR, and 1,461 (daily) observations spanning the same period at GRY. The 5 observation groups (i.e. F_1, F_2, F_3, *COR* and *GRY*) also formed the categories for the subsequent linear uncertainty analysis.

The WaSiM model was then linked with PEST (Doherty, 2019) – a model-independent, gradient-based parameter estimation tool which uses the Levenberg-Marquardt algorithm. PEST repeatedly runs the model, altering the calibration parameter values each iteration in an attempt to minimise the objective function. PEST was selected primarily due to its efficiency, which is considerably higher than the more commonly applied Monte Carlo-oriented approaches. Indeed, parameter search efficiency was crucial given the relatively high computational demands of the energy balance-based snow model. Practically speaking, the coupling was achieved by implementing routines to i) extract the spatial and temporal model outputs corresponding to the observations and ii) calculate the required statistics (see Thornton et al., 2019). The final parameters values obtained are presented in Table 3.1.

3.4.3 Predictive uncertainty and data worth analyses

Following calibration, a linear analysis was conducted to quantify the pre- and post-calibration uncertainty associated with selected individual "predictions" of interest (the term predictions is not used here in its future sense); namely, the SWE at COR on 1 April in each of the four simulated hydrological years (2015-2018), and the F_1 spatial metric for 22 May 2017. This approach enables any reduction in uncertainty achieved through the calibration process to be evaluated.

1 April SWE at station locations is an indicator commonly employed by environmental managers in snowmelt dependent regions to assess likely water availability throughout the subsequent summer. The spatial prediction was included because few (if any) previous studies have specifically considered uncertainty in predictions of snow patterns.Analyses quantifying the contribution of individual parameters to pre- and post-calibration uncertainty variance, as well as the information provided by the five observation groups to the calibration process (i.e. "data worth"), were also undertaken. To achieve all of these tasks, tools from PEST's GENLINPRED suite were applied. For a through description, readers are referred to Doherty (2010) and Doherty (2019).

In contrast to the model calibration phase, an identical weight was assigned to all non-zero weighted observations for these analyses (zero-weighed observations being the predictions of interest). Following the advice of Doherty (2010), this weight was estimated by taking the number of non-zero weighted observations (here 36,570), calculating its square root, and dividing the result by the calibrated model objective function (91,150) – giving a value of 0.002098.

3.4.4 Estimating glacial melt, liquid precipitation, and potential evapotranspiration

To generate comprehensive forcing data for subsequent distributed hydrological modelling (Chapter 5), four additional datasets were also generated using the model. These are liquid precipitation, firn melt, ice melt, and ET_{p}. Firstly, to account for liquid precipitation in addition to snowmelt, grids which are referred to as "snowcover outflow" were written at each time-step. These represent the sum of liquid precipitation on snow-free pixels and snowmelt (as calculated by the snow model) from snow-covered pixels. As Section 3.3.1 explained, modest fixed corrections were applied to the original liquid precipitation measurements to account for undercatch. Accordingly, for snow-free pixels, the "snowcover outflow" values correspond to any (corrected, interpolated) rainfall falling.

As the aerial proportion of glaciers in the study catchment is small (<3%), glacial melt makes a much smaller contribution to annual, catchment-averaged meltwater input than snowmelt here. Nevertheless, localised glacial meltwater generation in summer can be considerable. As such, a dynamic glacier model accounting for the accumulation, dynamics, and ablation (with radiation correction) was applied in WaSiM. The parameters of this model were not calibrated due to the overall dominance of snowmelt and a lack of glacier-related data; the Glacier des Martinets, for instance, has not actively monitored since 1975 (SCNAT, 2018).

For snow on the glaciers, an approach identical to the main snow model was applied. In this way, separate hourly, 25 m resolution grids representing snowmelt, firn melt, and ice melt from glacierised areas were produced. The final WaSiM control file is provided in the associated data and code (Thornton et al., 2019). Besides containing all the optimised snow-related parameters, this file indicates the values of the (fixed) parameters that were applied in generating these additional datasets. It is envisaged that With only slight modification (possibly related to the distinction between snow and bare glacier ice in the NDSI images), the approach could be easily transferred to much more glacierised catchments.

More specifically, the meltwater outputs from the glacier model had to be normalised according to the glacier covered fraction of each cell at each time-step, which ranged between 0 and 1. Having done this, the "snowcover outflow" rasters at each timestep could be summed together the corresponding normalised "snowmelt on glacier", "firn melt", and "ice melt" grids, thereby producing a single set of hourly rasters representing all liquid water arriving at the surface (a.k.a. "surface water input"). These calculations were carried out by executing batch GDAL scrips via OSGeo4W (GDAL, n.d.; OSGeo4W, n.d.). Raster units were also converted in a similar fashion in preparation for the subsequent hydrological modelling in Chapter 5.

Finally, the Penman-Monteith method was used to estimate 25 m resolution, hourly ET_{p}. To achieve this, classes in the the land cover map that was developed for WaSiM from existing swisstopo datasets (swisstopo, n.d.) (Supplementary Figure B.3) were attributed with appropriate physical parameters (e.g. Leaf Area Index; LIA). See Fuhrer and Jasper (2012) for further details. No additional processing of the ET_{p} grids was required (apart from unit conversion for subsequent hydrological modelling).

In having identical spatio-temporal resolution, and having moreover been generated using predominantly physically-based approaches, all resultant datasets can be considered broadly commensurate with one another.

3.5 Results and discussion

3.5.1 Estimated parameter values

The parameter values estimated via inversion (Table 3.1 can be considered an initial set of "results" in their own right. Two in particular are interesting to briefly consider. Firstly, the high value of 1.45 taken by the wind speed-independent snow correction constant, *snob*, which actually reached the upper bound permitted, attests to the considerable underestimation bias generally contained within the winter station precipitation measurements. It must be remembered that in the approach applied herein, this constant factor is combined with the wind speed-dependent factor, *snoa*, which was estimated to be 0.0283 (i.e. an increase of 2.83% per additional $m \cdot s^{-1}$ of wind speed), and the interpolated wind speed to determine effective precipitation. Secondly, *idwedr* took on its lowest permitted value, i.e. improved fits were obtained when a strong elevational gradient was enforced upon the interpolated precipitation fields.

The magnitude of the estimated solid precipitation correction factor is broadly consistent with existing literature. For instance, Sevruk (1985) suggested that overall, precipitation in Switzerland is underestimated by between 4% (in summer at low elevations) and approximately 40% (at high altitudes in winter). Pan et al. (2016), meanwhile, found the sheltering effect of surrounding vegetation to be an important influence on the magnitude of any underestimation in northern Canada, with well-sheltered sites requiring much less correction. At open sites, the bias corrections they applied increased annual precipitation by between 15 and 34%. At windy sites with high snowfall proportions, it was noted even larger corrections – even exceeding 50% – can be necessary. Finally, in their simulation of a 200 km^2 region of Switzerland, Bavera et al. (2014) applied a fixed 30% factor to solid precipitation.

3.5.2 Correspondence with observations

The spatial goodness-of-fit statistics (i.e. F_1, F_2, and F_3) obtained following calibration are shown in Table 3.3. The corresponding observed and simulated snow maps from which these statistics were calculated, meanwhile, are shown in Supplementary Figure B.4.

Date	F_1	F_2	F_3
08/04/2015	0.852	0.847	0.696
24/04/2015	0.786	0.698	0.511
20/12/2015	0.838	0.798	0.699
21/01/2016	0.999	0.999	0.999
10/04/2016	0.871	0.849	0.819
03/10/2016	0.910	0.621	0.399
06/12/2016	0.750	0.596	0.199
13/04/2017	0.744	0.569	0.504
20/04/2017	0.790	0.752	0.508
29/04/2017	0.567	0.561	0.561
22/05/2017	0.846	0.626	0.434
13/10/2017	0.958	0.131	0.073
14/11/2017	1.000	1.000	1.000
02/02/2018	0.997	0.997	0.996
22/03/2018	0.963	0.963	0.963
25/05/2018	0.773	0.584	0.348
19/06/2018	0.844	0.328	0.089
mean	**0.852**	**0.701**	**0.576**

Table 3.3: Post-calibration F-statistics quantifying the spatial goodness-of-fit for each of the 17 days.

The F-statistics are generally reasonably high; across the 17 days, the average of the percentage of correctly simulated pixels being 85%. As expected, the scores decline progressively from F_1 to F_3. Moreover, a relatively high degree of variably in the statistics from one image to another was observed, the fit scores achieved naturally being best on completely snow covered mid-winter days. The lowest F_1 value was returned for the 29 April 2017 when a late season snowstorm that briefly blanketed the catchment was unfortunately missed by the model.

Figure 3.6, meanwhile, shows the comparison between simulated and observed SWE time-series at the two measurement stations.

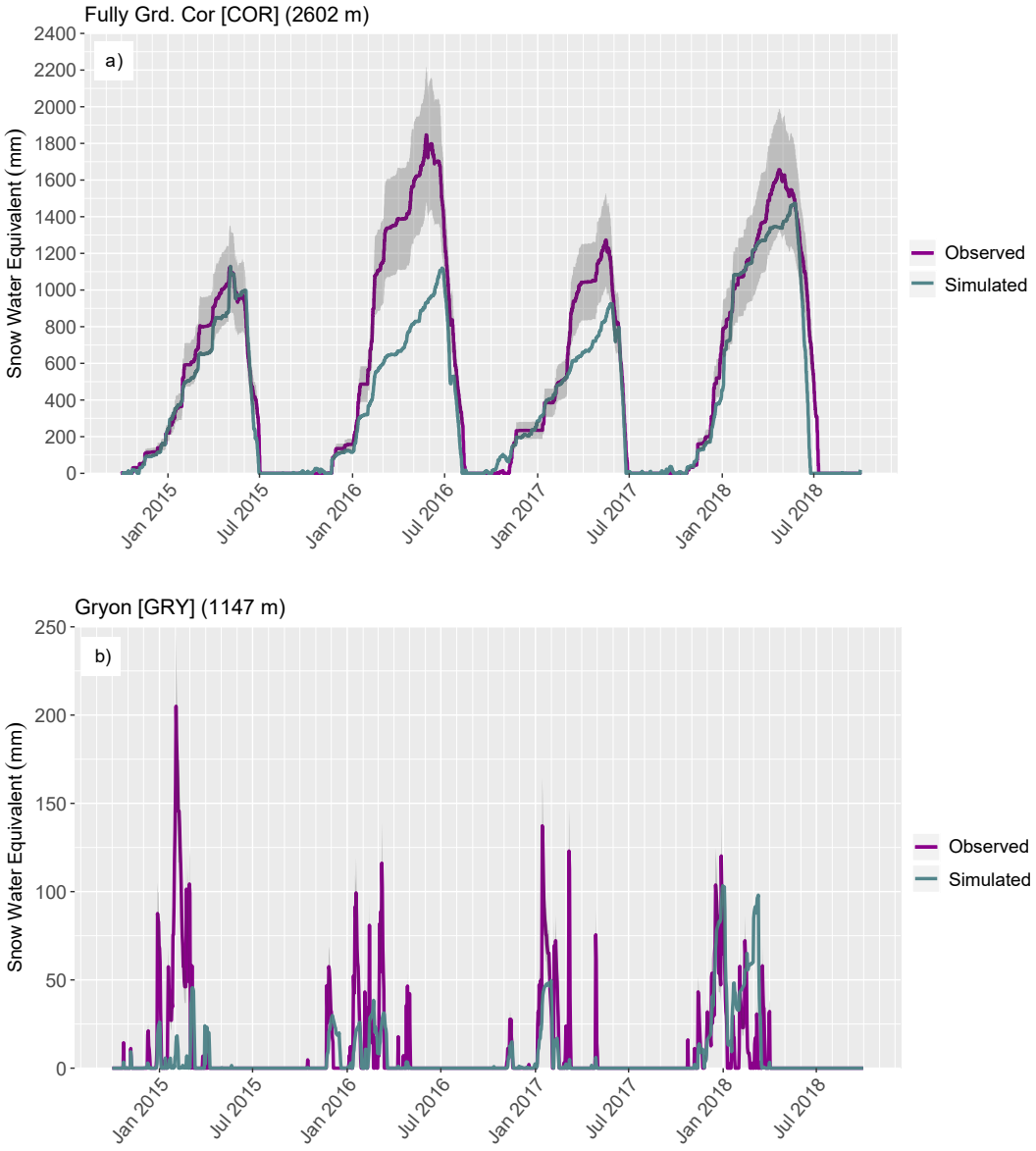

Figure 3.6: Observed and simulated Snow Water Equivalent (SWE) time-series at the two measurement stations, Fully Grand Cor (a: COR, hourly) and Gryon (b: GRY, daily). The observations are not direct measurements of SWE, but rather are reconstructions based on snow depth and other measurements at COR, and purely snow depth at GRY. The grey bar of $\pm 20\%$ is added around the reconstructed "observed" series to reflect the pixel-point nature of these comparisons.

The dynamics of snowpack evolution are replicated adequately, including the contrast between seasonal snowpack at the higher elevation station (COR) and the more intermittent pattern at the lower elevation one (GRY). The colder prevailing conditions at COR allow the results to

be discussed explicitly in terms of the accumulation and ablation phases. This simulated onset of accumulation closely matches the observations, as do changes in the rate of accumulation. The timing and rate of ablation is likewise broadly consistent with the observations. However, there does seem to be a general tendency towards underestimation of the accumulation totals. A similar underestimation is evident in the first three years at GRY. Across both stations, the best reproduced observations are those from winter 2017/2018.

In evaluating these results, it must be emphasised that the key meteorological variables of precipitation at COR, and both precipitation and temperature at GRY, were not actually measured at these locations but rather had to be spatially interpolated (onto the corresponding model cells) from station measurements elsewhere. As such, much of the residual post-calibration remaining likely arises from uncertainties in these interpolations. In addition, it should be re-emphasised that the "observations" are in not in fact direct measurements, but were themselves reconstructed via modelling; with two different methods being used according to data availability. Finally, the observations were made at discrete station locations, whilst the simulated values correspond to the 25 m pixel within which each station was located. Hence, should the terrain at the station locations not be entirely representative of its immediate surroundings, this represents another potential source of mismatch. A shaded region corresponding to $\pm 20\%$ around the observations was added to the plots to reflect this – that being roughly the maximum SWE mismatch one could expect for this reason (T. Jonas, *pers. comm.*).

3.5.3 Comparison of simulated spatial statistics with previous studies

In Figure 3.7, the F-statistics obtained in this study are compared those reported in previous studies which also employed F-statistics to quantify the fit between distributed snow models and snow extent maps derived from Landsat imagery. Three such studies are known of, each of which only reported the statistics for a small number of days (between one and three). More specifically, Schöber et al. (2010) only presented F_1 values for two days, but did so for numerous different catchments, while Bernhardt et al. (2012) and Warscher et al. (2013) provided all three F-statistics for their respective study catchments and selected days. Unlike this study, which also included mid-winter and late summer days in the calibration image catalogue, the previously published statistics correspond exclusively to spring and early summer periods (i.e. partially snow-covered conditions). As such, to enable the fairest possible comparison, only statistics from this study corresponding to spring and early summer were considered. The underlying

data are complied in Supplementary Table B.2.

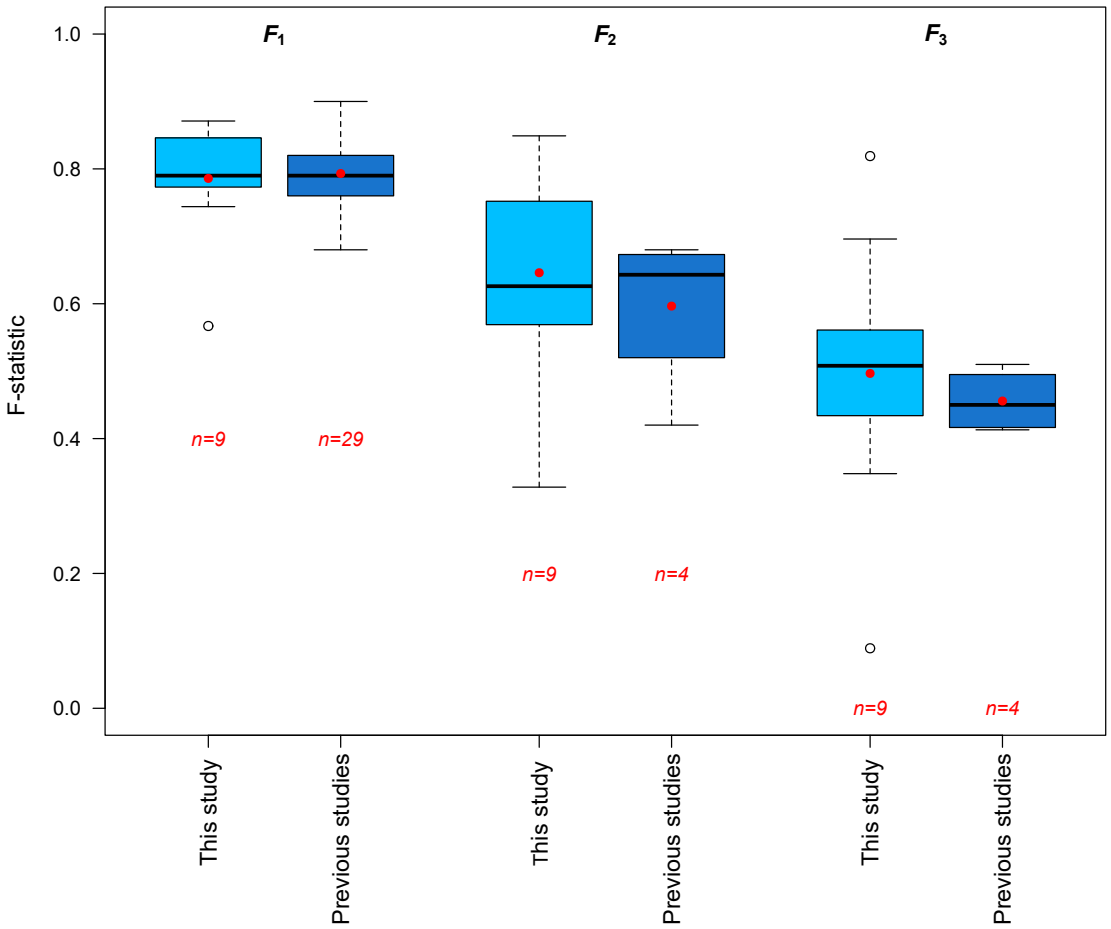

Figure 3.7: Comparison between the spatial model fits obtained in the present study and previously reported equivalents (i.e. the same metrics generated with respect to Landsat imagery). For the fairest possible comparison, only the F-statistics from this study that corresponded to spring and early summer (i.e. 08/04/2015, 24/04/2015, 10/04/2016, 13/04/2017, 20/04/2017, 29/04/2017, 22/05/2017, 25/05/2018, 19/06/2018) are included. The medians are shown using a thick black line in the traditional fashion, whilst the means are indicated by the red dots.

The F-statistic distributions obtained in this study seem to have a tendency to be slightly higher than those of previous studies, even if the mean and median of F_1 are marginally lower than those calculated from the previously published values. This tendency appears to be most pronounced for F_2 and F_3; in both cases the mean values obtained in this study are higher than counterparts from previously published studies. It is important and interesting to note that, with the possible exception of Schöber et al. (2010) who may have used the spatial snow observations

in an informal fashion to adjust certain parameters in their snow model (ambiguity remains as this step was not fully explained), the previous studies used the spatial data purely for model evaluation (i.e. in contrast to the present study, in which they formed calibration targets).

As such, while perhaps slightly disappointing that the explicit calibration did not yield higher F_1 scores, a real benefit of calibration can arguably seen in the noticeably higher F_2 and F_3 scores. Indeed, it may be recalled that these metrics were assigned enhanced weight in the calibration processes. That said, the small sample sizes must be bourne in mind when making such interpretations.

An additional consideration is that the calibration was not informed solely by the observed snow extent maps, but rather sought to obtain an acceptable balance between fits according to both the maps and reconstructed SWE time-series. It is likely that improved spatial fits could have been achieved if the maps alone comprised the objective function, but this may have come at the expense of a reduced accuracy in the simulated catchment-wide snow water storage.

In summary, a much fuller catalogue of previously published F-statistics would certainly be required to assess the statistical significance of these results, i.e. whether or not the calibration approach proposed does lead to real improvement in the capabilities of distributed snow models to reproduce high-resolution observed snow extents. Nevertheless, the comparisons presented confirm the overall appropriateness of the approach taken, and perhaps even allude to the value it adds. Finally, given the variability in the F-statistics obtained between days, the larger number of days for which performance statistics were presented here to shed light upon this is a positive distinguishing feature of this study; previous studies report the statistics from a small number of days, and so it is unclear how consistent in time the (generally good) performance of the previously published models might be.

3.5.4 Snowpack evolution and hydrological plausibility

A key benefit of the model (and indeed any distributed, transient simulator) is that is "fills in the gaps" in space and time between the available spatial and temporal observations. To visualise this, Animation B.1 (Appendix B) presents the simulated evolution of SWE at a daily time-step during Winter 2017/2018. The redistribution of snow from steep slopes is particularly apparent in the animation, and the simulated redistribution is broadly consistent with both field experience (Figure 3.2) and the elevated avalanche activity that occurred in the region more generally (Bühler et al., 2019).

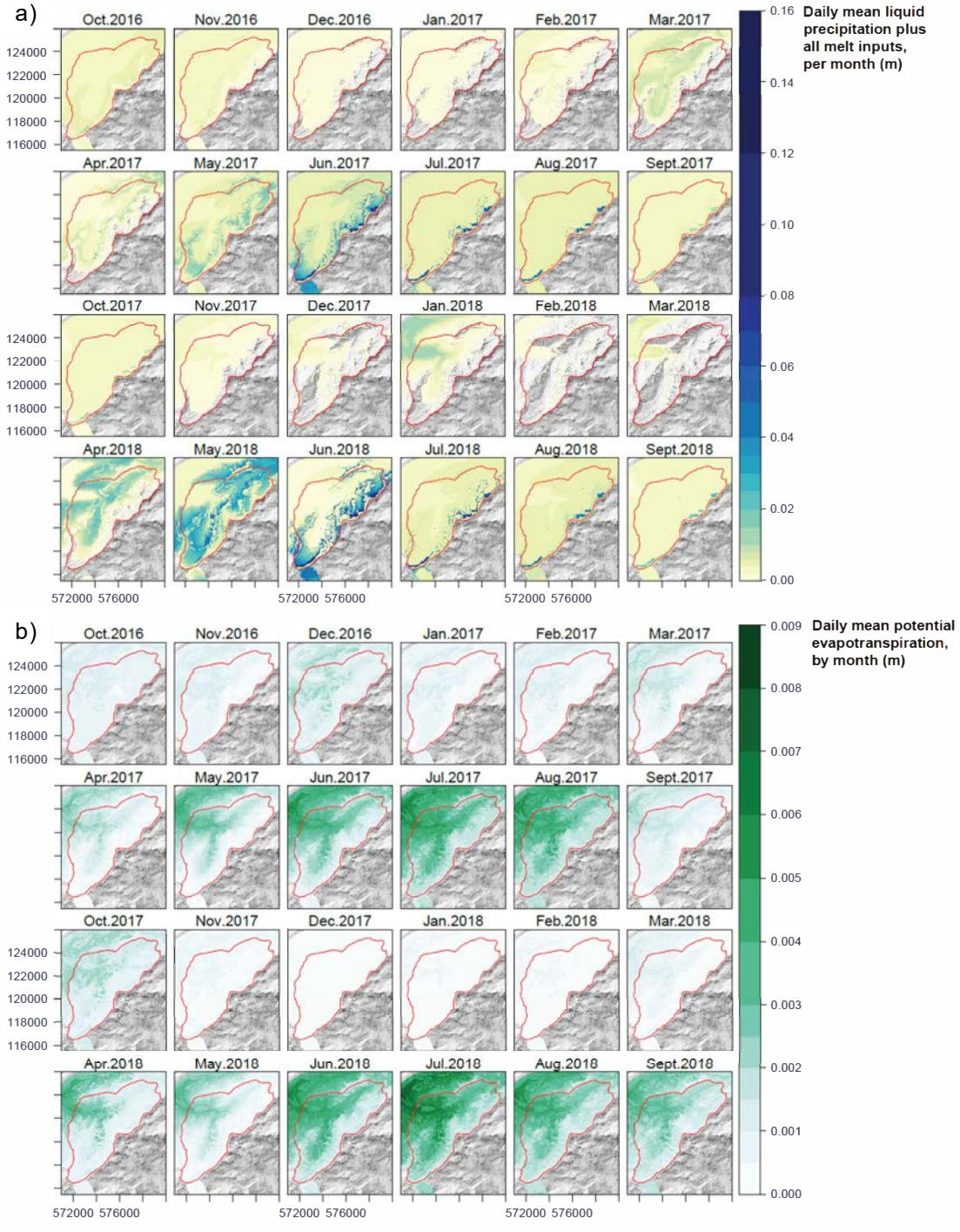

Figure 3.8: Spatio-temporal patterns of a) liquid water arriving at the surface (i.e. liquid precipitation + snowmelt + firn melt + ice melt), and b) potential evapotranspiration (ET_p) generated using the optimised model configuration over the two hydrological years 2017-2018. The underlying hourly data are expressed as daily mean values in metres (m), averaged across calendar months.

Figure 3.8 illustrates the spatio-temporal distribution of i) the arrival of water at the land surface (comprised of liquid precipitation, snowmelt, firn melt and ice melt) and ii) ET_p over the last hydrological years of the simulation period, aggregated on a monthly basis.

As expected, very little meltwater input is simulated to occur during the winter months, when temperatures are generally below freezing. Conversely, the highest meltwater volumes are generated during the spring melt, especially the months of April, May, and June, with the increasing elevation at which the majority of melt water is produced as the season progresses and the localised contribution of the glaciers during the summer months also being discernible features. Of course, liquid precipitation during the summer and autumn months, which in such environments can be highly concentrated in space and time, is "smoothed out" in these plots, appearing as a fairly low and constant daily mean value in non-glacierised areas. The graphs in Supplementary Figure B.5, however, present the same underlying data in a different way – as hourly, catchment-averaged series – indicating the dynamics of the system. In terms of the spatial pattern of ET_p, strong seasonality and elevational influences are apparent, with low values being estimated widely in winter but restricted to higher elevations in summer.

To further verify the hydrological plausibility of these results (but without recourse to a full hydrological model – that comes in Chapter 5), simulated "snowcover outflow" and observed discharge for the Vallon de Nant sub-catchment were compared. In Figure 3.9a, hourly catchment-averaged "snowcover outflow" (i.e. snowmelt from non-glaciated areas plus any liquid precipitation) is plotted against hourly observed, catchment area-normalised discharge (measured at the Avannçon Weir; Figure 3.1) over spring 2018 (April to June inclusive). A straightforward comparison of the two cumulative totals produces an estimated runoff ratio of 0.61 within this three-month period, although this value is tentative given uncertainties associated with precipitation, the model, and observed discharge.

At the diurnal timescale, snowmelt leads increasing streamflow, which seems reasonable. Dependence remains present on slightly longer timescales also. For example, the decrease in measured streamflow just before the start of May coincides with a marked reduction in simulated water inputs. Extending this plot to later in the summer (not shown) revealed that a certain proportion of the "excess" spring melt inputs arrive in the stream later (which can be considered the "buffering" capacity of relatively shallow groundwater storage), whilst some meltwater will be lost to actual evapotranspiration and perhaps also deeper groundwater storage and/or groundwater exportation across topographic divides. Figure 3.9b, meanwhile, shows the relationship between these data aggregated to a daily time-step (as the lagged and strongly dampened streamflow response relative to the melt inputs complicates such comparisons using the hourly data).

A clear relationship between the variables can be seen, and can be approximated by a power-law function (illustrated by the estimated non-linear least squares regression regression line). A certain hysteresis is also present in the relationship, meaning that less meltwater is "required" to produce a given magnitude of flow response as the season progresses. This is consistent with increasing groundwater storage and saturation conditions throughout this period.

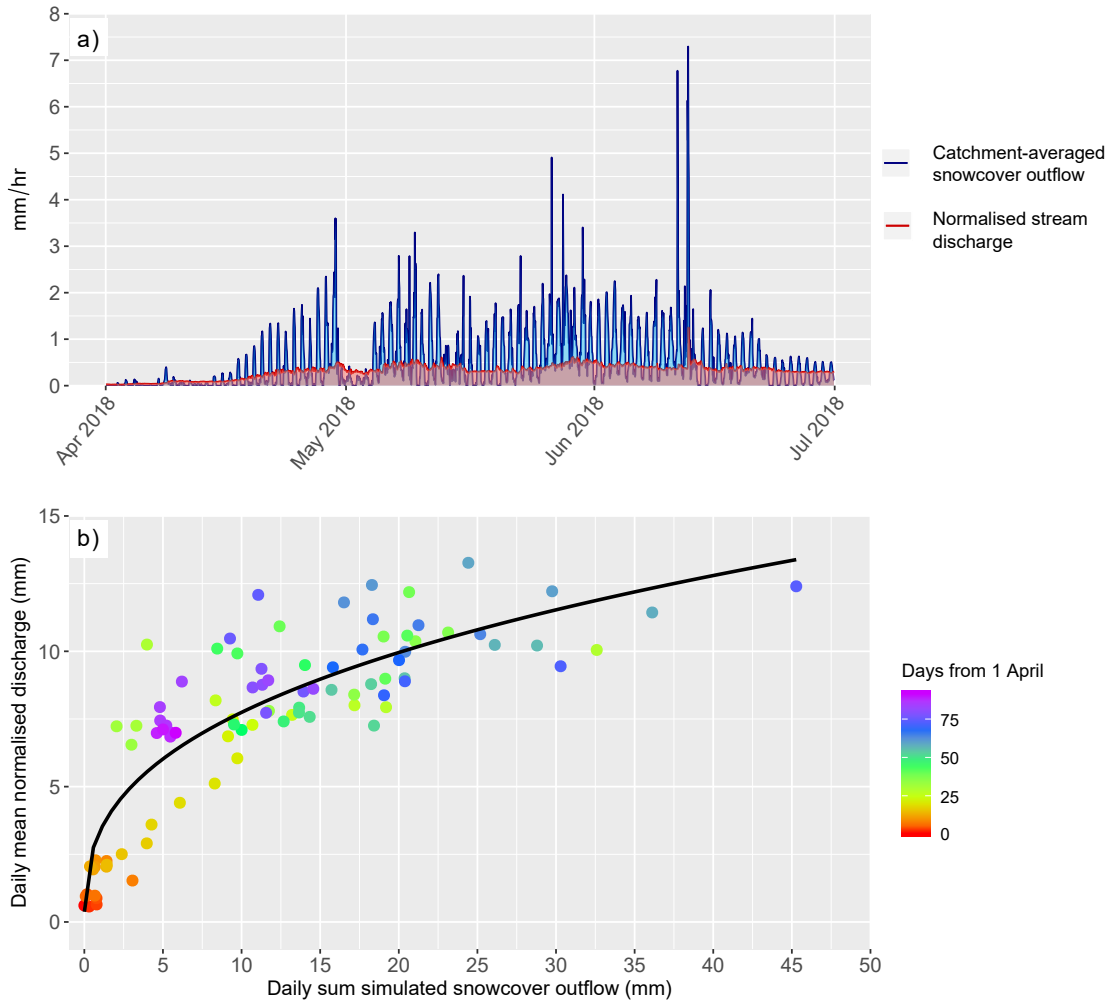

Figure 3.9: a) Hourly simulated catchment-averaged "snowcover outflow" (i.e. snowmelt from non-glaciated areas plus any liquid precipitation) vs. hourly observed normalised stream discharge for the Vallon de Nant sub-catchment for spring 2018 (discharge gauged at Avançon Weir and normalised according to catchment area), and (b) daily sum simulated snowcover outflow vs. daily mean normalised observed discharge, again at the Avançon Weir station, for the same 3-month period.

These lines of evidence therefore further reinforce the hydrological plausibly of the snow simulations, and therefore provide confidence that the datasets generated will form suitable inputs, alongside a specifically developed 3D model of bedrock geology (Chapter 2; Thornton et al., 2018) and recent geophysical surveys and related work (Chapter 4), to one forthcoming application; the development of a sophisticated, fully-integrated surface-subsurface hydrological model.

3.5.5 Predictive uncertainty and data worth

Table 3.4 shows the estimated pre- and post-calibration uncertainty standard deviation of the selected predictions. For all, the uncertainty associated with the prediction in question is seen to be substantially reduced (by a factor of approximately four) by the calibration process.

Prediction	**Pre-calibration uncertainty standard deviation**	**Post-calibration uncertainty standard deviation**
SWE 01/04/2015	219.09 (mm)	57.87 (mm)
SWE 01/04/2016	200.81 (mm)	57.82 (mm)
SWE 01/04/2017	628.54 (mm)	151.63 (mm)
SWE 01/04/2018	320.29 (mm)	82.13 (mm)
F_1 22/05/2017	0.0537 (-)	0.0365 (-)

Table 3.4: Pre- and post-calibration uncertainty standard deviation of selected snow predictions. The SWE predictions are at COR.

An indication of contribution of the different model parameters to the uncertainty variance, both pre- and post-calibration, is given for two of the five predictions in Figure 3.10. In these plots, the uncertainty variance contributions have been normalised with respect to the pre-calibration uncertainty variance associated with the respective predictions.

Figure 3.10a, which concerns the prediction of SWE on 1 April 2016, reveals firstly that many parameters that either do not (or hardly) contribute to predictive uncertainty either before or after calibration, i.e. the prediction is insensitive to these parameters. A slight reduction in the contribution to uncertainty variance can however be observed for *idwedr*, *snob*, and *snoa*. The presence of many parameters that do not contribute to either the pre-or post-calibration uncertainty in the SWE prediction is to be expected. This is because most of these parameters concern the gravitational redistribution component of the model, whereas the COR measurement station will have undoubtedly been sited strategically, such that the measurements are generally

unaffected by such processes. Another striking feature of this plot is the large reduction in the predictive uncertainty associated with the longwave correction parameters, *lwin* and *lwout*, that calibration induced. The results for the three other 1 April SWE predictions were similar, and so are not presented in the interests of space.

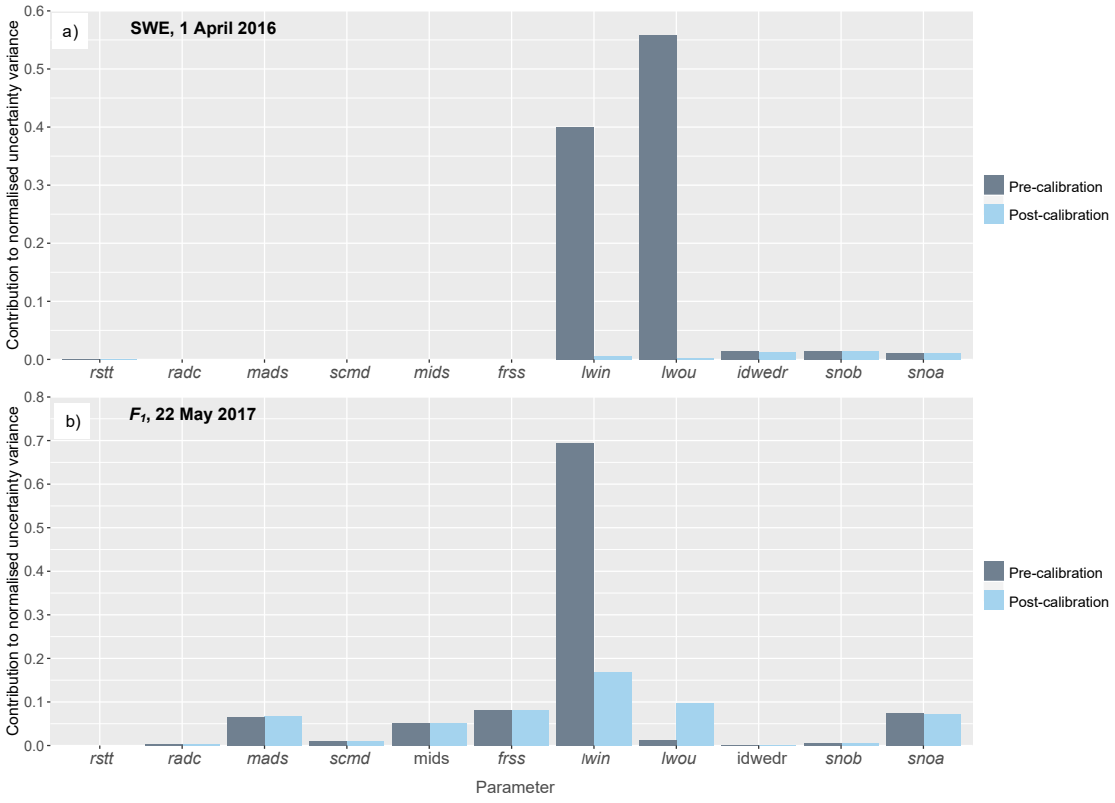

Figure 3.10: Parameter contributions to predictive uncertainty variance pre- and post-calibration for the predictions of a) Snow Water Equivalent on 1 April 2016, and b) snow pattern (summarised by F_1) on 22 May 2017.

For the prediction of spatial snow extent on the 22 May 2017 quantified according to the F_1 statistic (Figure 3.10b), practically all parameters make some discernible contribution to uncertainty variance both pre-and post calibration. Interestingly, and as with the SWE prediction, a large reduction in the post-calibration uncertainty associated with *lwin* is observed, but the post-calibration uncertainty associated with *lwou* in relation to this prediction is actually higher than the pre-calibration value. This counterintuitive situation can can occasionally arise when a parameter to which the prediction is insensitive can only be made in conjunction with another parameter to which the prediction is indeed sensitive; see Doherty (2010) for further explanation. For all other parameters, the uncertainty contribution post-calibration is very similar to the

pre-calibration level, suggesting a certain insensitivity of the simulated snow extents to varying these parameter values. The "robustness" that the similarity between pre- and post-calibration parameter contributions to uncertainty in the spatial prediction indicates could in fact be particularly beneficial in instances where the spatial snow patterns as opposed to volumes of water stored are of primary importance (e.g. in studies seeking to better understand the influence of snow patterns on vegetation species distributions).

Figure 3.11 provides two alternative representations of the worth of the observations belonging to the five different groups in the calibration process. Figure 3.11a firstly shows the increase in post-calibration predictive uncertainty variance associated with each of the five selected predictions – again relative to pre-calibration uncertainty variance – that is incurred by omitting each observation group from the calibration dataset in turn. Removing either F_1, F_2, or F_3 is observed to have very little adverse effect on any of the predictions. This can be explained by the fact that when one of these groups is omitted, very similar information is retained in other two groups. The comparatively small number of observations in these groups, coupled with the uniform weighing applied to all observations for the purposes of this analysis, could also partially explain these results. This plot furthermore reveals the notable contribution that both time-series, but most especially that at GRY, make to the prediction; the prediction's uncertainty variance increases markedly if either of these groups of observations are removed. It is also interesting to highlight that four of the five predictions under consideration correspond to the SWE predicted at the high elevation COR station. In light of this, the analysis suggests, perhaps surprisingly, that removing the data at GRY from the calibration dataset has a more detrimental effect than removing the other observations at COR itself (the very location of the predictions).

Figure 3.11b, meanwhile, provides an indication of the decrease in uncertainty variance accrued relative to the pre-calibration uncertainty variance when each observation group comprises the sole member of the calibration dataset.

Including any one of the observation groups F_1, F_2, or F_3 alone in the calibration datasets is seen to lead to only modest reductions in the pre-calibration uncertainty variance associated with the predictions (although this is not to say that they do not have a more pronounced effect in combination). In contrast, including either of COR or GRY SWE time-series observations as the sole calibration dataset leads to similarly large reductions in the uncertainty associated with the prediction of SWE at COR. The uncertainty around the F1 prediction on 22 May 2017 is also greatly reduced by including either of these groups as the sole calibration dataset, although only by about half as much as the reduction seen for the 1 April SWE predictions. This result, that even including only one of the time-series as the sole calibration dataset substantially reduces

the uncertainty in the spatial prediction, is indicative of an important flow of information from the time-series to the predicted spatial snow patterns, and can probably be generalised to the other days on which simulated spatial patterns were compared with observations.

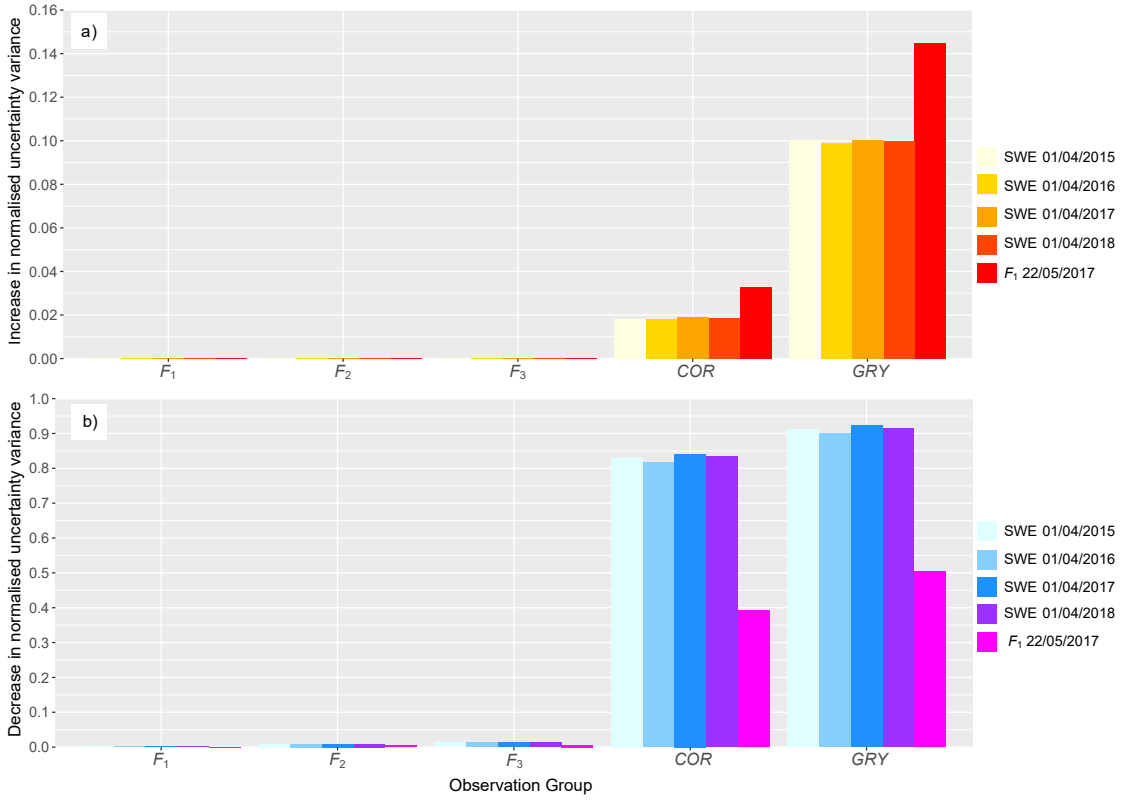

Figure 3.11: a) Increase in relative (to the pre-calibration uncertainty variance) post-calibration predictive uncertainty variance associated with each of the five selected predictions that is incurred by omitting each observation group from the calibration dataset in turn, and b) decrease in relative (again to the pre-calibration uncertainty variance) uncertainty variance accrued when each observation group comprises the sole member of the calibration dataset. The "redundancy" or commonality of information between the three spatial observation groups (i.e. F_1, F_2, and F_2) is clearly apparent.

The apparent significance of the GRY data that both analyses indicate is especially notable given that the number of observations at this site is substantially lower than at GRY (due to lower measurement frequency). It could be that being straddled more frequently by the 0°C isotherm, the SWE time-series at GRY contains more important information about temperature (and therefore temperature gradients) and snow limits than the COR data, in which distinct accumulation and ablation phases are apparent.

The notable contributions that the time time-series data seem to make more generally demonstrates the importance of obtaining alternative, complementary types of data and employing them within a multi-objective approach. This result is consistent with the conclusion of Tuo et al. (2018), who also showed that SWE data can be included to good effect in the calibration of hydrological models of alpine catchments.

Lastly with regards to uncertainty, it should be highlighted that since an important aim of this study was to generate the best possible inputs for subsequent hydrological modelling (that also coincide in time with other measurements from the study region, e.g. groundwater levels; not shown), no snow observations were specifically withheld for evaluation. Future research should certainly explore the influence of the specific calibration period, and/or assess model's performance under different conditions. That said, the uncertainty analysis presented acts as an alternative to a more traditional split-sample model calibration and evaluation framework.

3.5.6 Potential sources of residual mismatch

Uncertainty in the observed snow data aside, a large proportion of the residual spatio-temporal mismatch between the simulations and observations can probably be attributed to the meteorological forcing data. In light of the combination of relatively low station density and variable but sometimes high frequency of data gaps (Supplementary Figures B.1 and B.2), the interpolated spatial fields of meteorological variables are undoubtedly uncertain. More specifically, whilst the temporal data coverage and therefore crossover of the meteorological data varies throughout the simulation period, the parameters in the model are of a global nature.

Therefore, the rain-snow threshold temperature (*rstt*) and solid precipitation correction factors (*snoa* and *snob*), for example, are applied constantly in time and space. Hence, when these parameter are estimated though the calibration processes, "best overall" estimates respect to the observations are returned. In reality, however, the error distribution associated with precipitation measurements, for instance, actually varies on a station-by-station, event-by-event basis. The spatial dependencies in meteorological variables away from the station locations, which the interpolation processes attempts to recreate, also probably demonstrate some non-stationarity in reality (e.g. differences between frontal and convective precipitation).

In other words, it may be that the model structure, in not allowing any bespoke corrections to be made on a per-station/event basis, is insufficiently flexible to fully compensate for deficiencies in the meteorological measurements during certain periods and/or at certain locations. In this sense, improved fits could perhaps have been achieved by simply scaling relatively complete

time-series measured at (an) individual location(s) using linear, elevation-dependent relationships, although such an approach would have been less satisfactorily during periods with high meteorological data availability, since much of it would have essentially been discarded.

3.5.7 Some remarks on wind redistribution

Spatially distributed drift correction factors have been successfully applied in an attempt to account for the influence of wind transport processes on snowpack heterogeneity (e.g. Hanzer et al., 2016; Marshall et al., 2019). However, as mentioned earlier, after extensive testing, the wind redistribution algorithm available in WaSiM was not applied in the final model; doing so was found to lead to poorer fits with observations.

The algorithm in question computes a temporally invariant, spatially-distributed correction factor grid that is applied as a multiplier to the interpolated precipitation fields such that precipitation falling on predominantly sheltered slopes and on the leeward side of ridges is augmented (deposited), whilst that falling on exposed slopes is reduced (scoured). The generation of such a grid requires that a single prevailing wind direction (in fact, a sector) be prescribed. However, analysis of the relationship between high elevation, winter wind speeds (these conditions being those under which snow redistribution by wind is of most concern) revealed that no such prevailing wind direction exists across the study site (Supplementary Figure B.6); strong winter winds can apparently can originate from contrasting directions, likely as a function of larger-scale synoptic meteorology. Some influence of the complex local topography on wind patterns also seems to be present.

In addition, the range of the calculated wind redistribution factors also seemed somewhat high (leading to both too much "deposition" and "scouring", depending upon pixel exposition). Another potential complicating factor is that unlike the gravitational redistribution algorithm that was applied, the wind redistribution approach does not conserve mass within a given area (e.g. a catchment). It may thus simply be that in mountainous regions where large scale meteorological phenomena interacting with extremely complex topography give rise to considerable spatio-temporal variability in near-surface wind fields, such comparatively simple algorithms of this nature cannot be expected to produce snow representations that match highly resolved, site-specific observations.

As such, the development of extended empirical approaches that perhaps include directly measured high-elevation wind directions and/or are calibrated explicitly to observed redistribution magnitudes in the vicinity of ridges could form an appropriate intermediate-complexity approach

(needed until physics-based wind-induced snow transport simulations can be simulated physically at high resolution across entire catchments). In any case, it can be stated with some confidence that at this study site, snow redistribution by wind is of secondary hydrological importance to that by gravitational forces.

3.5.8 Ongoing debates regarding model calibration

There remains some debate concerning the most appropriate approach for including snow data in the calibration or evaluation of hydrological models. It has been argued on the one hand that since the volumetric information contained within discharge measurements is complementary to the internal spatial pattern information embedded in distributed snow observations (Finger et al., 2011), these two types of observations should be considered simultaneously. This approach was pursued, for example, by Finger et al. (2011), Duethmann et al. (2014), and Shrestha et al. (2014). The argument runs that the constraint provided by discharge can help ensure that, in aggregate, the simulated amount of water in the system is approximately correct – which is important given the uncertainties associated with precipitation measurements and gridded products – whilst the observed snow pattern constraints help to ensure that the runoff is being generated from the right areas.

However, others have posited that calibrating such models is better tackled in a more sequential fashion, whereby snow simulations are focussed upon initially, and only then does one proceed to simulate any other intermediate hydrological variables of interest and, ultimately, discharge. The principal argument in favour of this approach is that simultaneous calibration may allow for error compensation (Ragettli and Pellicciotti, 2012; Magnusson et al., 2015) that can be hidden or easily missed (at least unless extremely careful evaluative work with respect to observed spatial patterns in conducted, which remains rare).

Here, the view was taken that provided a given set of snow observations are sufficiently informative (and it is hoped those employed here – whilst limited by practical considerations e.g. the risks associated with conducting regular winter snow surveys in such terrain – are), then employing them "alone" as a constraint in what may eventually amount to the first step in a wider, sequential calibration processes should in itself be enough to ensure that the total water volumes are reasonably accurate.

The hydrological plausibly assessment undertaken provides reassurance that this is indeed the case. Indeed, for this very reason, both binary spatial and volumetric time-series at contrasting sites contributed the snow model calibration here. In this way, the potential for model param-

eters related to the surface or subsurface to compensate for poor snow simulations should be minimised. An additional reason for splitting the calibration phases is that the development of a comprehensive, integrated 2D-3D surface-subsurface hydrological model able to simulate the remainder of the study catchment's hydrological cycle is in prospect (see Chapter 5). Being somewhat more complex than standard approaches, this will require sufficient explanation, and so falls out of scope for the time being.

Either way, one thing that is clear is that neglecting to verify internal models states at all should be avoided.

3.6 Conclusion

A novel and computationally efficient approach to the calibration and uncertainty analysis of distributed snow models in extremely steep and rugged alpine catchments has been presented an exemplified. The physically-based core of the model enables spatio-temporal variably in energy balance components, which is largely responsible for heterogeneous snow patterns and therefore melt rates in such terrain, to be explicitly captured. Physically-oriented snow models of this nature moreover have stronger credentials for generating more reliable predictions under modified climatic conditions than their simpler counterparts.

That said, certain processes that can also substantially influence meltwater patterns in steep mountainous regions, such gravitation snow redistribution, cannot presently be represented on an entirely physical basis at catchment scales or above. To address this, a pragmatic empirical gravitational redistribution algorithm was therefore applied alongside the energy balance-based core. Substantial additional uncertainties related to biased solid precipitation measurements and other observational deficiencies were likewise tackled by the introduction of empirical correction factors.

Reconstructing the spatio-temporal evolution of SWE as reliably as possible in such a challenging region therefore hinged upon the task of parameter estimation, which was not trivial given that the "forward" model was associated with reasonable computational expense (with a single simulation taking several hours in a parallelised configuration). To this end, a novel multi-objective calibration methodology was established that incorporated two types of complementary, high-resolution snow observations. One component of the objective function was explicitly spatial, with misfits at the pixel level being penalised. Indeed, this is believed to be the instance in which a distributed snow model has actually been calibrated in this fashion (i.e.

using F-statistics with reference to observed snow maps derived from Landsat data).

Following calibration, snow dynamics were satisfactorily reproduced. The spatial fit metrics obtained also compared quite favourably with the few equivalent statistics that have been reported in previous studies. Interestingly, substantial corrections to measured winter precipitation totals were required to minimise simulation-observation mismatches. Subsequent uncertainty and data worth analyses indicated that: i) the uncertainty variance of indicative predictions of snow states, both spatial and volumetric, were substantially reduced through calibration, ii) including two parameters that enable the longwave component of the surface energy balance to be adjusted, and thus potential errors in cloudiness and albedo compensated for, was especially beneficial, and iii) the SWE time-series at the lower elevation station (GRY) was particularly informative, despite the comparatively small number of observations at this site. Any uncertainties in the snow observations notwithstanding, it is likely that a large proportion of the residual matches between simulations and observations is associated with the meteorological forcing data; both the raw measurements themselves and their spatial interpolation. As such, research efforts to better understand and account for the uncertainties and biases inherent with mountain meteorological measurements and interpolated/downscaled gridded data products should assume high priority.

Furthermore, a feasible, useful, and generic (i.e. model and concept-independent) approach to quantifying the uncertainties and data worth associated with snow model predictions – a rarely attempted task in snow hydrology – has been demonstrated. Such work should be undertaken more routinely as part of snow simulation exercises. Calibration-constrained simulations of snow dynamics and their resultant meltwater datasets such as those generated herein have great potential to be used extensively to inform the next generation of comprehensive, physically-based, distributed hydrological modelling efforts in alpine terrain, which are in turn urgently needed to improve our understanding of ongoing alpine hydrological system change.

Contribution statement

I (The Author) conceived this sub-project independently and conducted the vast majority of the work, including obtaining and processing the meteorological, satellite, and GRY SWE time-series data, establishing the model, designing and implementing the calibration approach, preparing the figures, and drafting the manuscript. Dr. T. Brauchli conducted the simulation using the SNOWPACK model at the COR station and provided guidance regarding some of the meteorological data. Professors G. Mariethoz and P. Brunner provided advice at various stages, and all of the aforementioned individuals participated in the finalisation of the manuscript.

Data and code availability

All model-rated datasets and code that the can be shared have been uploaded to an online repository (Thornton et al., 2019). High-resolution versions of the supplementary figures are also available at this location, as is the supplementary animation. The meteorological data obtained from MeteoSwiss, and the terrain and land cover data obtained from swisstopo remain subject to restrictions. Therefore, processed model inputs relating to these aspects are not included; requests for these datasets should be directed to the respective organisation. Third-party executables are similarly excluded, but are obtainable as follows: WaSiM executables and documentation can be downloaded from http://www.wasim.ch/en/products.html, whilst PEST executables and documentation can be downloaded from http://www.pesthomepage.org/Downloads.php

Acknowledgments

The work was conducted as part of the IntegrAlp project, funded by the Swiss National Science Foundation. I thank Professor B. Schaefli for useful discussions, and Dr. J. Schulla for answers to questions regarding the use of WaSiM. The padr package (Thoen, 2019) was useful for processing the time-series, and the rasterVis package (Perpiñán and Hijmans, 2019) was useful for the preparation of the animation, as well as some of the more complex map-based figures.

References

Addor, N., Rössler, O., Köplin, N., Huss, M., Weingartner, R., and Seibert, J. (2014). Robust changes and sources of uncertainty in the projected hydrological regimes of Swiss catchments. *Water Resources Research* 50, 7541–7562.

Aronica, G., Bates, P. D., and Horritt, M. S. (2002). Assessing the uncertainty in distributed model predictions using observed binary pattern information within GLUE. *Hydrological Processes* 16, 2001–2016.

Barnett, T. P., Adam, J. C., and Lettenmaier, D. P. (2005). Potential impacts of a warming climate on water availability in snow-dominated regions. *Nature* 438, 303–309.

Bavera, D., Bavay, M., Jonas, T., Lehning, M., and De Michele, C. (2014). A comparison between two statistical and a physically-based model in snow water equivalent mapping. *Advances in Water Resources* 63, 167–178.

Beniston, M. et al. (2018). The European mountain cryosphere: a review of its current state, trends, and future challenges. *The Cryosphere* 12, 759–794.

Benoit, L., Allard, D., and Mariethoz, G. (2018). Stochastic rainfall modeling at sub-kilometer scale. *Water Resources Research* 54, 4108–4130.

Berezowski, T., Chormański, J., and Batelaan, O. (2015). Skill of remote sensing snow products for distributed runoff prediction. *Journal of Hydrology* 524, 718–732.

Bernhardt, M., Schulz, K., Liston, G. E., and Zängl, G. (2012). The influence of lateral snow redistribution processes on snow melt and sublimation in alpine regions. *Journal of Hydrology* 424-425, 196–206.

Bini, A. et al. (2009). *Switzerland during the Last Glacial Maximum (LGM), 1: 500,000*.

Blöschl, G., Kirnbauer, R., and Gutknecht, D. (1991). Distributed snowmelt simulations in an Alpine catchment: 1. Model evaluation on the basis of snow cover patterns. *Water Resources Research* 27, 3171–3179.

Bolch, T. et al. (2012). The State and Fate of Himalayan Glaciers. *Science* 336, 310–314.

Bormann, K. J., Brown, R. D., Derksen, C., and Painter, T. H. (2018). Estimating snow-cover trends from space. *Nature Climate Change* 8, 924–928.

Brauchli, T., Beria, H., Michelon, A., Larsen, J., and Schaefli, B. (2018). Estimating the precipitation in a high-alpine catchment combining local meteo stations and Swiss-wide meteo products. *Swiss Geoscience Meeting 2018*. Bern.

Brauchli, T., Trujillo, E., Huwald, H., and Lehning, M. (2017). Influence of slope-scale snowmelt on catchment response simulated with the Alpine3D model. *Water Resources Research* 53, 10723–10739.

Bründl, M. et al. (2019). *Analyse des évènements de la situation avalancheuse de janvier 2018*. Tech. rep. WSL Institut pour l'étude de la neige et des avalanches SLF, Davos, p. 162.

Bühler, Y., Hafner, E. D., Zweifel, B., Zesiger, M., and Heisig, H. (2019). Where are the avalanches? Rapid SPOT6 satellite data acquisition to map an extreme avalanche period over the Swiss Alps. *The Cryosphere* 13, 3225–3238.

Casassa, G., López, P., Pouyaud, B., and Escobar, F. (2009). Detection of changes in glacial run-off in alpine basins: examples from North America, the Alps, central Asia and the Andes. *Hydrological Processes* 23, 31–41.

Ceperley, N. et al. (2018). *Salt gauging and stage-discharge curve, Avançon de Nant, outlet Vallon de Nant catchment*.

Clark, M. P., Hendrikx, J., Slater, A. G., Kavetski, D., Anderson, B., Cullen, N. J., Kerr, T., Örn Hreinsson, E., and Woods, R. A. (2011). Representing spatial variability of snow water equivalent in hydrologic and land-surface models: A review. *Water Resources Research* 47.

Clark, M. P., Slater, A. G., Barrett, A. P., Hay, L. E., McCabe, G. J., Rajagopalan, B., and Leavesley, G. H. (2006). Assimilation of snow covered area information into hydrologic and land-surface models. *Advances in Water Resources* 29, 1209–1221.

Cochand, M., Christe, P., Ornstein, P., and Hunkeler, D. (2019). Groundwater storage in high Alpine catchments and its contribution to streamflow. *Water Resources Research* 55, 2613–2630.

Costa, A., Molnar, P., Stutenbecker, L., Bakker, M., Silva, T. A., Schlunegger, F., Lane, S. N., Loizeau, J.-L., and Girardclos, S. (2018). Temperature signal in suspended sediment export from an Alpine catchment. *Hydrology and Earth System Sciences* 22, 509–528.

Dierauer, J. R., Whitfield, P. H., and Allen, D. M. (2018). Climate controls on runoff and low flows in mountain catchments of western North America. *Water Resources Research* 54, 7495–7510.

Doherty, J. (2019). *PEST: Model-Independent Parameter Estimation*. 7th Edition. Watermark Numerical Computing, Brisbane, Australia.

Doherty, J. (2010). *Methodologies and Software for PEST-Based Model Predictive Uncertainty Analysis*. Tech. rep. Watermark Numerical Computing.

Dozier, J. (1989). Spectral signature of alpine snow cover from the landsat thematic mapper. *Remote Sensing of Environment* 28, 9–22.

Duethmann, D., Peters, J., Blume, T., Vorogushyn, S., and Güntner, A. (2014). The value of satellite-derived snow cover images for calibrating a hydrological model in snow-dominated catchments in Central Asia. *Water Resources Research* 50, 2002–2021.

Engel, M., Notarnicola, C., Endrizzi, S., and Bertoldi, G. (2017). Snow model sensitivity analysis to understand spatial and temporal snow dynamics in a high-elevation catchment. *Hydrological Processes* 31, 4151–4168.

Etter, S., Addor, N., Huss, M., and Finger, D. (2017). Climate change impacts on future snow, ice and rain runoff in a Swiss mountain catchment using multi-dataset calibration. *Journal of Hydrology: Regional Studies* 13, 222–239.

Fatichi, S., Rimkus, S., Burlando, P., Bordoy, R., and Molnar, P. (2015). High-resolution distributed analysis of climate and anthropogenic changes on the hydrology of an Alpine catchment. *Journal of Hydrology* 525, 362–382.

Finger, D., Pellicciotti, F., Konz, M., Rimkus, S., and Burlando, P. (2011). The value of glacier mass balance, satellite snow cover images, and hourly discharge for improving the performance of a physically based distributed hydrological model. *Water Resources Research* 47, 1–14.

Förster, K., Garvelmann, J., Meißl, G., and Strasser, U. (2018). Modelling forest snow processes with a new version of WaSiM. *Hydrological Sciences Journal* 63, 1540–1557.

Franz, K. J., Butcher, P., and Ajami, N. K. (2010). Addressing snow model uncertainty for hydrologic prediction. *Advances in Water Resources* 33, 820–832.

Freudiger, D., Kohn, I., Seibert, J., Stahl, K., and Weiler, M. (2017). Snow redistribution for the hydrological modeling of alpine catchments. *Wiley Interdisciplinary Reviews: Water* 4, 1232.

Fuhrer, J. and Jasper, K. (2012). Demand and supply of water for agriculture: Influence of topography and climate in pre-Alpine, mesoscale catchments. *Natural Resources* 03, 145–155.

Gallice, A., Bavay, M., Brauchli, T., Comola, F., Lehning, M., and Huwald, H. (2016). StreamFlow 1.0: An extension to the spatially distributed snow model Alpine3D for hydrological modelling and deterministic stream temperature prediction. *Geoscientific Model Development* 9, 4491–4519.

GDAL (n.d.). *GDAL*. URL: https://gdal.org/.

Giaccone, E., Luoto, M., Vittoz, P., Guisan, A., Mariéthoz, G., and Lambiel, C. (2019). Influence of microclimate and geomorphological factors on alpine vegetation in the Western Swiss Alps. *Earth Surface Processes and Landforms* 44, 3093–3107.

Grand, S., Rubin, A., Verrecchia, E. P., and Vittoz, P. (2016). Variation in soil respiration across soil and vegetation types in an Alpine valley. *PLOS ONE* 11. Ed. by W. L. Araujo.

Grayson, R. B. and Blöschl, G. (2001). *Spatial patterns in catchment hydrology: Observations and modelling*. Cambridge: Cambridge University Press.

Grayson, R. B., Blöschl, G., Western, A. W., and McMahon, T. A. (2002). Advances in the use of observed spatial patterns of catchment hydrological response. *Advances in Water Resources* 25, 1313–1334.

Grünewald, T., Schirmer, M., Mott, R., and Lehning, M. (2010). Spatial and temporal variability of snow depth and ablation rates in a small mountain catchment. *Cryosphere* 4, 215–225.

Hanzer, F., Helfricht, K., Marke, T., and Strasser, U. (2016). Multilevel spatiotemporal validation of snow/ice mass balance and runoff modeling in glacierized catchments. *The Cryosphere* 10, 1859–1881.

Härer, S., Bernhardt, M., Siebers, M., and Schulz, K. (2018). On the need for a time- and location-dependent estimation of the NDSI threshold value for reducing existing uncertainties in snow cover maps at different scales. *The Cryosphere* 12, 1629–1642.

He, M., Hogue, T. S., Franz, K. J., Margulis, S. A., and Vrugt, J. A. (2011). Characterizing parameter sensitivity and uncertainty for a snow model across hydroclimatic regimes. *Advances in Water Resources* 34, 114–127.

Herrnegger, M., Nachtnebel, H.-P., and Haiden, T. (2012). Evapotranspiration in high alpine catchments – an important part of the water balance! *Hydrology Research* 43, 460.

Hock, R. (2003). Temperature index melt modelling in mountain areas. *Journal of Hydrology* 282, 104–115.

Huss, M. and Hock, R. (2018). Global-scale hydrological response to future glacier mass loss. *Nature Climate Change* 8, 135–140.

Huss, M. et al. (2017). Toward mountains without permanent snow and ice. *Earth's Future* 5, 418–435.

Jenicek, M., Seibert, J., Zappa, M., Staudinger, M., and Jonas, T. (2016). Importance of maximum snow accumulation for summer low flows in humid catchments. *Hydrology and Earth System Sciences* 20, 859–874.

Jennings, K. S., Winchell, T. S., Livneh, B., and Molotch, N. P. (2018). Spatial variation of the rain-snow temperature threshold across the Northern Hemisphere. *Nature Communications* 9, 1–9.

Jonas, T., Marty, C., and Magnusson, J. (2009). Estimating the snow water equivalent from snow depth measurements in the Swiss Alps. *Journal of Hydrology* 378, 161–167.

Kerr, T., Clark, M., Hendrikx, J., and Anderson, B. (2013). Snow distribution in a steep mid-latitude alpine catchment. *Advances in Water Resources* 55, 17–24.

Kirchner, J. W. (2006). Getting the right answers for the right reasons: Linking measurements, analyses, and models to advance the science of hydrology. *Water Resources Research* 42.

Klein, G., Vitasse, Y., Rixen, C., Marty, C., and Rebetez, M. (2016). Shorter snow cover duration since 1970 in the Swiss Alps due to earlier snowmelt more than to later snow onset. *Climatic Change* 139, 637–649.

Kochendorfer, J., Nitu, R., et al. (2017). Analysis of single-Alter-shielded and unshielded measurements of mixed and solid precipitation from WMO-SPICE. *Hydrology and Earth System Sciences* 21, 3525–3542.

Kochendorfer, J., Rasmussen, R., et al. (2017). The quantification and correction of wind-induced precipitation measurement errors. *Hydrology and Earth System Sciences* 21, 1973–1989.

Kurylyk, B. L. and Hayashi, M. (2017). Inferring hydraulic properties of alpine aquifers from the propagation of diurnal snowmelt signals. *Water Resources Research* 53, 4271–4285.

Lane, S. N., Borgeaud, L., and Vittoz, P. (2016). Emergent geomorphic-vegetation interactions on a subalpine alluvial fan. *Earth Surface Processes and Landforms* 41, 72–86.

Lane, S. N. and Nienow, P. W. (2019). Decadal-scale climate forcing of Alpine glacial hydrological Systems. *Water Resources Research* 55, 2478–2492.

Lehning, M., Bartelt, P., Brown, B., and Fierz, C. (2002). A physical SNOWPACK model for the Swiss avalanche warning Part III: Meteorological forcing, thin layer formation and evaluation. *Cold Regions Science and Technology* 35, 169–184.

Lehning, M., Völksch Ingo, I., Gustafsson, D., Nguyen, T. A., Stähli, M., and Zappa, M. (2006). ALPINE3D: A detailed model of mountain surface processes and its application to snow hydrology. *Hydrological Processes*. Vol. 20. (10), pp. 2111–2128.

Leonarduzzi, E., Molnar, P., and McArdell, B. W. (2017). Predictive performance of rainfall thresholds for shallow landslides in Switzerland from gridded daily data. *Water Resources Research* 53, 6612–6625.

Magnusson, J., Wever, N., Essery, R., Helbig, N., Winstral, A., and Jonas, T. (2015). Evaluating snow models with varying process representations for hydrological applications. *Water Resources Research* 51, 2707–2723.

Marshall, A. M., Link, T. E., Abatzoglou, J. T., Flerchinger, G. N., Marks, D. G., and Tedrow, L. (2019). Warming alters hydrologic heterogeneity: simulated climate sensitivity of hydrologyâbased microrefugia in the snowâtoârain transition zone. *Water Resources Research* 55, 2122–2141.

Mas, A., Baraer, M., Arsenault, R., Poulin, A., and Préfontaine, J. (2018). Targeting high robustness in snowpack modeling for Nordic hydrological applications in limited data conditions. *Journal of Hydrology* 564, 1008–1021.

Meeks, J., Moeck, C., Brunner, P., and Hunkeler, D. (2017). Infiltration under snow cover: Modeling approaches and predictive uncertainty. *Journal of Hydrology* 546, 16–27.

MeteoSwiss (n.d.). *IDAWEB*. URL: https://gate.meteoswiss.ch/idaweb/more.do.

Micheletti, N. and Lane, S. N. (2016). Water yield and sediment export in small, partially glaciated Alpine watersheds in a warming climate. *Water Resources Research* 52, 4924–4943.

Michelon, A., Schaefli, B., Ceperley, N. C., and Beria, H. (2017). *Weather dataset from Vallon de Nant, Switzerland, until July 2017*.

Mott, R., Scipión, D., Schneebeli, M., Dawes, N., Berne, A., and Lehning, M. (2014). Orographic effects on snow deposition patterns. *Journal of Geophysical Research: Atmospheres* 119, 1419–1439.

Mott, R. and Lehning, M. (2010). Meteorological modeling of very high-resolution wind fields and snow deposition for mountains. *Journal of Hydrometeorology* 11, 934–949.

Musselman, K. N., Pomeroy, J. W., Essery, R. L. H., and Leroux, N. (2015). Impact of windflow calculations on simulations of alpine snow accumulation, redistribution and ablation. *Hydrological Processes* 29, 3983–3999.

Mutzner, R., Weijs, S. V., Tarolli, P., Calaf, M., Oldroyd, H. J., and Parlange, M. B. (2015). Controls on the diurnal streamflow cycles in two subbasins of an alpine headwater catchment. *Water Resources Research* 51, 3403–3418.

Naseer, A., Koike, T., Mohamad, R., Ushiyama, T., and Shrestha, M. (2019). Distributed hydrological modelling framework for quantitative and spatial bias correction for rainfall, snowfall, and mixed-phase precipitation using vertical profile of temperature. *Journal of Geophysical Research: Atmospheres* 124, 4985–5009.

Oke, T. (1987). *Boundary Layer Climates*. 2nd Ed. London and New York: Routledge.

OSGeo4W (n.d.). *OSGeo4W*. URL: https://trac.osgeo.org/osgeo4w/.

Pan, X., Yang, D., Li, Y., Barr, A., Helgason, W., Hayashi, M., Marsh, P., Pomeroy, J., and Janowicz, R. J. (2016). Bias corrections of precipitation measurements across experimental sites in different ecoclimatic regions of western Canada. *The Cryosphere* 10, 2347–2360.

Papathoma-Köhle, M., Kappes, M., Keiler, M., and Glade, T. (2011). *Physical vulnerability assessment for alpine hazards: State of the art and future needs*.

Parajka, J. and Blöschl, G. (2008). The value of MODIS snow cover data in validating and calibrating conceptual hydrologic models. *Journal of Hydrology* 358, 240–258.

Pepin, N. et al. (2015). Elevation-dependent warming in mountain regions of the world. *Nature Climate Change* 5, 424–430.

Perpiñán, O. and Hijmans, R. (2019). *Package 'rasterVis'*.

Pritchard, H. D. (2019). Asia's shrinking glaciers protect large populations from drought stress. *Nature* 569, 649–654.

Ragettli, S., Cortés, G., Mcphee, J., and Pellicciotti, F. (2014). An evaluation of approaches for modelling hydrological processes in high-elevation, glacierized Andean watersheds. *Hydrological Processes* 28, 5674–5695.

Ragettli, S. and Pellicciotti, F. (2012). Calibration of a physically based, spatially distributed hydrological model in a glacierized basin: On the use of knowledge from glaciometeorological processes to constrain model parameters. *Water Resources Research* 48, 1–20.

Raleigh, M. S., Livneh, B., Lapo, K., and Lundquist, J. D. (2016). How does availability of meteorological forcing data impact physically based snowpack simulations? *Journal of Hydrometeorology* 17, 99–120.

Randin, C. F., Dedieu, J. P., Zappa, M., Long, L., and Dullinger, S. (2015). Validation of and comparison between a semidistributed rainfall-runoff hydrological model (PREVAH) and a spatially distributed snow-evolution model (SnowModel) for snow cover prediction in mountain ecosystems. *Ecohydrology* 8, 1181–1193.

Rittger, K., Painter, T. H., and Dozier, J. (2013). Assessment of methods for mapping snow cover from MODIS. *Advances in Water Resources* 51, 367–380.

Rössler, O., Froidevaux, P., Börst, U., Rickli, R., Martius, O., and Weingartner, R. (2014). Retrospective analysis of a nonforecasted rain-on-snow flood in the Alps – A matter of model limitations or unpredictable nature? *Hydrology and Earth System Sciences* 18, 2265–2285.

Schöber, J., Achleitner, S., Kirnbauer, R., Schöberl, F., and Schönlaub, H. (2010). Hydrological modelling of glacierized catchments focussing on the validation of simulated snow patterns – applications within the flood forecasting system of the Tyrolean river Inn. *Advances in Geosciences* 27, 99–109.

Schulla, J. (2017). *WaSiM (Water balance Simulation Model) Model Description*. Tech. rep. Zürich: Hydrology Software Consulting J. Schulla, p. 332.

SCNAT (2018). *GLAMOS 1881-2018, The Swiss Glaciers 1880-2016/17*.

Sevruk, B. (1985). Systematischer Niederschlagsmessfehler in der Schweiz. *Der Niederschlag in der Schweiz*. Ed. by B. Sevruk. Beitr. Geol. Schweiz Hydrol., 31, 65â75.

Shrestha, M., Wang, L., Koike, T., Tsutsui, H., Xue, Y., and Hirabayashi, Y. (2014). Correcting basin-scale snowfall in a mountainous basin using a distributed snowmelt model and remote-sensing data. *Hydrology and Earth System Sciences* 18, 747–761.

Slater, A. G., Barrett, A. P., Clark, M. P., Lundquist, J. D., and Raleigh, M. S. (2013). Uncertainty in seasonal snow reconstruction: Relative impacts of model forcing and image availability. *Advances in Water Resources* 55, 165–177.

SLF (n.d.[a]). *Description of automated stations*. URL: https://www.slf.ch/en/avalanche-bulletin-and-snow-situation/measured-values/description-of-automated-stations.html.

SLF (n.d.[b]). *niVis*. URL: https://models.slf.ch/p/niviz/.

Sommer, C. G., Lehning, M., and Mott, R. (2015). Snow in a Very Steep Rock Face: Accumulation and Redistribution During and After a Snowfall Event. *Frontiers in Earth Science* 3, 1–13.

Staudinger, M., Stoelzle, M., Seeger, S., Seibert, J., Weiler, M., and Stahl, K. (2017). Catchment water storage variation with elevation. *Hydrological Processes* 31, 2000–2015.

Strasser, U., Bernhardt, M., Weber, M., Liston, G. E., and Mauser, W. (2008). Is snow sublimation important in the alpine water balance? *The Cryosphere* 2, 53–66.

Sturm, M., Goldstein, M. A., and Parr, C. (2017). Water and life from snow: A trillion dollar science question. *Water Resources Research* 53, 3534–3544.

Swisstopo (n.d.). *DHM25*. URL: https://shop.swisstopo.admin.ch/en/products/height_models/dhm25.

swisstopo (n.d.). *Land cover*. URL: https://www.geo.admin.ch/en/geo-information-switzerland/geodata-index-inspire/surface-representation/land-cover.html.

Tague, C. and Grant, G. E. (2009). Groundwater dynamics mediate low-flow response to global warming in snow-dominated alpine regions. *Water Resources Research* 45, 1–12.

Thoen, E. (2019). *Package 'padr'*. URL: https://cran.r-project.org/web/packages/padr/padr.pdf.

Thornton, J. M., Mariethoz, G., Brauchli, T. J., and Brunner, P. (2019). *Shareable data, code, and supplementary figures related to the establishment and calibration of a spatially-distributed, catchment-scale model of alpine snow dynamics*. URL: https://doi.org/10.6084/m9.figshare.9016154.v1.

Thornton, J. M., Mariethoz, G., and Brunner, P. (2018). A 3D geological model of a structurally complex alpine region as a basis for interdisciplinary research. *Scientific Data* 5, 1–20.

Tobin, C., Nicotina, L., Parlange, M. B., Berne, A., and Rinaldo, A. (2011). Improved interpolation of meteorological forcings for hydrologic applications in a Swiss Alpine region. *Journal of Hydrology* 401, 77–89.

Tuo, Y., Marcolini, G., Disse, M., and Chiogna, G. (2018). A multi-objective approach to improve SWAT model calibration in alpine catchments. *Journal of Hydrology* 559, 347–360.

Vittoz, P., Randin, C., Dutoit, A., Bonnet, F., and Hegg, O. (2009). Low impact of climate change on subalpine grasslands in the Swiss Northern Alps. *Global Change Biology* 15, 209–220.

Viviroli, D. et al. (2011). Climate change and mountain water resources: overview and recommendations for research, management and policy. *Hydrology and Earth System Sciences* 15, 471–504.

Vögeli, C., Lehning, M., Wever, N., and Bavay, M. (2016). Scaling precipitation input to spatially distributed hydrological models by measured snow distribution. *Frontiers in Earth Science* 4, 1–15.

Vuille, M. et al. (2018). Rapid decline of snow and ice in the tropical Andes – Impacts, uncertainties and challenges ahead. *Earth-Science Reviews* 176, 195–213.

Wagner, T., Themeßl, M., Schüppel, A., Gobiet, A., Stigler, H., and Birk, S. (2017). Impacts of climate change on stream flow and hydro power generation in the Alpine region. *Environmental Earth Sciences* 76, 4.

Wang, L., Zhang, F., Zhang, H., Scott, C. A., Zeng, C., and Shi, X. (2018). Intensive precipitation observation greatly improves hydrological modelling of the poorly gauged high mountain Mabengnong catchment in the Tibetan Plateau. *Journal of Hydrology* 556, 500–509.

Wang, X.-Y., Wang, J., Jiang, Z.-Y., Li, H.-Y., and Hao, X.-H. (2015). An Effective Method for Snow-Cover Mapping of Dense Coniferous Forests in the Upper Heihe River Basin Using Landsat Operational Land Imager Data. *Remote Sensing* 7, 17246–17257.

Warscher, M., Strasser, U., Kraller, G., Marke, T., Franz, H., and Kunstmann, H. (2013). Performance of complex snow cover descriptions in a distributed hydrological model system: A case study for the high Alpine terrain of the Berchtesgaden Alps. *Water Resources Research* 49, 2619–2637.

Wayand, N. E., Marsh, C. B., Shea, J. M., and Pomeroy, J. W. (2018). Globally scalable alpine snow metrics. *Remote Sensing of Environment* 213, 61–72.

Wulf, H., Bookhagen, B., and Scherler, D. (2016). Differentiating between rain, snow, and glacier contributions to river discharge in the western Himalaya using remote-sensing data and distributed hydrological modeling. *Advances in Water Resources* 88, 152–169.

4 | Estimating the geometries of potential unconsolidated Quaternary aquifers across rugged Alpine headwaters

Photograph: *The alluvial fan in the central part of the Vallon de Nant, photographed in September 2018*

"We have not made much progress in linking the small-scale understanding of individual aquifers to watershed-scale hydrogeology"

(Hayashi, 2019)

Abstract

Our collective understanding of the hydrological behaviour of the various unconsolidated Quaternary landforms that are commonly encountered in alpine headwater catchments has been substantially enhanced by dedicated field campaigns. However, even under present-day climatic conditions (never mind possible future ones), the contributions that such unconsolidated aquifers make to the broader catchment systems within which they are embedded often remains much less clear. Applying sophisticated physically-based, spatially distributed, groundwater or integrated surface water-groundwater hydrological models at catchment scale represents one promising means by which this key knowledge gap might be closed. In order to do so, alongside other tasks, the three-dimensional (3D) geometries of all potentially important unconsolidated aquifer features within a given study area must be estimated as accurately as possible. The distinctive nature of alpine environments typically hampers the usefulness of approaches that are routinely deployed to meet this objective in other settings. Whilst certainly more efficient, classical desk-based geomorphometrical procedures are afflicted by various drawbacks of their own, many of which are accentuated in complex alpine terrain. Consequently, the few instances in which otherwise sophisticated numerical modelling of alpine hydrology has been undertaken have tended to involve the prescription of very simple Quaternary configurations (e.g. formations of uniform thickness). A clear need therefore exists for efficient and widely applicable methods that are nevertheless – on account of their comparatively high information content – able to incorporate constraints derived from geophysics wherever dedicated surveys are possible. As such, this chapter presents a simple approach to the estimation of 3D bedrock interfaces and, by extension, unconsolidated sediment geometries that combines a spline-based geomorphometical procedure with geophysical inferences where available (in this case from an Electrical Resistivity Tomography survey). Certain ambiguities and constraints arose in the application to the present study site that somewhat limit the confidence that should be placed in the resultant estimates. More generally, a singular ideal solution remains elusive. That said, the proposed approach does facilitate the generation reasonable first-order geometrical estimates which, in turn, should enable more plausible subsurface configurations to be employed in contemporary 3D hydrological models of (rapidly changing) alpine catchments.

4.1 Introduction

Whilst the general hydrological importance of unconsolidated Quaternary aquifers has long been recognised from both water resources and ecological perspectives, the influences between unconsolidated geologies and streamflow dynamics are only now beginning to be assessed in more rigorous, quantitative fashions (Carlier et al., 2019; Wirth et al., 2020). In consistence with this trend, and as already discussed in Section 1.2.1, intensive fieldwork campaigns have greatly elucidated the hydrological storage and flow characteristics of various types of unconsolidated sedimentary deposit features like talus slopes, moraines, rock glaciers, and suchlike that are commonly encountered in alpine settings. Many such features have been shown to be capable of storing and then subsequently releasing sufficient quantities of water that the responses of the headwater streams they are noticeably "buffered" or dampened with respect to snowmelt, ice melt, and rainfall inputs. The geometries, internal structures, and even hydraulic properties of many such formations have also been characterised through the application of apposite field techniques. However, in large part due to practical constraints, unconsolidated features – which have limited spatial extents – have thus far mostly been considered on a individual, even isolated basis. Consequently, their hydrological roles within the broader headwater systems of which they form part, including the extent to which they sustain downstream baseflow through hotter and/or dryer conditions (or might do so in future), has received very little attention.

Applying the latest generation of spatially distributed, fully-integrated surface-subsurface flow models (see Section 1.3) at catchment scale represents one emerging means by which such crucial broader aspects might be addressed; in theory, such models offer ample opportunity for integrating and synthesising an array of observational data types, testing competing hypotheses of system functioning, and quantifying the hydrological influence of unconsolidated aquifers not merely in conjunction or relation with one another, but also with respect to other prominent system components such as soils, bedrock, and vegetation. Finally, and perhaps most importantly of all, such models should enable more reliable predictions of future mountainous water availability than those hitherto possible to be made. However, with the exception of the contribution of Rogger et al. (2017), little numerical modelling of this nature (i.e. in which numerous potential unconsolidated aquifers and other elements are represented in detail with the a view to holistically reproducing internal spatio-temporal hydrological dynamics) has been attempted to date. The majority of the (still few) studies which have already applied integrated models at catchment scale in mountainous terrain (see Section 5.1 for further details) have not considered unconsolidated formations especially comprehensively, with uniform thicknesses commonly be-

ing assumed (e.g. Ala-aho et al., 2017).

To improve the realism of such simulations, the three-dimensional (3D) geometries of all potentially important unconsolidated aquifer features present in a given study area should be determined as accurately as possible; only having done so can appropriate hydraulic properties of said formations, which also naturally strongly control hydrological responses to a given forcings, be assigned or estimated via inversion with respect to field observations. In other words, constraining the geometries as tightly as possible beforehand should help minimise the risk of parameters assuming unrealistic values in order to compensate for structural deficiencies. It follows, then, that if the applicability of such advanced models in notoriously data-sparse mountainous terrain is to be improved, methods and guidance for producing the requisite estimates must be forthcoming. The steep, rugged, snow-covered (for much of the year), often inaccessible, and frequently protected nature of many alpine headwater systems complicate this task substantially, especially relative to lowland regions.

That said, given the increasingly widespread existence of geological and geomorphological mapping products, high resolution aerial and drone imagery, and digital terrain models (DTMs) even in high mountain regions, the very first phase – of establishing the two-dimensional (2D) surficial extents of potential unconsolidated aquifer features – usually presents few problems. All else failing, surveying the features on foot using a handheld Global Positioning System (GPS) device may remain feasible. Thence, the 3D geometries corresponding to the superficial extents must be deduced. Several possible approaches to this task exist, and can be grouped into three main categories: i) geomorphometric methods (essentially desk-based), ii) geophysical methods (field-based, non-invasive), and iii) borehole drilling (field-based, but invasive). It is important to emphasise at this juncture that not all studies that have used such methods to estimate unconsolidated sediment geometries have done so with hydrological applications in mind; many have simply intended to quantify sediment storage volumes.

Geomorphometric methods shall be considered first. As already mentioned, having identified and perhaps also classified the features, the simplest way of assigning a 3D character to them involves simply assuming uniform mean thicknesses based upon prior knowledge or expert judgement (Smoorenburg, 2015; Floriancic et al., 2018). Needless to say, such features rarely thicknesses uniformity in reality, however. At the next level of sophistication, certain features such as talus slopes and debris cones can be approximated using simplified 3D geometrical forms which are able to be described with small number of measurable deterministic parameters, as Figure 4.1 illustrates. Once again, the detraction here relates to the realism of these simplified forms. For example, should a bedrock valley wall behind a talus slope be undercut (as is common in

glaciated landscapes) it would be more concave than the planar surface assumed, and hence sediment volumes would be underestimated (Otto et al., 2008).

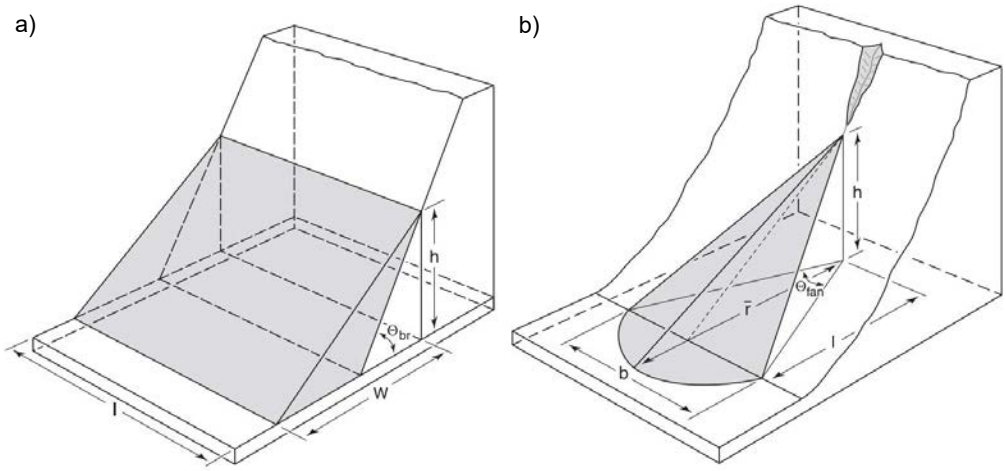

Figure 4.1: Simple geometric approximations to storage volumes for a) talus slopes, and b) debris cones. Source: Campbell and Church (2003).

Moving to the larger scale of valley cross-sections, several different geomorphometic approaches to estimating the sediment/bedrock interface have been considered. Incidentally, at a conceptual level, this challenge resembles that of estimating the bedrock interface beneath present-day glaciers to determine ice thickness distributions, although glaciological theory and contemporary measurements like surface mass balances and rates of ice thickness change can also be brought to bear on that endeavour (Farinotti et al., 2009; James and Carrivick, 2016). Perhaps the most straightforward approach involves simply projecting hillslope gradients into the subsurface (Hinderer, 2001). The fitting of power laws (Svensson, 1959) and quadratic functions (Wheeler, 1984) to empirical cross-section data have also proved rather popular (James, 1996; Li et al., 2001), even if much of this work was undertaken in attempts to try and better understand valley formation processes, whereby the fitted parameter values are interpreted (for instance, a power law exponent, b, approaching two is taken to be indicative of parabolic "U-shaped" glacial valleys, whilst values closer to one are considered to signify fluvially incised "V-shaped" valleys).

Despite this, such methods are mentioned here because if elevation points along the profiles corresponding to the sedimentary fill are removed prior to curve fitting, erosional upper bedrock surfaces can be reconstructed using them (Harbor and Wheeler, 1992). A fairly dense array of cross-sections must usually be considered to capture any longitudinal variability in the 2D

profiles, and a final interpolation undertaken to produce a 3D result. Schrott et al. (2003), for instance, took such an approach in a small catchment in the Bavarian Alps, Germany, but found that the surfaces produced by polynomial fitting overestimated sediment thicknesses compared to coincident seismic refraction surveys. Not dissimilarly, Rogger et al. (2017) provide an example of using a geomorphometrical approach to augment geophysical insights; sediment thicknesses were estimated at many different cross-sections by "extending the bare rock surface below the sediment deposit through a parabola fitted to the bedrock slopes at the outcrop boundaries", as shown in Figure 4.2.

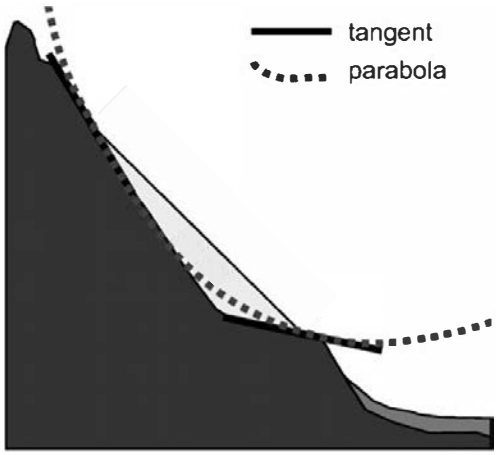

Figure 4.2: A parabola fitting approach to estimate unconsolidated sediment thickness in complement to geophysical survey data, with the ultimate intention of catchment-scale mapping and hydrological modelling. Source: modified after Rogger et al. (2017).

Major drawbacks have been identified with both the power law and quadratic methods, however (Harbor and Wheeler, 1992; Pattyn and Van Huele, 1998). Specifically, power law functions must be fitted to both sides of a given valley cross-section independently, since the variable representing horizontal distance cannot take negative values. Additionally, power law functions must pass through the origin of the coordinate system used, yet where this location should be is generally unknown at the outset – above all when the very aim is to interpolate the bedrock surface beneath sedimentary fill deposits. This issue renders the results sensitive to the choice of origin. The logarithmic transformation that is typically applied to solve for the constants of power law equations compounds the problem, since it causes more weight to be placed upon those points located near the origin than those towards the profile's extremities. Quadratic functions, meanwhile, assume that the cross-sectional form is parabolic and symmetrical, and are hence poorly suited to representing any form of asymmetry in such profiles.

A more modern but related approach to the estimation of glacial valley bedrock forms is the Sloping Local Base Level (LSBL) method (Jaboyedoff and Derron, 2005). This technique requires a DTM as input. Via the iterative calculation of quadratic parabolas, the topographic surface within the region of sedimentary fill is then progressively "excavated" , leaving a curved 3D bedrock surface. A crucial impediment to the wider implementation of this technique is that the maximum expected depth to bedrock, must be specified *a priori* (Otto et al., 2009), yet this is typically a key unknown to be determined.

More recently, Mey et al. (2015) presented an approach to the estimation of valley fill thickness/bedrock surface topography that revolves around training a machine learning algorithm using geometrical landscape data – specifically, the sectoral distance to the nearest bedrock hillslope, with the training data being generated by artificially filling DTMs. The approach hinges on the morphological similarity of the hillslope above the valley fill and the bedrock interface beneath it. Whilst results were promising with respect to estimating the thicknesses of sediments stored in the floor of large, almost horizontal intermontane valleys, the method would appear to be less immediately applicable to smaller alpine headwater catchments with their steeper sloping deposits.

As this last point alludes to, a further limitation of all the aforementioned geomorphometrical methods – and one which is particularly important given the complex nature of the bedrock geology at the present study site – is that geometric similarity above and below the fill level is assumed. In other words, no account is taken of lithological contrasts which, where present, bring about discontinuities in the cross-sectional profiles and terrain morphology more generally. The geostatistical approach developed by Castilla-Rho et al. (2014) used splines – a geomorphometrical technique that is better able to account for cross-sectional variability – in conjunction with various other datasets to estimate the bedrock interfaces of fluvial valleys. Indeed, that approach is somewhat similar to that eventually employed here, although replicating the stochastic quantification of interface uncertainty fell beyond the scope of this thesis.

In summary, given the now widespread availability of DTMs and associated geospatial data processing tools, such desk-based approaches can yield cost-effective estimates across larger areas, even if their accuracy is not necessarily entirely guaranteed.

Geophysical subsurface imaging techniques represent the main alternative to geomorphometrical approaches. Studies reporting on intensive geophysics campaigns in alpine areas include those of Sass (2006), McClymont et al. (2011), and McClymont et al. (2012); see also Christensen et al. (2017). Amongst such methods, seismic refraction and ground penetrating radar

(GPR) are perhaps the most popular, although Electrical Resistivity Tomography (ERT) is also fairly widely used. Such techniques often provide much more "concrete" information on depths to bedrock (i.e. sediment thicknesses). Moreover, being non-invasive, they are particularly attractive in sensitive alpine environments where strong environmental protection regulations are often in place. Another potentially important benefit of geophysical investigations over geomorphometric approaches is that they support certain inferences with respect to internal sediment structures.

Unlike in sediment budget-oriented studies, internal structure can be crucial from a hydrological perspective, but raises further challenges. Valley fill sediments in particular tend to be characterised by complex sequences of overlain and intercalated gravels, sands, and clays that may have been deposited by a variety of different processes (namely alluvial, colluvial, glacial, and mass movement processes). Figure 4.3, for instance, shows the idealised structure of a debris flow alluvial fan.

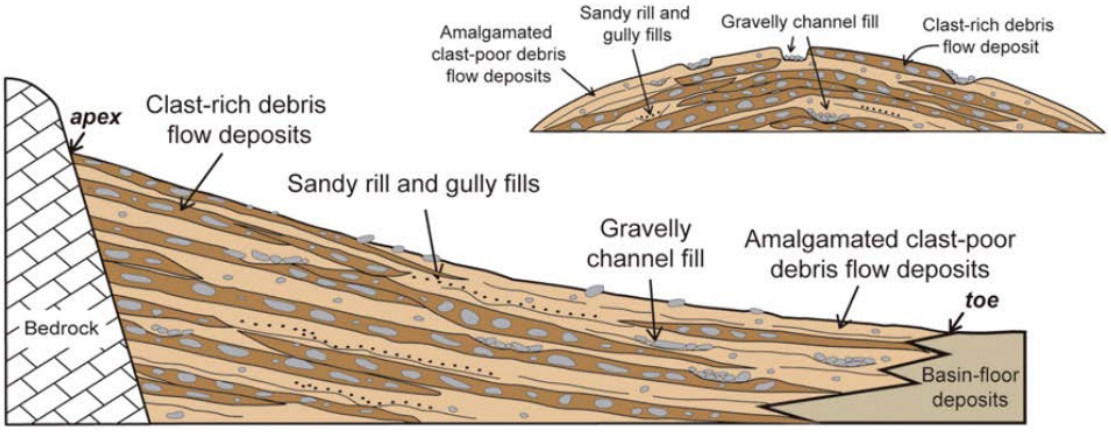

Figure 4.3: Sections through an idealised debris flow alluvial fan, showing the complex arrangements of unconsolidated sedimentary facies. Source: Moscariello (2018).

Crucially, they hydraulic properties of such facies are highly contrasting. One implication of this is that the bedrock interface does not necessarily correspond to the base of the aquifer. Rather, should an extensive layer of "tight" clay-rich sediments be present at only a few metres depth, then even if unconsolidated sediments extend several tens or even hundreds of metres beneath this, the zone would essentially be decoupled from the active near-surface hydrological system (although it could host several deeper confined aquifers).

In this sense, accurately representing "active" aquifer geometries should be considered more important than capturing the volumes of unconsolidated sediments *per se*. One possibility once the

overall unconsolidated volumes are known is to apply advanced statistical procedures to generate many plausible realisations of internal structures (e.g. Comunian et al., 2011). However, the disconnect between the capabilities of such algorithms and the approaches that are available for estimating their bounding geometries in the first place seems to be widening. Moreover, when such structures are generated stochastically, it is hard if not impossible to enforce them to be "in the right places".

The main drawbacks associated with geophysics in rugged alpine terrain are the time and costs involved, and more specifically the constraints that these factors place on extensiveness of the surveys that can practically be undertaken (e.g. with reference to the scale triplet of "extent", "spacing", and "support", for instance; Blöschl and Sivapalan, 1995). Although the number, lengths, and locations of profiles that can feasibly be surveyed will be greater is considerable manpower and other resources are available, activities will inevitably be curtailed as terrain becomes steeper and more inaccessible (Mey et al., 2015). As such, it is rarely possible to densely survey all potential aquifer features across moderately-sized headwater catchments. In addition, direct information can obviously only be recovered along the 2D transects surveyed, with uncertainties elsewhere (although 3D inversions can be undertaken to "fill the gaps" if surveying a dense network of overlapping profiles is possible). Furthermore, local restrictions may also impinge on the specific geophysical methods that can be contemplated.

The final technique – drilling a network of boreholes and analysing the resultant cores – is widely in other settings. However, this approach is generally impractical in rugged alpine terrain, especially those with stringent environmental protection regulations and/or where vehicular access is impossible. Deep boreholes are thus usually sporadic if not entirely absent in alpine headwaters.

From this review, it would seem that no straightforward, universally applicable approach to the challenge of estimating bedrock interfaces beneath unconsolidated sedimentary features presently exists. Undertaking as much geophysics as possible, ideally using multiple complementary techniques, is certainly recommendable. Regarding the more efficient geomorphometrical methods, it is noteworthy that the capabilities of spline-based functions, which are local (or piecewise) interpolators that produce smooth, minimum curvature surfaces yet are able to follow sharp variability (e.g. related to lithology) where present in the data have received relatively little exposure. Prior to the widespread availability of digital terrain data, such algorithms were used for interpolating between contours to generate topographic or bathymetric maps (Smith and Wessel, 1990), and more latterly have been successfully applied to the "opposite problem" to that under consideration here; the reconstruction of pre-erosional topography (Bergonse and Reis, 2015).

This chapter therefore proposes a simple 2D and 3D spline-based geomorphometrical approach that involves the targeted extraction of digital terrain and geological map data. Where available, bedrock interface constraints inferred from geophysics – in the case an ERT survey – can easily be incorporated. This combined approach can be considered a pragmatic compromise between the more accurate information that extensive geophysics can yield and the more extensive spatial coverage afforded by geomorphometrical methods. Ultimately, it is hoped that the approach provides a means by which catchment-scale groundwater and integrated surface-subsurface model structures can be refined, avoiding the need for the sort of extremely simple assumptions that have previously been resorted to.

4.2 Study Area

Extensive information regarding the study area has already been provided elsewhere in this thesis. In the context of this chapter, it is merely worth re-emphasising that the region was subjected to repeated periods of glacial advance and retreat throughout the Quaternary Period (i.e. the last 2.6 Ma), including during the last glacial cycle (Seguinot et al., 2018). Figure 4.4 shows the estimated ice extent at the Last Glacial Maximum (LGM), approximately 24,000 ka.

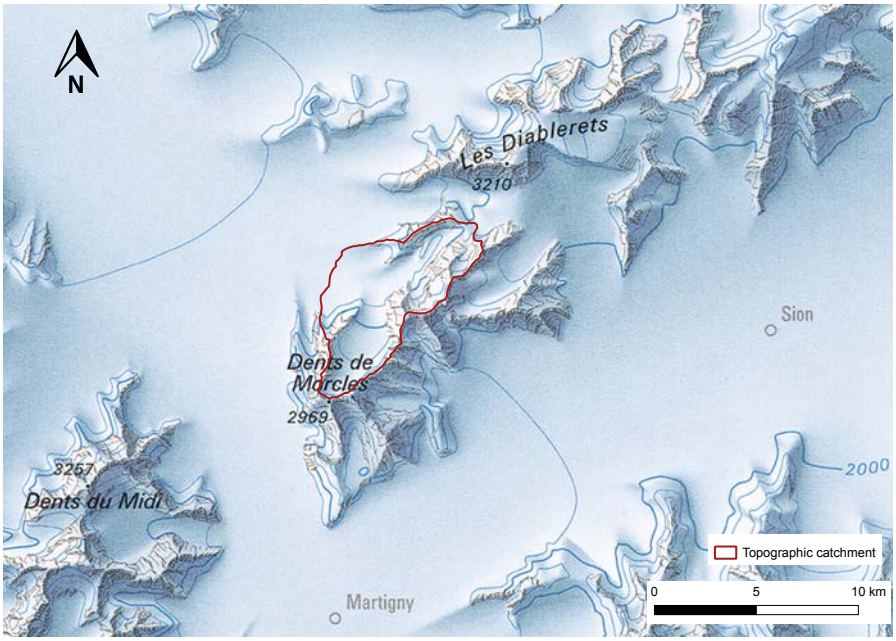

Figure 4.4: Estimated ice coverage in the study region at the height of the Last Glacial Maximum (LGM). Source: Bini et al. (2009). The study catchment is outlined in red.

As a result of this active history, accumulations of unconsolidated alluvial, colluvial, and glacial sedimentary materials overly the bedrock in several places. Figure 4.5, for instance, shows the coarse proglacial moraine sediments of the small Glacier des Martinets (Vallon de Nant).

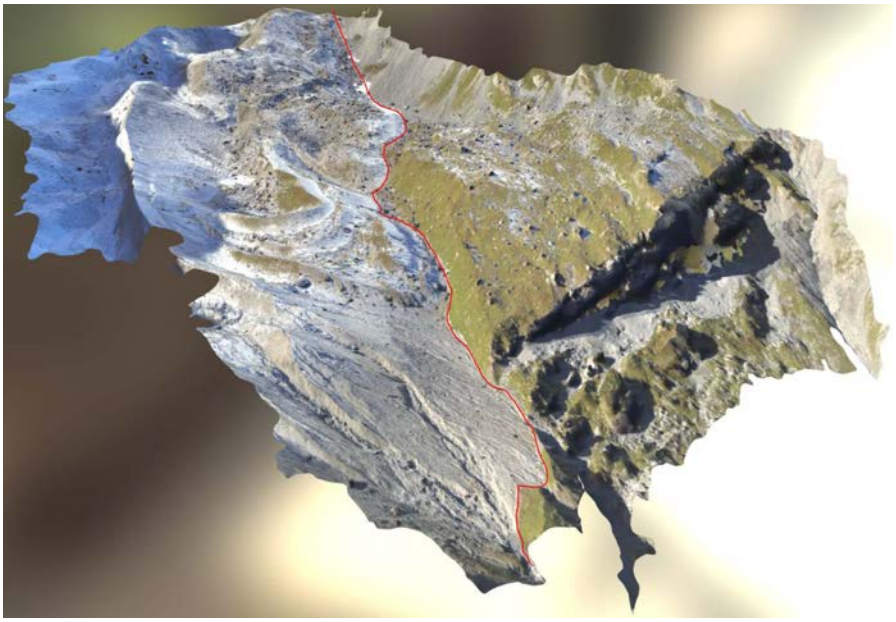

Figure 4.5: Photogrammetry model of the proglacial sediments (left of the red line) of the Glacier des Martinets, Vallon de Nant looking towards the south-west. These data were captured using a SenseFly eBee RTK drone. Source: SR-PROD (2016).

4.3 Methods

4.3.1 Preliminary fieldwork and sedimentary feature identification

The first step of the methodology involved identifying any major sedimentary features with the potential to act as aquifers (i.e. have the ability to store and subsequently release meaningful quantities of water) and establishing their surficial extents.

As it would in most instances, this step required some general understanding of the hydrogeological system – especially qualitative knowledge of where the major aquifers are located. This understanding was developed by making some basic field measurements and reviewing various existing datasets. For instance, on four days in summer 2017, several indicators of subsurface residence times including water temperature, electrical conductivity, major ion concentrations were measured at various locations in both surface and subsurface waters. Radon activities were

also measured on one day. Figure 4.6, for example, shows the electrical conductivities and calcium ion concentrations measured/sampled on the 5 August.

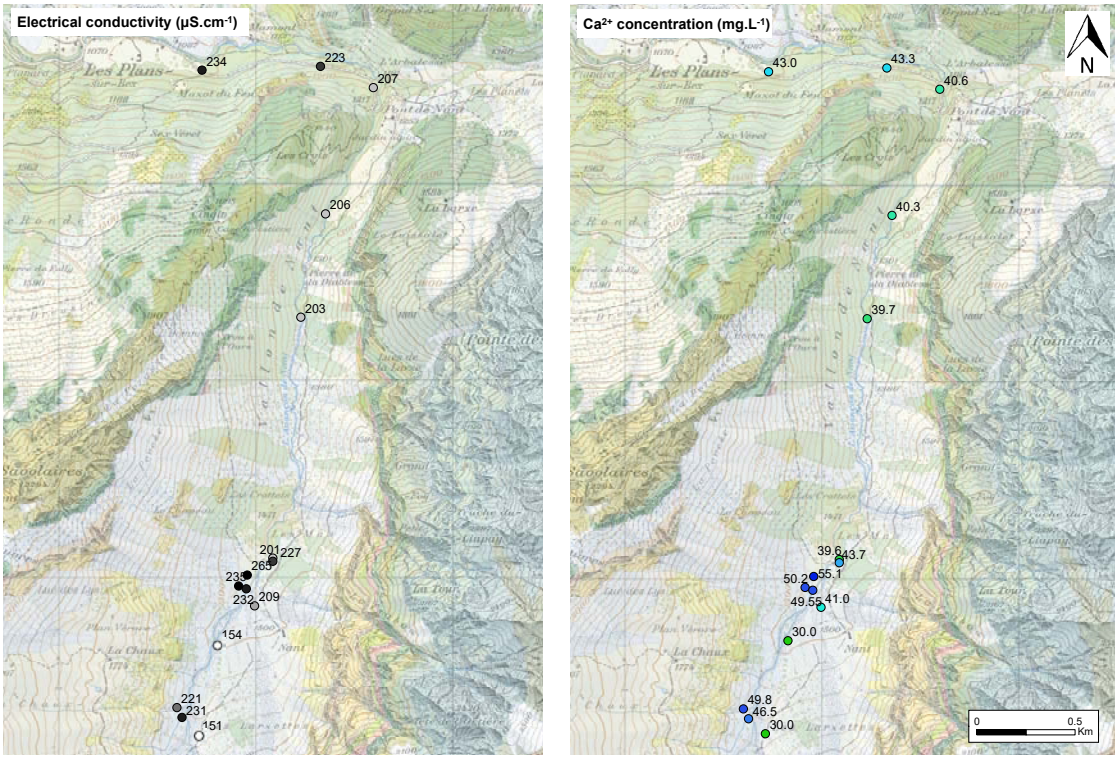

Figure 4.6: Spatial snapshot of electrical conductivity and calcium ion concentrations measured in various surface and spring waters on 5 August 2017. Several other parameters were also measured at these locations, and the measurements/sampling was repeated on four different days throughout summer 2017.

Stream water originating directly from the glacier had the lowest solute concentrations. Springs emerging from the deposits at La Chaux in the east had more elevated concentrations, as did groundwaters sampled in shallow piezometers (see Section 5.3) and numerous riparian springs and "seeps" in the vicinity of the main alluvial fan feature in the Vallon de Nant. The locations of these springs, which are strongly activated during the snowmelt period, were also mapped in June 2017 (see Figure 4.12). Together, these data and observations – alongside non-negligible Radon activities (data not shown) – display unambiguous groundwater signatures. As such, the two sedimentary features mentioned could be identified as important aquifers. Proceeding downstream, the water in the main channel becomes progressively more concentrated, which can be interpreted groundwater constituting an increasing proportion of the total discharge. Such patterns were broadly consistent across the different sampled days.

Elsewhere in the catchment, feature identification placed reliance on existing detailed (pre-digitised) surface geological maps (the GeoCover25 dataset; swisstopo) and a high (2 m) resolution terrain "hillshade" map which was developed from the swissALTI^{3D} dataset (swisstopo). Unconsolidated sedimentary deposits were marked on the geological maps, and are furthermore clearly discernible in the "hillshade" map. Previous studies pertaining to the hydrogeological function of certain types of features (e.g. proglacial moraines) were also consulted as necessary. In this way, the following five principal features were identified:

- A large alluvial fan system, referred to henceforth as ***Nant***
- High proglacial moraine sediments of the Glacier des Martinets (as shown in Figure 4.5) – ***Les Martinets***
- Glacial drift sediments – ***La Chaux***
- Generic unconsolidated fill sediments in a karstic, topographically closed depression (i.e. a doline) – ***Vare Upper***, and;
- Generic unconsolidated fill sediments – ***Vare Lower***

These five features were treated as distinct zones so that in the subsequent integrated model, different hydraulic properties reflecting their specific histories and constituent materials could be assigned to each (Chapter 5). The spatial extents of these features were extracted as shapefiles from the GeoCover25 maps, and verified with reference to the hillshade map. The resultant areas are presented in Figure 4.7.

In a final preliminary step, the x,y, and surface elevation, z, attributes of points spaced at 5 m intervals along the feature boundaries (i.e. where sediment thickness = 0) were extracted from the DTM, and the resultant coordinate triplets recorded along with an identifier of the feature to which they correspond. The topographic profiles and electrode positions also shown in Figure 4.7 are explained shortly.

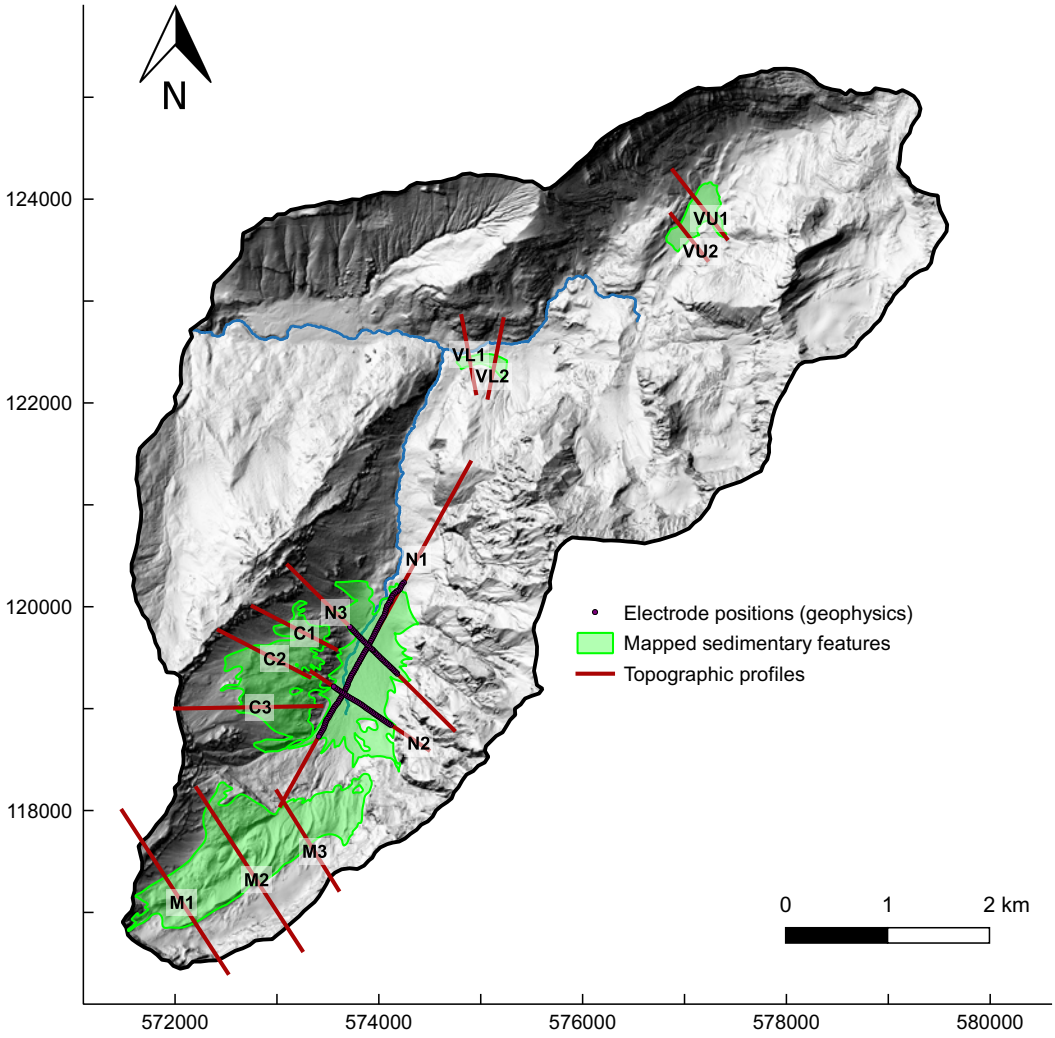

Figure 4.7: The major unconsolidated sedimentary feature extents considered in this study. The locations of electrodes that were placed during the geophysics campaign and the topographical cross-sections that were established as a basis for interpolating the bedrock interfaces are also shown. N denotes *Nant*, M *Martinets*, C *La Chaux*, and VU *Vare Upper*, and VL *Vare Lower*. The underlying hillshade map was generated from the swissALTI^{3D} digital terrain model (swisstopo).

4.3.2 Geophysics campaign

As previously discussed, in seeking to estimate Quaternary aquifer geometries, as much geophysics as possible should ideally be conducted. That said, the practical and monetary constraints to such approaches are elevated in rugged alpine terrain. With such considerations in

mind, and within the very broad scope of this thesis, only one geophysical technique could be deployed here, and only a single unconsolidated formation surveyed. Since the main alluvial fan in the central part of the Vallon de Nant (i.e. *Nant*) was believed to constitute the most important unconsolidated formation in hydrological terms, attention was focussed here. This feature also happened to be comparatively accessible; having obtained the necessary special permissions, off-road vehicular access was possible as far as Chalet Nant – a now uninhabited farm building in the alpine pasture (Figure 4.8b).

The survey's primary objective was to determine the spatial distribution of depth to bedrock; any potential insights that could be gleaned with regards to internal structure would be considered a bonus. Seismic methods (used by Schrott et al., 2003, amongst many others) were discounted due to the Natural Reserve's regulations, whilst the depth of information provided by GPR is very limited. ERT was identified as the most appropriate technique by elimination. A four-day long field campaign was conducted in favourable meteorological (dry and sunny conditions) in September 2018 – the first attempt to image the subsurface of this pristine Alpine valley.

With the objectives in mind, the intended profile layouts and electrode spacings were planned in advance. Three separate profiles were identified; one long one of 1,780 m running approximately parallel to the main valley axis (N1), and two shorter perpendicular profiles of 700 m each (N2 and N3). The former sought to capture any longitudinal variability in the bedrock interface (i.e. along the valley axis), for instance due to glacial over-deepening, which is common in such settings. The two intersecting transverse profiles sought to provide some 3D constraints on the morphology of the upper bedrock surface (and hence the unconsolidated sediment thickness); the ultimate goal being to develop a 3D flow model after all. In order to image to more deeply that usual, a uniform 20 m electrode spacing was chosen.

Once in the field, where conditions allowed, the stainless-steel electrodes were hammered in to a depth of 10-20 cm. The length of N1 necessitated a "roll-along" technique. At locations without soil cover (see e.g. Figure 4.8b), electrodes were positioned firmly in the silty sediments between larger boulders and pebbles, and sponges dampened with salt water were applied to decrease the contact resistance. Typically, contact resistances between electrodes of less than 5 kΩm were achieved. The electrode positions were measured accurately using a Lecia Differential GPS device; these are plotted in Figure 4.9. Fortunately, relatively straight profiles could be maintained, and so any 3D distortive effects in the results should be minimal.

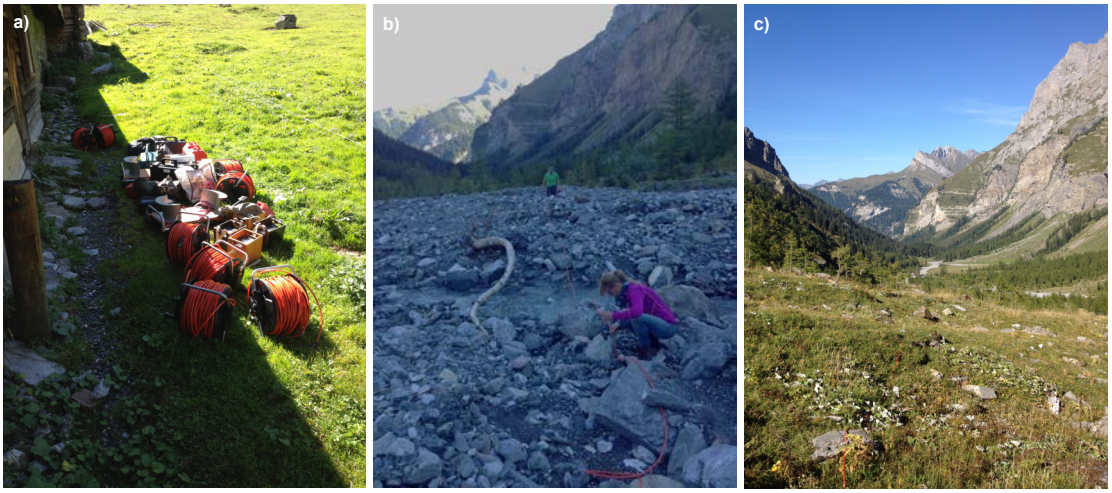

Figure 4.8: Photographs taken during the geophysics campaign of September 2018: a) Some of the geophysics equipment, which had to be transported on foot from this point onwards, b) ensuring good electrode contact in stream bed gravels, and c) looking down from the top of profile N1, with the cable visible in the foreground.

The apparent resistivity measurements were acquired in both dipole-dipole and Wenner-Schlumberger configurations using an IRIS Syscal Pro instrument. The current injection cycles (500 ms) were repeated four times and stacked in order to improve the signal-to-noise ratios. Prior to inversion, the data from the Wenner-Schlumberger and dipole-dipole surveys were combined, giving a total of 3,353 measurements for N1, and 793 measurements for N2 and N3, before any measurements whose standard deviation exceed 3% were removed. The inversions were performed in a fairly standard fashion using the code BERT (Günther et al., 2006). Robust data reweighting and compact inversion using iteratively-reweighted least-squares were employed to reduce the influence of outliers and to image sharper interfaces, respectively. The inversion process converged in 10 iterations, with a final relative root-mean square error of <5%.

The three resultant resistivity images were interpreted both independently and in combination. To facilitate the latter, they were georeferenced and visualised in conjunction with the surface topography within a virtual environment. This step also enabled the coherence of the inversion results near the profiles' intersection points to be verified. Next, a plausible bedrock interface was tentatively identified and annotated on the images (along with other possible interpretations). Finally, the spatial coordinates (x,y,z) of points placed at regular intervals along the identified subsurface interface were extracted.

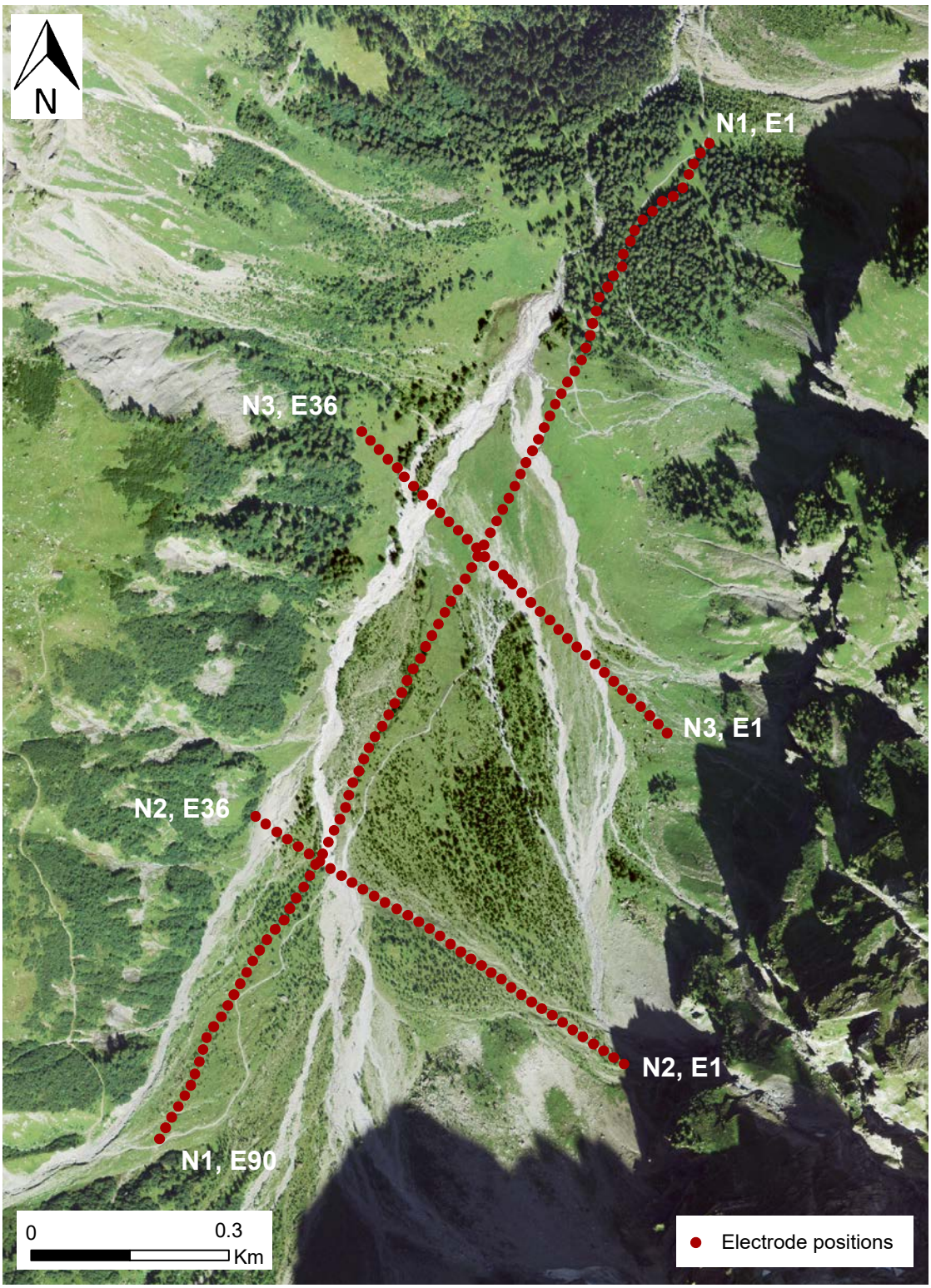

Figure 4.9: The arrangement of electrode positions along the three transects in the *Nant* alluvial fan that were surveyed using electrical resistivity tomography (ERT). The profiles were named N1, N2, and N3, and the electrodes were numbered sequentially along each profile.

4.3.3 Geomorphometrical approach

4.3.3.1 2D interpolations

The geophysics transects in *Nant* were extended to produce the topographical profiles N1, N2, and N3 shown in Figure 4.7. For the other features (where no geophysics was undertaken), similar topographic profiles – approximately perpendicular to their primary axes, and extending beyond their extents – were laid out. Points were generated at 5 m intervals along the full profiles, the surface elevation (z) extracted from the DTM, and the horizontal distance from the respective profile start points recorded.

Then, for each feature independently, the surface elevation points were plotted against the horizontal distances, and any points falling within the unconsolidated sediment extents (identified via spatial intersection with the feature shapefiles) were removed. These points are represented in red in Supplementary Figure C.1 (Appendix C). Following that, using the "stats" package (R Core Team, 2019), cubic splines were fitted to interpolate between the remaining points. As a class of functions, splines are local interpolators which seek to fit the empirical data points exactly (or extremely closely, by minimising the sum of the squared residuals) whilst simultaneously maximising smoothness, or penalising roughness (Mitas and Mitasova, 1999). They are generally favoured over high-order polynomials because the latter can result in strong oscillations. The specific technique of cubic spline fitting involves establishing piece-wise third-order polynomials that pass through all of the control points.

In this way, the upper bedrock surfaces along each transect were estimated. For the three profiles in the *Nant* feature, the additional subsurface interface derived from the geophysics results were included in the 2D interpolations in exactly the same fashion as the topographic points beyond the feature extents. Note that where such subsurface interfaces are available, the interpolation could also have been undertaken using the potential field approach of GeoModeller, as described in Chapter 2 (but with an "Erode" relationship specified with the rest of the pile). However, this approach would have been unsuited to the other formations for which no interface information was initially available, and so was not applied here.

The smoothness of the resultant interpolations makes splines well-suited to the task of reconstructing "U-shaped" glacial valleys; the smooth interfaces they propose beneath the sediment-obscured regions correspond to the simplest possible models. Simultaneously, in being able to follow sharp elevation discontinuities in the bedrock outcrops, which arise here due to lithological contrasts, these points do not influence the reconstructed interfaces. In other words, the

upper bedrock surface estimates along each transect were consistent with the bedrock gradients immediately beyond the feature extents.

It follows that should any lithological "steps" occur beneath the zones of sediment fill, these would not be captured. Such "steps" are generally not too problematic in this case, however; in the Vallon de Nant, for instance, the lowest bedrock formation (the Flysch, e6o1; see Figure 4.12) is "already" visible beyond the unconsolidated region area and extends fully beneath it. Thus, no hidden "steps" can be present here.

Unsurprisingly given the method but perhaps more importantly in terms of the results, the interpolated interfaces in certain instances demonstrated a high degree of sensitivity to the elevation gradient immediately beyond the sedimentary feature extents, and hence to the inclusion/exclusion of sampled points near the sediment/bedrock interfaces. This is similar to the finding of Mey et al. (2015), who also noted a certain sensitivity to the accuracy of the mapped feature "mask".

In fact, in the present case, no hard condition even to stipulate that the resultant interpolated surface remains beneath the topographic surface existed. That said, the original surficial extent mapping (and hence the distinction between which points lay within the unconsolidated region and which lay beyond it) was certainly not perfect. This observation justified the manual addition or removal of a few points in certain cases in these boundary regions, leading to interface profiles that were i) more consistent with prior expectations, and ii) were sufficiently coherent with others in the same feature. The final resultant splines are shown as the light blue lines in Supplementary Figure C.1.

The surface coordinates (i.e. *x,y*) of regular points along the interpolated spline function beneath the sedimentary fill were calculated using trigonometry and recorded along with the elevation estimates, (*z*). Finally, the triplets (*x,y,z*) were grouped by feature, and pooled with the corresponding surficial extent triplets (i.e. where thickness = 0) that had been generated previously (in Section 4.3.1). For illustration, Supplementary Figure C.2 shows all points prior to 3D interpolation for the *Les Martinets* feature.

4.3.3.2 3D interpolations

For each feature independently, all 3D (i.e. *x,y,z*) points which corresponded to an observed of estimated sediment thickness of zero (i.e the bedrock interface) were interpolated using Thin Plate Spline (TPS) functions – which imitate thin steel sheets forced to pass through the points – to give a spatially continuous 3D surface (with 10 m horizontal resolution). The "fields" package

in R (Nychka et al., 2019) was applied to achieve this. The smoothing parameter was identified automatically by generalised cross-validation. Where necessary, the resultant raster dataset was clipped to the feature boundaries. Finally, to express the results in terms of the spatial sediment thickness distribution, the estimated interface was subtracted from the (appropriately resampled) DTM.

4.4 Results and interpretation

4.4.1 Bedrock topography

4.4.1.1 Electrical resistivity fields in *Nant*

Figure 4.10 shows the inverted geophysical measurements made in the *Nant* feature. Animation C.1, meanwhile, represents these profiles – having been georeferenced – in a virtual environment along with the topographic surface. It should be remembered that the information content of these images is not constant throughout, but rather drops appreciably towards the margins and with depth.

Despite having been inverted separately, the three resistivity fields demonstrate a high degree of coherence within one another – as evidenced by the similar values at the intersection points (see Animation C.1; Appendix C). Another noticeable feature, at least compared to other studies that have sought to characterise unconsolidated sediment-bedrock interfaces via ERT in other geological settings, is that no sharp transition to substantially higher resistivity values that would usually demark the bedrock interface is apparent. The composition of the bedrock known to underlie the alluvial fan explains this; the marly shales of the Flysch (e6o1; Figure 4.12) are expected to be somewhat clay-rich. Had the bedrock been of non-sedimentary bedrock type (e.g. granite), a much sharper change in resistivity would have been produced.

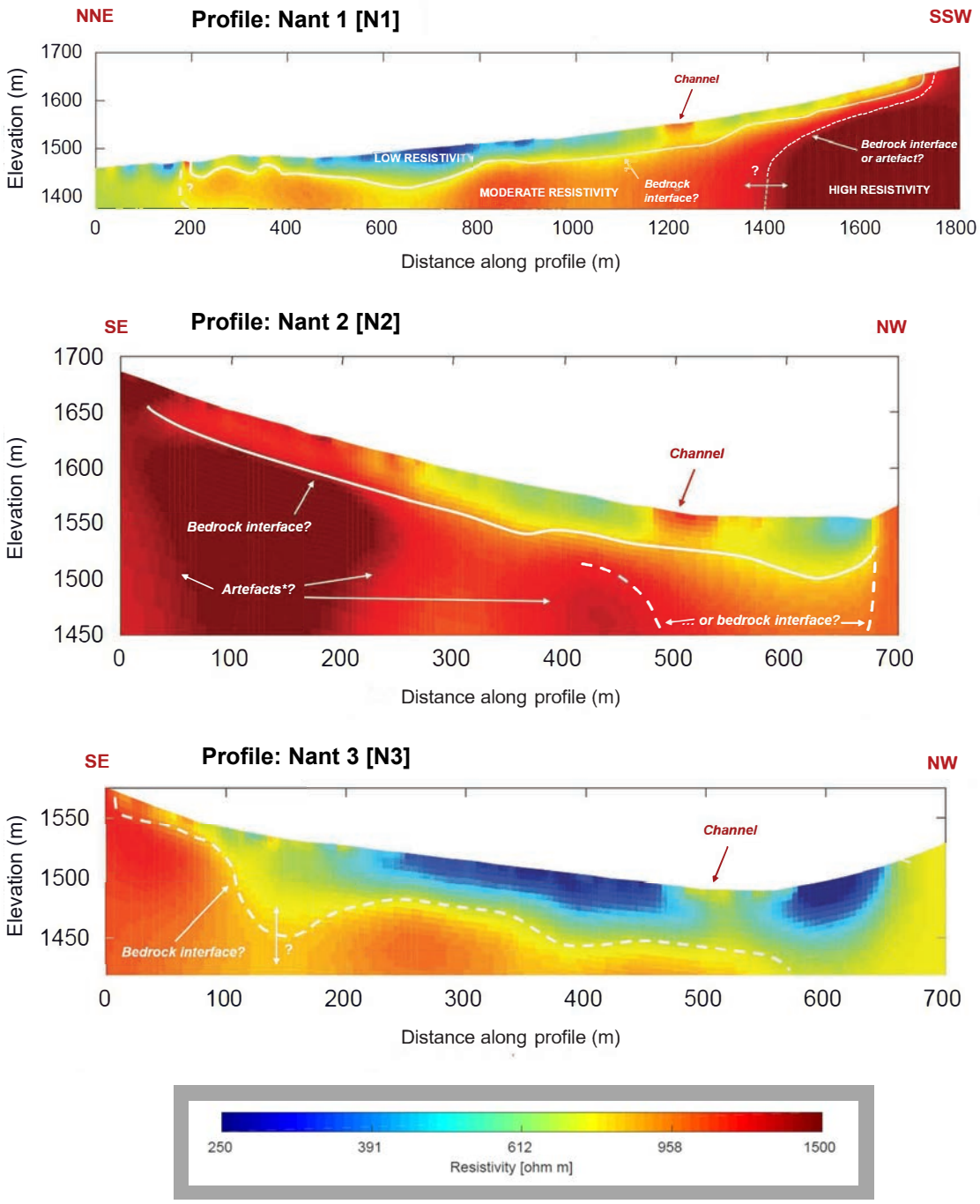

Figure 4.10: Inverted electrical resistivity fields for each of the three surveyed profiles in the *Nant* alluvial fan. A common resistivity scale is used. Annotations indicate the inferred bedrock interface and other interpretations, in some cases only tentative.

In light of this absence of a sharp resistivity contrast, the, the two transverse profiles (N2 and N3) were helpful in establishing a plausible bedrock interface,even despite the information content being lower at the extremities (as noted above). This is because, as Figures 4.9 and 4.12 reveal, these profiles extend close to the bedrock outcrops at both ends. As such, and given what was known about the fundamental bedrock morphology, the bedrock should be encountered at relatively shallow depths at the transverse profile extremities, with the depth to interface then increasing towards the profile centres. The inferred interface was annotated onto the resistivity images. (Note that these delineations were not based on a strict iso-value, however.

The digitised interfaces (pink dots in Animation C.1) were taken included alongside the topographic points beyond the feature's extent in the 2D (and by extension the 3D) interpolation of the bedrock surface beneath the *Nant* feature. Identifying the bedrock interface with greater confidence in future would probably require a seismic survey to be conducted (if permitted).

4.4.1.2 Interpolated 2D cross-sections

The 13 2D bedrock interfaces that were interpolated beneath the unconsolidated fill material are presented in Supplementary Figure C.1. Despite the simplicity of the geomorphometrical method, the results can be considered plausible, even if in certain instances it was necessary to add or remove a few points near the bedrock-unconsolidated boundary to ensure this, as mentioned above. The approach assumes that the bedrock gradients immediately beyond the sedimentary feature is indicative of the surfaces' extensions into the subsurface. As such, it assumes that no hidden bedrock "steps", at which the gradient changes with lithological contrasts, are present below the fill surface. Accordingly, the method is most applicable at sites where the lowest bedrock formation underlying a given sedimentary feature has already outcropped above topographic surface. As previously highlighted, this is generally the case at this site, although towards the south-eastern end of profile N2 – for example – a final potential "step" could be present (see Figure 4.12), but at least additional geophysical information was available here. More generally, the method depends on there being a pronounced morphological contrast between bedrock outcrops (perhaps mantled by a very thin soil layer) and regions of sedimentary fill. In more smoothly undulating regions (i.e. older mountain chains and hilly uplands), it may therefore be less directly applicable.

4.4.1.3 Final 3D unconsolidated sediment thickness estimates

The final estimated unconsolidated sediment thickness distribution is shown in Figure 4.11.

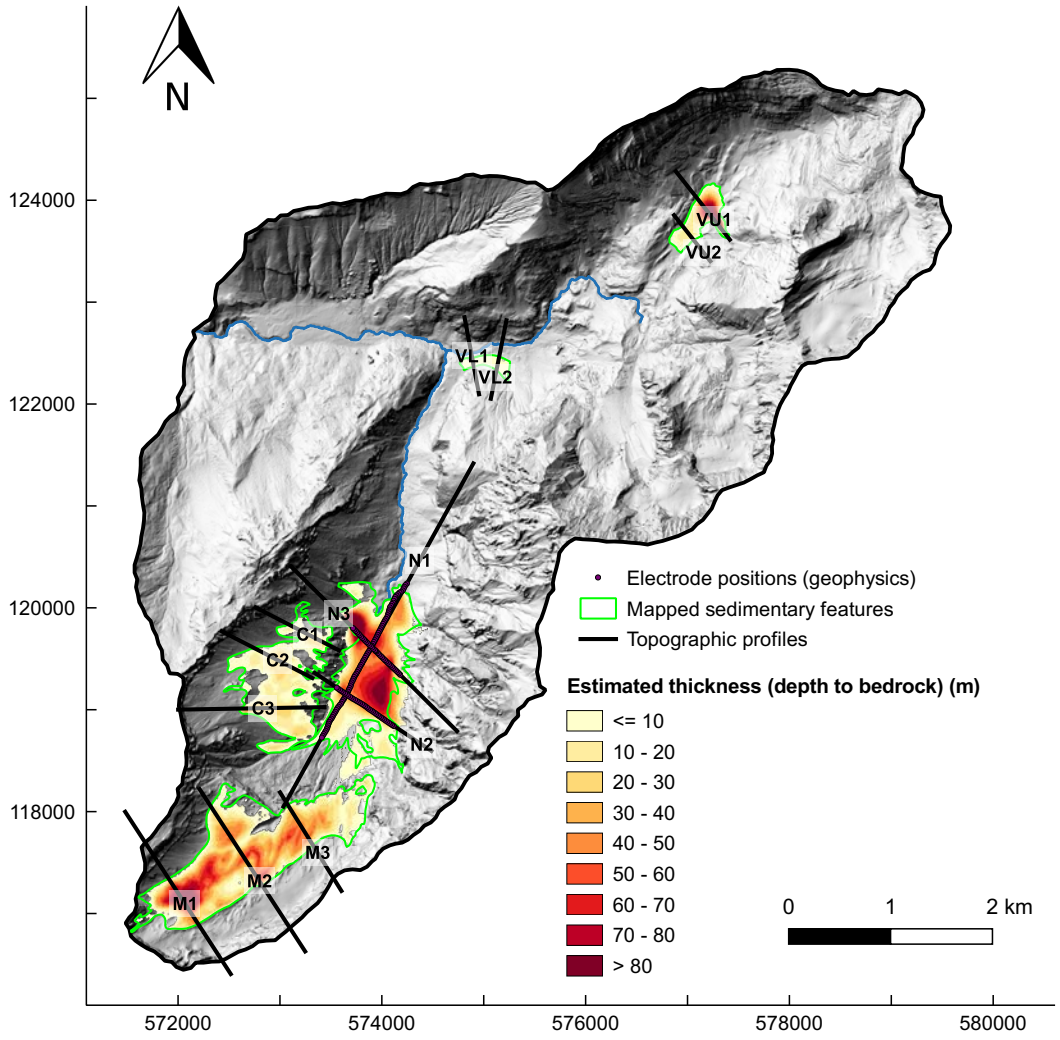

Figure 4.11: Estimated depth to bedrock within unconsolidated sedimentary features that were identified as potentially to host important aquifers. In the case of *Nant*, the result was generated by combining bedrock interfaces inferred from electrical resistivity images along the three profiles and the results from the geomorphometric method. As the other features could not practically be surveyed with geophysics, the purely desk-based geomorphometric method was used for these features.

4.4.2 What can be said regarding internal structure?

Whilst broadly reasonable estimates of bedrock geometries and therefore total sediment thicknesses seems to have been possible using the approach presented, establishing the internal structures (i.e. sub-zonation, both horizontally and vertically) of these sediments is more challenging still. Yet, as Section 4.1 discussed, such internal structures can be complex, and can have major hydrological implications. Unfortunately, the geometrical approach cannot provide any information regarding internal structure, and so it had to be assumed, for the purposes of the subsequent numerical modelling, that the features whose geometries were estimated in this fashion are "hydrologically active" to their full depth. This discussion is therefore limited to any possible insights that the geophysics survey could bring into the internal structure of the *Nant* feature.

In the resistivity images (Figure 4.6), a region of relatively low resistivities (dark blue colours) is located approximately one third of the distance along N1, as well in N3. Given a groundwater resistivity of approximately 45 Ωm (the inverse of the electrical conductivities shown in Figure 4.6), these values are consistent with coarse, rather porous non-consolidated materials, with a clay fraction of up to perhaps 10%. This can be identified as the main (saturated) alluvial aquifer.

By the time of year the survey was conducted (September), the groundwater level in the alluvial fan system will have decreased substantially from their peak during the snowmelt a few months previously. It is therefore unclear whether the slightly higher resistivities observed in the shallow subsurface in the upper half of N1 and N2 correspond to similarly coarse gravel materials to the previously highlighted conductive material which had simply become desaturated by this point, or rather whether their composition is different. If anything, one would generally expect sediment sizes to fine with distance down-fan (Bowman, 2019). As such, on balance, the former possibility can perhaps be tentatively favoured.

Just as the lack of strong resistivity contrasts made definitively establishing the bedrock interface problematic, it equally prevents much further being said regarding internal structure; the various materials that one would expect to encounter in such a setting – alluviums, clays, marls, limestones, and shales – all have similar expected resistivity values. Indeed, the possible resistivity ranges of such materials (depending on their degree of saturation) overlap substantially (Loke, 2015), rendering the determination of precise subsurface composition on the basis of these measurements alone practically impossible. In addition, the electrode spacing and resultant effective resistivity image resolution can be expected to prevent any very shallow features from being resolved, and cause any small or thin features more generally to be subsumed. Therefore, the vertical structure as a whole – including the effective thickness of the upper gravel aquifer –

remained highly uncertain on the basis of the geophysical data alone.

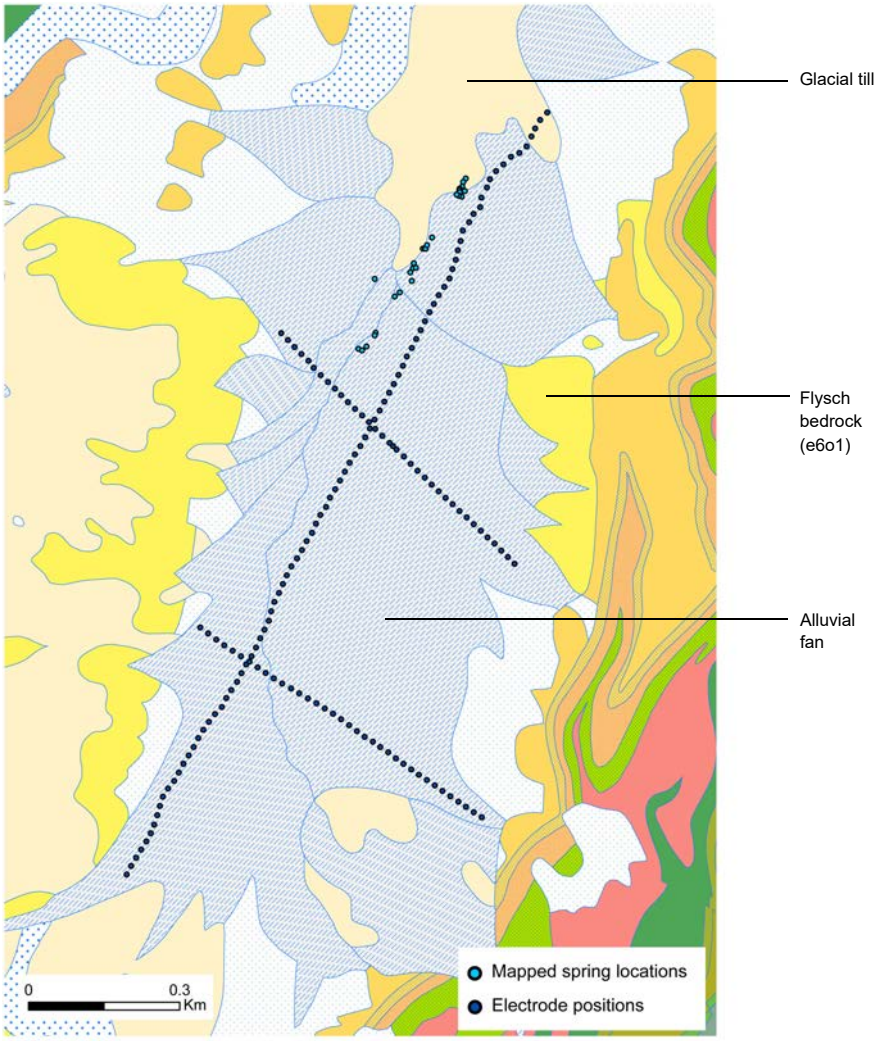

Figure 4.12: The geophysics profiles plotted on the GeoCover25 geological map (Source: Swiss Federal Office of Topography). Spring locations, which were georeferenced using a handheld GPS device (lateral location accuracy typically < 5 m), are seen to be concentrated at the interface between the distal part of the alluvial fan feature and the glacial till.

By combining the geophysics results with other information, however – namely the existing geological maps, and the georeferenced locations of springs that emerge near the interface between the distal part of the alluvial fan and a region of glacial till (Figure 4.3) – some possibilities may at least be suggested. According to these datasets, it can be considered unlikely that the alluvial fan is "hydrologically active" to its full depth (i.e. all the way to the bedrock interface). Rather,

would seem probable that the glacial till overlies the bedrock, upon which the alluvial fan subsequently developed. The till sediments should be both fine (i.e. clay-rich) and compressed, and therefore have very low hydraulic conductivity.

Within the alluvial feature itself, a complex internal architecture similar to that illustrated in Figure 4.3 is likely, even if hydraulic connections through the coarser facies (i.e. between the finer layers) remain possible (Bowman, 2019). As mentioned earlier, hydraulic conductivity could also be expected to decrease strongly with distance down-fan due to the progressive fining of sediments (ibid.). Representing such compartmentalisation and the attendant heterogeneity in hydraulic properties it surely indices represents a major outstanding challenging in the development and calibration of not only catchment-scale but also aquifer scale numerical models in similar settings.

On that note, interesting observations were made on a field visit was undertaken (for other purposes) in late September 2019 – approximately one year after the geophysics survey. An erosive flow event some time previously had incised and hence exposed the hitherto largely obscured subsurface alluvial fan architecture. In several distributed locations, including along the surveyed profiles, a shallow clay-rich layer was visible (Figure 4.13). Of course, the relatively wide electrode spacing employed in the geophysics survey was designed to detect an anticipated bedrock interface at much greater depths, and so could not have been expected to resolve such a feature. Nevertheless, should such a shallow intermediate clay-rich layer be spatially continuous, the implications for the flow system and its numerical representation would be considerable.

In summary, assuming that the bedrock interface identified does indeed correspond to the bedrock, at least two main "groups" of ambiguities remain; i) whether the glacial till does indeed extend beneath the entirety of the *Nant* feature, and if so, what its spatial thickness distribution is, and ii) how spatially extensive the shallow clay layer that was observed in the field really is, whether or not it is truly distinct from the glacial till formation, whether there are similar thin clay layers and greater depth, and if so how many of them there are, and how spatially extensive they are.

Unravelling these questions more definitively could ultimately require several deep boreholes to be drilled, and the layers of the recovered sediment cores carefully correlated, although such a strategy would not be appropriate in many sensitive alpine regions (including the present one). As such, a certain amount of structural uncertain may have to be accepted.

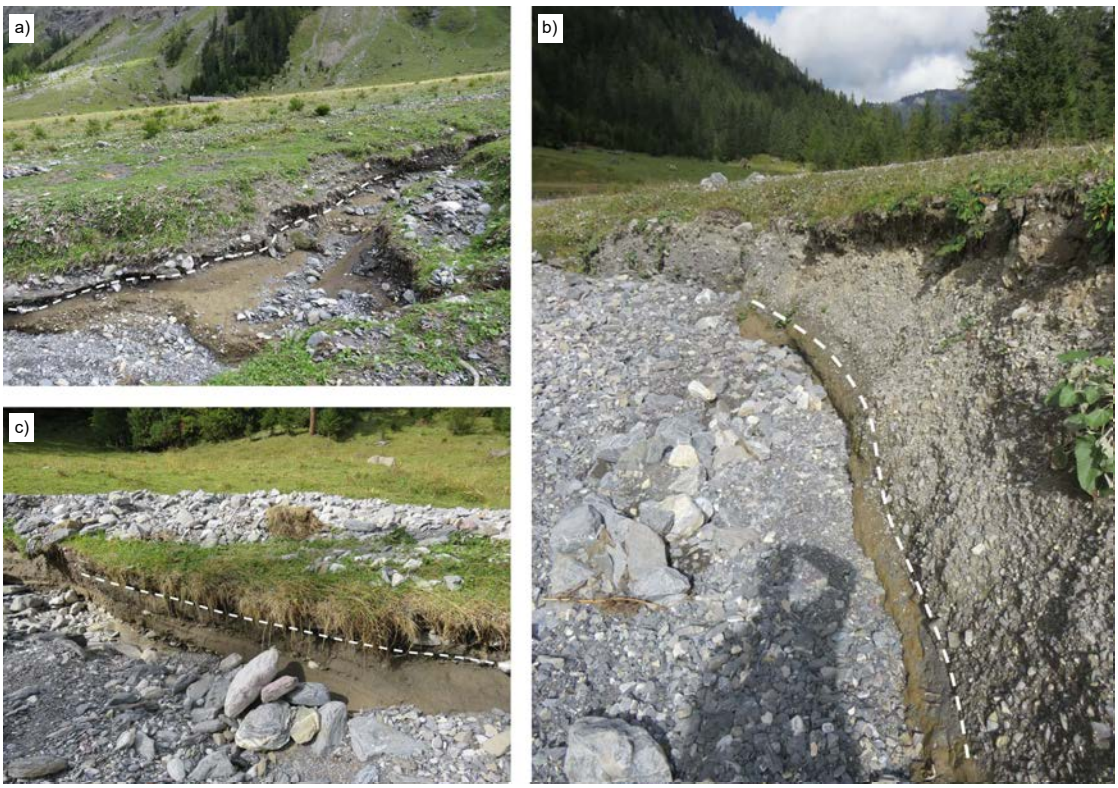

Figure 4.13: Photographs taken on 30 September 2019 showing the apparently spatially extensive shallow clay layer in the *Nant* feature that was more visible on this occasion than previously. Approximate locations are: a) 573740, 119090, b) 573992, 119875, and c) 573735, 119583.

4.4.2.1 Estimating the "hydrologically active" alluvial fan thickness for subsequent numerical modelling

In the end, the entire depth to bedrock beneath the alluvial fan was not defined as being eminently permeable for the purposes of the subsequent numerical modelling. Instead, only the upper third of the total thickness was considered as such, with the lower permeability till/clay assumed to comprise the remaining volume. This is essentially akin to defining the alluvial fan base according to a lower resistivity isosurface than the bedrock interface in Figure 4.10; somewhere in the light blue region. Such an approach is justified by the fact the ERT appears to be mapping the fan and the till as a common low-resistivity feature above the bedrock interface. The technique is also known to have a tendency to somewhat overestimate the size of conductive anomalies – in this case the coarse gravel region of the fan.

4.5 Conclusions

For reasons of practicality and cost, surveying all unconsolidated hydrogeological "functional units" in a given headwater catchment using geophysical methods is generally infeasible. Likewise, invasive techniques are rarely an appropriate choice in such terrain. Furthermore, the results of traditional geomorphometrical approaches may not yield consistently accurate results, especially when notable lithological "steps" in cross-sectional profiles are present.

Overall, few efficient and reliable approaches to characterising sediment thickness – never mind internal structures – of unconsolidated deposits at catchment scale in alpine terrain are currently available. Unfortunately, the resultant lack of data is now restricting the sophisticated, comprehensive simulation of the hydrological cycle in such environment, which in turn is preventing detailed knowledge gained through dedicated field campaigns being upscaled (to management-relevant scales) and is holding back the development of perhaps more reliable future predictions

In this context, and taking into account both the generic characteristics of alpine terrain (i.e. rugged, inaccessible, and geologically complex) and the specific nature of the present study site (strict environmental protection rules), this chapter proposed an approach revolving around spline fitting, which can also be classified as a geomorphometrical technique. Interestingly, such an approach seems to have been little applied to the problem of unconsolidated sediment thickness estimation to date.

Although inspired by "classical" work, high-resolution digital terrain data and digital geological maps were integrated. Overall, it can be considered a relatively simple, practical, and efficient means by which to estimate unconsolidated sediment geometries at catchment scale in mountainous terrain. A principal limitation of the method is the sensitivity of the interpolated interfaces to the bedrock gradients immediately beyond the sedimentary feature extents. That said, by judiciously adding or removing a small number of points in these regions – which is justifiable as the original mapped extents themselves are not perfectly accurate – minimum curvature surfaces representing the bedrock topography could be produced that both respected the data points and broadly aligned with prior expectations. Another important limitation is that, in having to also develop numerous other components for a complex integrated surface-subsurface hydrological model, the uncertainty in the estimated interfaces could not be quantified in the time available.

It is already recognised in the literature that, where possible, such geomorphometric methods be constrained by information derived from geophysics. As such, in this case study, an ERT survey was conducted in the (*Nant*) alluvial fan system. As it happens, this survey represents

the subsurface imagery of the Vallon de Nant; a rare example of a pristine headwater catchment in the European Alps, and moreover one in which an increasing amount of interdisciplinary environmental research is now being undertaken. Despite only moderate electrical resistivity contrasts, a probable bedrock interface could be proposed with some confidence, and could easily be incorporated into the 3D geometry estimation.

Another clear limitation of the geomorphometric method is that it yielded no insight whatsoever into internal structures of the sedimentary formations in question. This could explain why such techniques have historically been applied mainly studies seeking to merely quantify total unconsolidated sediment volumes. It was also slightly unfortunate that in this case the geophysics survey did not permit any firm conclusions to be drawn regarding the internal structure of the *Nant* alluvial fan system. That said, by carefully considering the geophysical data within the broader context (e.g. known geological setting and insights from other fieldwork, including the prevalence of springs at the downstream interface between the alluvial fan and the glacial till), it could be tentatively suggested that the unconsolidated sediments are unlikely to be "hydrologically active" throughout their entire depth (i.e. to the bedrock interface). Instead, the alluvial fan probably developed upon "tight", clay-rich glacial sediments, which themselves lie above the (similarly low hydraulic conductivity) Flysch bedrock.

In accordance with the structural model of an idealised debris flow alluvial fan presented in Figure 4.3, additional field observations indicated the presence of further "intermediate" fine deposits at shallow depths whose spatial extensions are presently unknown. These sediments are likely to have been deposited by periodic flood or debris flow events. However, since the measured resistivites were not extremely low, it is unlikely that these clay layers are terribly voluminous (although of course they would not necessarily have to be to still exert a substantial influence on aspects such as subsurface flow pathways and surface-subsurface interactions).

To account for the expected influence of these clay-rich formations in the subsequent integrated model in a simple fashion, the relatively coarse and permeable alluvial feature was assumed to comprise only the upper third of the total estimated depth to bedrock. With hindsight, maybe the main objective of the geophysics campaign – to image the bedrock interface – may not have been ideal; using an alternative technique able to provide shallower but more detailed information, or more than one method in combination, could have been preferable.

Developing an extremely comprehensive description of unconsolidated sediments, such as that presented by Orsi et al. (2016), fell beyond the scope of this thesis; here, topography, bedrock, snow, and land cover information all had to eventually be incorporated within a novel, com-

plex fully-integrated model (Chapter 5). Nevertheless, coupling state-of-the-art integrated flow models with probabilistic, geostatistically-generated realisations of subsurface interfaces and/or internal heterogeneity in future would represent an attractive potential approach to assess the impact of model structural uncertainties on hydrological predictions, both in mountainous terrain and other settings where comparable complexity is encountered.

To better constrain the internal structures (and indeed bedrock interfaces) at this site, additional geophysical surveys should be prioritised in future work. Ideally, several complementary methods would be employed, ultimately enabling the reliability of the interpretations proposed here on the basis of limited data and a simple method to be evaluated or refined. A greater number of similar catchments should also be characterised in this fashion. Given the spatial scales and rough terrain, further exploring the potential of air- and helicopter-borne geophysical techniques could also prove fruitful (see review by Siemon et al., 2009).

Finally, an alluring avenue for future research would involve investigating the sensitivity of hydrological model predictions to alternative plausible unconsolidated aquifer geometries. This framework could even enable some statements to be made as to the validity or plausibility of alternative possible plausible unconsolidated structures (e.g. by simulating hydrological responses under different structural assumptions or possibilities and then making the apposite comparisons with field measurements). However, parametric uncertainty could cause difficulties; model parameters could assume values that essentially compensate for inadequate structures, such that observations can still be satisfactorily reproduced. Distinguishing such cases from those in which both appropriate structures and parameters produce good comparisons could be difficult. More generally, it is certainly worth emphasising that structural uncertainties remain comparatively overlooked at the expense of parametric uncertainty. In essentially seeking to identify and then "fix" a single acceptable structure – both for the unconsolidated formations (this chapter), the bedrock formations (Chapter 2), and the forcing data (Chapter 3) before proceeding to consider parametric uncertainty (Chapter 5) – the model developed in this thesis is admittedly far from revolutionary in dealing better with structural uncertainties.

Contribution statement

I (The Author) proposed that a geophysics campaign be conducted in the study area as part of the thesis, contributed to its planning and organisation. I also developed and implemented the geomorphometrical approach, prepared all figures except Figure 4.10, and drafted the text. Dr. Emily Voytek and Professor Niklas Linde were involved in planning the geophysics field cam-

paign, and were wholly responsible for operating the measurement device and undertaking the geophysical inversions (thereby producing Figure 4.10). All of the aforementioned individuals were involved in the interpretation of the geophysics results. Others who kindly volunteered to assist with the fieldwork component are sincerely thanked once again.

References

Ala-aho, P., Soulsby, C., Wang, H., and Tetzlaff, D. (2017). Integrated surface-subsurface model to investigate the role of groundwater in headwater catchment runoff generation: A minimalist approach to parameterisation. *Journal of Hydrology* 547, 664–677.

Bergonse, R. and Reis, E. (2015). Reconstructing pre-erosion topography using spatial interpolation techniques: A validation-based approach. *Journal of Geographical Sciences* 25, 196–210.

Bini, A. et al. (2009). *Switzerland during the Last Glacial Maximum (LGM), 1: 500,000*.

Blöschl, G. and Sivapalan, M. (1995). Scale issues in hydrological modelling: A review. *Hydrological Processes* 9, 251–290.

Bowman, D. (2019). Groundwater. *Principles of Alluvial Fan Morphology*, pp. 101–105.

Campbell, D. and Church, M. (2003). Reconnaissance sediment budgets for Lynn Valley, British Columbia: Holocene and contemporary time scale. *Canadian Journal of Earth Sciences* 40, 701–713.

Carlier, C., Wirth, S. B., Cochand, F., Hunkeler, D., and Brunner, P. (2019). Exploring geological and topographical controls on low flows with hydrogeological models. *Groundwater* 57, 48–62.

Castilla-Rho, J. C., Mariethoz, G., Kelly, B. F., and Andersen, M. S. (2014). Stochastic reconstruction of paleovalley bedrock morphology from sparse datasets. *Environmental Modelling and Software* 53, 35–52.

Christensen, C. W., Hayashi, M., and Bentley, L. R. (2017). Scanning Calgary's 'Water Towers': Applications of Hydrogeophysics in Challenging Mountain Terrain. *CSEG Recorder* 42, 28–35.

Comunian, A., Renard, P., Straubhaar, J., and Bayer, P. (2011). Three-dimensional high resolution fluvio-glacial aquifer analog - Part 2: Geostatistical modeling. *Journal of Hydrology* 405, 10–23.

Farinotti, D., Huss, M., Bauder, A., Funk, M., and Truffer, M. (2009). A method to estimate the ice volume and ice-thickness distribution of alpine glaciers. *Journal of Glaciology* 55, 422–430.

Floriancic, M. G., van Meerveld, I., Smoorenburg, M., Margreth, M., Naef, F., Kirchner, J. W., and Molnar, P. (2018). Spatio-temporal variability in contributions to low flows in the high Alpine Poschiavino catchment. *Hydrological Processes* 32, 3938–3953.

Günther, T., Rücker, C., and Spitzer, K. (2006). Three-dimensional modelling and inversion of dc resistivity data incorporating topography - II. Inversion. *Geophysical Journal International* 166, 506–517.

Harbor, J. M. and Wheeler, D. A. (1992). On the mathematical description of glaciated valley cross sections. *Earth Surface Processes and Landforms* 17, 477–485.

Hayashi, M. (2019). Alpine hydrogeology: the critical role of groundwater in sourcing the headwaters of the world. *Groundwater*, gwat.12965.

Hinderer, M. (2001). Late Quaternary denudation of the Alps, valley and lake fillings and modern river loads. *Geodinamica Acta* 14, 231–263.

Jaboyedoff, M. and Derron, M. (2005). A new method to estimate the infilling of alluvial sediment of glacial valleys using a sloping local base level. *Geografia Fisica e Dinamica Quaternaria* 28, 37–4.

James, A. (1996). Polynomial and power functions for glacial valley cross-section morphology. *Earth Surface Processes and Landforms* 21, 413–432.

James, W. H. and Carrivick, J. L. (2016). Automated modelling of spatially-distributed glacier ice thickness and volume. *Computers and Geosciences* 92, 90–103.

Li, Y., Liu, G., and Cui, Z. (2001). Glacial valley cross-profile morphology, Tian Shan Mountains China. *Geomorphology* 38, 153–166.

Loke, H. (2015). *2-D and 3-D ERT surveys and data interpretation*. URL: http://ftp.geologipiemonte.it/atti%20download/006PIE15%20Loke%20TO-Sept_2015.pdf.

McClymont, A. F., Hayashi, M., Bentley, L. R., and Liard, J. (2012). Locating and characterising groundwater storage areas within an alpine watershed using time-lapse gravity, GPR and seismic refraction methods. *Hydrological Processes* 26, 1792–1804.

McClymont, A. F., Roy, J. W., Hayashi, M., Bentley, L. R., Maurer, H., and Langston, G. (2011). Investigating groundwater flow paths within proglacial moraine using multiple geophysical methods. *Journal of Hydrology* 399, 57–69.

Mey, J., Scherler, D., Zeilinger, G., and Strecker, M. R. (2015). Estimating the fill thickness and bedrock topography in intermontane valleys using artificial neural networks. *Journal of Geophysical Research: Earth Surface* 120, 1301–1320.

Mitas, L. and Mitasova, H. (1999). Spatial interpolation. *Geographical information systems: principles, techniques, management and applications*. Vol. 1. (2). Citeseer.

Moscariello, A. (2018). Alluvial fans and fluvial fans at the margins of continental sedimentary basins: Geomorphic and sedimentological distinction for geo-energy exploration and development. *Geological Society Special Publication* 440, 215–243.

Nychka, D., Furrer, R., Paige, J., and Sain, S. (2019). *Package 'fields'*. URL: https://cran.r-project.org/web/packages/fields/fields.pdf.

Orsi, G., Burger, U., Marschallinger, R., and Nocker, C. (2016). Geological model of an alpine lateral valley with implications for the design of a groundwater monitoring network â the example of the padaster valley (Eastern Alps, Austria). *Austrian Journal of Earth Sciences* 109.

Otto, J.-C., Schrott, L., Jaboyedoff, M., and Dikau, R. (2009). Quantifying sediment storage in a high alpine valley (Turtmanntal, Switzerland). *Earth Surface Processes and Landforms* 34, 1726–1742.

Otto, J.-C., Goetz, J., and Schrott, L. (2008). Sediment storage in Alpine sedimentary systems-quantification and scaling issues. *Sediment Dynamics in Changing Environments*. Vol. 325. IAHS Publ, pp. 258–265.

Pattyn, F. and Van Huele, W. (1998). Power law or power flaw? *Earth Surface Processes and Landforms* 23, 761–767.

SR-PROD (2016). *Vallon de Nant - Les Martinets - eBee drone scan*. URL: https://sketchfab.com/3d-models/vallon-de-nant-les-martinets-ebee-drone-scan-cb512401911e4f68890e3b93c1878f73.

R Core Team (2019). *R: A language and environment for statistical computing*. URL: https://www.r-project.org/..

Rogger, M., Chirico, G. B., Hausmann, H., Krainer, K., Brückl, E., Stadler, P., and Blöschl, G. (2017). Impact of mountain permafrost on flow path and runoff response in a high alpine catchment. *Water Resources Research* 53, 1288–1308.

Sass, O. (2006). Determination of the internal structure of alpine talus deposits using different geophysical methods (Lechtaler Alps, Austria). *Geomorphology* 80, 45–58.

Schrott, L., Hufschmidt, G., Hankammer, M., Hoffmann, T., and Dikau, R. (2003). Spatial distribution of sediment storage types and quantification of valley fill deposits in an alpine basin, Reintal, Bavarian Alps, Germany. *Geomorphology* 55, 45–63.

Seguinot, J., Ivy-Ochs, S., Jouvet, G., Huss, M., Funk, M., and Preusser, F. (2018). Modelling last glacial cycle ice dynamics in the Alps. *The Cryosphere* 12, 3265–3285.

Siemon, B., Christiansen, A. V., and Auken, E. (2009). A review of helicopter-borne electromagnetic methods for groundwater exploration. *Near Surface Geophysics* 7, 629–646.

Smith, W. H. F. and Wessel, P. (1990). Gridding with continuous curvature splines in tension. *Geophysics* 55, 293–305.

Smoorenburg, M. (2015). Flood behavior in alpine catchments examined and predicted from dominant runoff processes. PhD thesis. ETH Zürich.

Svensson, H. (1959). Is the cross-section of a glacial valley a parabola? *Journal of Glaciology* 3, 362â363.

Wheeler, D. A. (1984). Using parabolas to describe the cross-sections of glaciated valleys. *Earth Surface Processes and Landforms* 9, 391–394.

Wirth, S. B., Carlier, C., Cochand, F., Hunkeler, D., and Brunner, P. (2020). Lithological and tectonic control on groundwater contribution to stream discharge during low-flow conditions. *Water* 12, 821.

5 | Fully-integrated simulation of Alpine headwater dynamics under present and plausible future conditions

A manuscript based on this chapter is currently in preparation as:

Thornton, J.M., Therrien, R., Mariethoz, G., Voytek, E.B., Linde, N., Deluigi, N., Scherrer, D. and Brunner, P. (*in prep.*) Fully-integrated simulation of hydrological dynamics in complex Alpine headwaters under present and plausible future conditions.

Photograph: *L'Avançon de Nant during spring flow conditions, looking south with Dent Favre in the background*

"Parsimony is convenient, but complexity is often necessary"

(Fatichi et al., 2016)

Abstract

Temperature mountainous catchments are highly susceptible to ongoing climate change. Fully-integrated surface-subsurface hydrological models theoretically hold great potential to elucidate the holistic and spatio-temporally explicit functioning of such systems under both present and plausible future conditions. Whilst several predominantly crystalline mountainous catchments in the North American Cordillera have now been simulated using these tools, their utility in even more rugged and geologically complex (i.e. "truly Alpine") terrain remains untested. Moreover, the automated calibration of catchment-scale integrated models has not been attempted in mountainous environments. Herein, the development and calibration of an integrated HydroGeoSphere model representing two adjacent steep, snow-dominated, and geologically complex headwater catchments in the western Swiss Alps is initially presented. On account of the distinctive characteristics of the study region, substantial advancements were made over previous mountainous integrated models in terms of structure. More specifically, the detailed 3D geological and highly resolved (25 m) forcing datasets described previously (the snowmelt component of which was was generated via an energy balance snow model combined with an advanced optimisation procedure) were both incorporated. Calibration was undertaken with respect to internally measured streamflows and groundwater levels, but due to substantial model execution times could only be undertaken using monthly frequency forcing data. Thereafter, a recent period was simulated using both daily and hourly frequency forcing data. With the latter, streamflows at the principal gauging station could be reproduced over an independent 11-month evaluation period with a Nash-Sutcliffe Efficiency (NSE) coefficient of 0.75. The model also captured the strong seasonality of observed groundwater levels, although obtaining precise matches at each site remained elusive – probably due to unrepresented local scale variability in hydraulic properties. Simulated spatio-temporal patterns of several other important variables were also visualised, giving a sense of the capabilities of such a modelling approach. Finally, with a view to assessing the relative hydrological of plausible direct (i.e. climate change) vs. indirect (i.e. concomitant vegetation and permafrost changes), the model was forced using scenarios corresponding to a "moderate" warming towards the end of the century; these numerical experiments represent the first hydrological climate change impact assessments undertaken using a fully-integrated surface-subsurface model anywhere in the European Alps. Substantial

anticipated changes in snow dynamics and atmospheric demand for moisture are expected to propagate through, when summed across a three-year period, to a catchment-scale increase in total evapotranspiration of up to 44%, and a decline in total streamflow of up to 10% relative to the simulated baseline. Direct climatic changes will likely dominate, with the modulating effect of land cover and permafrost being more moderate.

5.1 Introduction

Partial differential equation-based, spatially distributed, fully-integrated surface-subsurface hydrological models are increasingly being used to address questions pertaining to real-world terrestrial hydrological systems. Indeed, reported applications of such models now span a considerable range of environmental settings and spatial scales (Smerdon et al., 2007; Sulis et al., 2011; Ala-aho et al., 2015; Maxwell et al., 2015; Hwang et al., 2018; Jaros et al., 2019; Tolley et al., 2019). In mountainous terrain, however, their uptake has been more limited, especially at a global level. Upon first glance, this situation could be considered surprising; the vital water resources derived from many of earth's high-elevation regions are increasingly threatened by ongoing climate change (Immerzeel et al., 2020; Hock et al., 2019), and so the need to better understand and quantify the functioning of mountainous hydrological systems under both current and plausible future conditions is now pressing. Crucially, integrated models have already demonstrated capabilities with respect to such tasks in many complex lowland environments, and furthermore should enable many of the limitations which afflict their more widely used conceptual counterparts to be circumvented.

Indeed, integrated models would appear especially suited to the simulation of distinctive Alpine hydrological regimes. Besides accounting for the vast majority of relevant hydrological processes in a physically-based and spatially and temporally explicit fashion, integrated models are capable of ingesting 3D information regarding the arrangement of subsurface formations. As such, they should enable any influence that (inherently complex) alpine geologies exert on broader hydrological processes to be explicitly represented. Additionally, integrated models simultaneously account for surface water flows – which hold considerable importance in terms of hydropower production, natural hazards, and sediment transport in steep mountainous terrain (Turowski et al., 2009; Lane et al., 2017; Costa et al., 2018).

Perhaps the greatest attraction of integrated models in alpine contexts, however, relates to the simulation of free bi-directional exchange between the surface and subsurface domains that they afford. Headwater torrents and streams are often ephemeral (Durighetto et al., 2020) – with

profound implications for in-stream ecology (Ward et al., 1999; Datry et al., 2014; Leigh et al., 2016) – or else demonstrate spatio-temporal variability in "losing" and "gaining" patterns more broadly. Since the stream network in fully-integrated models is able to evolve dynamically in accordance with to physical laws as a function of the boundary conditions and surface and subsurface properties prescribed, they theoretically support the replication of such dynamics. Integrated models therefore contrast greatly with alternative types of hydrological models, wherein fixed stream locations must usually be defined *a priori*.

Glaciers and snowpacks are not the only components of Alpine environmental systems that are responding to ongoing climatic change; components such as the vegetation (Macias-Fauria and Johnson, 2013; Goulden and Bales, 2014) and permafrost/soils (Evans et al., 2018; Rasouli et al., 2019; Wang et al., 2019) are also responding (and are expected to do so increasingly in future), albeit on contrasting timescales. Since such components are also involved in the hydrological cycle, and are linked together via an array of often subtle interactions and feedback mechanisms, the broader response of entire systems could modulate any direct climate-driven hydrological changes (Barnett et al., 2008). However, this possibility is often neglected in hydrological climate change impact assessments. A further potential benefit of integrated models, then, is that they often incorporate many important system components and interactions within a single coherent framework – even if further code developments would be required if the fully-dynamic co-evolution of hydrology and vegetation, and/or hydrology and geomorphology, for instance, is to be accounted for (Partington et al., 2017). By investing in such tools, it may be possible to generate more reliable predictions of the overall fate of the alpine hydrological systems to ongoing change than those hitherto possible.

A strong dichotomy exists between the extensive data requirements of such models and the generally more limited nature (in terms of quality, quantity, and spatial representativeness) of the information that is available in mountainous regions. Perhaps due to this and other challenges that shall be introduced shortly, the global uptake of integrated models in mountainous areas remains extremely limited. Nevertheless, some studies seeking to exploit the considerable potential of advanced contemporary numerical models – including in some cases fully-integrated ones – in mountainous contexts have begun to emerge lately. Efforts thus far have been predominantly focussed on catchments underlain by crystalline and other low permeability/storage bedrock types that are encountered widely across the west North America, and typically induce quite high water-table configurations.

In perhaps the first major contribution, Gleeson and Manning (2008) conducted a series of synthetic experiments using the fully-integrated code HydroGeoSphere (HGS; Aquanty Inc., 2016)

to unravel the influence of topography and hydrogeological properties on regional (i.e. inter-watershed) three-dimensional (3D) groundwater flow in idealised mountainous terrain. The ratio of recharge to subsurface hydraulic conductivity was found to strongly control water table position, and hence headwater streamflow ephemerality. Shortly thereafter, the first highly-detailed, catchment-scale representations of real mountain systems which went beyond simply treating the bedrock as impermeable were presented. Huntington and Niswonger (2012) employed GSFLOW (Markstrom et al., 2008) to simulate the hydrology of three watersheds in the eastern Sierra Nevada under numerous future climate scenarios, concluding that marked decreases in summertime stream discharge are likely. Voeckler et al. (2014), meanwhile, used a MIKE SHE model (Graham and Butts, 2005) to demonstrate that approximately 27% of annual precipitation in a small headwater catchment in British Columbia, Canada, contributed to bedrock recharge, thereby calling the then-prevailing assumption that deep groundwater is a negligible water budget component in crystalline mountain catchments into question. Note that GSFLOW and MIKE SHE provide only coupled (as opposed to a fully-integrated) representations of surface and subsurface flows, however.

Markovich et al. (2016) subsequently applied the prominent integrated code ParFlow.CLM (Maxwell and Miller, 2005) to quantify the influence of geology on the interplay between water balance components in two contrasting hypothetical 2D alpine hillslope transects – one of which was assigned typical crystalline properties, the other more transmissive volcanic-type properties – under progressively warmer conditions. Again, the results suggested that modified recharge and evapotranspiration (*ET*) dynamics will probably induce declines in groundwater storage and streamflow. Somewhat similarly, albeit in a real catchment (East River, Colorado) and with the intention of comparing the relative impacts of possible future climate change with those of land cover change, Pribulick et al. (2016) simulated three headwater transects, again using ParFlow.CML. Although it was found that simulated climate-driven hydrological impacts are likely to dominate those associated with vegetation change, their combination (i.e. both climate and vegetation change) led to even more accentuated streamflow shifts than either individual scenario. This implies the involvement of a feedback mechanism (or mechanisms), in this case positive, of the type alluded to above. The simulated responses of each transect were also highly contrasting.

3D integrated models of real basins – which account for spatial variably far more explicitly than models of 2D transects – should enable the dominant controls and changes to be established more confidently at catchment scale. Thanks to ever-growing computational power and commensurate model codes, research is now progressing in this direction. Ala-aho et al. (2017)

established a 3D fully-integrated model to glean insights into the spatio-temporal contributions of groundwater to runoff generation in small headwater in the Scottish Highlands. Three even more recent contributions together largely encapsulate the current state-of-the-art. Firstly, Penn et al. (2016) developed a comprehensive ParFlow.CLM model and altered vegetation parameters to assess the hydrological impacts of mountain pine beetle-induced tree mortality in another Coloradoan headwater – that of the Big Thompson River. Secondly, the GSLOW model of the entire East River constructed by Carroll et al. (2019) showed groundwater to be an important and stable contributor to mountain streamflow. Finally, Maina and Siirila-Woodburn (2020) used ParFlow.CLM to investigate hydrological responses following fire dynamics in a Californian watershed spanning a considerable elevational range.

Mountainous environments elsewhere in the world may exhibit (even) more complexity in terms of topography, geology, and/or the number and diversity of important hydrological processes than those systems to which integrated models have already been applied. Being geologically younger and more widely sedimentary, the European Alps – and most especially the calcareous parts thereof, which comprise approximately 30% by area (Goldscheider, 2005) – fit squarely in this category. The utility of integrated models in such contexts remains entirely untested.

Importantly, as the system complexity increases, many of the simplifying assumptions that featured in previous studies may no longer remain appropriate, especially those related to the subsurface. For instance, certain previous studies simply treated the bedrock as impermeable by assigning a no-flow boundary at its upper surface (Ala-aho et al., 2017; Camporese et al., 2019). At a slightly more complex level, single bedrock zone of homogeneous hydraulic conductivity values (Voeckler et al., 2014; Markovich et al., 2016) or a few sub-parallel geological layers (Huntington and Niswonger, 2012), have variously been considered sufficient – although Engdahl and Maxwell (2015) did employ a somewhat richer hydraulic conductivity field. In addition, the vast majority of these relatively simple configurations permitted only shallow simulated groundwater circulation. Whilst the general decline in hydraulic conductivity with depth in crystalline settings (Welch and Allen, 2014) may provide some justification for this shallowness, it should be highlighted that even in crystalline settings, field evidence for much deeper mountain groundwater circulation than that typically represented in models is emerging (e.g. Frisbee et al., 2017).

Across much of the Alps, sequences of limestones, shales, and marls have been folder and faulted into complex geological arrangements. It is well established that in these regions, groundwater flowpaths can be deep, with patterns strongly influenced by the geometries of aquifer-aquitard interfaces besides topogrpahy. Thus, 3D representations of bedrock geology should ideally in-

form the structures of integrated flow models in such settings. Unfortunately, such data has traditionally been been severely lacking (Thornton et al., 2018). Whilst not straightforward, Chapter 2 demonstrated that the development of geological models with the requisite attributes for hydrogeological applications is now possible in even the most challenging Alpine terrain.

Several other factors may also have impeded progress in integrated Alpine hydrological modelling. Firstly, the considerable spatial variability of meteorological phenomena that arises through the interaction of strong elevational gradients and rugged topography (e.g. shading effects, complex wind fields, etc.) means that high resolution spatial forcing datasets – on the order of tens or, at most, perhaps hundreds of metres – are required. Unlike other hydrological model codes, integrated models do not (yet?) include convenient pre-processing routines to apply any necessary corrections (e.g. for precipitation undercatch) and spatially interpolate meteorological station data onto a grid. Similarly, as a result of strong diurnal energy fluctuations and the prevalence of short-lived but intense convective precipitation events, high frequency (e.g. hourly) forcing data are generally considered necessary in mountain hydrology simulation exercises. However, applying spatially distributed, transient boundary conditions to complex integrated models with such high resolution and frequency is currently highly atypical. Certain code limitations can also be mentioned here; GSFLOW, for instance, only runs at a daily timestep. Gridded meteorological data products, meanwhile, are rarely reliable nor high-resolution and high-frequency enough to be applied directly in mountainous regions.

A more specific challenge in extremely rugged and steep Alpine catchments relates to the representation of snow dynamics; snow constituting another dominant, even defining hydrological influence in terms of both annual streamflow and groundwater recharge. Put simply, accurate snow simulations are imperative if spatio-temporal patterns of meltwater arrival at the land surface are to be satisfactory represented, but limited and uncertain meteorological data (as alluded to immediately above) and the considerable spatio-temporal variability and complexity of the snow processes involve impede the generation of such simulations. In fact, despite being highly advanced in most regards, certain integrated models – perhaps belying their origins in the groundwater modelling community – offer only simple index-based snow modelling approaches whose ability to satisfactorily capture alpine snow dynamics is questionable (Warscher et al., 2013). Note that ParFlow.CLM uses an energy-balance snow modelling scheme, and so is partially excepted from this criticism.

The MIKE SHE model of Voeckler et al. (2014), for example, as well as the recent applications of HGS in non-mountainous but strongly snow-influenced settings by Cochand et al. (2019) and Schilling et al. (2019) involved only temperature-index schemes. Presumably on account of

the now generally modest hydrological importance of snow in the Scottish Highlands, Ala-aho et al. (2017) felt able to neglect snow processes altogether. Furthermore, no integrated codes are currently known to incorporate snow redistribution processes (e.g. gravitational transfers), whose omission can produce undesirable model artefacts in steep, rugged topography (Freudiger et al., 2017). As with 3D geological models, efforts to ameliorate the simulation of snow dynamics independently of integrated models remain ongoing, for instance using distributed physics-based, multi-layered distributed snow models (Brauchli et al., 2017) or more hybrid physical-empirical models conditioned on various snow observations, such as that presented in Chapter 3 (see also Griessinger et al., 2019). However, such efforts have not yet been combined with a fully-integrated 2D/3D description of surface-subsurface flow dynamics.

Integrated models also are notoriously computationally intensive. Their long execution times (often days to weeks; Miller et al., 2018) can confound formal automated model calibration and uncertainty analyses, which require many forward iterations (von Gunten et al., 2014). Reflecting this, out of all the mountainous integrated modelling studies discussed hitherto, only Ala-aho et al. (2017) attempted any sort of automated calibration, with remainder relying on manual calibration and/or simple sensitivity analyses (see also Foster and Maxwell, 2019). Nonetheless, because "mountains do not give up their secrets easily" (Klemeš, 1990), calibration and uncertainty analyses should arguably assume an even more central importance than elsewhere.

Spatial discretisation can pose further headaches, affecting as it does both the numerical stability of the (non-linear) equation solutions and – in a partly dependent fashion – simulation times. Representing a steep, rugged Alpine landscape replete with sharp peaks, ridges, incised streams and suchlike with a given "fidelity" evidently requires a more finely resolved surface mesh than would be required to represent a flatter region of equal size in a comparable fashion (Smerdon et al., 2009). Elements should also be sufficiently small to represent spatial variability in key non-topographic surface properties (e.g. land cover), whilst the total domain should ideally be extensive enough that any potential subsurface water transfers across topographical boundaries are not artificially restricted. Beyond these considerations, the specific way in which surface topography is represented depends heavily on the code employed. Most integrated codes use regular orthogonal grids, which provide a more restricted topographic representation (or at least require a very large number of elements to approximate the true topography) – although "terrain following" modifications have been made to improve this aspect (Maxwell, 2013).

In contrast, other codes, including HGS (the particular option chosen here), can accept partially-unstructured meshes, wherein the surface is represented using a sheet of triangular elements, and these sheets are then replicated in a series of layers to furnish the mesh with its vertical dimen-

sion. Regarding vertical discretisation, in complex Alpine settings the extent should firstly be sufficiently extensive so as not to preclude the possibility of deep flows, as discussed above. The vertical resolution, meanwhile, should ideally be fine enough to minimise "information loss" in the transfer of spatially continuous 3D geological models that may contain complex geometries and thin layers. Recumbent folds pose a particular problem to the partially-unstructured approach, at least insofar as an extortionately fine mesh cannot be resorted to. This is because their presence prevents a more parsimonious mesh in which the subsurface layers are simply warped to several sub-parallel formation interfaces, defined by raster surfaces, from being generated.

In practice, limited computational resources demand that an appropriate balance between fine discretisation (and hence accuracy of the numerical solution) on one hand, and the total number of nodes/elements (and hence simulation times) on the other be struck. Unfortunately, determining the "minimum acceptable discretisation" requires extensive testing with numerous mesh versions, which can be time-consuming to undertake (von Gunten et al., 2014). In addition, attempts to coarsen the discretisation can easily become unstuck should solution accuracy (Wang et al., 2018) and/or numerical stability become compromised. Finally, and more generally, other distinctive aspects of the alpine systems like the presence of extremely steep slopes, high vertical hydraulic gradients, some very low hydraulic conductivity formations, and thick unsaturated zones have the potential to cause further numerical and/or runtime nuisances, including during (but not limited to) the model initialisation or "spin-up" phase (Seck et al., 2015).

In this context, and with a view to evaluating the utility of 3D, fully-integrated models in the some of the most complex Alpine terrain, this chapter sought firstly to develop and calibrate an integrated model of two steep, adjacent, snow-dominated, and geologically-complex Alpine headwater such that observed hydrological dynamics could be satisfactorily reproduced. One major novelty lies in the incorporation of a detailed, complex geological model and a sophisticated representation of snow dynamics into a catchment-scale integrated simulator of a mountainous catchment. In addition, in implementing an automated, multi-objective calibration procedure with respect to measured streamflows and groundwater levels, the study represents one of (if not the) first attempt to calibrate such a model in an automated fashion. Furthermore, the selected code, HGS – whose flexible mesh support offers more efficient terrain representation than its main competitors, as mentioned earlier – is not thought to have ever previously been applied in any real (as opposed to synthetic) mountainous terrain whatsoever.

The second aim was to subsequently apply the model to explore the possible hydrological impacts of not only plausible future climate change but also attendant vegetation and permafrost changes that could be expected under a "moderate" scenario towards the end of the century; the

first climate change impact assessment using a fully-integrated surface-subsurface hydrological model anywhere in the European Alps. In particular, the intention was to assess the possible impacts of changing temperature, precipitation, vegetation, and permafrost on – as applicable – aspects such as snow accumulation and melt dynamics, atmospheric demand for moisture (i.e. potential evapotranspiration, ET_p), the quantity and timing of liquid water arrival at the land surface, its subsequent partitioning into interception, surface runoff, and actual evapotranspiration (ET_a), groundwater levels, and – ultimately – downstream discharge. In so doing, many of the interactions shown in Figure 1.11 were considered.

5.2 Study area and field instrumentation

The $\sim$37 km^2 study area, which is identical to that of Chapters 3 and 4, is shown in Figure 5.1.

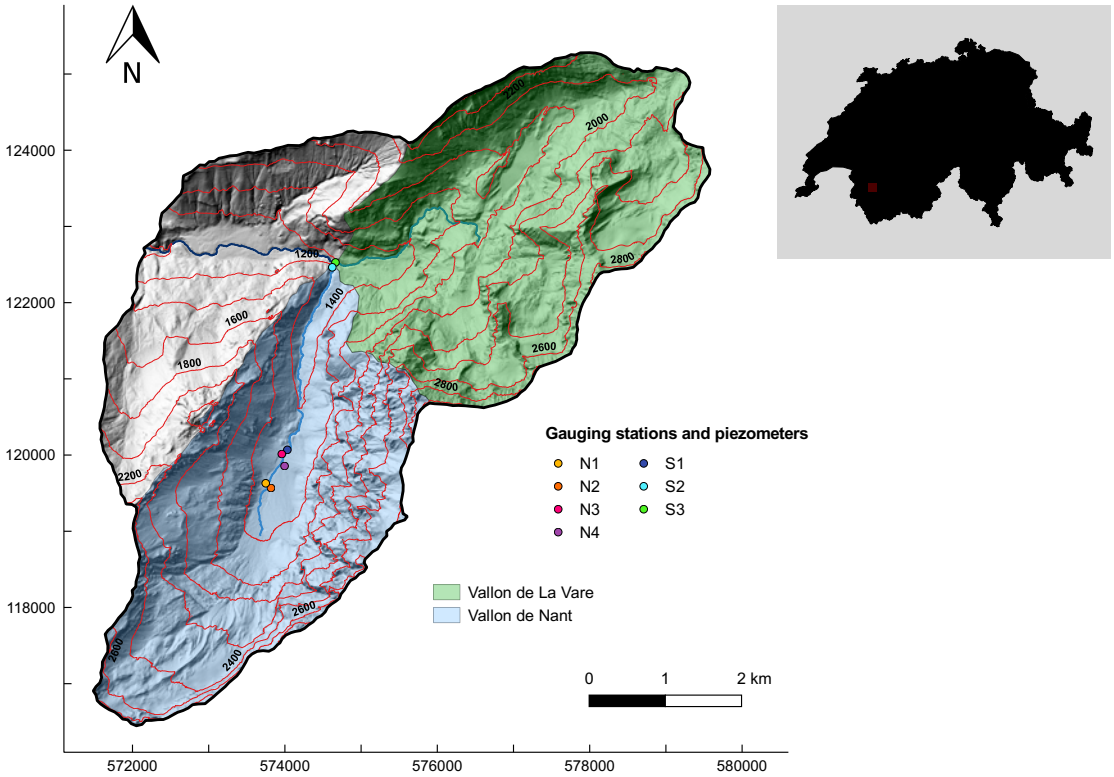

Figure 5.1: The study area and its situation within Switzerland. Stream discharge (S1-S3) and groundwater level (N1-N4) measurement station locations are indicated. Elevation (in metres) is represented using contours, whilst the background hillshade map provides an impression of the steepness and ruggedness of the surface topography.

The surface elevations extend from 950 m to over 3,050 m, slopes are accordingly steep, and the topography rugged. The area was delineated based on the review of the region's known or hypothesised general hydrological and hydrogeological functioning presented in Chapter 2. In particular, it was decided that the study catchment should extend beyond the confluence of Le Richard with L'Avançon (i.e. the limits of the two gauged sub-basins) since a certain proportion of precipitation falling within the topographical catchment in the north-western ridge of the Vallon de Nant is known to drain in a north westerly direction to a spring (Le Rippaz), thereby bypassing gauging station S2. Extending the simulation domain therefore averted the possible introduction of an artificial boundary effect, though this obviously had consequences in terms of the size of the simulation domain and hence the model's eventual node count and execution time. Some precipitation incident on the eastern cliffs of the Vallon de Nant may be similarly transported in a south-easterly direction across the topographic divide, ultimately emerging several kilometres away at a spring near Saillon in the Rhône Valley (Figure D.3). However, for practical reasons (e.g. execution times, data availability) the simulation domain could not be extended to encompass this entire area. Slightly artificial model boundary effects might therefore be present in this part of the model.

Geologically, the region lies within the Nappe de Morcles; the lowest of a series of large nappe thrust folds that together form the Helvetic Nappes. Alternating sequences of limestones are interspersed with much lower permeability marls and shales (Badoux, 1971). These Mesozoic sequences have been folded and faulted into complex geometrical arrangements by tectonic forces. Consequently, the configurations of the various (non-planar) aquifer-aquitard interfaces are expected to influence patterns of groundwater flow. Indeed, the two adjacent valleys – the Vallon de Nant and the Vallon de La Vare – actually lie within different zones of the first-order fold structure, with the upshot that their near-surface geologies are somewhat contrasting. As such, this arrangement potentially forms an attractive site to investigate, amongst other aspects, the influence of bedrock geology on hydrology. Further information on the area's bedrock geology and expected hydrogeological functioning is provided in Chapter 2.

Land cover is varied, with densely forested lower reaches giving way, with increasing elevation, to more open alpine pastures and then to sparsely vegetated regions of unconsolidated rock and bedrock outcrops/cliffs. Soils are generally thin or even non-existent in the upper parts, but are better developed in the valley bottoms. Small glaciers persist in the north-facing upper reaches. Recent permafrost potential mapping using the method of Deluigi et al. (2017) indicates that some can be expected at the highest elevations in the uppermost reaches – an assessment corroborated by the geophysical survey presented by Giaccone et al. (2019) – but that permafrost

is unlikely to be extensive. As Chapter 4 explained, various unconsolidated sedimentary features of Quaternary age overly the bedrock, several of which are likely to function as aquifers. Debris flows and avalanches occur frequently in the more geomophologically active upper parts of the catchment, somewhat limiting the colonisation of the upper slopes by forest.

Being situated in the western high Alps, the area receives abundant precipitation – approximately 40% of which falls as snow. Snowmelt dominates the annual streamflow regime, and is also likely to contribute disproportionately to groundwater recharge. Since the study catchment spans a considerable elevational range, the rain-snow limit falls somewhere within it for much of a typical year; as such, the system could be highly sensitive to small shifts in air temperature. Intense localised convective storms in summer are a further noteworthy feature of the meteorological regime. The surficial hydrology of the Vallon de Nant is characterised by the eponymous "Nants"; temporary torrents whose discharge responds rapidly to rain and snowmelt. Likely due its more permeable bedrock, surface water is less conspicuous in the Vallon de La Vare.

The area is a rare example of a section of the European Alps that has remained relatively unaffected by anthropogenic activity, light summer grazing notwithstanding. Indeed, the Vallon de Nant has been a designated Natural Reserve since 1969. Coupled with the number and diversity of potentially important hydrological processes operating within it, this makes it an excellent natural laboratory, albeit a challenging one to simulate in the fashion intended here; whilst the pristine nature of the environment is in many ways a great attraction, there is no long-term history of systematic hydrometeorological observation in the region, i.e. the hydrological system was poorly characterised and understood at the outset. A key step towards ameliorating this situation was the funding and construction of a concrete weir by a consortium of stakeholders downstream of Pont de Nant (S2 in Figure 5.1, see also Figure 5.2a). This development played an important role in the area being really "opened up" as a feasible site for hydrological investigations. Indeed, having such a well-constructed gauging station so high up an Alpine stream network, and crucially prior to any anthropogenic influences on the flow, is fairly exceptional. Water level measurements are made automatically at regular intervals which, by applying a rating curve developed via salt dilution gauging (Ceperley et al., 2018), can be translated into a relatively complete discharge record from April 2016 onwards. Substantial subsurface flows beneath the station are not thought to occur here.

Even at this regular cross-section, however, shifting channel configurations immediately upstream undermine the temporal consistency of the record a little, leading not only to fairly high but also temporally variable discharge uncertainties – especially at low flows. (High flow estimates are also naturally uncertain as the rating curve was developed from punctual discharge

gaugings at low to moderate flows). Temporary gauges were also installed (by collaborators) at two further locations – S1 and S3 (Figure 5.1), but these sites only provide estimated discharge series for much shorter periods. Note that none of these gauges are situated at the outlet of the simulated entire catchment; S1 is an internal site within the Vallon de Nant, whilst S2 is located further down L'Avançon de Nant, just above its confluence with Le Richard. The flow of Le Richard, which (partially) drains the Vallon de La Vare, is measured at S3.

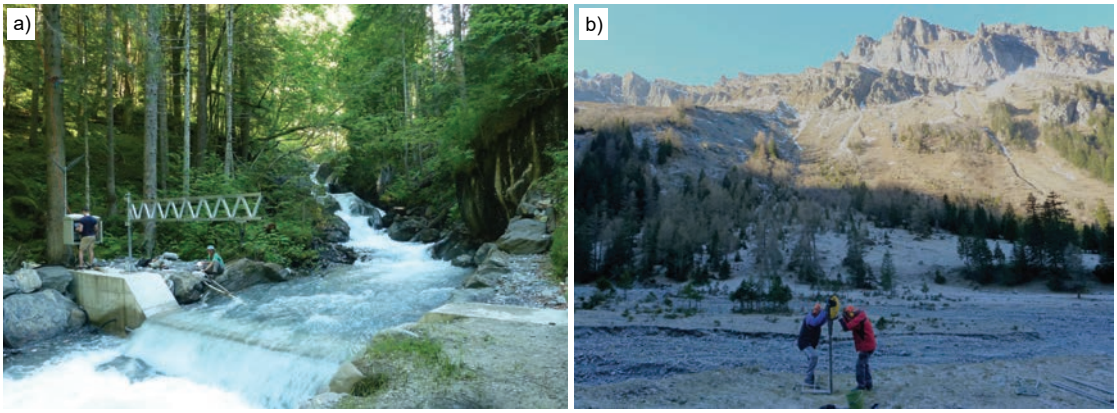

Figure 5.2: Photographs showing a) the concrete weir gauging station S2, and b) the installation of piezometer N4.

To complement the stream discharge observations and provide greater insight into hydrogeological processes, four relatively shallow (up to 6.5 m deep), small-diameter groundwater observation wells (or piezometers) were installed in vicinity of the large alluvial fan system in the central part of the Vallon de Nant (N1-N4 in Figure 5.1; see also Figure 5.2b). The piezometers were screened over at least their lower half, and were equipped with the pressure loggers in June 2017. From this point forth, they provide half-hourly groundwater level observations, although at three of the four sites levels fell below the bases for substantial periods.

5.3 Model setup and calibration

HGS (Aquanty Inc., 2016) is a fully-integrated simulator which simultaneously solves the diffusion wave approximation to the Saint-Venant equations for shallow 2D surface flow and a modified form of Richards' equation for 3D variably-saturated subsurface flow. Here, the coupling between these domains was conceptualised using the first-order-exchange method. Although some formations are expected to be karstified and soil macropores are also likely present, the subsurface was treated as an Equivalent Porous Media (EPM). As such, parameters must be

considered effective at the elemental scale. Interception and evapotranspiration are simulated according to Kristensen and Jensen (1975). HGS was chosen over possible alternatives on account of its support for (partially, in this case) unstructured finite element meshes, which compared with structured meshes offer improved representation of the study area's complex topography and other physical features. Several work phases were required to establish the model's structure, as outlined below.

5.3.1 Finite element mesh generation

A 2D triangular mesh was generated using Algomesh (HydroAlgorithmics, 2016), which employs multi-level optimisation and Delaunay refinement.

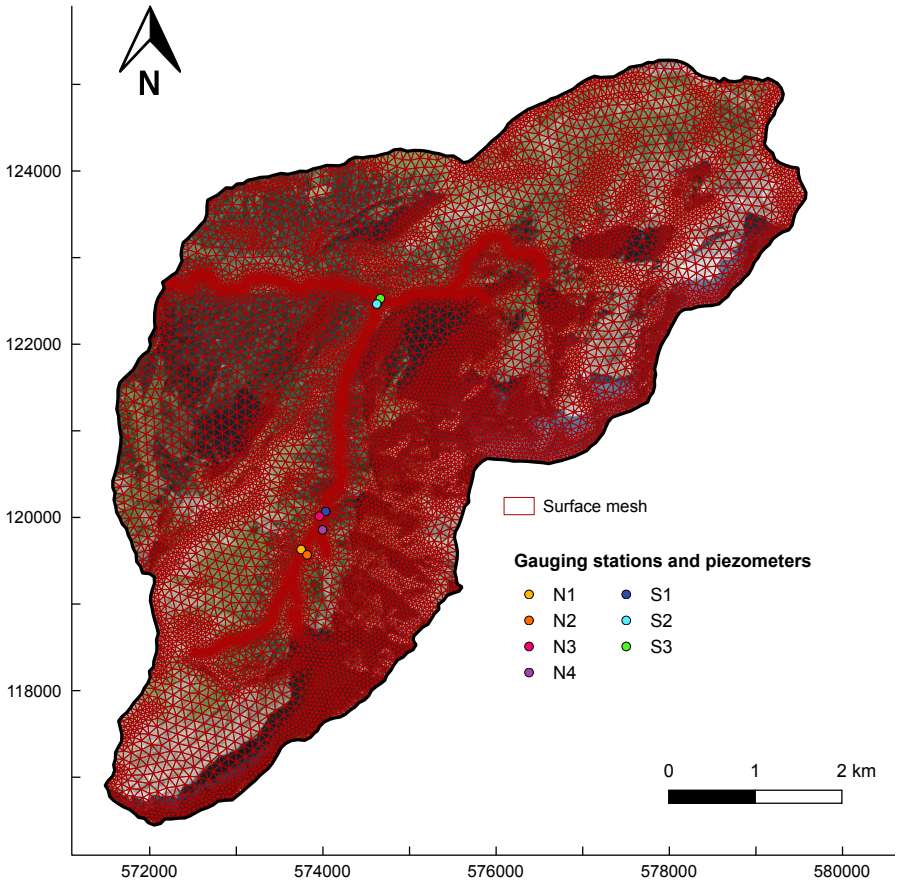

Figure 5.3: The 2D surface triangular mesh, underlain by a high resolution aerial photograph (Source: © swisstopo). Refinement is highest in the riparian zone and in steep areas. Care was also taken to ensure that nodes existed at the precise coordinates of the observation points.

Taking into account the need to extend the domain beyond S2 and S3 (as explained above), the catchment boundary and "usual" stream location polylines were first generated via an analysis of the swissALTI^{3D} Digital Terrain Model (DTM) (horizontal resolution of 2 m; swisstopo); these vector datasets represent the main surface constraints for mesh generation.

Nodes were spaced at approximately 20-25 m intervals along the stream lines, with spacing increasing with distance from the riparian areas. The mesh was also refined in very steep areas, and care was taken to ensure that nodes coincided precisely with the gauging station and piezometer locations. The final surface mesh is shown in Figure 5.3.

It is common practice in integrated modelling to modify the digital terrain data in a pre-processing step such that the nodal elevations decreases monotonically down the stream network (Käser et al., 2014); doing so can improve numerical convergence. However, the topographically closed basins in the limestone landscape of the Vallon de La Vare meant that such an approach was inappropriate here. Node elevations were therefore extracted directly from the swissALTI^{3D} DTM. The final surface mesh is comprised of 11,349 nodes (22,007 triangular elements).

Thereafter, the mesh was extruded vertically in 23 layers, resulting in 3D mesh comprised of 272,376 nodes (507,771 prismic elements) (Figure 5.4). (Note that HGS automatically adds an extra node sheet at the surface to in order to apply the "dual nodes" approach). Vertical resolution was highest near the surface, with sheets created at depths of 0.25, 0.5, 1.0, 2.0, 4.0, and 6.0 m. This scheme ensured that mesh layers were present at the assumed soil thickness depths, and that nodes also existed at approximately the same depths as the pressure transducers in the piezometers. Beneath this, the next three layers were spaced at 5 m intervals, except within the major unconsolidated feature extents considered in Chapter 4; here, the lowermost of these three layers corresponded to the estimated feature bases (i.e. depth to bedrock in all cases except the *Nant* alluvial fan), with the remaining two layers stretched such that three were equally distributed up to the 6.0 m layer. The spacing of the remaining 14 lower sub-parallel layers began with 20 m and increased with depth until the constant specified base elevation of 800 m a.s.l was reached.

Overall, a mesh that satisfactorily represented both steep slopes and incised mountain streams, and had additionally reasonably fine vertical discretisation was generated, thereby overcoming one of the limitations encountered by Smerdon et al. (2009), for instance.

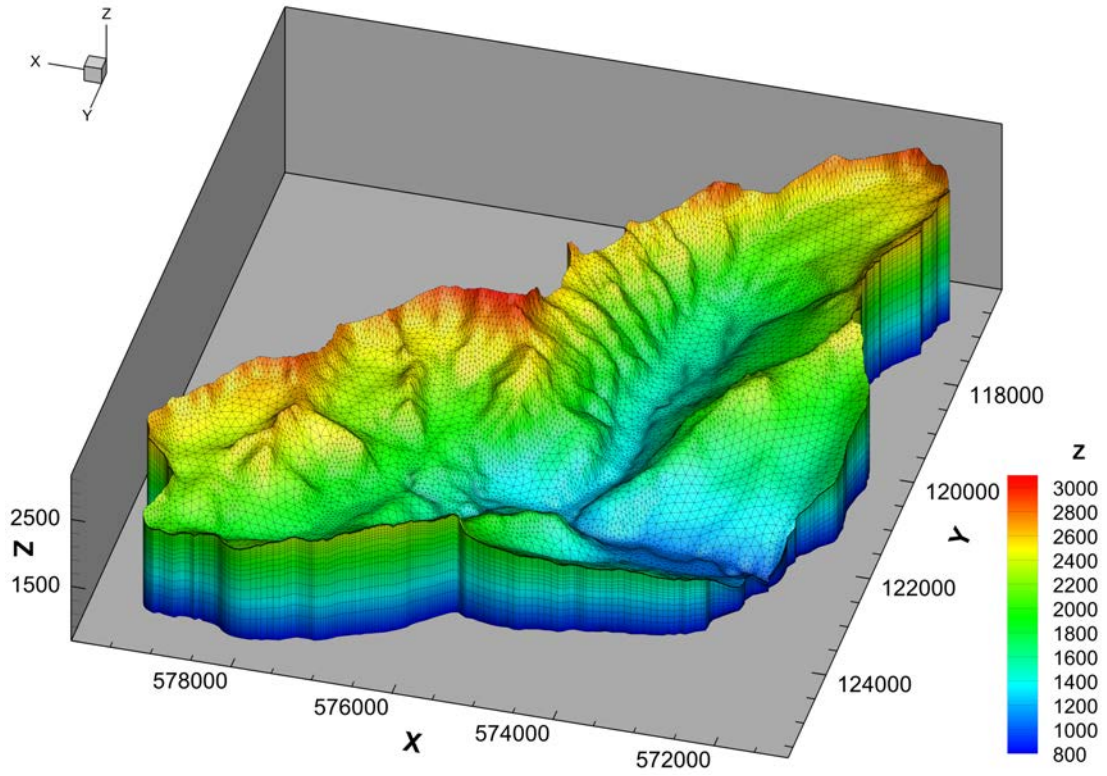

Figure 5.4: The 3D partially-unstructured prismic mesh. Z denotes elevation in metres above sea level (a.s.l.). The surface mesh was refined close to the streams and in very steep areas. Discretisation in the vertical plane was finest near the surface and coarsened with depth.

The rationale for representing such an extensive vertical range and employing a fairly high vertical resolution, in marked contrast to most applications of such models (S. Berg, *personal communication*), is linked to the geology of the area. Essentially, as Chapter 2 described, sequences of hydrologically contrasting formations, including some thin layers, have been folded and faulted into highly complex arrangements. Hence, whilst it is inevitable that some structural information from the spatially continuous 3D geological model will be lost as it is resampled or transferred onto the sub-parallel layers of the numerical grid, using as fine a vertical discretisation as possible minimises this loss. Unlike in crystalline mountainous catchments (Welch and Allen, 2014), where a strong decline in hydraulic conductivity with depth could limit the importance of deep flow pathways and therefore justify the use of only a few and/or shallow subsurface layers, deep flow paths are somewhat expected at the present site. That said, not least because of the extensive vertical range, some trade off between layer thicknesses and the total number of nodes/elements was necessary. Indeed, several different meshes had to be developed and test simulations con-

ducted with each of them before the final one presented here could be settled on as an appropriate compromise between feature representation, numerical performance, and the number of nodes.

5.3.2 Definition of zones

5.3.2.1 Surface

The spatial distribution of zones (i.e. regions to be assigned uniform parameters, in some cases to be estimated via calibration) for the surface and *ET* domains of the integrated model were defined according to a present-day land cover map (see Figure 5.13a), which was developed on the basis of swisstopo data. Since the resolution of this map was higher than that of the mesh, triangular elements were assigned a distinct zone based on the dominant land cover class by area within each. Elements were thus attributed with one of seven primary surface classes.

A present-day permafrost probability map, developed following the methodology of Deluigi et al. (2017) was superimposed upon the land cover map. Since the presence of permafrost in rock walls depends strongly on air temperatures, it can usually be determined fairly confidently. This type of permafrost was therefore represented using a binary map. Predicting the spatial distribution of permafrost occurrence in unconsolidated sediments, however, is considerably more demanding – since it depends on numerous complex and inter-related factors. As such, the distribution of permafrost in unconsolidated sediments was represented probabilistically, with only pixels with values > 0.5 – i.e. estimated more likely than not to be permafrost – being defined as permafrost here. Permafrost presence or absence was treated as a sub-category in the zonation scheme such that categories such as "unconsolidated rock with permafrost" and "unconsolidated rock without permafrost" were permitted.

5.3.2.2 Subsurface

Subsurface zones were defined according to three sources of information. The first is the 3D model of bedrock geology representing 18 distinct formations and their associated features (major faults and secondary folds) developed specifically for this purpose in Chapter 2. The bedrock information was transferred onto the mesh by extracting codes identifying the geological formation present (see Table 2.2) at each mesh element centroid. As with the land cover map, it is inevitable that a certain loss of information from the spatially continuous geological model occurs as a result of this process (which, as discussed already, the comparatively fine vertical mesh resolution sought to minimise).

The estimated volumes of five unconsolidated Quaternary sedimentary features likely to host important aquifers (Chapter 4) constitute the second information source. The formation codes of any elements whose centroids fell within one of the five feature volumes were overwritten with those of the respective Quaternary formation – this reassignment being necessary because all elements were initially assigned a code from the bedrock model (that dataset extends to the surface, and does not represent unconsolidated sediments). Where bedrock did not outcrop at the surface beyond the extents of these major unconsolidated formations, a generic moraine layer with an assumed thickness of 2 m beneath the surface was also included in the model to represent the thin superficial unconsolidated hillslope cover present in these areas.

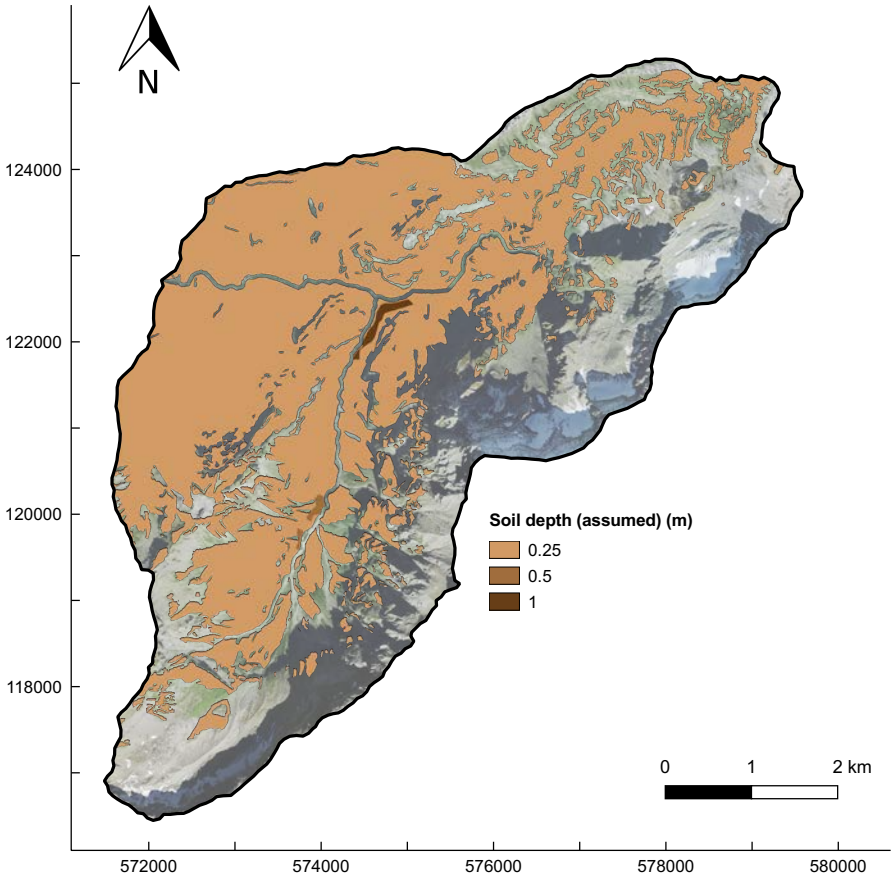

Figure 5.5: The spatial distribution of soil depth that was assumed in the integrated model in the absence of any detailed, high-resolution spatial information on soil depths and properties. Where the underlying aerial imagery is visible, no soil layer is represented.

Finally, in the absence of any more detailed information on the spatial distribution of soil depths and their associated textural or hydraulic properties – the existing "official" spatially distributed

data regarding soils (OFAG, 1980) being dated and of questionable suitability – a very simple soil depth map was generated (Figure 5.5). Soil was treated as a single homogeneous zone in the model, with the same "overwriting" process as previously used assign the appropriate elements. Whilst the volume of the soil zone is very small compared to the unconsolidated and consolidated geological volumes, being located at the land surface and thus having the potential to regulate the partitioning of incident water into runoff and infiltration, soils are likely to exert a disproportionately strong hydrological influence.

Overall, 24 distinct subsurface zones were defined. As a result of this phase, the model's structure was constrained as tightly as possible before the parameter values began to be considered. Some important structural uncertainties did remain, however, notably regarding the unconsolidated aquifer volumes and the soil.

5.3.3 Boundary conditions

To allow water to leave the model domain, a "critical depth" boundary condition was applied to all surface boundary nodes This condition forces the flow depth at these nodes equal to the critical depth, i.e. the depth at which specific energy is minimal for a given discharge (Froude number = 1). The sides and base of the domain were treated as "no flow" boundaries.

The 25 m resolution "all liquid water" (i.e. snowmelt, ice melt, firn melt, and rain) and potential evapotranspiration (ET_p) datasets generated in Chapter 3 – which span the period 1 October 2014 to 30 September 2019 and therefore partially coincide with the *in situ* observations – were prepared for the model at their underlying temporal resolution of one hour. Daily and monthly aggregations were also made, allowing the data to be applied as the "rain" and "potential evapotranspiration" model boundary conditions flexibly across these three different frequencies.

As a reminder, in Chapter 3, an energy balance-based snow modelling approach that also accounted for gravitational redistribution was optimised on the basis of Snow Water Equivalent (SWE) time-series and snow extent maps derived from satellite imagery. ET_p was estimated using the Penman-Monteith method at an identical spatio-temporal resolution. Applying these externally-generated forcing datasets enabled the limitations associated with the simple temperature-index snow model of HGS to be circumvented, and moreover enabled estimation of ET_p using a physically-based approach that was suitable for rugged mountain areas (e.g. with terrain shading effects accounted for).

5.3.4 Preliminary run: impermeable matrix

Using the daily frequency forcing data, a preliminary simulation of the full historical period was undertaken with only the surface domain activated (i.e. with subsurface flow and ET switched off). This was achieved by applying the *"impermeable matrix"* switch in HGS. This initial experiment had several aims; to further confirm that the incoming component of the water balance as determined in Chapter 3 was reasonably well estimated, to verify that the surface mesh was of sufficiently high resolution and quality to enable good model convergence, and to ensure the plausibility of the initial surface domain parameterisation. The convergence criteria for this simulation were set relatively tightly (*Newton absolute* = 1×10^{-3} m, *Newton residual* = 10 m). Figure 5.6 compares the streamflow levels simulated under this assumption with their observed counterparts.

With respect to the numerics, the model ran extremely smoothly and the tight convergence criteria could be satisfied, indicating the soundness of the surface mesh geometry. A good correspondence between the timing of the simulated and observed streamflow peaks is observed, and accordance between the flow magnitudes more generally is good. This confirms that the results of Chapter 3 are reasonable. The temporal pattern in the relative under/overestimation also aligns well with expectations; with infiltration and subsurface storage precluded, the simulated peaks are higher than their observed counterparts, whilst baseflows (which are clearly ordinarily sustained by groundwater discharge) are underestimated. The results at the highest gauging station, S1, are particularly interesting in this regard; they indicate that even without the representation of losses to ET_a, if it was not for the sustaining influence of groundwater discharge, streamflow would frequently become negligible in summers following snow-poor winters (like 2016/2017).

That said, the overall degree of similarly between these simulated streamflows and the observations suggests that the true response of the Vallon de Nant in particular is not greatly dissimilar to the *"impermeable matrix"* case, which is to say that groundwater storage is not extensive. It must also be emphasised that in reality (and also in the fully-integrated version of the model), a certain proportion of incident precipitation will be returned to the atmosphere via ET_a, and hence never become streamflow. One should therefore expect to see a certain degree of overestimation in these simulated streamflows with respect to the observations (some of the difference being ET_a). A small overestimation does indeed appear to to evident at S1 and S2.

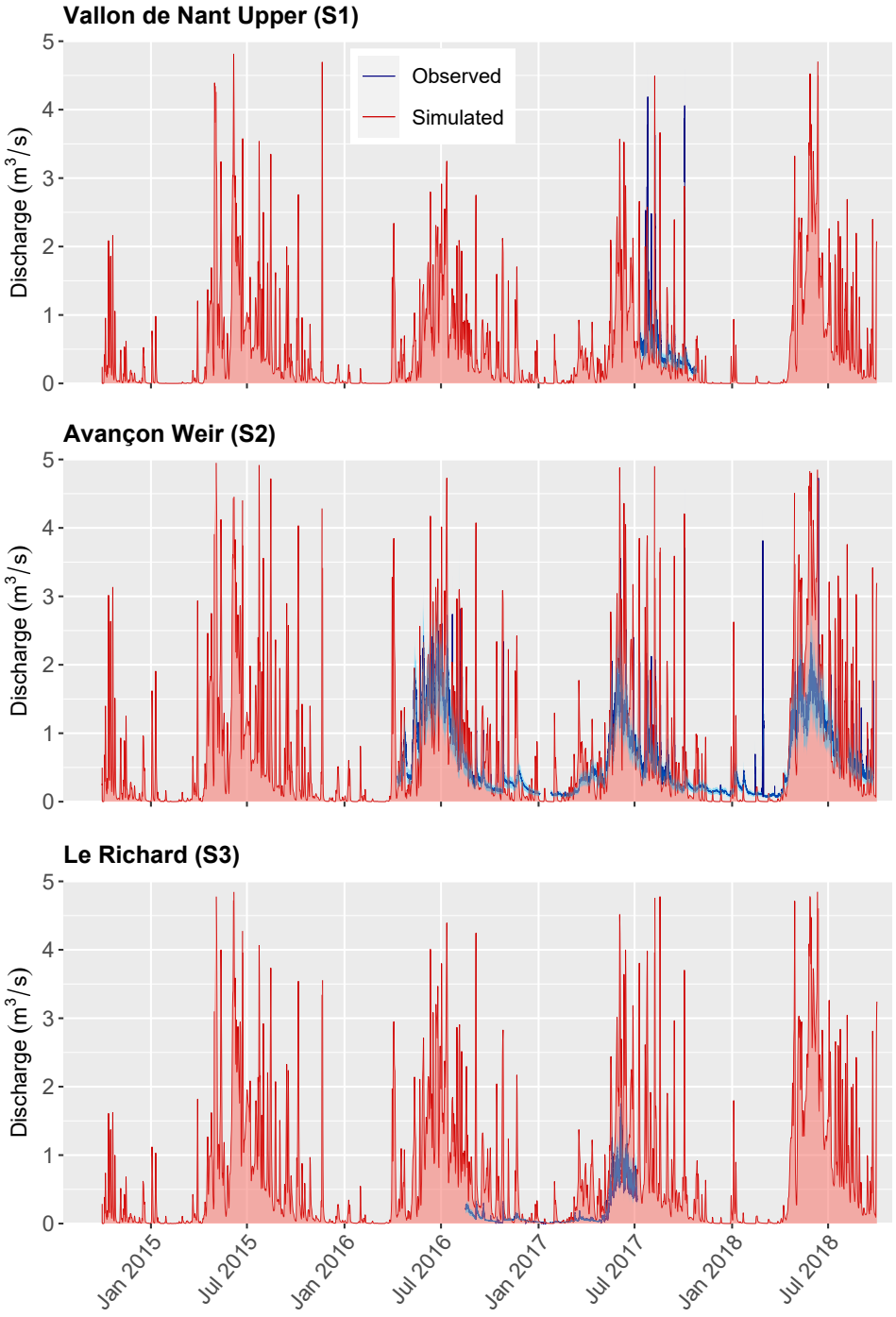

Figure 5.6: Simulated streamflows at each of the three gauging stations over the four year historical period under an *"impermeable matrix"* assumption (i.e. "surface only", with subsurface flow and evapotranspiration (*ET*) deactivated). The forcing data were applied at daily frequency in this case. Estimated uncertainty in the observed streamflow data is represented by a shaded region (light blue) corresponding to $\pm 30\%$.

The simulated streamflows under this *"impermeable matrix"* configuration are overestimated most at S3. This is likely to be related to the bedrock geology in the Vallon de La Vare, which – as explained in Chapter 2 – is expected to be more eminently permeable than that in the bottom of the Vallon de Nant. As such, in reality, subsurface flow pathways in the former valley should be longer and deeper, leading to a greater disparity between these simulations and the observations. Indeed, as was also noted in Chapter 2, Lugeon and Gagnebin (1928) proved a hydrogeological connection between the topographically closed basin of La Varre (which is naturally damned to a height of around 20 m) and La Chambrette – a spring which joins the main channel downstream of S3. Unsurprisingly, inspection of the spatial model output revealed that under this configuration, a unrealistically substantial lake forms in La Varre.

5.3.5 Integrated model initialisation

The initialisation of fully-integrated models can be a time-consuming process (Ajami et al., 2014; Seck et al., 2015). Beginning with a set of prescribed initial conditions, the model in question must be run using either steady or recursive transient forcing data until a state of equilibrium (or "dynamic equilibrium", in transient cases) is attained. Traditional options for the initial conditions are a water table that is coincident with the surface (a so-called "wet start"), a completely dry domain (a "dry start"), or a water table configured to some shallow but arbitrary constant depth beneath the surface (e.g. 1-5 m; Seck et al., 2015). In some codes, including HGS, an initial water table surface can also be generated as a function of elevation, which theoretically enables concepts such as the Topographic Wetness Index (TWI; Beven and Kirkby, 1979) to be used.

However, the annual mean water table distribution in this catchment is expected to take a complex form, being influenced not only by topography but also by geology. For example, unsaturated zones beneath mountain ridge lines may be thick. As such, taking one of the aforementioned approaches to prescribing initial conditions would likely have resulted in very lengthy simulation times being required to approach a state of (dynamic) equilibrium. A "bespoke" approximate initial water table distribution was therefore generated by interpolating the surface coordinates (x,y,z) sampled along normally perennial steams, springs, and wetland locations (i.e. where the water table can be expected to be at or near the surface) in 3D. Using the resultant water table distribution as a starting point, the integrated model was then run by applying the monthly frequency forcing data corresponding to the hydrological year 2014/15 recursively. The initial (or prior) parameter estimates were applied in this stage (see the next subsection). This process was considered complete when the simulated surface water hydrographs and groundwa-

ter levels at the various observation points ceased to demonstrate marked inter-annual trends.

5.3.6 Automated calibration strategy

The hydraulic properties of the subsurface formations and surface zones are essentially unknown, at least at model-effective scales (if not more fundamentally). Some form of calibration is therefore required. Whilst this is still frequently attempted manually on a trial-and-error basis, the relatively large number of parameters involved here would have confounded such a strategy. An automated approach was therefore implemented. Based on a combination of lithological descriptions (in the case of the bedrock formation), values presented in relevant previous studies, and informed judgement, an initial parameterisation scheme was devised. A subset of the models parameters, 46 in total, were identified as calibration targets. Tables 5.1 to 5.3 present the parameterisation scheme by model "domain".

To facilitate calibration, the model was linked with PEST_HP (v17) (Doherty, 2020) – a code-independent, gradient-based parameter estimation tool which uses the Levenberg-Marquardt algorithm to minimise an objective function in a least-squares sense. Since the outputs of models like that under consideration here are typically highly non-linear with respect to varied parameter values, calibration is an iterative process.

All available hourly (mean) streamflow measurements and half-hourly (instantaneous) groundwater level measurements between 9 April 2016 (i.e. from the commencement of measurements at S2) and 31 October 2017 contributed to the definition of the objective function. It must be emphasised, however, that data coverage is far from continuous throughout this period; S1 and S3 were not permanently gauged, the groundwater pressure transducers were only installed in June 2017, and the groundwater records contain gaps during periods in which the level fell below the base of the shallow wells.

The observed streamflow data have already been presented, whilst the observed groundwater levels are plotted in Figure 5.8 alongside their (post-calibration) simulated counterparts. For every new set of parameter values proposed by PEST, an initial "re-initialisation" period beginning on 1 October 2015, approximately six months before the first observations are available, was first simulated. The intention here was to enable the internal system state, whose initial condition was identical for each run, to become better equilibrated with the corresponding parameter values. Following a split-sample strategy, the remaining observations (i.e. those spanning the period from November 2017 to September 2018 inclusive) were used for independent evaluation.

Zone/Domain	Evapotranspiration												
	d_e (m)	d_r (m)	LAI range (seasonal) (m)	C1 (-)	C2 (-)	C3 (-)	H_{wp} (m)	H_{fc} (m)	H_{ol} (m)	H_{al} (m)	H_{et1} (m)	H_{et2} (m)	c_{int} (m)
Grass	0.2	0.2	2.0 to 4.0	0.30	0.05	1.00	-150	-5	0	0	-5	-0.2	5.00×10^{-4}, (1.60×10^{-4} to 1.50×10^{-3}), **4.93×10^{-4}**
Bedrock	-	-	-	-	-	-	-	-	-	-	-	-	-
Glaciers	-	-	-	-	-	-	-	-	-	-	-	-	-
Unconsolidated rock	-	-	-	-	-	-	-	-	-	-	-	-	-
Bushes	0.5	2.0	2.5 to 4.5	0.30	0.05	1.00	-150	-5	0	0	-5	-0.2	6.50×10^{-4}
Forest	0.5	3.5	1.5 to 9.5	0.30	0.05	1.00	-150	-5	0	0	-5	-0.2	7.50×10^{-4}, (2.50×10^{-4} to 2.25×10^{-3}), **8.25×10^{-4}**
Streambed	-	-	-	-	-	-	-	-	-	-	-	-	-

Table 5.1: Evapotranspiration parameter values in the integrated model, rounded to two significant figures. d_e is evaporation depth, d_r root depth, LIA range gives the annual minimum and maximum Leaf Area Index (with monthly variability between these values), C1, C2, and C3 are transpiration fitting parameters, and H_{wp}, H_{fc}, H_{ol}, and H_{al} are the pressure heads at the wilting point, field capacity, oxic limit, and anoxic limits, respectively. c_{int} is the canopy storage parameter. For parameters that were subjected to calibration, the upper and lower permitted bounds are specified (in parentheses), as is the "final" value obtained after two calibration iterations (in bold). Free parameters in all "domains" were log-transformed to improve the numerical robustness of the process. Evaporation from the bedrock, glaciers, unconsolidated rock, and streambed zones was deactivated in the model.

Zone/Domain	**Surface**			
	n_{xy} ($m^{-1/3} \cdot d^{-1}$)	h_{ds} (m)	h_o (m)	l_{exch} (m)
Grass	4.05×10^{-7}, (1.35×10^{-7} to 1.22×10^{-6}), **4.24×10^{-7}**	0.010	0.015	0.2*
Bedrock	4.63×10^{-7}	0.020	0.010	0.2*
Glaciers	2.55×10^{-7}	0.005	0.005	0.2*
Unconsolidated rock	4.63×10^{-7}, (1.54×10^{-7} to 1.85×10^{-6}), **5.63×10^{-7}**	0.050	0.030	0.2*
Bushes	8.10×10^{-7}	0.010	0.020	0.2
Forest	1.74×10^{-6}	0.010	0.030	0.2
Streambed	3.47×10^{-7}, (1.16×10^{-7} to 8.10×10^{-7}), **4.07×10^{-7}**	0.010	0.030	1.0

Table 5.2: Surface parameter values in the integrated model, rounded to two significant figures. n_{xy} is the Manning's roughness coefficient, h_{ds} is the depression (or rill) storage height, h_o is the obstruction storage height, l_{exch} is the surface-subsurface coupling length. For parameters that were subjected to calibration, the upper and lower permitted bounds are are specified (in parentheses), as is the "final" value obtained after two calibration iterations (in bold). *Except where permafrost, in which case l_{exch} was given a value of 50 m.

Zone/Domain	**Subsurface**					
	k_{xy} ($m \cdot d^{-1}$)	k_z ($m \cdot d^{-1}$)	θ (-)	S_s (m^{-1})	α (m^{-1})	β (-)
a	2.73×10^{-4}	2.73×10^{-4}	1.00×10^{-3}	1.60×10^{-4}	-	-
i1i	8.64×10^{-4}	8.64×10^{-4}	1.50×10^{-3}	1.60×10^{-4}	-	-
i1s	8.64×10^{-3}	8.64×10^{-3}	2.00×10^{-3}	1.60×10^{-4}	-	-
i2	2.73×10^{-2}	2.73×10^{-2}	1.50×10^{-3}	1.60×10^{-4}	-	-
i3_4	8.64×10^{-4}	8.64×10^{-4}	1.50×10^{-3}	1.60×10^{-4}	-	-
i5	**7.08×10^{-2}**	**7.08×10^{-2}**	**3.44×10^{-3}**	1.60×10^{-4}	-	-
i6_8	**3.03**	**3.03**	**9.59×10^{-3}**	1.60×10^{-4}	-	-
i8c2	**1.17×10^{-2}**	**1.17×10^{-2}**	**1.02×10^{-3}**	1.60×10^{-4}	-	-
c2k	**2.96**	**2.96**	**6.46×10^{-3}**	1.60×10^{-4}	-	-
c3	**0.36**	**0.36**	**8.94×10^{-3}**	1.60×10^{-4}	-	-
c4	**1.15×10^{-2}**	**1.15×10^{-2}**	**1.89×10^{-3}**	1.60×10^{-4}	-	-
c4_5	**3.71**	**3.71**	**1.16×10^{-2}**	1.60×10^{-4}	-	-
c6_8	**5.91×10^{-2}**	**5.91×10^{-2}**	**3.49×10^{-3}**	1.60×10^{-4}	-	-
e5	**4.09×10^{-2}**	**4.09×10^{-2}**	**1.47E-03**	1.60×10^{-4}	-	-
e6c	**3.12×10^{-2}**	**3.12×10^{-2}**	**3.43×10^{-3}**	1.60×10^{-4}	-	-
e6k	**7.25×10^{-3}**	**7.25×10^{-3}**	**1.69×10^{-3}**	1.60×10^{-4}	-	-
e6o1	**2.19×10^{-3}**	**2.19×10^{-3}**	**9.50×10^{-4}**	1.60×10^{-4}	-	-
Basement	2.73×10^{-4}	2.73×10^{-4}	**1.49×10^{-3}**	1.60×10^{-4}	-	-
Moraine	**0.14**	**0.14**	**0.10**	1.10×10^{-5}	-	-
Nant	**103.27**	**16.64**	**0.14**	1.10×10^{-5}	-	-
La Chaux	**21.75**	**21.75**	**0.10**	1.10×10^{-5}	-	-
Martinets	**864.0**	**864.0**	**0.16**	1.10×10^{-5}	-	-
Vare Lower	4.79	4.79	**0.30**	1.10×10^{-5}	-	-
Vare Upper	23.17	108.35	**0.35**	1.10×10^{-5}	-	-
Soil	**0.13**	**0.13**	**0.38**	1.10×10^{-5}	2.00	1.41

Table 5.3: Subsurface parameter values in the hydrological model, rounded to an appropriate degree of precision. k_{xy} is horizontal saturated hydraulic conductivity, k_z is vertical saturated hydraulic conductivity, θ is effective porosity, S_s is specific storage, and α and β are parameters of the Van Genuchten unsaturated retention functions. These functions were simplified for all subsurface formations except soils. In the interests of space, only the initial values (for non-calibrated parameters, plain text), or the "final" values obtained after two calibration iterations (bold) are presented here. For the initial values and ranges prescribed, the PEST control file (*"pest_control_v5.pst"*) which is provided in the Supplementary Material in Appendix A should be consulted. Likewise, the *"subsurface.mrops"* file in the same location details the simplified unsaturated parameterisation applied in non-soil zones.

The objective function (OF) can be expressed as:

$$OF = \sum_{i=1}^{20409} [wGWL(GWL_{sim} - GWL_{obs})^2] + \sum_{i=1}^{13184} [wQS_2(QS_{2sim} - QS_{2obs})^2] + \sum_{i=1}^{60533} [wQS_{1,3}(QS_{1,3sim} - QS_{1,3obs})^2] \quad (5.1)$$

where $wGWL$, wQ_{S2}, and $wQ_{S1,3}$ are the relative weights that were assigned to each observation group, i.e. the groundwater levels, the streamflows at S2, and the streamflows at S1 and S3, respectively. Here, $wGWL$ = 0.38, wQ_{S2} = 5.50×10^{-5}, and $wQ_{S1,3}$ = 9.00×10^{-5}. GWL_{sim} and GWL_{obs}, QS_{2sim} and QS_{2obs}, and $QS_{1,3sim}$ and $QS_{1,3obs}$ are the simulated and observed values at the N1-4, S2, and S1 and S3, respectively.

Given the contrasting number and magnitudes of observations within the different groups, and the unknown degree of initial mismatch, it was only possible to establish the final weights in Equation 5.1 after the model had been run once with the initial parameters; the PEST utility PWTADJ1 was used to adjust the weights such that each observation group remained "visible" to the calibration process, but with a greater emphasis placed on streamflow (for the reasons explained immediately below).

Streamflow measurements represent an integrated response, whilst distributed groundwater level observations provide more spatially explicit information, i.e. have a reduced spatial support. As such, these two data types can be considered complementary (Paniconi and Putti, 2015). That said, the latter can be heavily influenced by very local phenomena, and this was indeed the case here, as evidenced by the somewhat contrasting patterns at the different piezometers. It was realised that without introducing sub-zone heterogeneity in material properties, which lay out of scope, it would essentially be impossible to reproduce these distinct responses. To try and prevent the calibration process from magnifying this particular model deficiency, modest weights were assigned to the groundwater level observations, such that their contribution to the initial objective function was only around 11%.

After having gathered the necessary data, developed all the other model components, settled on an appropriate mesh resolution, established an initial parameterisation scheme, and initialised the model, limited time remained for the calibration phase. In an attempt to nevertheless realise automated calibration, similarly to Ala-aho et al. (2017), various simplifications were made.

Firstly, the re-initialisation and calibration periods described above were fairly short. Although this was partly dictated by the availability of the observed data and a desire to maintain an independent evaluation period, a shorter simulation period obviously reduces overall computation times. Given the pronounced seasonality of the catchments' hydrological regimes, it was considered important that the calibration period was not less than one year, however.

Model execution times were found to increase substantially with the temporal frequency at which the forcing data were applied. In relation to this, in another major simplification, the calibration runs were undertaken using the monthly frequency forcing data. Slightly surprisingly, however, the simulated seasonal dynamics do not vary drastically depending on whether monthly or daily frequency data are prescribed (see Supplementary Figure D.2), providing some justification for this approach.

Additionally, the unsaturated zone (pressure head–saturation, and pressure head–relative hydraulic conductivity) relationships for all subsurface zones except the soil were represented using a small number of data points and somewhat linearised. This is defensible because the nature of these relationships in consolidated, potentially fractured, and/or karstified bedrock are poorly understood. In the case of soils, the van Genuchten parameters listed in Table 5.3 were used; van Genuchten, 1980). Similarly, the slope term in the surface water flow equations was assumed equal to the topographic slope, and thereby also linearised.

The model's convergence criteria were relaxed greatly for calibration (*Newton absolute* = 1×10^{-3} m, *Newton residual* = 750 m) before being re-tightened for subsequent runs with optimised parameters (*Newton absolute* = 1×10^{-3} m, *Newton residual* = 150 m). The latter settings led to a mean mass balance error, expressed as a percentage of liquid water input, of $\lesssim 5\%$.

As a final simplification, the coupling length parameter for all surface zones except the streambed was set to a somewhat higher (and fixed) value (0.2 m) than it might ordinarily be; values closer to zero is generally recommended to approximate the Continuity of Pressure (COP) approach, but are typically associated with longer execution times (Liggett et al., 2012). Simple sensitivity tests were undertaken to ensure that model outputs of interest were not substantially affected. In the field, a fine layer of silty sediments was observed in the streambed. To mimic the greater surface-subsurface disconnection that such an layer could induce, the coupling length for the streambed zone was fixed to the higher value of 1.0 m.

After some experimentation on a High Performance Computing (HPC) cluster, the calibration runs were eventually carried out Windows machine (Intel(R) Xeon(R) CPU E-2699 v4 @ 2.20 GHz, 64.0 GB RAM, 44 cores), with 12 agents running in parallel (i.e. using only part of the

entire resource). Each instance of HGS was also distributed across 2 cores. Two iterations of the calibration process (133 model calls in total; simulation time approximately 2 weeks) was the most that could be completed in the time available. After these two iterations, the *OF* was reduced to 0.73 of its original value. This calibration process remains ongoing, and it is possible that the *OF* can eventually be reduced further; the results presented here were generated with the parameter values obtained after two iterations, however.

5.4 Model applications, results, and discussion

5.4.1 Present-day conditions

With the partially optimised parameters, the integrated model was applied over the extended period (i.e. including the evaluation period) using the daily gridded forcing data. Distributed over two cores again, thus simulation took approximately five days to complete. The outputs enabled an initial assessment of the model's performance under historical conditions to be made. This simulation also served as a baseline for the subsequent future scenario runs.

5.4.1.1 Streamflows and groundwater levels at the observation points

In Figures 5.7 and 5.8, the streamflows and groundwater levels simulated under the configuration described above are plotted against their corresponding observations. It should be noted that the observed data remain at their original temporal resolution (i.e. hourly or higher frequency) in these figures. In considering these results, it may firstly be remarked that fit levels attainable with such complex, physically-based models are generally lower than can be produced with simpler, more data-driven alternatives (Mendoza et al., 2015).

Figure 5.7 reveals that the general seasonality of observed streamflow is reproduced reasonably well at S1 and S2. In using daily frequency forcing, one would not necessarily expect to reproduce the sharp, singular peaks that are present in the observations – these having been plotted at their underlying frequency, as already stated. Considering S2 specifically, which has the most extensive observed record, whilst the simulated annual water balance looks reasonable, the onset of high spring flows is delayed in the model with respect to observations, and the peak levels attained are slightly too low. In both regards, this situation is more pronounced in spring 2016 than spring 2017, suggesting that, if the forcing data are indeed reasonable, imperfect initial conditions may be at least partly responsible – a subject that shall be returned to shortly.

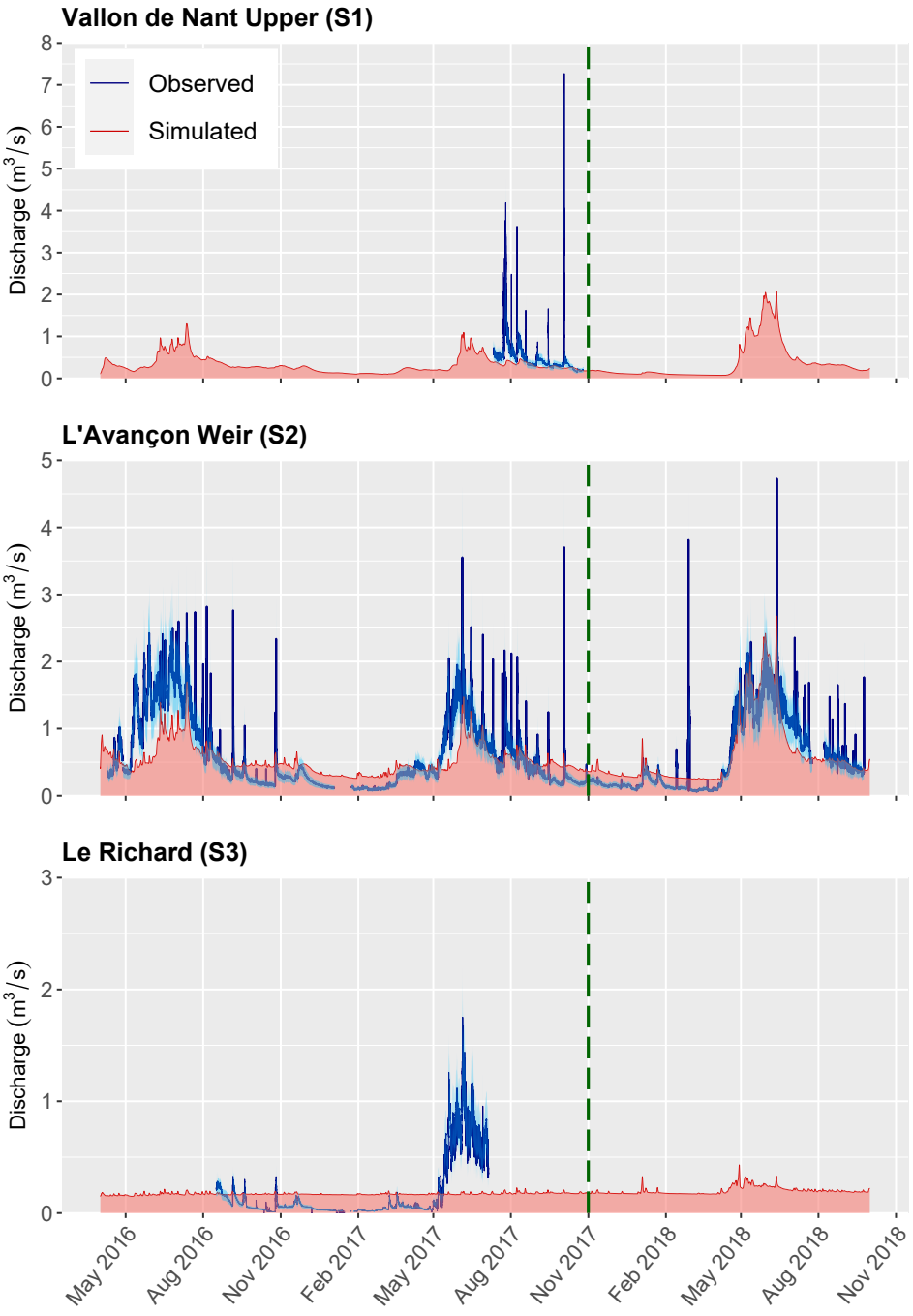

Figure 5.7: Simulated streamflows at the three gauging stations over the calibration and evaluation periods (left and right of the green dashed line, respectively) using the partially calibrated model with daily frequency forcing vs. observations. Estimated uncertainty in the observed streamflow data is represented by the shaded light blue region, which corresponds to $\pm 30\%$.

Another feature of the comparison at S2 is that the baseflow level is consistently overestimated by a factor of approximately two. This mismatch could suggest that too much infiltration and recharge is permitted in the model, and/or that the seasonal recharge is not able to drain rapidly enough, and/or that not enough overland flow (via either the Horton or Dunne mechanisms) occurs. At the higher station in the Vallon de Nant, S1, based on the reduced record available, any baseflow overestimation appears less evident if present at all. In light of this, the issue with overestimated baseflow at S2 can be tentatively attributed in spatial terms to only those surface and subsurface zones which influence flow downstream of S1.

In terms of the main spring snowmelt-driven peak, the fit achieved is much better at S2 over the independent evaluation period (i.e. November 2017 – September 2018 inclusive; to the right of the green dashed line), even if the preceding baseflows remain overestimated. The simulated discharge also declines too rapidly with respect to the observations in mid-summer, which could be indicative of a possible overestimation of evaporative losses. Incidentally, the substantial observed peak shown in mid-winter 2018 has now been identified as spurious data associated with channel freezing.

Similarly, a large boulder became lodged beneath the water level sensor around the start of August 2018 compromised the temporal consistency of the record, explaining the gap during this period (A. Michelon, *pers. comm.*). Such examples highlight the challenges associated with making even fundamental hydrological measurements continuously and consistently in such terrain. Regarding the potential issue of flow beneath the gauge, an assessment of the simulated subsurface to surface flow ratio through time found it to be extremely small at this site. In this sense, the model apparently confirms that the station is appropriately sited.

The level of fit obtained at S3 is extremely poor, with the simulations bearing little resemblance to the observations. More specifically, the simulated series is extremely constant, whereas the (short) observational record is much more dynamic. Interestingly, this seemingly rapid observed response occurs despite the bedrock formations in Vallon de La Vare, the catchment which contributes to streamflow at S3, being known to be relatively permeable. It may be that the initial parameterisation scheme resulted in an unduly low initial water table configuration, which in turn enabled too much infiltration and recharge (ultimately producing a steady discharge) at the expensive of rapid surface runoff.

That said, in reality, the high, topographically closed basin of La Varre clearly does drain somehow, possibly via a discrete fracture, as discussed by Lugeon and Gagnebin (1928). A strong "duality" in this part of this hydrological system is therefore possible, whereby snowmelt and

rainfall waters in the upper part of the catchment either drain directly into the subsurface or else arrive at La Varre via surface torrents, whence they disappear into the subsurface. Some of this water may ultimately arrive in Le Richard (S3) via slow pathways, but it is not known what this proportion could be. In contrast, a hydrogeological connection from La Varre that bypasses S3 entirely has been definitively proven (Lugeon and Gagnebin, 1928). Snowmelt and rainfall in the remaining, lower part of the catchment, meanwhile, would seem to flow more rapidly in surface torrents, producing the relatively flashy observed response at S3. In its present configuration, the model is essentially unable to replicate such complexity.

During initial parameterisation and early qualitative tests, maybe undue emphasis was placed on ensuring that an artificial lake did not develop in La Varre (by approximating the effect of the possible fracture through effective parameter values), thus inducing a water table that was unduly low throughout the catchment more broadly. It is furthermore conceivable that even if PEST then proposed more appropriate parameter values (i.e. parameters which would ordinarily lead to a more direct streamflow response and hence a better match at S3), given the response times of the internal storages, the six-month re-initialisation period that was simulated prior to each calibration run may have been insufficient for "enough" re-initialisation to occur. In fact, because the re-initialisation period corresponded predominantly to a period of recession, this possibility actually seems fairly likely.

In future work, ensuring that any re-initialisation period used in automated calibration attempts includes at least one full annual cycle, and ideally runs – iteratively if necessary – for as long as the system in question requires to equilibrate fully with each set of parameters. The length of this period would thus be variable for each model run. Models or model zones with relatively low permeability parameter values could be most problematic in this regard, since the storages in higher permeability formations should respond more rapidly. Interestingly, this interplay between initial conditions, parameter values proposed by automated calibration tools, and the length of any re-initialisation period required has received very little attention to date in the groundwater modelling literature, never mind that concerning fully-integrated modelling.

In future, should simulating an indeterminate re-initialisation period until trends in storages or predictions at observation points become minimal be impossible due to constraints related to execution times, as was the case here, the "observation re-referencing" capabilities of PEST could be implemented to at least ensure that the initial conditions at the start of each iteration correspond to the final conditions generated with the best parameter set from the prior one. As it was, in this study, the same set of initial conditions were returned to for each and every model run.

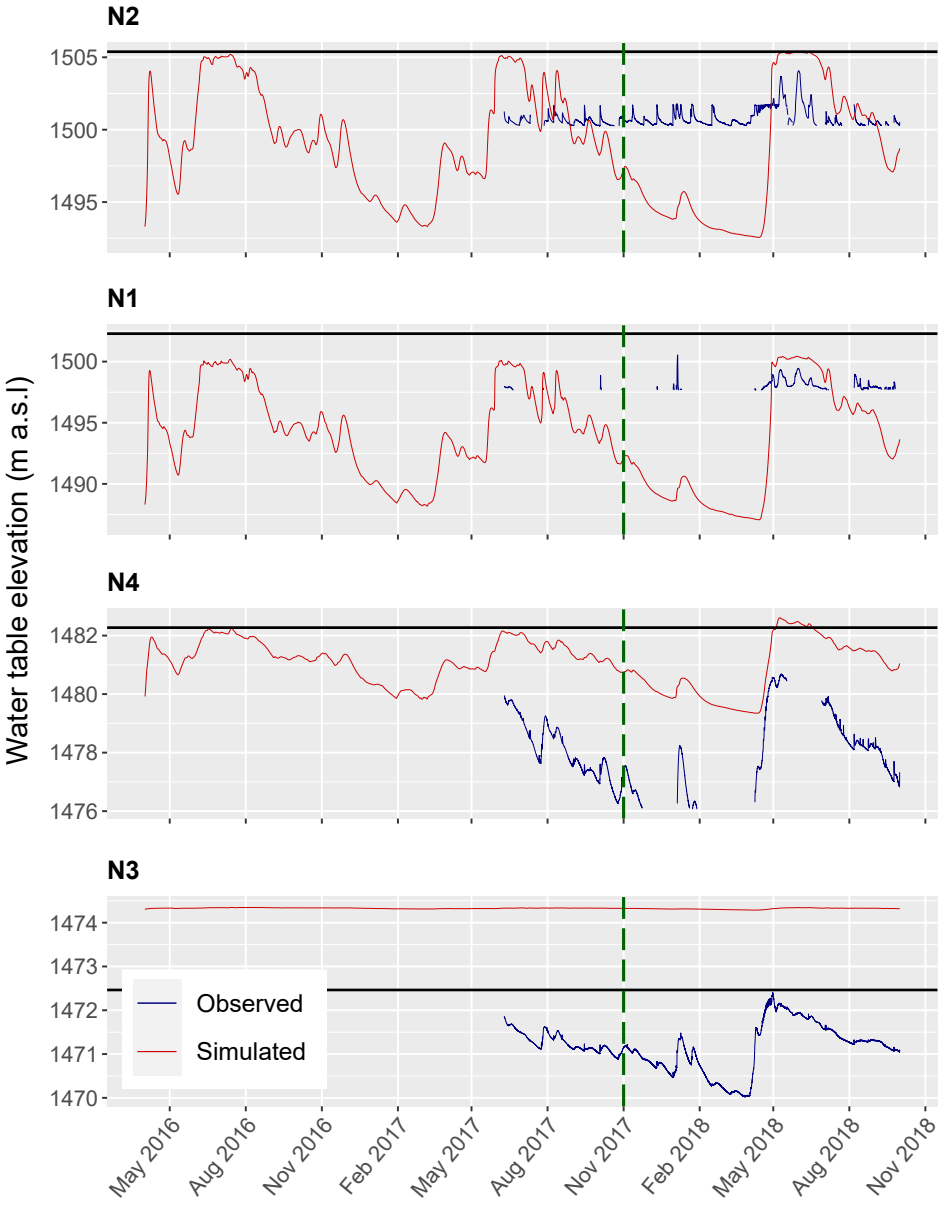

Figure 5.8: Simulated groundwater levels at the four piezometers over the calibration and evaluation periods (left and right of the green dashed line, respectively) using the partially calibrated model with daily frequency forcing vs. observations. The black horizontal lines indicate the surface elevations at each piezometer.

In the groundwater level comparisons presented in Figure 5.8, the simulation show a strong seasonal signal comprised of a peak associated with the snowmelt followed by a more gradual decline. In this sense, the observed trends at N3 and N4 – if not the precise levels themselves – are well captured. Again, whilst rainfall-related peaks are superimposed upon the recession in the observations at N4 in particular, one cannot necessarily expect these features to be reproduced using the daily forcing frequency of the simulation. As discussed previously, the groundwater level observation at these different sites demonstrate contrasting signals, whereas the simulated trends are fairly similar (although the higher elevation sites, N1 and N2, demonstrate greater variability). Consequently, the distinctive signals at N2, and to a lesser extent, N1, could not be reproduced.

It should firstly be highlighted that there are few observations within the calibration period at these sites. In addition, N2 is thought to be situated within a former stream channel, which would explain its flashy response. The lower groundwater level here is also remarkably constant, which a shallow, clay-rich layer of the sort discussed in Chapter 4 may be responsible for maintaining. Of course, since the model does not represent variability in hydraulic properties on such local scales, it could hardly even have been hoped to reproduce these contrasting responses. With this in mind, simulations using an Iterative Ensemble Smoother (IES; White, 2018), which can enable the estimation of very large number of parameters (e.g. k per-element) with a greatly reduced number of runs than the standard PEST procedure would require, are ongoing. Reassuringly, however, the dynamics at N4, which being nearest to the main gravelly part of the alluvial fan can be considered the most spatially representative of the four sites, generally match well, albeit with too high a level in the simulations. It is not particularly alarming that groundwater levels were overestimated at N3 since this location is less than 10 m from a small stream where groundwater persistently upwells (see Figure 5.10).

Next, to further investigate the impact of forcing frequency on the simulated hydrological responses, the most recent hydrological year (i.e. 2017/2018) was simulated using the hourly datasets. Figure 5.9 presents streamflow and groundwater level results at S2 and N4, respectively. The generally good streamflow match obtained with the daily forcing data was maintained. Indeed, a Nash-Sutcliffe Efficiency (NSE) coefficient of 0.75 over the independent evaluation period denotes a good performance. The improved match over this independent period compared to the two preceding years, which formed part of the calibration period, could simply be attributable to the forcings having been better estimated over this period in Chapter 3 – e.g. due to increased meteorological data availability (see Figure 3.6). The underestimation of streamflow during the latter half of June that was also highlighted in the simulation with daily

forcing, meanwhile, could indicate an overestimation of evaporative losses during this warm period, perhaps due to some lack of temporal transferability of parameters identified over the somewhat different conditions of the calibration period.

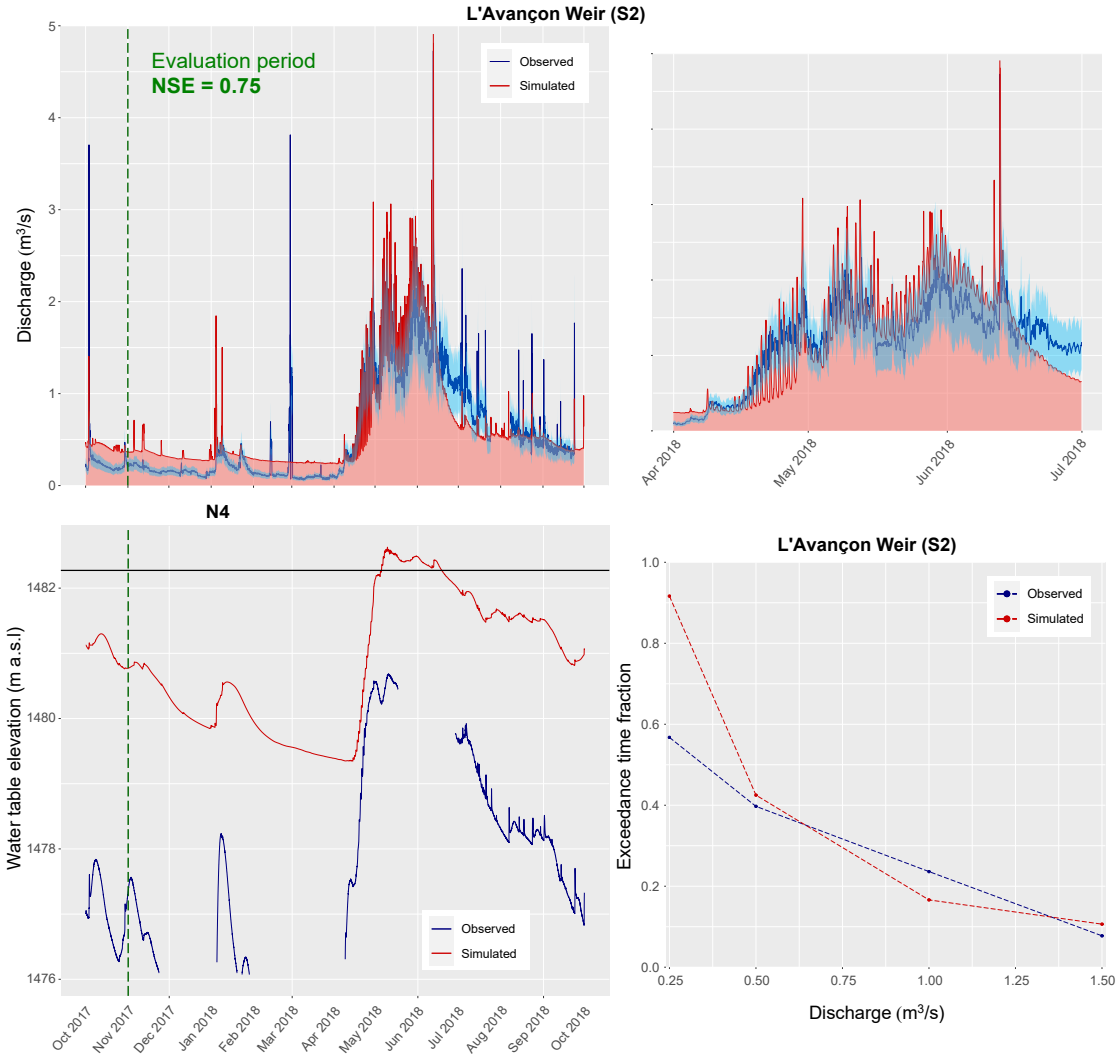

Figure 5.9: Simulated streamfow and groundwater levels simulated at S2 and N4, respectively, using the partially calibrated model with hourly frequency forcing vs. observations. The upper-right pane shows an enlarged version of the streamflow comparison during the spring and early summer, whilst the lower-right pane shows a comparison between the simulated and observed proportions of the total evaluation period that certain flow rate thresholds were exceeded at S2. As noted previously, despite the concrete weir at this location, the observed streamflow measurements are themselves subject to uncertainty, especially at flow extremes. Once again, this estimated uncertainty is represented by the shaded light blue region, which corresponds to $\pm 30\%$.

During the first part of the simulated period, due to the water table being overestimated, the small rainfall events lead to flow peaks that are accentuated with respect to the observations. For the remaining period, however, applying hourly forcing data clear provides a better representation of the singular observed peaks. In the upper right-hand pane of Figure 5.9, which shows a subset of the evaluation period, strong simulated diurnal snowmelt-driven cycles are also evident, as in the observed series.

The lower right-hand pane shows a comparison of derived streamflow data; namely the proportion of the evaluation period during which simulated and observed flow levels exceeded certain pre-defined thresholds. This is mainly to point out that such derived metrics could have been included, or even used in place of the raw data, in defining the OF.

In terms of the N4 groundwater levels simulated with hourly forcing (lower-left pane), the structure simulated with the daily forcing is again maintained, but small rainfall-related peaks are now visible. These peaks are not as pronounced as those in the observations, however. The depressed variability and slight lag in the simulated versus observed groundwater levels could be related to the simplified unsaturated zone functions that were applied.

5.4.1.2 Spatially distributed outputs

One of the key benefits of such integrated models is that diagnostics are not merely limited to time-series comparisons at observation points. On the contrary, the boundary conditions applied and resultant simulated responses of several model state variables can be visualised and/or extracted at any spatio-temporal location within the model domain. This provides ample opportunities for the coherency of the system's simulated hydrological behaviour to be assessed in more holistically. More qualitative (or "soft") evaluations can also be made. Exploring model outputs in this fashion can prove invaluable for better understanding complex hydrological systems, and can also lead to a fuller appreciation for the regards in which a given numerical representation might remain imperfect. To illustrate this, several examples are taken from the partially-calibrated model run with daily forcing data.

Firstly, reference is made to a thermal drone image that was captured in the central part of the Vallon de Nant early on 7 December 2016. No precipitation had fallen in the preceding 10 days, and – unusually for the time of year – due to the late onset of snowfall, the ground remained clear. As such, any water present in the channel could be confidently and exclusively identified as groundwater. Under these conditions (i.e. in winter), appearing being several degrees warmer than the surrounding dry land surface in the image, the region where groundwater exfiltrates

from the dry stream bed can be clearly identified (Figure 5.10a). A direct comparison can be made with the exchange flux simulated by the model in the same area on the same date (Figure 5.10b). (Note: positive values here indicate a simulated flux of groundwater to surface water). This comparison demonstrates that groundwater emerges into the channel in the simulation at approximately the same location in reality. Moreover, water is present in the stream from this point forth in the simulation (Figure 5.10c), which is also consistent with the observation (since the discrete "warm" region continues downstream in the thermal image).

Animation D.1 (Appendix D), meanwhile, shows the spatio-temporal variability of the two meteorological boundary conditions (i.e. "all liquid water", which was treated as "rain" in HGS, and potential evapotranspiration) alongside the simulated response of two key variables – surface water depth and ET_a, over the hydrological year 2017/2018. Note that the scales applied to the ET_p and ET_a data are identical but inverted since HGS writes out the latter as a negative flux by default. During the first part of the hydrological year, dynamics are subdued as the catchment gradually drains. With the onset of the snowmelt, which naturally begins at lower elevations, the surface water network begins to expand. However, these spatial outputs suggest that the multiple small, steep torrents which transmit snowmelt (and indeed rainfall) extremely efficiently to larger channels may not form extensively enough in the model as compared to reality, at least not with the daily frequency forcing. It may be that for this to have occurred, these discrete features would have had to have been "picked out" more explicitly in the surface mesh, although (under the established meshing approach used) this would have resulted in a larger mesh and even longer execution times. Surface water bodies up to a few metres deep can also still be seen to form in the topographic depressions of the Vallon de La Vare. A strong effect of elevation, and hence temperature, is apparent in both the ET_p and ET_a outputs.

Finally, Animation D.2 shows the interplay between simulated saturation, both at the surface and – using slices – at depth. The simulated streamflow response at S2 is also shown. In this animation (upper-right), the generally lower water table in the Vallon de La Vare that was discussed earlier is clearly visible. The near-surface saturation increases across the catchment through the snowmelt period, followed by the arrival of spring flow peak. Lastly, the shallow simulated (and indeed observed) surface flow depths at S2 highlight the extent to which this system, presumably like many other small Alpine headwaters, lie fairly close to the "wet-dry limit" even under the present climate. As such, and in light of the non-linear processes involved, it could be purported that reproducing such a system using such an approach as taken here is more challenging than reproducing more voluminous flows along larger rivers, for instance.

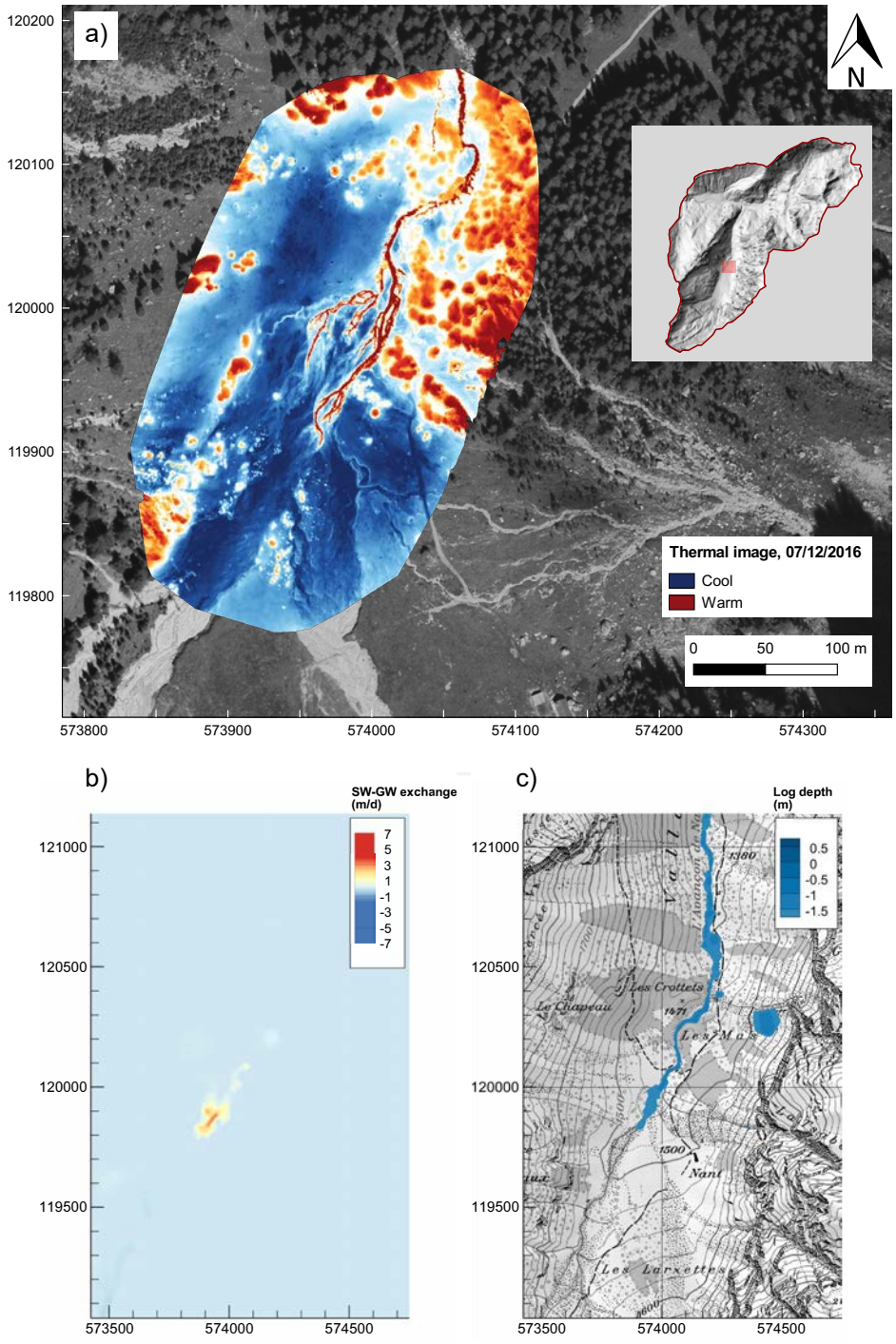

Figure 5.10: Spatial pattern of a) relative skin surface temperature in the distal part of the *Nant* alluvial fan on 7 December 2016 from which "observed" subsurface-surface exchange flux was inferred (data: R. Vallat), b) subsurface-surface exchange flux simulated by the model, and c) simulated surface water presence (both on the same date).

5.4.2 Investigating a plausible future climate, landcover, and permafrost scenario

Having ensured that the partially calibrated model could reproduce historical observations to some degree and produce broadly coherent outputs, attention could turn to applying modified climate and land cover scenarios to assess possible future changes to such systems. Given the models strong physical basis, it is not unduly problematic that the observations were not replicated perfectly since any simulated changes still remain meaningful relatively.

Due to the substantial integrated model execution times, only a single scenario could be considered within the scope of this thesis. Previous integrated model applications, including those cited in Section 5.1, also tended to involve only relatively simplistic change scenarios. A "moderate" climate scenario (i.e. based on RCP 4.5) was selected as being most appropriate; RCP 2.6 now probably being too optimistic, and RCP 8.5 arguably to pessimistic (Hausfather and Peters, 2020). To provide some time for ongoing changes to materialise whilst not being so distant that the uncertainties involved become overwhelming, around the year 2075 was identified as an appropriate target period. Basing the scenario upon the model ensemble medians from CH2018 (CH2018, 2018) was deemed most appropriate. As such, the new scenarios could not be used in their fully transient form, since such information is only available for the independent GCM-RCM combinations.

Instead, simple approximate (already bias corrected) seasonal temperature and precipitation change factors applicable to the region and future period in question were extracted from Figures 4.4 and 4.5 of the CH2018 report and applied directly to the hourly meteorological station time-series that formed the input to the WaSiM model described in Chapter 3. In other words, the "delta change" approach was used. The aforementioned factors are listed in Table 5.4. Their possible future evolution presently being rather unclear, all other meteorological variable were considered to be invariant.

In taking this approach, it was assumed that the period 1 October 2014 to 30 September 2018 still "aligns" in climatic terms with the CH2018 reference period of 1980-2010. This assumption may not actually hold, i.e. by 2014 the underlying temperature and precipitation distributions may have already shifted slightly relative to the reference period. However, with such a short four-year period of "realisations" drawn from it, any changes would be impossible to distinguish from natural variability in probabilistic terms. It should simply be borne in mind, then, that the scenario employed could be marginally more pessimistic than a "true" RCP 4.5 outcome.

	Change factor	
Season	Temperature (°C)	Precipitation (%)
Winter (DJF)	+ 2.0	+ 10.0
Spring (MAM)	+ 1.6	+ 4.0
Summer (JJA)	+ 2.2	− 8.0
Autumn (SON)	+ 1.9	0.0

Table 5.4: Seasonal change factors that were applied to the 2014-2018 hourly meteorological data to generate a climate scenario akin to what could be expected by around the year 2075 under the "moderate" RCP 4.5. This is the "CC" scenario referred to below.

By forcing the (optimised) WaSiM model that was described in Chapter 3 with these modified meteorological datasets, a new set of 25 m resolution grids (at both daily and hourly resolution) of i) ET_p, and ii) liquid water arriving at the land surface, i.e. snowmelt and rain (hereafter referred to as "snowcover outflow") were generated. Given the strong likelihood that the small remaining glaciers in the study area will have disappeared by 2075, the glacier module was also deactivated in this simulation.

5.4.2.1 Projected change in snow storage, "snowcover outflow", and potential evapotranspiration

Figure 5.11 compares the catchment-averaged hourly total snow storage (i.e. Snow Water Equivalent, SWE) simulated under the modified climate with the corresponding results from the original, unmodified model. In quantitative terms, taking the Vallon de Nant as an example, the predicted change in catchment-average annual maximum snow storage, averaged across the four year period, is -34%. Additionally, one observes that winters which are relatively snow-poor historically (e.g. 2016/17) are liable to become disproportionately more so than snowier winters.

Equivalent comparisons are presented for ET_p and "snowcover outflow" in Figure 5.12. These results suggest that ET_p would increase sharply under such a scenario; again for the Vallon de Nant again, catchment-averaged annual ET_p is estimated to increase by around 10%. Reflecting seasonally contrasting expected precipitation changes that largely cancel one another out on an annual basis, projected changes in overall annual mean catchment-averaged "snowcover outflow" are much modest (<+ 1%), although seasonal differences are of course larger.

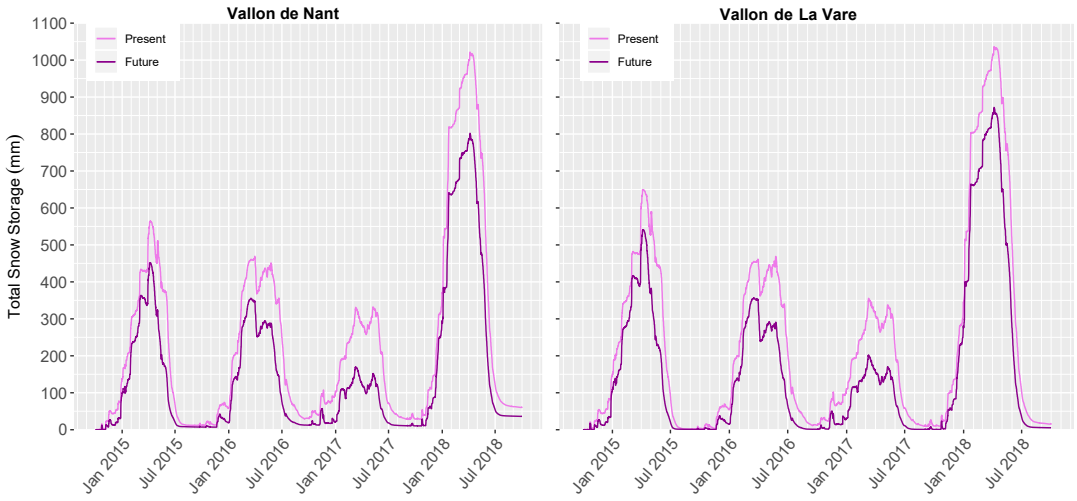

Figure 5.11: Simulated hourly catchment-averaged total snow storage (i.e. SWE) over the historical reference period (present), and with the change factors listed in Table 5.4 applied to represent a plausible "moderate" climate change scenario by approximately the year 2075 (future). These data were simulated using the WaSiM model described in Chapter 3.

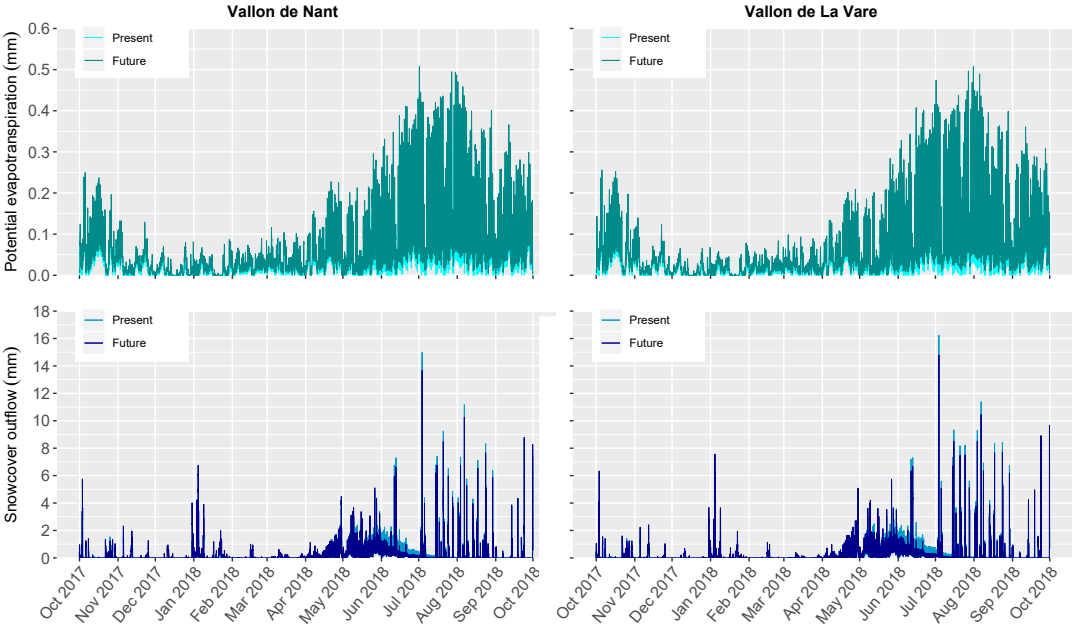

Figure 5.12: Simulated hourly catchment-averaged potential evapotranspiration (ET_p; upper) and "snowcover outflow" (lower) over the historical reference period (present), and with the change factors listed in Table 5.4 applied to represent a plausible "moderate" climate change scenario by approximately the year 2075 (future). An in Figure 5.11, these data were simulated using the WaSiM model described in 3. Only a reduced period – the hydrological year 2017/18 – is shown for clarity.

5.4.2.2 Projected change in land cover and permafrost

A future forest scenario was developed by forcing the dynamic vegetation model TreeMig (Lischke et al., 2006) with appropriate future climate scenario data, this time at monthly frequency. An interesting initial revelation from this simulation, which began in the year 1500 and proceeded in 25 year time-steps, is that the actual present-day forest distribution is considerably less extensive than climatic conditions alone (i.e. as per the model) would dictate. In other words, much of the grasslands in the area can be considered "artificial", i.e. below the true tree-line, having only been kept open through animal grazing.

As alluded to above, it its standard configuration, TreeMig takes no account of other factors like future soil evolution and avalanche or rockfall activity that could affect forest development besides climate. Therefore, to somehow represent such soil and geomorphological controls (Henne et al., 2011; Macias-Fauria and Johnson, 2013), the normalised difference vegetation index (NDVI) was calculated from a Landsat 8 scene captured on 26 June 2018. Based on this raster, future forest expansion excluded in regions with low, "non-vegetation" NDVI values. Thus, areas which are presently vegetated with grasses and suchlike were allowed to transition to forests in the model if the climate was also conducive, but forests were prevented from developing in areas which are presently vegetation free on the assumption that insufficient soil will have developed by the future period in question to support them.

Forest development was furthermore excluded from avalanche tracks, where vegetation successions are regularly "reset" (these areas were clearly visible in high resolution (25 cm) aerial imagery, from which they were digitised) , as well as from areas near the small settlements in the area presently open areas (on the assumption that grazing and other land management practices will prevent future forest developing here). The final exclusion mask area is shown in Supplementary Figure D.1. Present grazing pastures were not included in this mask; hence the future scenario can additionally be considered representative of a pasture abandonment scenario, which is an increasing non-climate-related occurrence in such areas.

Finally, a probabilistic permafrost map was also generated for the relevant climate scenario, and was classified into a binary format using the same procedure as that applied to the present-day map. Note that the future permafrost map corresponds only to unconsolidated sediments (whose response to changing air temperatures is complex and can be fairy slow). As was discussed earlier, permafrost in rock walls rapidly tracks annual mean air temperature, and so given the relatively low elevation of the study site (in Alpine permafrost terms), it can be safely assumed that most rock-wall permafrost will have disappeared by the period in question. Even under present

conditions, permafrost is not especially extensive in the area. In this respect, had the intention of this thesis been to focus specifically on hydrology–permafrost interactions, then an alternative site would have certainly been selected. The resultant future land cover and permafrost maps are presented in Figure 5.13.

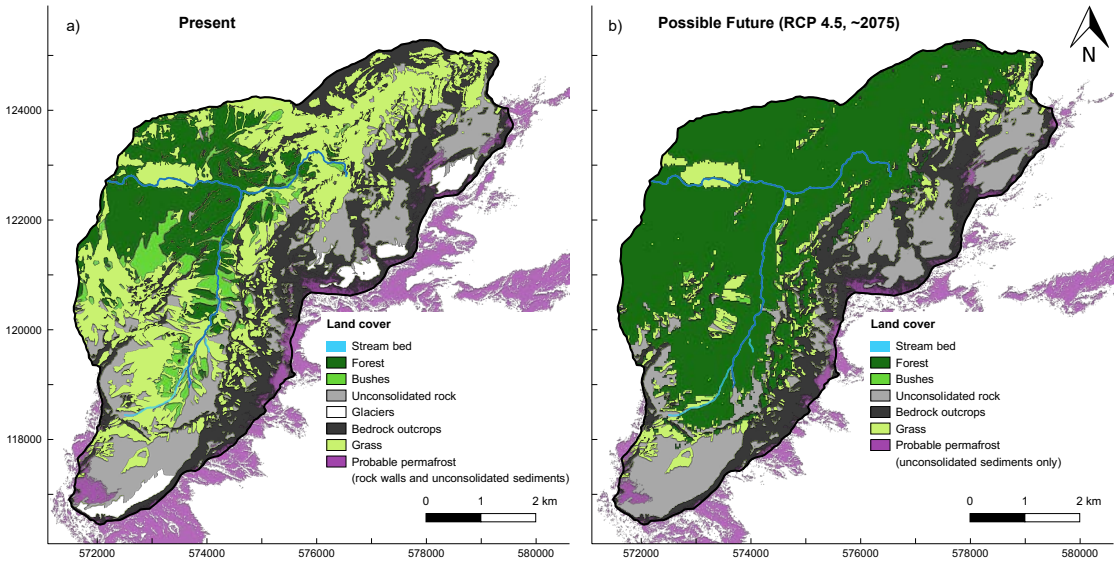

Figure 5.13: a) Present-day and b) plausible future land cover map of the study area, including permafrost distribution, under a plausible "moderate" climate change scenario by approximately the year 2075.

5.4.2.3 Projected changes in integrated hydrological response

Two final integrated model simulations were undertaken using the information generated in the above subsections (with daily forcing frequency). The first sought to explore the possible hydrological impacts of the changed climate alone ("CC"), whilst the second sought to investigate the extent to which contemporaneous forest and permafrost changes could act as secondary modulators ("CC + LC + PF"). The projected impacts at S2 and N4 are shown in Figure 5.14.

The results indicate that substantial reductions in late spring streamflow can be anticipated under the CC scenario. Indeed, there could be some years in which a snowmelt-related peak is hardly evident at all. Conversely, the potential for mid-winter high flow events appears to be significantly elevated under this scenario. Baseflows, on the other hand, are predicted to remain fairly stable, presumably because i) winter precipitation total are expected in increase according to the climate scenario applied, and ii) more of this precipitation will fall as rain (and hence may not be stored for so long before being translated into streamflow).

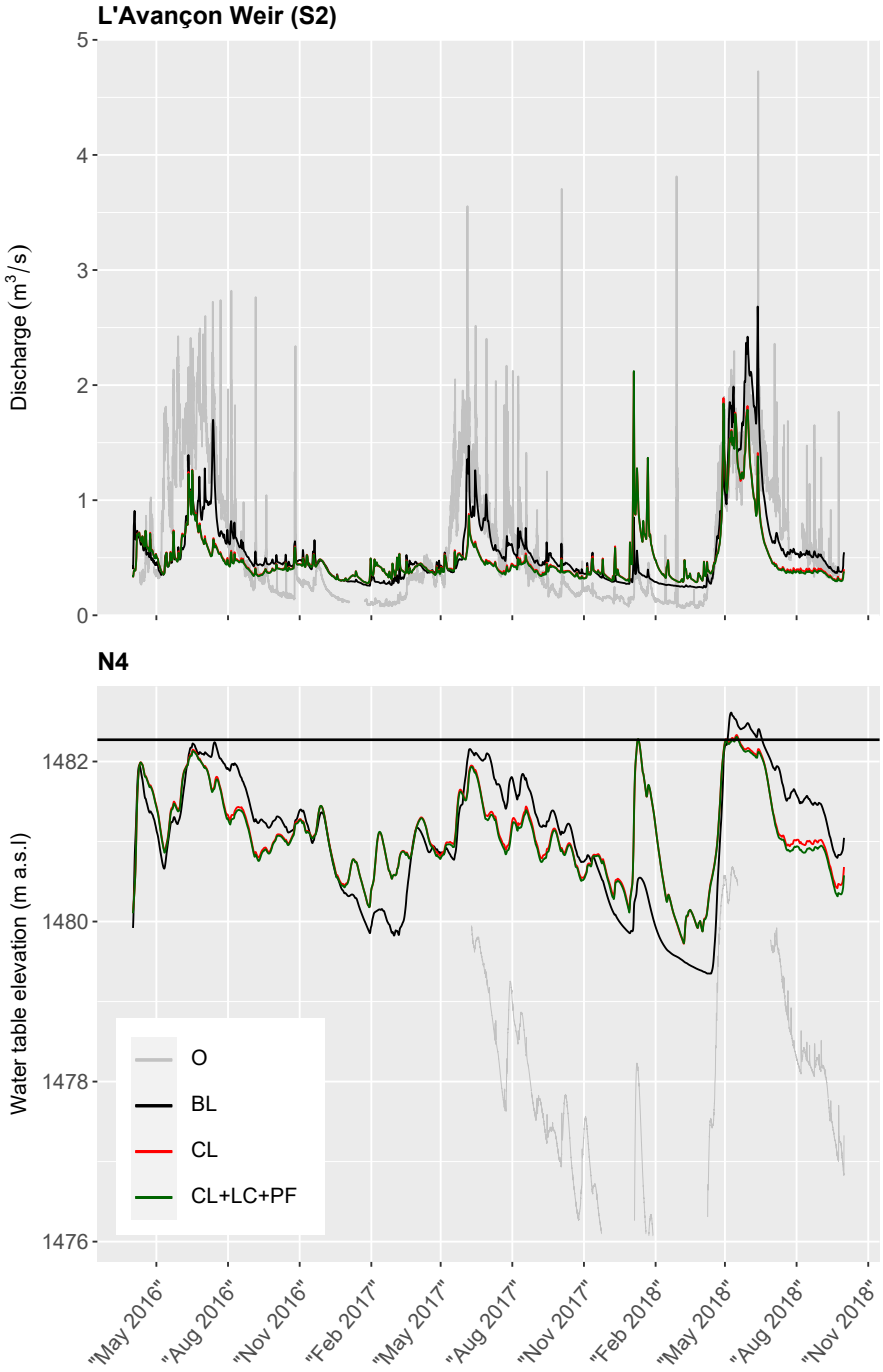

Figure 5.14: Projected changes in streamflow and groundwater levels at S2 and N4, respectively, under the plausible modified climate scenarios ("CC") and with additional plausible land cover and permafrost changes ("CC + LC + PF"). The baseline simulation (as presented above; "B") and historical observations ("O") are also shown.

For groundwater levels, the most apparent feature of simulated future change with respect to the historical baseline is a pronounced decline in seasonality, which is again consistent with a reduced snowmelt influence and elevated quantities of liquid precipitation in winter.

Considering the simulated future series with and without the additional land cover and permafrost changes, one observes that climate changes alone are expected to dominate, with the land cover and permafrost changes only having a small modulating effect. This could be due to the effects of forest expansion and permafrost degradation offsetting one another somewhat (as discussed in Chapter 1, permafrost degradation alone could be expected to generally raise groundwater levels). However, due to time constraints, these scenarios were not run independently, although that would have been ideal. That said, due to the more extensive area affected, the hydrological impacts of forest expansion could be expected to prevail, and the fact that both streamflows are groundwater levels are expected to be marginally lowered with the land cover and permafrost changes compared with the climate only change seems to be in accordance with this hypothesis (more interception, and *ET*). On the other hand, it could be that the vegetation and permafrost changes reinforce one another; permafrost degradation leading to more deep infiltration into the mountain massifs, perhaps leaving to reduced mountain front recharge and ultimately contributing to reduced valley-floor groundwater levels. A more detailed spatial exploration of the scenarios would be required to shed light on such aspects, but the underlying outputs from these simulations would enable such work to be undertaken.

By integrating the water balance outputs from HGS for these three scenarios ("BL", "CC", and "CC + LC + PF") for the entire simulation domain between 1 April 2016 and 30 September 2018, the overall predicted changes in key variables such as streamflow at the outlet and ET_a were quantified. This analysis showed that were the historical period to be repeated under the "CC" scenario, total catchment-averaged ET_a over the three year-period could be expected to be increased by approximately 36%, whilst total stream discharge would reduce by approximately 9%. Adding the land cover and permafrost changes, further changes of +8.3 and -1.2% (relative to the baseline values) are expected for ET_a and discharge, respectively.

This work represents the first hydrological climate change assessment to be presented in the European Alps using an integrated hydrological model. By simulating an entire catchment, one gains something of an appreciation of the larger scale, integrated response, which similar studies which only simulated a few transects (e.g. Pribulick et al., 2016) do not support. That said, it must be emphasised firstly that various sources of model-related uncertainty remain, the secondly that the direct co-evolution of vegetation and hydrology are not directly coupled in the model. For such an approach, readers are referred to Speich et al. (2020), although the code

employed in this work was a much simpler conceptual one. A more general limitation of using fully-integrated models for such assessments is that it is challenging to place projected changes within their broader climatic contexts (i.e. expressed relative to natural variability).

5.4.3 General model limitations

As stated earlier, the model overlooks sub-zone heterogeneity in hydraulic properties and assumes that the system could be represented using the EPM assumption. Moreover, soil freeze-thaw processes, which can influence infiltration capacities (Bayard et al., 2005), are not accounted for. The current version of HGS already offers possibilities in this regard (Schilling et al., 2019), though at present it is unclear how feasible including these processes in the simulation of a moderately-sized, real-world catchment may be. On a similar theme, the way in which permafrost presence was represented, using a large coupling length, was also rather simplistic. Another limitation is that fully 3D anisotropy of hydraulic properties was neglected, despite anisotropic flow being likely in certain bedrock formations, as Chapter 2 discussed. Again, an improvement could have been made in this regard; the formation orientations were actually extracted from the model of bedrock geology at every mesh element centroid during the transfer process. 3D anisotropic hydraulic conductivities could therefore have been assigned on a per-element basis using the *"K tensor"* command, similarly to the groundwater modelling study of Borghi et al. (2015). The caveats attached to the estimates of the unconsolidated sedimentary features discussed in Chapter 4, as well as the limited extent to which the future simulated changes could be placed within the broader context of internal climatic variability, should also be underlined.

Finally, whilst the model domain was extended below S2 and S3 so as to not artificially influence groundwater which is known to bypass these locations and emerge further downstream, to keep the spatial extent of the model somewhat manageable, the same approach was not taken on the eastern flank of the Vallon de Nant. As it was, the topographical boundary (ridge line) in this regions was specified as a no flow boundary. However, as Supplementary Figure D.2 reveals, the dip of the strata may permit the exportation of water across this boundary. As noted in Chapter 2, this water may ultimately end up at La Sarvaz spring, many kilometres away in the Rhône valley. The extreme slopes angles in the area would counteract this effect, however. Such exportations could even occur preferentially, with snowmelt and frontal rainfall – in arriving at the surface more gradually – perhaps being more likely to be retained in the topographical catchment than precipitation from intense convective storms. Overall, the results presented in 5.6 suggest that any exportations are not of major consequences in volumetric terms.

5.4.4 Did the overall calibration strategy work?

The large number of zones in the model is a direct consequence of the study area's geological and land cover diversity. The number of parameters potentially requiring calibration was therefore large. Of course, reducing the number of free parameters by fixing more at their prior estimates (a form of regularisation) would have been possible, but doing so can have adverse consequences. The calibration of a fairly large number of parameters was therefore attempted, which in turn required compromises elsewhere, such as in the temporal resolution of the calibration forcing data and the length of the re-initialisation period. In other words, using daily meteorological forcing, only are reduced number of parameters could feasibly have been calibrated. As has already been mentioned, somewhat contrary to initial expectations, the seasonal simulated general dynamics do not vary greatly according to whether monthly or daily frequency forcing data are applied (Supplementary Figure D.2), however, indicating that the strategy of calibrating with monthly data was a broadly appropriate one. This statement is naturally application dependent, however; to match peak/flood flows, a more focussed calibration strategy would be required.

Another comment that can be made on the calibration approach also relates to the expression of prior knowledge. Whilst prior parameter value estimates can easily be incorporated in PEST via the assignment of regularisation weights, including prior knowledge of inter-parameter relativities – which may actually be much better known than the values themselves – is much more challenging. Enforcing this type of knowledge on the calibration process is thus difficult. For example, in the present case, the hydraulic conductivity of a given shale formation was known to be lower than of a given limestone one, though not by precisely how much. Under such circumstances, it would be useful to allow such parameters to vary within independently specified bounds provided the relative relationship was maintained. As it was, imposing such a constraint would have required the bounds of these two exemplar formations to have been set so narrowly that they do not overlap. Maintaining wider bands (as was done here) thus came with a slight risk that, perhaps to compensate for deficits elsewhere in the model, the final parameter relativities contradict the prior estimates based on physical reasoning. Careful inspection of the relative parameter values attained suggested that this was not a major problem, however.

Overall, it can be concluded that the calibration strategy was moderately effective, with some improvement over the fits with observations generated with the initial parameter estimates. On balance, the model was considered able to reproduce the system sufficiently well to render it a useful tool for exploring future scenarios.

5.5 Conclusions

This chapter has presented the development, partial calibration, and application of a fully-integrated surface-subsurface hydrological model of a steep and rugged Alpine headwater catchment. The model is the first integrated surface-subsurface simulator to incorporate both a complex 3D geological model (including multiple bedrock and Quaternary formations) and results from an optimised, high resolution (25 m, hourly) energy balance-based representation of snow dynamics, liquid precipitation, and ET_{p} estimation. At a more general level, HGS is not thought to have been previously been applied in steep, mountainous real-world (as opposed to synthetic) mountainous terrain of any description.

Due to dichotomy between the limited availability of field data at the outset and the extensive data required to inform such models, as well as difficulties encountered with respect to striking an appropriate balance with respect to mesh resolution, numerical stability, and execution times, the model development phase itself was challenging and time-consuming. Even having made a number of simplifications, substantial execution times precluded automated calibration using the hourly or daily frequency forcing data. In fact, in the time that remained following the model's construction, only two calibration iterations using monthly frequency forcing data could be completed. Perhaps partly as a consequence, it was not possible to reproduce historical *in situ* observations with exceptionally high accuracy.

Nevertheless, the general dynamics of streamflow and groundwater levels were demonstrably captured adequately. A more qualitative assessment of the simulated spatio-temporal patterns of the applied forcing data and simulated response variables further reinforced the view that the numerical representation of the system was fundamentally sound. The model was deemed capable of acting as a meaningful baseline for two simple but plausible future scenarios. Applying the partially calibrated model with hourly forcing indicated that such frequencies may be necessary to replicate the extremely dynamic hydrological responses that strong energy diurnal cycles, rain-on-snow events, and convective thunderstorms induce in such environments. In instances where reasonably long simulation periods are required, this need for high frequency forcing data may raise considerable computational problems to future applications of integrated models in large (3D) catchments for many years to come – not only in the mountains but also other meteorologically dynamic environments.

With respect to possible future work that could follow directly on, if the observed hydrograph at N3 can be better reproduced following further model calibration, then it would be extremely

interesting to extract the water balance for each of the catchments (i.e. the Vallon de Nant and the Vallon de La Vare) seperately – which is now facilitated by a new HGS command – in order to quantify the influence of the contrasting bedrock geologies on hydrological partitioning at the land surface. Including satellite, drone-based, or *in situ* measurements of ET_a and/or (*in situ*) soil moisture measurements in the calibration and evaluation process of such sophisticated models could also prove fruitful.

Another straightforward test would be assess the sensitivity of simulated outputs in such steep terrain to the spatial resolution of the forcing data. This could be achieved by degrading it from the 25 m resolution that has been used throughout. For example, forcing data averaged across each sub-catchment could be applied uniformly at each time-step. The ease with which integrated models may be applied in such geologically complex regions, in particular where recumbent folder are present, may also be significantly enhanced by the development of new "blended" unstructured mesh generation approaches that are specifically designed to conform with surface features in the near-surface zone, but then to only subsurface structures beneath this. Such an approach would supersede the established layered approach that was used here. Activities related to the measurement and spatialisation of soil properties in mountainous areas, including at meaningful scales for numerical models, should likewise be reinvigorated.

In summary, this contribution has hopefully alluded to the considerable capabilities of fully-integrated hydrological models in Alpine terrain. Not only are such tools able to integrate and synthesise a wide variety of observed data, support multi-objective calibration and evaluation approaches, and drive improvements with regards to system understanding in a holistic sense, they also offer enhanced possibilities for revealing those regards in which improvements to the conceptual model and/or its numerical representation are still required, and why this might be the case. That said, given i) the substantial time required to establish such a model in the first place with as few as possible expedient assumptions, ii) the considerable computational costs associated with then simulating a "deep", catchment-scale domain for a reasonable time period and with appropriate frequency forcing data, and ii) particular complexities associated with the distinctive characteristics of such catchments which remain difficult to capture even with such advanced models, their application is presently only recommendable under certain particular situations, for example in exceptionally important or sensitive catchments.

Contribution statement

I (The Author) conducted the vast majority of the work, including collecting, sourcing, and preparing the required datasets, setting up, calibrating, and evaluating the model, preparing the figures, and writing the manuscript. Professor R. Therrien provided advice regarding the model, and made bespoke code modifications (which are now integrated in the commercial branch) to assist the study. Dr. N. Deluigi provided the permafrost maps, and Dr. D. Scherrer ran the future forest model (using climate data and exclusion mask prepared by The Author). Professors G. Mariethoz and P. Brunner provided advice and support throughout.

References

Ajami, H., McCabe, M. F., Evans, J. P., and Stisen, S. (2014). Assessing the impact of model spin-up on surface water-groundwater interactions using an integrated hydrologic model. *Water Resources Research* 50, 2636–2656.

Ala-aho, P., Rossi, P. M., Isokangas, E., and Kløve, B. (2015). Fully integrated surface-subsurface flow modelling of groundwater-lake interaction in an esker aquifer: Model verification with stable isotopes and airborne thermal imaging. *Journal of Hydrology* 522, 391–406.

Ala-aho, P., Soulsby, C., Wang, H., and Tetzlaff, D. (2017). Integrated surface-subsurface model to investigate the role of groundwater in headwater catchment runoff generation: A minimalist approach to parameterisation. *Journal of Hydrology* 547, 664–677.

Aquanty Inc. (2016). *HydroGeoSphere User Manual*. Tech. rep.

Badoux, H. (1971). *Carte et notice explicative, Feuille 1305 - Dt. de Morcles, Atlas géologique de la Suisse (1:25,000)*. Tech. rep.

Barnett, T. P. et al. (2008). Human-induced changes in the hydrology of the western United States. *Science* 319, 1080–1083.

Bayard, D., Stähli, M., Parriaux, A., and Flühler, H. (2005). The influence of seasonally frozen soil on the snowmelt runoff at two Alpine sites in southern Switzerland. *Journal of Hydrology* 309, 66–84.

Beven, K. J. and Kirkby, M. J. (1979). A physically based, variable contributing area model of basin hydrology. *Hydrological Sciences Bulletin* 24, 43–69.

Borghi, A., Renard, P., and Courrioux, G. (2015). Generation of 3D spatially variable anisotropy for groundwater flow simulations. *Groundwater* 53, 955–958.

Brauchli, T., Trujillo, E., Huwald, H., and Lehning, M. (2017). Influence of slope-scale snowmelt on catchment response simulated with the Alpine3D model. *Water Resources Research* 53, 10723–10739.

Camporese, M., Paniconi, C., Putti, M., and McDonnell, J. J. (2019). Fill and spill hillslope runoff representation With a Richards Equation-based model. *Water Resources Research* 55, 8445–8462.

Carroll, R. W. H., Deems, J. S., Niswonger, R., Schumer, R., and Williams, K. H. (2019). The importance of interflow to groundwater recharge in a snowmelt-dominated headwater basin. *Geophysical Research Letters* 46, 5899–5908.

Ceperley, N. et al. (2018). *Salt gauging and stage-discharge curve, Avançon de Nant, outlet Vallon de Nant catchment*.

CH2018 (2018). *CH2018 – Climate Scenarios for Switzerland: Technical Report*. Tech. rep. Zurich, p. 271.

Cochand, F., Therrien, R., and Lemieux, J. M. (2019). Integrated hydrological modeling of climate change impacts in a snow-influenced catchment. *Groundwater* 57, 3–20.

Costa, A., Molnar, P., Stutenbecker, L., Bakker, M., Silva, T. A., Schlunegger, F., Lane, S. N., Loizeau, J.-L., and Girardclos, S. (2018). Temperature signal in suspended sediment export from an Alpine catchment. *Hydrology and Earth System Sciences* 22, 509–528.

Datry, T., Larned, S. T., and Tockner, K. (2014). Intermittent rivers: a challenge for freshwater ecology. *BioScience* 64, 229–235.

Deluigi, N., Lambiel, C., and Kanevski, M. (2017). Data-driven mapping of the potential mountain permafrost distribution. *Science of the Total Environment* 590-591, 370–380.

Doherty, J. (2020). *PEST_HP: PEST for Highly Parallelized Computing Environments*. Tech. rep. Brisbane, Australia: Watermark Numerical Computing.

Durighetto, N., Vingiani, F., Bertassello, L. E., Camporese, M., and Botter, G. (2020). Intraseasonal Drainage Network Dynamics in a Headwater Catchment of the Italian Alps. *Water Resources Research* 56.

Engdahl, N. B. and Maxwell, R. M. (2015). Quantifying changes in age distributions and the hydrologic balance of a high-mountain watershed from climate induced variations in recharge. *Journal of Hydrology* 522, 152–162.

Evans, S. G., Ge, S., Voss, C. I., and Molotch, N. P. (2018). The role of frozen soil in groundwater discharge predictions for warming alpine watersheds. *Water Resources Research* 54, 1599–1615.

Fatichi, S. et al. (2016). An overview of current applications, challenges, and future trends in distributed process-based models in hydrology. *Journal of Hydrology* 537, 45–60.

Foster, L. M. and Maxwell, R. M. (2019). Sensitivity analysis of hydraulic conductivity and Manning's n parameters lead to new method to scale effective hydraulic conductivity across model resolutions. *Hydrological Processes* 33, 332–349.

Freudiger, D., Kohn, I., Seibert, J., Stahl, K., and Weiler, M. (2017). Snow redistribution for the hydrological modeling of alpine catchments. *Wiley Interdisciplinary Reviews: Water* 4, 1232.

Frisbee, M. D., Tolley, D. G., and Wilson, J. L. (2017). Field estimates of groundwater circulation depths in two mountainous watersheds in the western U.S. and the effect of deep circulation on solute concentrations in streamflow. *Water Resources Research* 53, 2693–2715.

Giaccone, E., Luoto, M., Vittoz, P., Guisan, A., Mariéthoz, G., and Lambiel, C. (2019). Influence of microclimate and geomorphological factors on alpine vegetation in the Western Swiss Alps. *Earth Surface Processes and Landforms* 44, 3093–3107.

Gleeson, T. and Manning, A. H. (2008). Regional groundwater flow in mountainous terrain: Three-dimensional simulations of topographic and hydrogeologic controls. *Water Resources Research* 44.

Goldscheider, N. (2005). Fold structure and underground drainage pattern in the alpine karst system Hochifen-Gottesacker. *Eclogae Geologicae Helvetiae* 98, 1–17.

Goulden, M. L. and Bales, R. C. (2014). Mountain runoff vulnerability to increased evapotranspiration with vegetation expansion. *Proceedings of the National Academy of Sciences* 111, 14071–14075.

Graham, D. and Butts, M. B. (2005). Flexible, integrated watershed modelling with MIKE SHE. *Watershed Models*. Ed. by V. Singh and D. Frevert. CRC Press. Chap. 10, pp. 245–272.

Griessinger, N., Schirmer, M., Helbig, N., Winstral, A., Michel, A., and Jonas, T. (2019). Implications of observation-enhanced energy-balance snowmelt simulations for runoff modeling of Alpine catchments. *Advances in Water Resources* 133, 103410.

Hausfather, Z. and Peters, G. P. (2020). Emissions - the 'business as usual' story is misleading. *Nature* 577, 618–620.

Henne, P. D., Elkin, C. M., Reineking, B., Bugmann, H., and Tinner, W. (2011). Did soil development limit spruce (Picea abies) expansion in the Central Alps during the Holocene? Testing a palaeobotanical hypothesis with a dynamic landscape model. *Journal of Biogeography* 38, 933–949.

Hock, R. et al. (2019). High Mountain Areas. *IPCC Special Report on the Ocean and Cryosphere in a Changing Climate*. Ed. by H.-O. Pörtner et al. Chap. 2.

Huntington, J. L. and Niswonger, R. G. (2012). Role of surface-water and groundwater interactions on projected summertime streamflow in snow dominated regions: An integrated modeling approach. *Water Resources Research* 48.

Hwang, H. T., Park, Y. J., Sudicky, E. A., Berg, S. J., McLaughlin, R., and Jones, J. P. (2018). Understanding the water balance paradox in the Athabasca River Basin, Canada. *Hydrological Processes* 32, 729–746.

HydroAlgorithmics (2016). AlgoMesh User Guide, 257.

Immerzeel, W. W. et al. (2020). Importance and vulnerability of the world's water towers. *Nature* 577, 364–369.

Jaros, A., Rossi, P. M., Ronkanen, A. K., and Kløve, B. (2019). Parameterisation of an integrated groundwater-surface water model for hydrological analysis of boreal aapa mire wetlands. *Journal of Hydrology* 575, 175–191.

Käser, D., Graf, T., Cochand, F., McLaren, R., Therrien, R., and Brunner, P. (2014). Channel representation in physically based models coupling groundwater and surface water: pitfalls and how to avoid them. *Groundwater* 52, 827–836.

Klemeš, V. (1990). The modelling of mountain hydrology: the ultimate challenge. *Hydrology of Mountainous Areas (Proceedings of the Strbské Pleso Workshop, Czechoslovakia, June 1988)*, 29–44.

Kristensen, K. J. and Jensen, S. E. (1975). A model for estimating actual evapotranspiration from potential evapotranspiration. *Hydrology Research* 6, 170–188.

Lane, S. N., Bakker, M., Gabbud, C., Micheletti, N., and Saugy, J. N. (2017). Sediment export, transient landscape response and catchment-scale connectivity following rapid climate warming and Alpine glacier recession. *Geomorphology* 277, 210–227.

Leigh, C., Boulton, A. J., Courtwright, J. L., Fritz, K., May, C. L., Walker, R. H., and Datry, T. (2016). Ecological research and management of intermittent rivers: an historical review and future directions. *Freshwater Biology* 61, 1181–1199.

Liggett, J. E., Werner, A. D., and Simmons, C. T. (2012). Influence of the first-order exchange coefficient on simulation of coupled surface-subsurface flow. *Journal of Hydrology* 414-415, 503–515.

Lischke, H., Zimmermann, N. E., Bolliger, J., Rickebusch, S., and Löffler, T. J. (2006). TreeMig: A forest-landscape model for simulating spatio-temporal patterns from stand to landscape scale. *Ecological Modelling* 199, 409–420.

Lugeon, M. and Gagnebin, E. (1928). L'origine des sources de la Chambrette aux Plans sur Bex (Alpes Vaudoises). *Bulletin de la Société vaudoise des Sciences* 56.

Macias-Fauria, M. and Johnson, E. A. (2013). Warming-induced upslope advance of subalpine forest is severely limited by geomorphic processes. *Proceedings of the National Academy of Sciences of the United States of America* 110, 8117–8122.

Maina, F. Z. and Siirila-Woodburn, E. R. (2020). Watersheds dynamics following wildfires: Nonlinear feedbacks and implications on hydrologic responses. *Hydrological Processes* 34, 33–50.

Markovich, K. H., Maxwell, R. M., and Fogg, G. E. (2016). Hydrogeological response to climate change in alpine hillslopes. *Hydrological Processes* 30, 3126–3138.

Markstrom, S. L., Niswonger, R. G., Regan, R. S., Prudic, D. E., and Barlow, P. M. (2008). GSFLOW – Coupled ground-Water and surface-water flow model based on the integration of the Precipitation-Runoff Modeling System (PRMS) and the Modular Ground-Water Flow Model (MODFLOW-2005). *U.S. Geological Survey*, 240.

Maxwell, R. M., Condon, L. E., and Kollet, S. J. (2015). A high-resolution simulation of groundwater and surface water over most of the continental US with the integrated hydrologic model ParFlow v3. *Geoscientific Model Development* 8, 923–937.

Maxwell, R. M. (2013). A terrain-following grid transform and preconditioner for parallel, large-scale, integrated hydrologic modeling. *Advances in Water Resources* 53, 109–117.

Maxwell, R. M. and Miller, N. L. (2005). Development of a coupled land surface and groundwater model. *Journal of Hydrometeorology* 6, 233–247.

Mendoza, P. A., Clark, M. P., Barlage, M., Rajagopalan, B., Samaniego, L., Abramowitz, G., and Gupta, H. (2015). Are we unnecessarily constraining the agility of complex process-based models? *Water Resources Research* 51, 716–728.

Miller, K. L., Berg, S. J., Davison, J. H., Sudicky, E. A., and Forsyth, P. A. (2018). Efficient uncertainty quantification in fully-integrated surface and subsurface hydrologic simulations. *Advances in Water Resources* 111, 381–394.

OFAG (1980). *Carte des aptitudes des sols de la Suisse*. URL: https://files.be.ch/bve/agi/geoportal/geo/lpi/BEK_2000_02_LANG_FR.PDF.

Paniconi, C. and Putti, M. (2015). Physically based modeling in catchment hydrology at 50: Survey and outlook. *Water Resources Research* 51, 7090–7129.

Partington, D., Therrien, R., Simmons, C. T., and Brunner, P. (2017). Blueprint for a coupled model of sedimentology, hydrology, and hydrogeology in streambeds. *Reviews of Geophysics* 55, 287–309.

Penn, C. A., Bearup, L. A., Maxwell, R. M., and Clow, D. W. (2016). Numerical experiments to explain multiscale hydrological responses to mountain pine beetle tree mortality in a headwater watershed. *Water Resources Research* 52, 3143–3161.

Pribulick, C. E., Foster, L. M., Bearup, L. A., Navarre-Sitchler, A. K., Williams, K. H., Carroll, R. W. H., and Maxwell, R. M. (2016). Contrasting the hydrologic response due to land cover and climate change in a mountain headwaters system. *Ecohydrology* 9, 1431–1438.

Rasouli, K., Pomeroy, J. W., and Whitfield, P. H. (2019). Are the effects of vegetation and soil changes as important as climatechange impacts on hydrological processes. *Hydrology and Earth System Sciences Discussions*, 1–33.

Schilling, O. S., Park, Y. J., Therrien, R., and Nagare, R. M. (2019). Integrated surface and subsurface hydrological modeling with snowmelt and pore water freeze–thaw. *Groundwater* 57, 63–74.

Seck, A., Welty, C., and Maxwell, R. M. (2015). Spin-up behavior and effects of initial conditions for an integrated hydrologic model. *Water Resources Research* 51, 2188–2210.

Smerdon, B. D., Allen, D. M., Grasby, S. E., and Berg, M. A. (2009). An approach for predicting groundwater recharge in mountainous watersheds. *Journal of Hydrology* 365, 156–172.

Smerdon, B. D., Mendoza, C. A., and Devito, K. J. (2007). Simulations of fully coupled lake-groundwater exchange in a subhumid climate with an integrated hydrologic model. *Water Resources Research* 43, 1416.

Speich, M. J. R., Zappa, M., Scherstjanoi, M., and Lischke, H. (2020). FORests and HYdrology under Climate Change in Switzerland v1.0: a spatially distributed model combining hydrology and forest dynamics. *Geoscientific Model Development* 13, 537–564.

Sulis, M., Paniconi, C., Rivard, C., Harvey, R., and Chaumont, D. (2011). Assessment of climate change impacts at the catchment scale with a detailed hydrological model of surface-subsurface interactions and comparison with a land surface model. *Water Resources Research* 47, 1–22.

Thornton, J. M., Mariethoz, G., and Brunner, P. (2018). A 3D geological model of a structurally complex alpine region as a basis for interdisciplinary research. *Scientific Data* 5, 1–20.

Tolley, D., Foglia, L., and Harter, T. (2019). Sensitivity analysis and aalibration of an integrated hydrologic model in an irrigated agricultural basin With a groundwater-dependent ecosystem. *Water Resources Research* 55, 7876–7901.

Turowski, J. M., Yager, E. M., Badoux, A., Rickenmann, D., and Molnar, P. (2009). The impact of exceptional events on erosion, bedload transport and channel stability in a step-pool channel. *Earth Surface Processes and Landforms* 34, 1661–1673.

Van Genuchten, M. T. (1980). A closed-form equation for predicting the hydraulic conductivity of unsaturated soils. *Soil Science Society of America Journal* 44, 892–898.

Voeckler, H. M., Allen, D. M., and Alila, Y. (2014). Modeling coupled surface water – groundwater processes in a small mountainous headwater catchment. *Journal of Hydrology* 517, 1089–1106.

Von Gunten, D., Wöhling, T., Haslauer, C., Merchán, D., Causapé, J., and Cirpka, O. A. (2014). Efficient calibration of a distributed pde-based hydrological model using grid coarsening. *Journal of Hydrology* 519, 3290–3304.

Wang, D., Liu, Y., and Kumar, M. (2018). Using nested discretization for a detailed yet computationally efficient simulation of local hydrology in a distributed hydrologic model. *Scientific Reports* 8, 5785.

Wang, X., Chen, R., Han, C., Yang, Y., Liu, J., Liu, Z., and Song, Y. (2019). Changes in river discharge in typical mountain permafrost catchments, northwestern China. *Quaternary International* 519, 32–41.

Ward, J. V., Malard, F., Tockner, K., and Uehlinger, U. (1999). Influence of ground water on surface water conditions in a glacial flood plain of the Swiss Alps. *Hydrological Processes* 13, 277–293.

Warscher, M., Strasser, U., Kraller, G., Marke, T., Franz, H., and Kunstmann, H. (2013). Performance of complex snow cover descriptions in a distributed hydrological model system: A case study for the high Alpine terrain of the Berchtesgaden Alps. *Water Resources Research* 49, 2619–2637.

Welch, L. A. and Allen, D. M. (2014). Hydraulic conductivity characteristics in mountains and implications for conceptualizing bedrock groundwater flow. *Hydrogeology Journal* 22, 1003–1026.

White, J. T. (2018). A model-independent iterative ensemble smoother for efficient history-matching and uncertainty quantification in very high dimensions. *Environmental Modelling and Software* 109, 191–201.

6 | Conclusions and outlook

6.1 Overview

In Chapter 1, a literature review of mountain hydrology and its simulation was conducted. Three major research gaps were identified. The first is that detailed hydrological and hydrogeological field investigations in alpine terrain rarely proceed to numerical modelling, making the generation of future predictions extremely difficult. The second is that most HCCIAs continue to rely on simplistic conceptual hydrological models, despite the complexity of alpine hydrological systems. The third, meanwhile, is that the possible hydrological impacts of contemptuous climate-driven changes in vegetation and permafrost are generally overlooked. These gaps provide the high level motivation for the research. As such, this thesis sought to assess the utility of fully-integrated surface-subsurface hydrological modelling in steep, snow dominated, geologically complex (calcareous) Alpine terrain; a type of landscape in which this class of sophisticated models have not previously been applied.

During the course of the research, several more specific (but still important) limitations associated with the status quo also became apparent, including: i) the lack of an appropriate 3D model of the study region's bedrock geology – for that matter, no such model existed anywhere in the Alps, meaning it was not initially apparent whether the development of such a model was even feasible, ii) the preponderance of empirical index-based snow simulation schemes in most alpine hydrological modelling exercises, which are inappropriate in very steep, rugged, and moderately sized headwater basins, iii) the lack of practical and efficient methods by which the geometries of potential unconsolidated Quaternary aquifers may be estimated across entire rugged alpine headwaters, iv) substantial uncertainty regarding whether or not a fully integrated model of a steep, snow-dominated, geologically complex alpine headwater that incorporated a considerable amount of the naturally inherent complexity could be feasibly developed, and of so, to what extent such a model would be capable of reproducing hydrological observations in such terrain, and v) continued debate surrounding the expected relative contributions of future direct vs. indirect system responses to overall future hydrological change; hydrological climate change impacts having never previously been assessed with a fully integrated model anywhere in the Alps. Hence, the original research contributed to addressing these issues, as well as the broader motivations.

Little of the extensive data that is required to inform such a comprehensive model was available at the outset, and so it was necessary for data collection and collation activities to proceeded simultaneously with the model development. On account of the distinctive nature of the study region, ambitious advancements were made over the simplified representations of subsurface

geometries and snow dynamics that are traditionally relied upon in most mountain hydrology simulation exercises (including those which employ otherwise sophisticated fully-integrated surface-subsurface codes). Indeed, by coupling two contemporary codes, it was possible to leverage the strengths of each of each whilst simultaneously mitigating against their respective limitations (namely the lack of options for interpolating meteorological fields and the simplified representation of snow in HydroGeoSphere, and the limited representation of subsurface flow associated with WaSiM). Below, the main outcomes of the thesis are evaluated with respect to the research questions that were initially posed.

6.2 Returning to the research questions

Is it possible to develop three-dimensional (3D) models of bedrock geology that are appropriate for subsequent numerical groundwater and/or integrated surface-subsurface flow modelling in even the most complex sedimentary Alpine settings?

In Chapter 2, a 3D model of the bedrock geology in the study region was developed. Even in such an exceptionally complex Alpine setting, and despite having been developed with much simpler subsurface environments in mind, an industry-standard geological modelling software tool (GeoModeller) was ultimately able to generate a spatially continuous representation of subsurface formations and their associated formations (e.g. faults) that corresponded well with inputs. The result is arguably the most comprehensive and highly resolved 3D geological model of a section of the Alps yet created. In summary, the first research question can now be answered affirmatively. Additionally, to promote its potential wider use, the model was published in open data formats. Besides making an independent contribution to the field of geological modelling, the output of Chapter 2 formed one of the several datasets that informed the fully-integrated surface-subsurface flow model.

How might different types of complementary snow observations be incorporated with physically-based, spatially distributed snow models in order to improve simulations of snow dynamics in rugged and comparatively data-sparse Alpine terrain?

Under present climatic conditions, melt of the seasonal snowpack typically dominates both annual streamflow and groundwater recharge in many Alpine catchments. However, snow is highly sensitive to climate change. Reflecting this, Chapter 3 concentrated upon the computational representation of snow dynamics. A novel and efficient simulation, optimisation, and uncertainty analysis framework was developed that facilitates the incorporation of complementary types of

snow observations within the calibration of a spatially distributed, physically-based snow model that additionally accounts for the gravitational redistribution of snow from steep slopes. More specifically, having established the model using the code WaSiM, several uncertain empirical parameters – whose inclusion in an otherwise physically-based model is justified by data deficiencies and the presence of an emperical algorithm – were optimised with respect to remotely sensed snow extent maps and reconstructed SWE time-series. As far as is known, Landsat 8 images had never previously been used to calibrate a distributed snow at the pixel level. Ultimately, snow observations could be reproduced satisfactorily, and (as far as the comparison allows) some improvement over previous studies in which this was not done was apparent. The reduction in uncertainty associated with key model predictions achieved through calibration and the worth of the different observation types in the process were also quantified. In so doing, one possible answer to the second research question was proposed, and an independent contribution to the field of snow hydrology made.

The framework also enables the generation of gridded ice melt, liquid precipitation, and potential evapotranspiration (ET_p) datasets alongside that corresponding to to snowmelt, at high spatio-temporal resolution – which is important given the large elevation-driven meteorological gradients and temporal dynamism of such systems – that can subsequently be used to force distributed hydrological models. The empirical adjustments involved should compensate somewhat for any deficiencies in meteorological observations, thereby helping to ensure that the representations are as accurate and reliable as possible. In the context of the overall thesis, the datasets generated in 3 formed the meteorological boundary conditions for the fully-integrated flow model, which was useful as the integrated code selected (HGS) i) offers no "pre-processing" functionally for spatially interpolating observed meteorological time-series onto a grid, and ii) includes only a fairly rudimentary representation of snow processes (which was likely to have been insufficient in such terrain).

To what extent can the geometries of potential unconsolidated Quaternary aquifers be estimated in a non-invasive and cost-effective fashion across entire moderately-sized, inaccessible Alpine headwater catchments?

A literature review conducted as part of Chapter 4 suggested that few feasible, cost-effective approaches to the estimation of potential unconsolidated aquifer geometries across rugged alpine headwaters are at the disposal of researchers and practitioners. This is problematic because such estimates constitute another form of information required to establish a comprehensive fully-integrated hydrological model. Therefore, with a view to addressing the fourth research question, Chapter 4 established a relatively simplistic approach to the estimation of bedrock

interfaces beneath unconsolidated Quaternary fill sediments. The approach draws heavily on existing digital terrain data, and geological mapping, although constraints from geophysical surveys can be easily integrated where available. Whilst plausible estimates could be generated, the purely geomorphometrical method should be applied with care, since it demonstrated fairly high sensitivity to the inclusion/exclusion of topographic data points in boundary areas. The challenge of determining unconsolidated sediment geometries at catchment-scale in such terrain essentially remains a substantial one, though it is certainly recommendable that as much geophysics be conducted as resources allow.

Can fully-integrated surface-subsurface hydrological models which include (even) more of the known complexity than previous efforts be developed, calibrated, and applied to reproduce spatio-temporal hydrological dynamics in complex headwaters under present climatic, land cover, and permafrost conditions?

Chapter 5 shows that with effort, such models can indeed be developed. Having collated or generated the necessary data, determining an appropriate level of spatial discretisation was a crucial initial challenge; if the discretisation was too fine, then model execution times become extortionate. Conversely, a certain level of discretisation was required to ensure that not too much underlying structural information was lost, and/or to prevent numerical difficulties being encountered. In fact, simply getting the model to converge well and execute in a reasonable period of time was a substantial challenge; a time-consuming trial and error approach to mesh generation and testing had to be adopted. Then, given the fairly finely resolved resultant mesh and the desire to calibrate a reasonably large number of parameters (reflecting the surface and subsurface heterogeneity of the study area) in an automated fashion over a calibration period exceeding one year (due to the strong seasonal dynamics), a pragmatic optimisation approach was required. Calibration using monthly frequency forcing data was therefore attempted. When the calibrated model was subsequently forced with daily and hourly frequency data, the principal features of the catchment's hydrological dynamics could be reproduced with some skill, even if obtaining extremely close matches was not possible. The interplay between initial conditions and re-initialisation (i.e. the period that should be simulated with every new set of parameters prior to the commencement of the calibration period) in such models should receive further research attention. It was nevertheless concluded that the model provides a suitable basis to proceed to explore a simple but plausible future scenario.

What insights can applying such models under a plausible future climatic, land cover, and permafrost scenario yield with respect to the magnitude and importance of possible drivers of future hydrological change?

The simulations under plausible future conditions, also presented in Chapter 5, suggest that climatic changes are likely to dominate those associated with forest expansion and permafrost degradation. The seasonality of both streamflow and groundwater levels is expected to reduce substantially. Overall, under the scenario considered, over a three-year simulation period, total streamflow is projected to decline by approximately 10%.

6.3 Limitations and recommendations for future research

Despite the generally satisfactory outcomes, a number of limitations associated with the research should be highlighted. In many cases, these provide impetus to recommendations for future work.

Firstly, a considerable effort was required to collate, collect, and generate all of the datasets needed to inform the integrated hydrological model. Numerous challenges were also then encountered in seeking to execute and calibrate it – simply getting the complete consistently, with an acceptably small mass balance error, and in a reasonable time period, was not trivial. For these reasons, it has only been possible in this thesis to explore a small subset of the many research questions that could theoretically be explored with such a model. Quantifying the importance of having such a complex 3D geology, for example, could be an interesting future objective.

Some more detailed remarks can be made regarding spatial discretisation. Although the mesh used included refinement around important surface features (which has been shown in a systematic study to improve both the accuracy of the flow solutions in these critical areas as well as execution times; Wang et al., 2018), the current approach to furnishing the integrated model grid with its vertical dimension by replicating the highly-resolved surface grid numerous times also resulted in more nodes/elements being in the 3D mesh than was perhaps necessary. The distinctive characteristics of alpine terrain certainly contributes significantly to the challenge here; the steepness and ruggedness of the topography meant that a relatively finely resolved surface mesh was required to achieve numerical stability, whilst the presence of recumbent folds and other complex subsurface features (e.g. many formations, some of which are thin) likewise demanded a mesh with many finely space vertical layers spanning an extensive vertical range. This is in contrast to most other applications in which a much more parsimonious discretisation, especially in the vertical plane, has proved adequate. Indeed, in simpler geological settings with a small number of sub-parallel formations, it has proved sufficient to employ meshes with many fewer

vertical layers, since the formation interfaces can be described using raster surface and the mesh layers warped so as to be conformant with these interfaces. The presence of recumbent folds at the present study site prevented this technique from being employed here. Consequently, the resultant mesh was large, which contributed to lengthy model execution times and in turn precluded a detailed assessment of parametric uncertainty.

To overcome this bottleneck and this enhance the efficiency of future fully-integrated model applications in such terrain, improved meshing techniques should be developed. This could be achieved by using fully-unstructured meshes which are concordant with salient features like streams, lakes, steep slopes, ridges, or even land over transitions in the uppermost few layers beneath the surface, but which exclusively reflect geological interfaces and faults at greater depths. As such, for the subsurface component, meshes should probably be tetrahedral – subsurface discretisation using structured hexahedral meshes (e.g. Jansen et al., 2017) can require extreme refinement to negate step-like features along formation boundaries. Previous work with a groundwater-only model suggests that such a transition to a fully-unstructured mesh could lead to substantial simulation accelerations (Clausnitzer et al., 2015), although this would be contingent on it being possible to maintain mesh quality over the complex geological structures at the present study site. The contributions of Fischer et al. (2015) and Zehner et al. (2015) could provide a useful starting point for such a development.

Finally, there remains a need for environmental monitoring and mapping efforts in mountainous areas (at model-relevant scales) to be prioritised more highly. The application of integrated models to mountainous systems in certain less developed countries, where the impacts of climate change on water resources are likely to be even more acute, should also be considered.

References

Clausnitzer, V., Cornaton, F., Schätzl, P., and Dufor, R. (2015). Comparing meshing approaches for groundwater modeling at a geometrically challenging mine site. *MODFLOW and More 2015: Modeling a Complex World*.

Fischer, T., Naumov, D., Sattler, S., Kolditz, O., and Walther, M. (2015). GO2OGS 1.0: a versatile workflow to integrate complex geological information with fault data into numerical simulation models. *Geoscientific Model Development* 8, 3681–3694.

Jansen, G., Sohrabi, R., and Miller, S. A. (2017). HULK – Simple and fast generation of structured hexahedral meshes for improved subsurface simulations. *Computers and Geosciences* 99, 159–170.

Wang, D., Liu, Y., and Kumar, M. (2018). Using nested discretization for a detailed yet computationally efficient simulation of local hydrology in a distributed hydrologic model. *Scientific Reports* 8, 5785.

Zehner, B., Börner, J. H., Görz, I., and Spitzer, K. (2015). Workflows for generating tetrahedral meshes for finite element simulations on complex geological structures. *Computers & Geosciences* 79, 105–117.

A | Supplementary material for Chapter 2

Instructions for visualising the geological model

To visualise the surfaces in **ParaView** (as in Fig. 2.11):

1. Download the software from https://www.paraview.org/, and install it.
2. Under “File”, select “Load State”.
3. Navigate to “Geological_Model_State_File.pvsm”.
4. Under “Load State Options”, select “Search file names under specified directory”, and ensure the directory path is correct.
5. Transparency of individual layers toggled by clicking on the “eye” symbol on the left hand side.

To visualise the voxel data in **SGeMS**:

1. Download the software from http://sgems.sourceforge.net/, and install it.
2. Select “Load Object”, navigate to the file “10 m.SGEMS”, and click “Open”.
3. In the “Select object type” dialogue box, choose “cartesian grid”, and click “Next”.
4. Provide a name for the grid, enter the values shown below in Figure A.1, then click “Finish”.
5. Once the data are loaded (which may take a few minutes), it may be viewed by checking the two tick boxes under the object tab.
6. The colour map can be changed if desired using the options under the “Preferences” tab. Also under this tab, by checking “Use Volume Explorer” and “Hide Volume”, a number of slices in the x, y, and z planes can be visualised using the sliders.

Note: Despite specifying the “No-Data-Value” on import, it does not seem possible make the grey area transparent. Nor does it seem possible to match the colour scheme in SGeMS to that used in the paper.

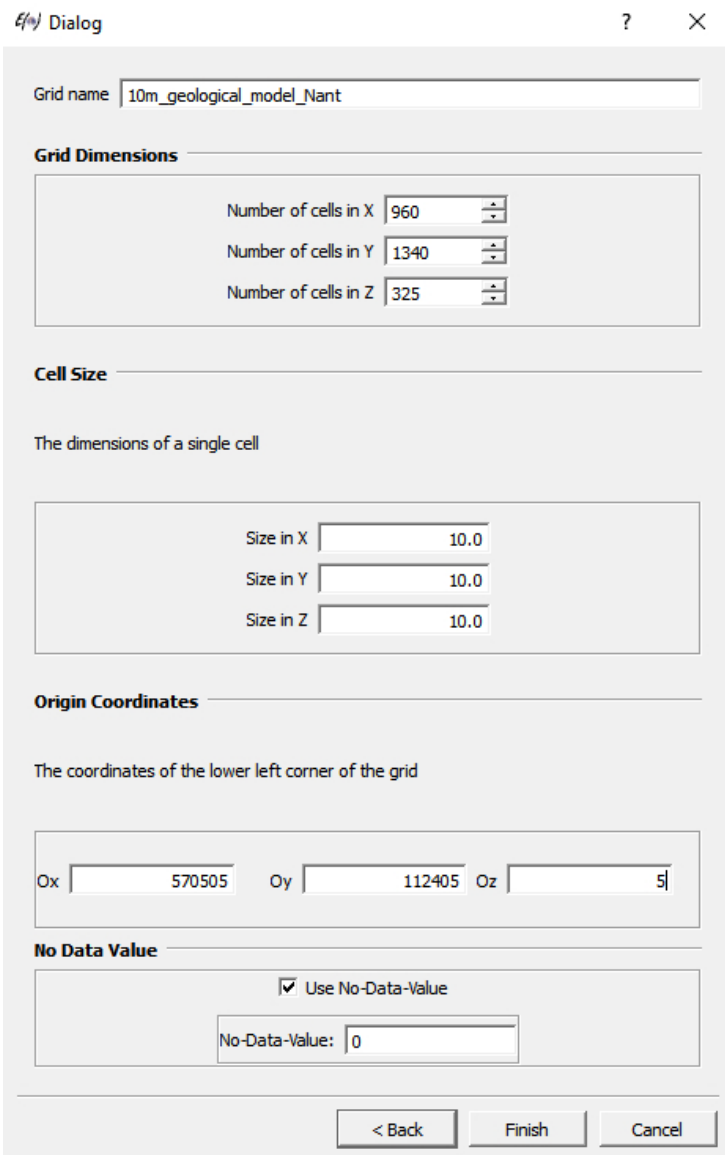

Figure A.1: The settings required to visualise the geological model in SGeMS.

Lastly, to visualise and/or work with the data in **GeoModeller** (licence required):

1. Launch GeoModeller
2. Open the project by navigating to the ".xml" file provided.

B | Supplementary material for Chapter 3

Tables, figures, and an animation

The figures below are reproduced for illustrative purposes only; for full resolution versions, please consult the folowing online repository: https://doi.org/10.6084/m9.figshare.9016154.v1.

The repository also contains i) plots of all the processed meteorological time-series that formed the WaSiM model input, and ii) an animation depicting the simulated daily evolution of Snow Water Equivalent (SWE) across the study catchment for the hydrological year 2018 (i.e. winter 2017/2018) (Animation B.1). The winter in question was extremely snow rich, especially at high elevations.

Station Name	Code	Responsible authority	Elevation (m)	Variables measured
Aigle	**AIG**	MeteoSwiss	381	ISWR, PSUM, RH, SD, TA, VP, WS
Anzeindaz	**ANZ**	UNIL	1,882	ISWR, PSUM, RH, TA, WS
Auberge Pont de Nant (Jardin)	**AUB**	UNIL	1,259	ISWR, PSUM, RH, TA, WS
Avançon-Scierie	**BEX AVA**	Canton of Vaud	450	PSUM
Bex	**BEX**	MeteoSwiss	402	PSUM
Chalet Nant (Alpage)	**CHN**	UNIL	1,487	PSUM, RH, TA, WS
Derborence	**DEB**	MeteoSwiss	1,366	PSUM
Evionnaz	**EVI**	MeteoSwiss	482	ISWR, PSUM, RH, SD, TA, VP, WS
Glacier des Martinets	**GLA**	UNIL	2,100	PSUM, RH, TA, WS
Fully Grand Chavalard	**CHA**	SLF	2,898	RH, TA, WS
Fully Grand Cor	**COR**	SLF	2,602	RH, TA, WS
La Peufaire	**PEU**	Canton of Vaud	730	PSUM
Les Diablerets	**DIA**	MeteoSwiss	2,964	ISWR, RH, SD, TA, VP, WS
Tsanfleuron	**DIS**	SFL	2,575	RH, TA, WS
Martigny	**MAR**	MeteoSwiss	461	ISWR
“Middle Bridge” (Vallon de Nant)	**MBR**	The Authors	1,470	TA
Salanfe	**SAL**	MeteoSwiss	1,965	PSUM
Solalex	**SOL**	UNIL	1,458	ISWR, PSUM, RH, TA, WS
Sorniot-Lac Inférieur*	**SOR***	MeteoSwiss	1,990	PSUM

Table B.1: Summary of the stations that contributed meteorological data to the present study. ISWR = Incoming Shortwave Radiation ($W \cdot m^{-2}$), PSUM = Precipitation (mm), RH = Relative Humidity (%), SD = Sunshine Duration (0-1), TA = Air Temperature (°C), VP = Vapour Pressure (hPa), and WS = Wind Speed ($m \cdot s^{-1}$). UNIL denotes the University of Lausanne. *The precipitation data at the SOR station were ultimately removed from input dataset as the measured totals seemed too low compared with nearby stations at similar elevations. Plots of the time-series can be downloaded from the online repository.

Metric								
F_1			F_2			F_3		
This study*	Previous studies	Reference	**This study***	Previous studies	Reference	**This study***	Previous studies	Reference
0.852	0.820	Schöber et al. (2010)	0.847	0.847	Warscher et al. (2013)	0.696	0.510	Warscher et al. (2013)
0.786	0.800	Schöber et al. (2010)	0.698	0.698	Warscher et al. (2013)	0.511	0.480	Warscher et al. (2013)
0.871	0.730	Schöber et al. (2010)	0.849	0.849	Warscher et al. (2013)	0.819	0.420	Warscher et al. (2013)
0.744	0.750	SchÃ¶ber et al. (2010)	0.569	0.569	Bernhardt et al. (2012)	0.504	0.413	Bernhardt et al. (2012)
0.790	0.770	Schöber et al. (2010)	0.752			0.508		
0.567	0.790	Schöber et al. (2010)	0.561			0.561		
0.846	0.790	Schöber et al. (2010)	0.626			0.434		
0.773	0.700	Schöber et al. (2010)	0.584			0.348		
0.844	0.770	Schöber et al. (2010)	0.328			0.089		
	0.760	Schöber et al. (2010)						
	0.800	Schöber et al. (2010)						
	0.890	Schöber et al. (2010)						
	0.790	Schöber et al. (2010)						
	0.820	Schöber et al. (2010)						
	0.790	Schöber et al. (2010)						
	0.810	Schöber et al. (2010)						
	0.780	Schöber et al. (2010)						
	0.790	Schöber et al. (2010)						
	0.810	Schöber et al. (2010)						
	0.740	Schöber et al. (2010)						
	0.750	Schöber et al. (2010)						
	0.680	Schöber et al. (2010)						
	0.790	Schöber et al. (2010)						
	0.880	Schöber et al. (2010)						
	0.750	Schöber et al. (2010)						
	0.840	Warscher et al. (2013)						
	0.900	Warscher et al. (2013)						
	0.830	Warscher et al. (2013)						
	0.881	Bernhardt et al. (2012)						

Table B.2: F-statistic results from this study and previous publications that were plotted in order to produce Figure 3.7. Statistics produced via the best model setup, i.e. SnowModel + SnowTran-3D + SnowSlide, were taken from Bernhardt et al. (2012). *Spring/early summer only.

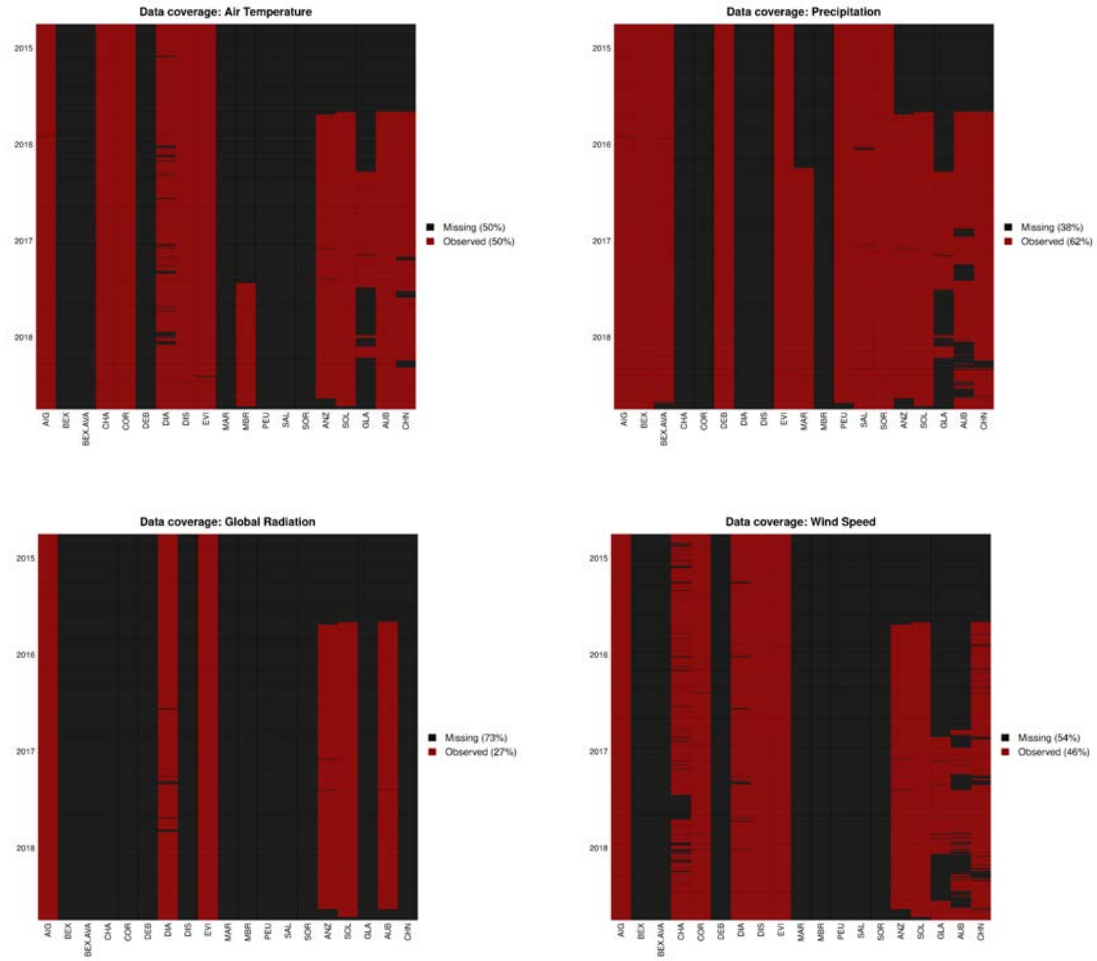

Figure B.1: Temporal coverage of air temperature, global radiation, precipitation and relative humidity data for the full simulation period (i.e. hydrological years 2015-2018). Each horizontal bar represents a period of one hour. See Table B.1 for the station names and locations that correspond to these codes. The mean percentage completeness statistics for each parameter were calculated on an hourly basis, and correspond to the period 1 October 2014-30 September 2018 inclusive. Note that the SOR data were eventually removed from the model inputs.

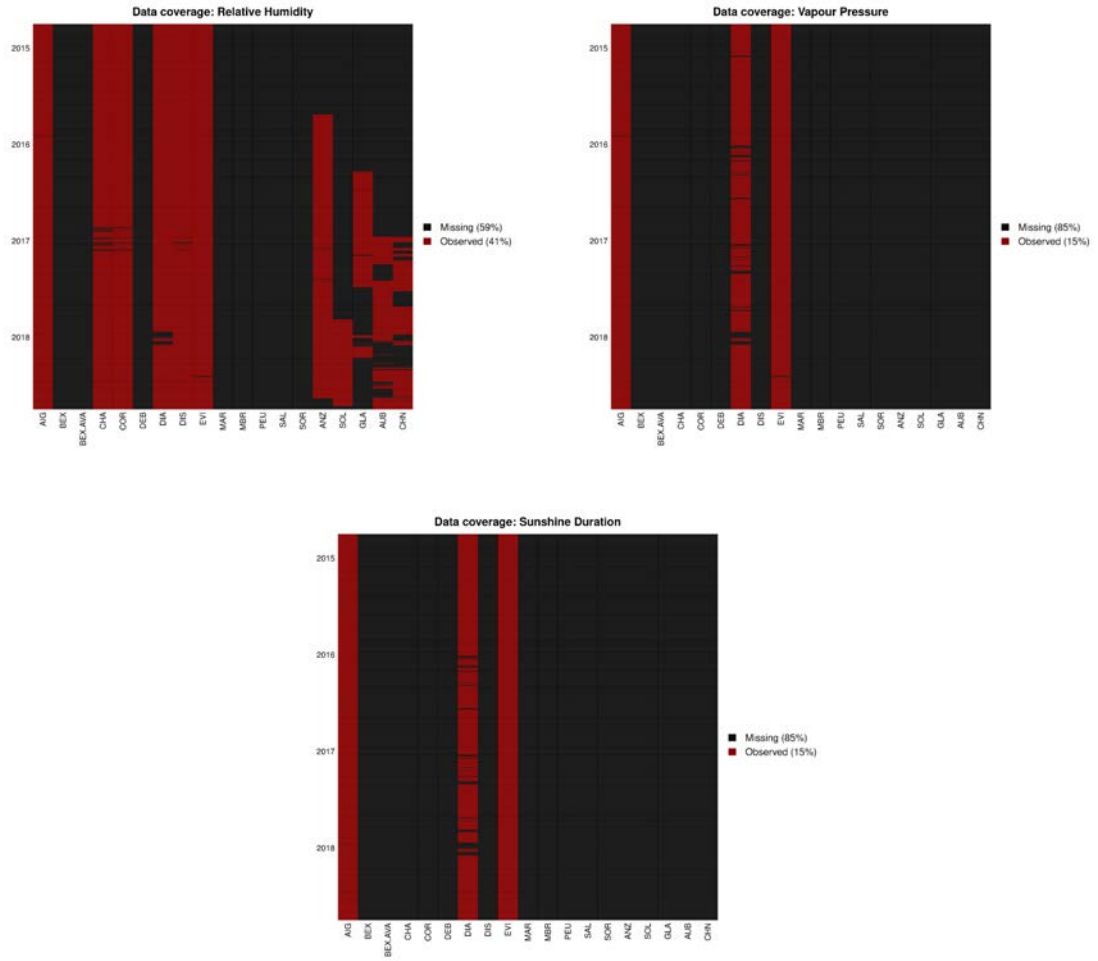

Figure B.2: Temporal coverage of vapour pressure, sunshine duration, and wind speed data for the full simulation period (i.e. hydrological years 2015-2018). Each horizontal bar represents a period of one hour. See Table B.2 for the station names and locations that correspond to these codes. The mean percentage completeness statistics for each parameter were calculated on an hourly basis, and correspond to the period 1 October 2014-30 September 2018 inclusive. Note that the SOR data were eventually removed from the model inputs.

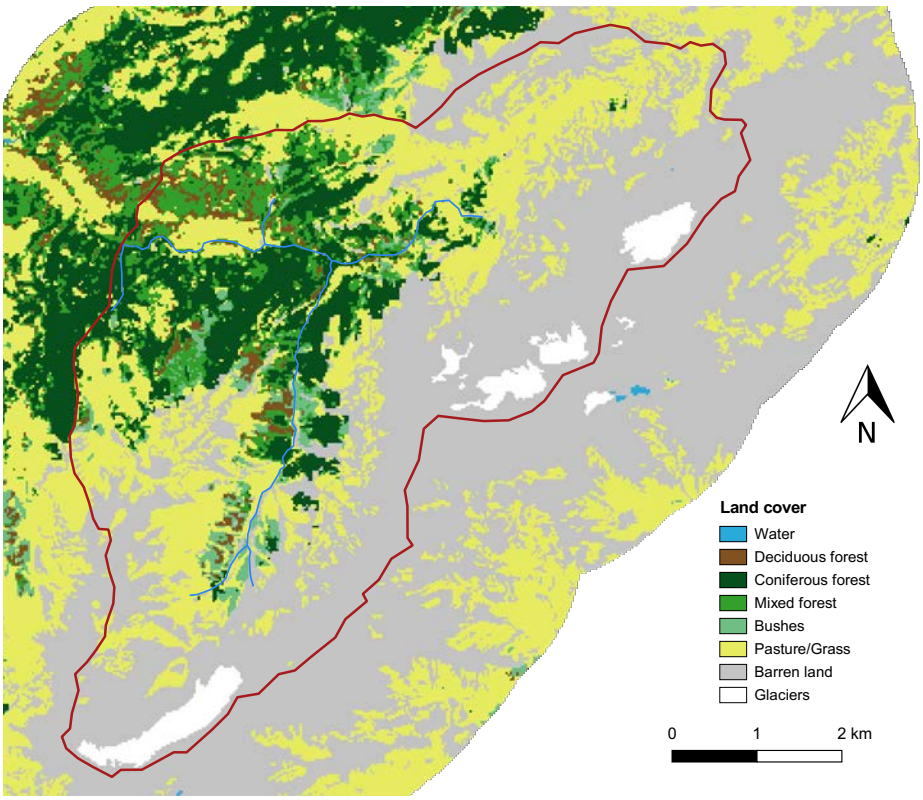

Figure B.3: The land cover map that was developed at 25 m resolution for WaSiM.

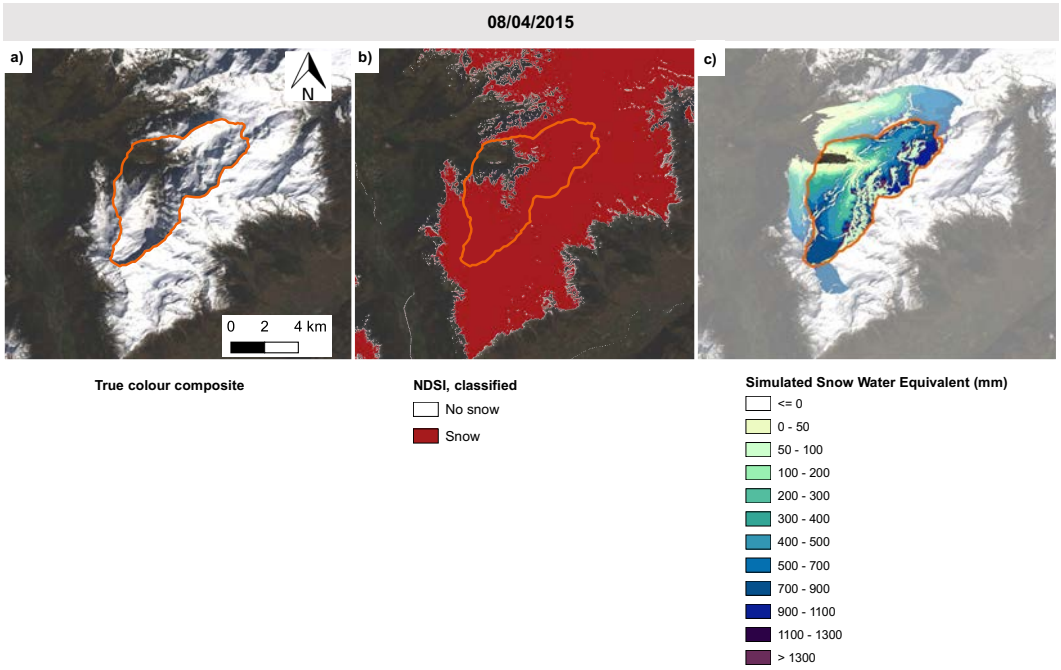
08/04/2015
a)
b)
c)
N
0 2 4 km
True colour composite
NDSI, classified
No snow
Snow
Simulated Snow Water Equivalent (mm)
<= 0
0 - 50
50 - 100
100 - 200
200 - 300
300 - 400
400 - 500
500 - 700
700 - 900
900 - 1100
1100 - 1300
> 1300

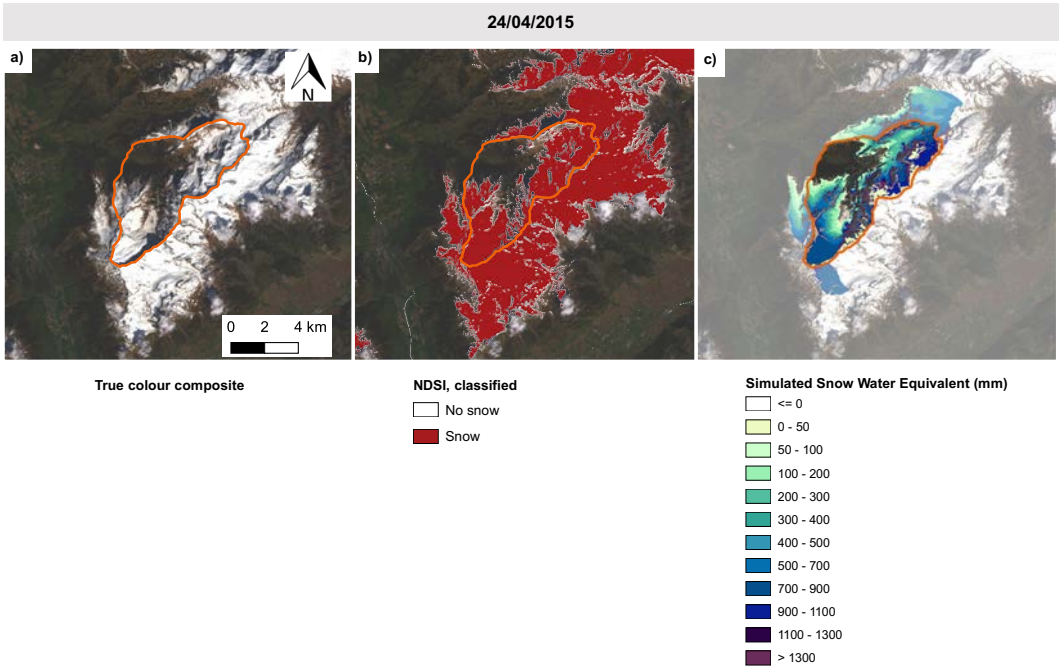
24/04/2015
a)
b)
c)
N
0 2 4 km
True colour composite
NDSI, classified
No snow
Snow
Simulated Snow Water Equivalent (mm)
<= 0
0 - 50
50 - 100
100 - 200
200 - 300
300 - 400
400 - 500
500 - 700
700 - 900
900 - 1100
1100 - 1300
> 1300

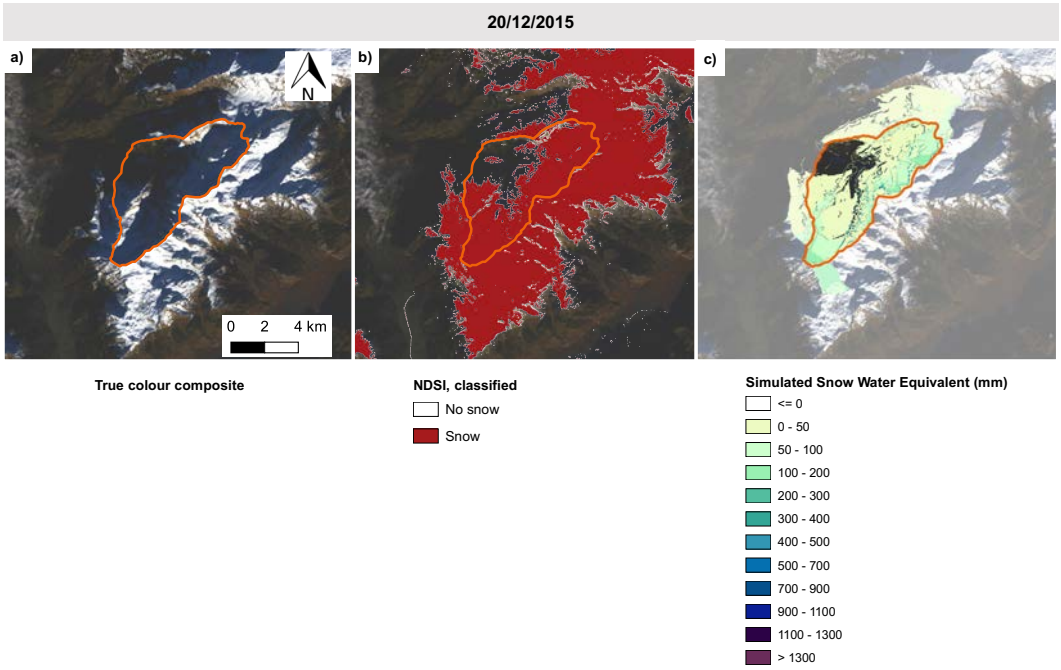
20/12/2015
a)
b)
c)
N
0 2 4 km
True colour composite
NDSI, classified
No snow
Snow
Simulated Snow Water Equivalent (mm)
<= 0
0 - 50
50 - 100
100 - 200
200 - 300
300 - 400
400 - 500
500 - 700
700 - 900
900 - 1100
1100 - 1300
> 1300

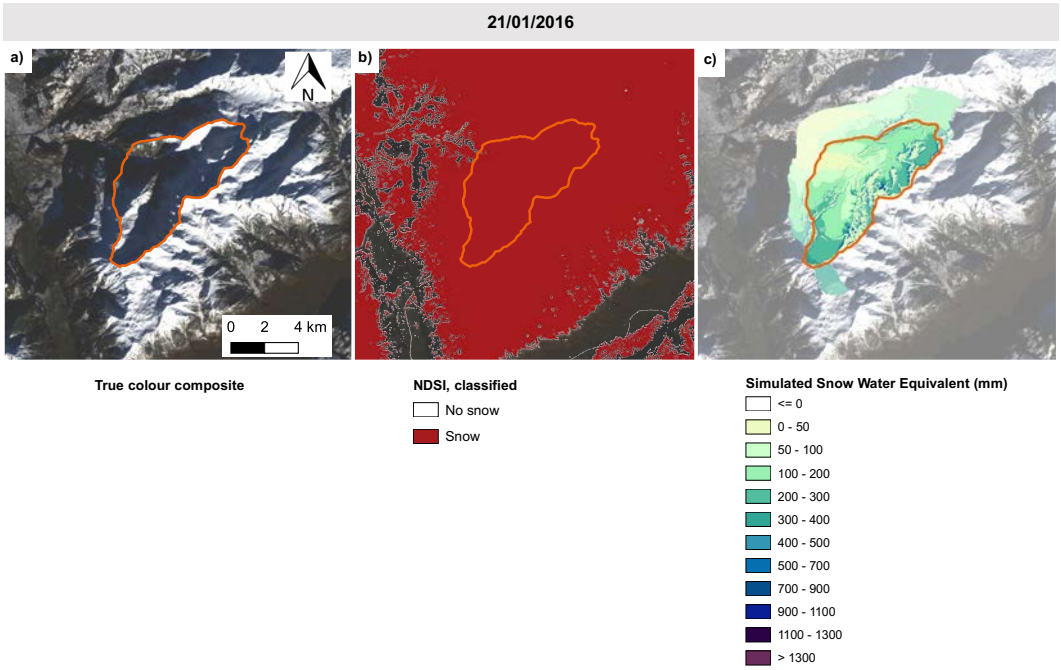
21/01/2016
a)
b)
c)
N
0 2 4 km
True colour composite
NDSI, classified
No snow
Snow
Simulated Snow Water Equivalent (mm)
<= 0
0 - 50
50 - 100
100 - 200
200 - 300
300 - 400
400 - 500
500 - 700
700 - 900
900 - 1100
1100 - 1300
> 1300

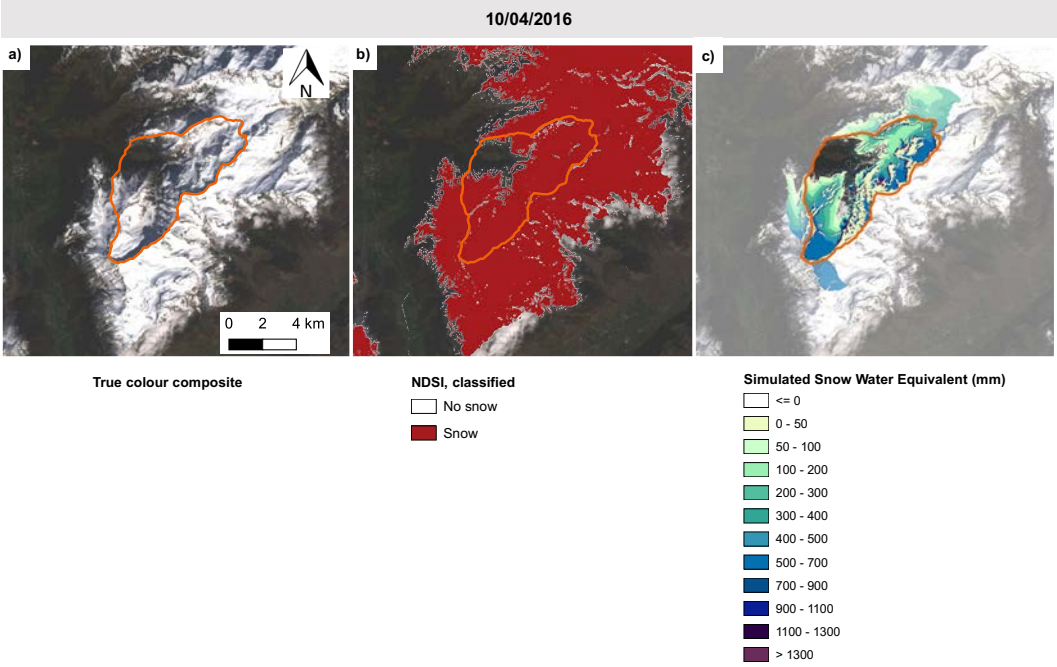
10/04/2016
a)
b)
c)
N
0 2 4 km
True colour composite
NDSI, classified
No snow
Snow
Simulated Snow Water Equivalent (mm)
<= 0
0 - 50
50 - 100
100 - 200
200 - 300
300 - 400
400 - 500
500 - 700
700 - 900
900 - 1100
1100 - 1300
> 1300

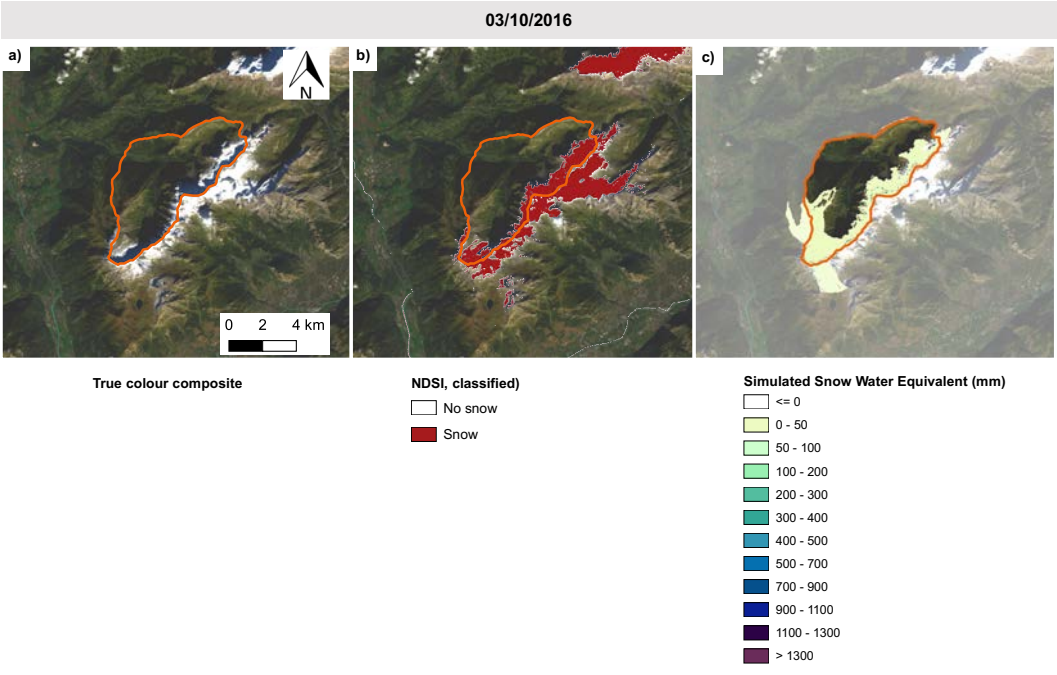
03/10/2016
a)
b)
c)
N
0 2 4 km
True colour composite
NDSI, classified)
No snow
Snow
Simulated Snow Water Equivalent (mm)
<= 0
0 - 50
50 - 100
100 - 200
200 - 300
300 - 400
400 - 500
500 - 700
700 - 900
900 - 1100
1100 - 1300
> 1300

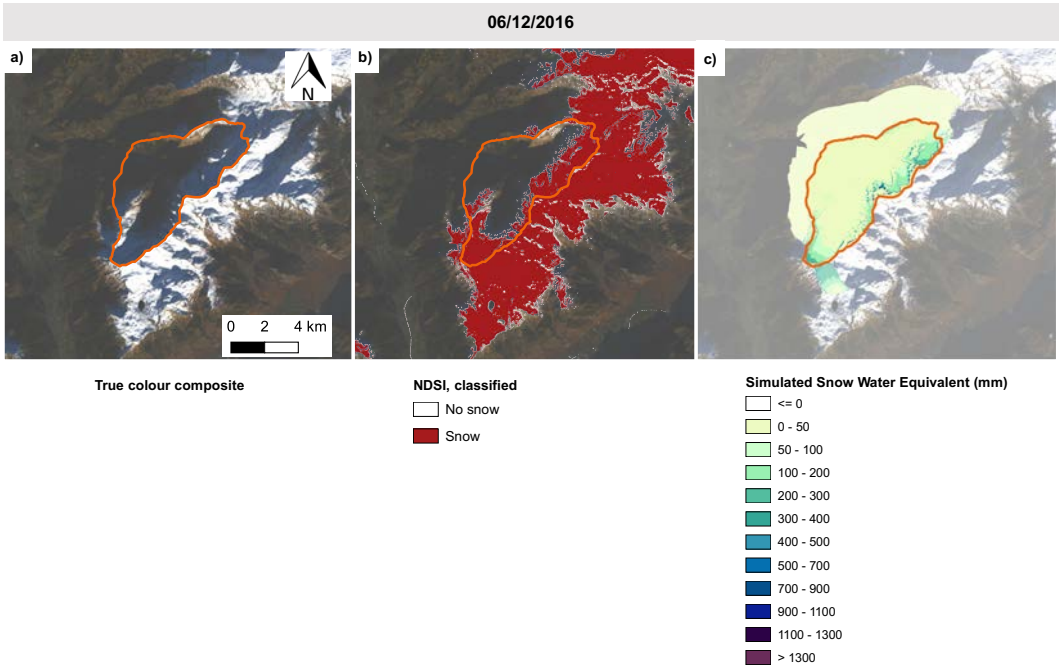
06/12/2016
a)
b)
c)
N
0 2 4 km
True colour composite
NDSI, classified
No snow
Snow
Simulated Snow Water Equivalent (mm)
<= 0
0 - 50
50 - 100
100 - 200
200 - 300
300 - 400
400 - 500
500 - 700
700 - 900
900 - 1100
1100 - 1300
> 1300

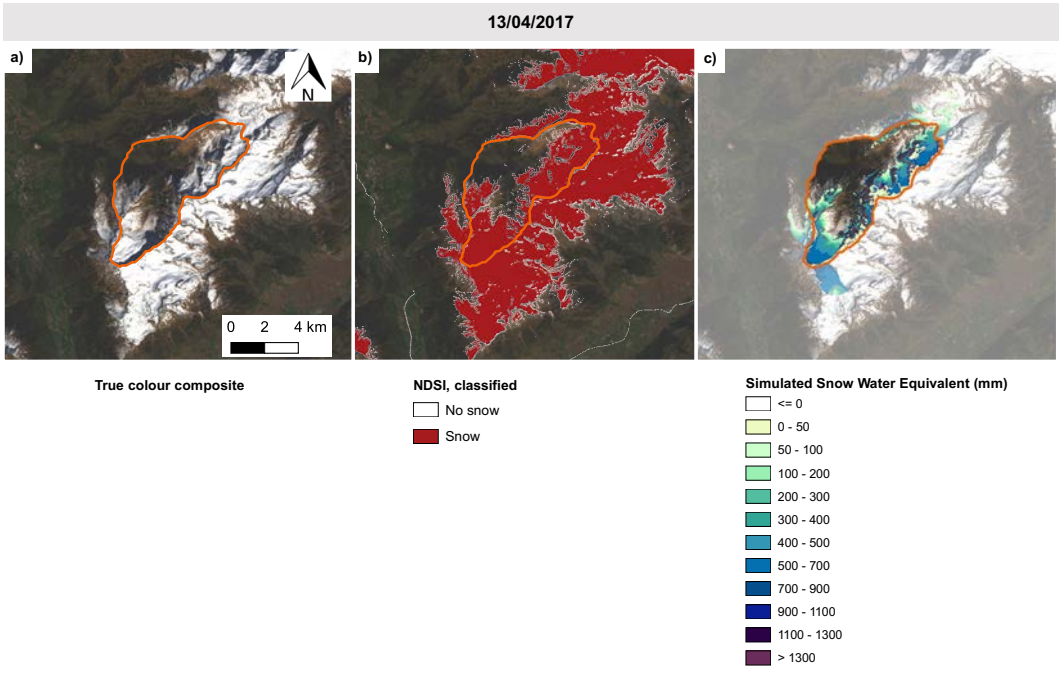
13/04/2017
a)
b)
c)
N
0 2 4 km
True colour composite
NDSI, classified
No snow
Snow
Simulated Snow Water Equivalent (mm)
<= 0
0 - 50
50 - 100
100 - 200
200 - 300
300 - 400
400 - 500
500 - 700
700 - 900
900 - 1100
1100 - 1300
> 1300

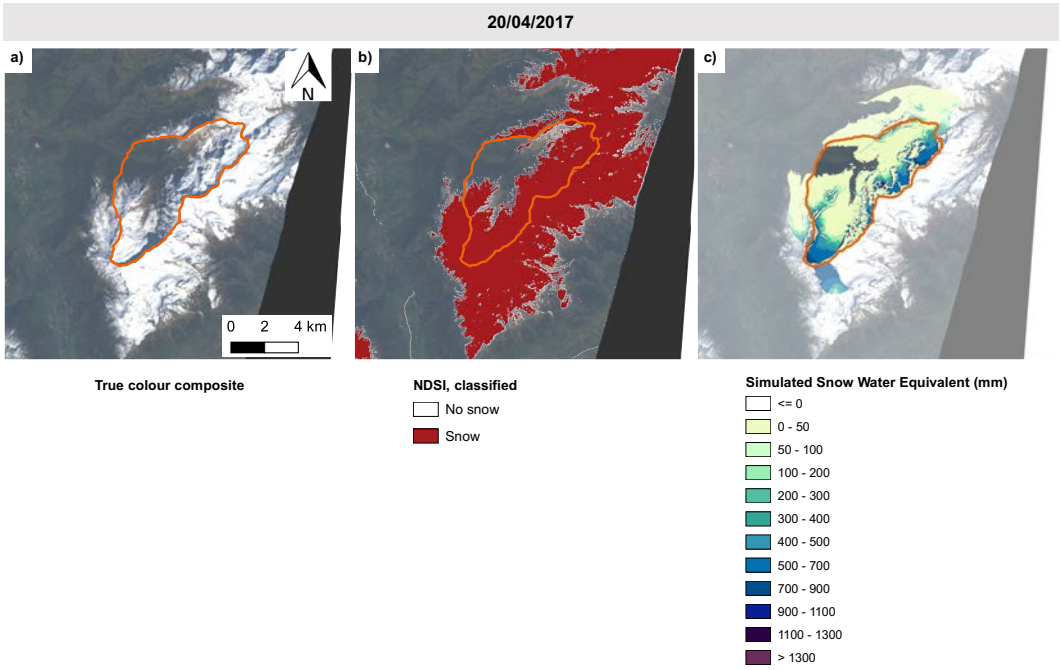
20/04/2017
a)
b)
c)
N
0 2 4 km
True colour composite
NDSI, classified
No snow
Snow
Simulated Snow Water Equivalent (mm)
<= 0
0 - 50
50 - 100
100 - 200
200 - 300
300 - 400
400 - 500
500 - 700
700 - 900
900 - 1100
1100 - 1300
> 1300

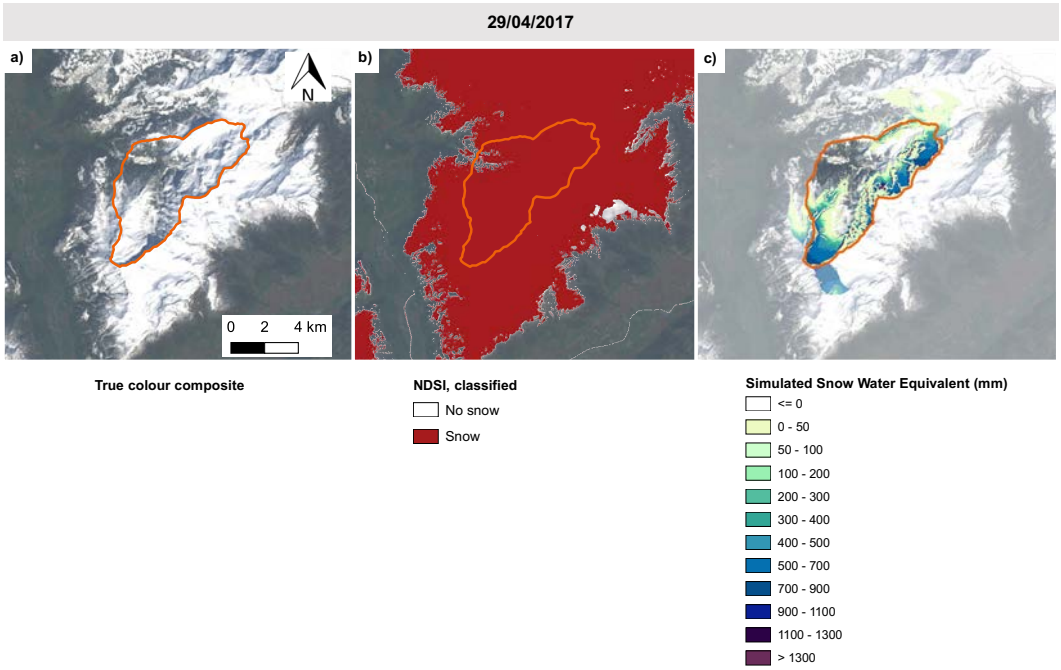
29/04/2017
a)
b)
c)
N
0 2 4 km
True colour composite
NDSI, classified
No snow
Snow
Simulated Snow Water Equivalent (mm)
<= 0
0 - 50
50 - 100
100 - 200
200 - 300
300 - 400
400 - 500
500 - 700
700 - 900
900 - 1100
1100 - 1300
> 1300

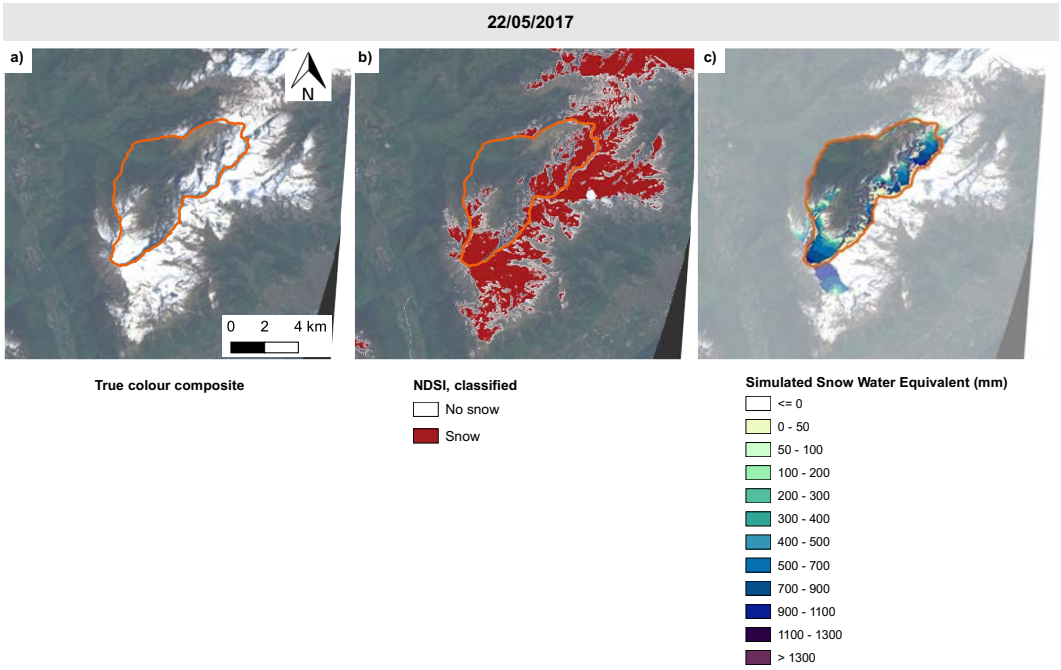
22/05/2017
a)
b)
c)
N
0 2 4 km
True colour composite
NDSI, classified
No snow
Snow
Simulated Snow Water Equivalent (mm)
<= 0
0 - 50
50 - 100
100 - 200
200 - 300
300 - 400
400 - 500
500 - 700
700 - 900
900 - 1100
1100 - 1300
> 1300

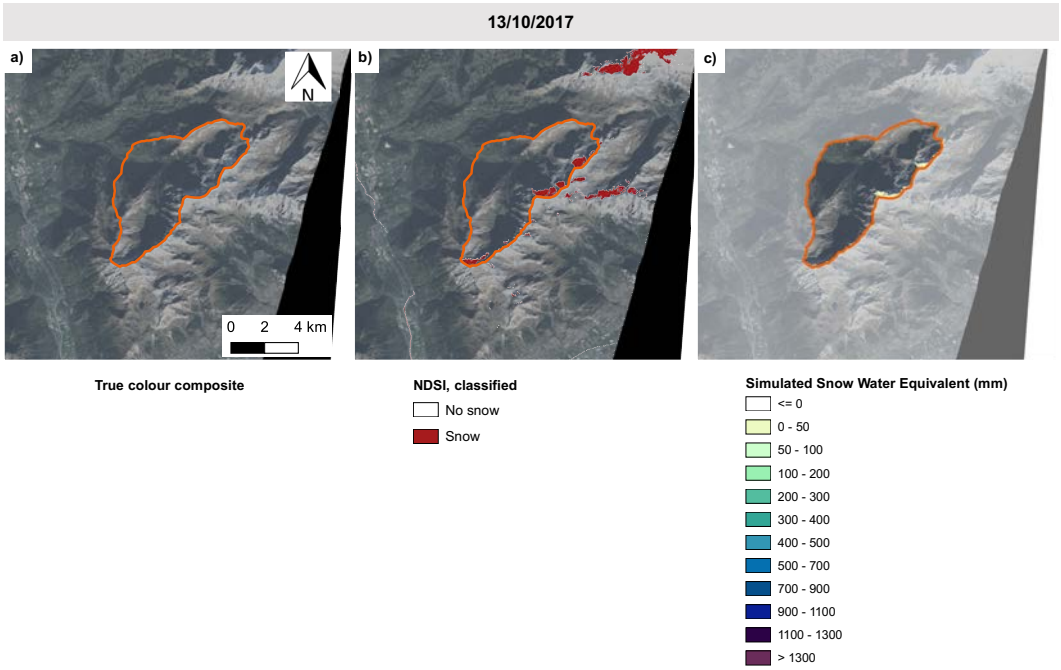
13/10/2017
a)
b)
c)
N
0 2 4 km
True colour composite
NDSI, classified
No snow
Snow
Simulated Snow Water Equivalent (mm)
<= 0
0 - 50
50 - 100
100 - 200
200 - 300
300 - 400
400 - 500
500 - 700
700 - 900
900 - 1100
1100 - 1300
> 1300

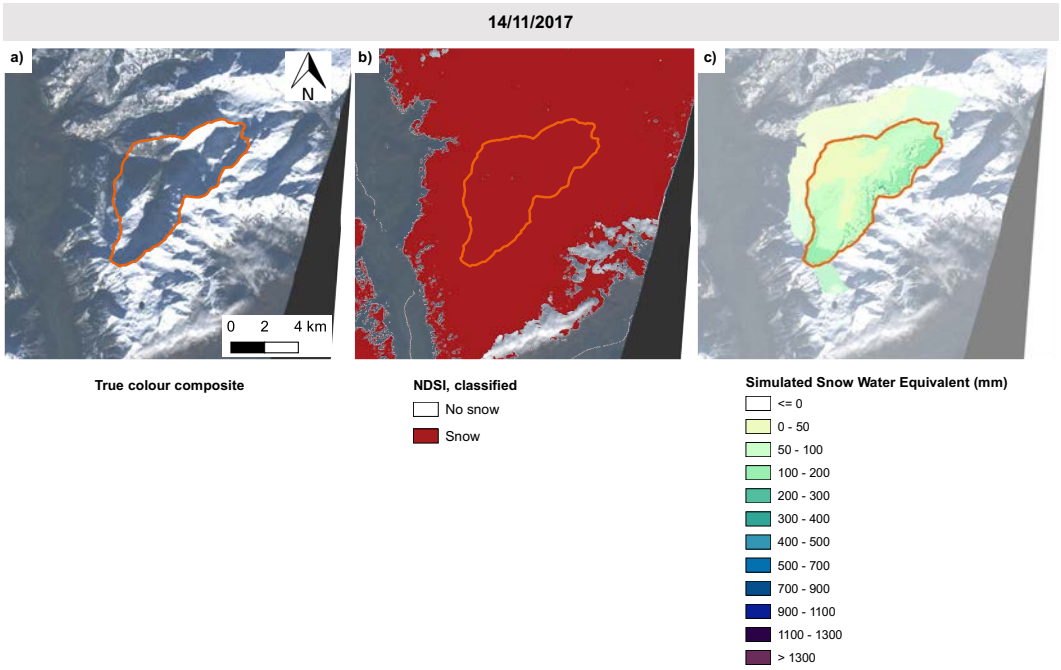
14/11/2017
a)
b)
c)
N
0 2 4 km
True colour composite
NDSI, classified
No snow
Snow
Simulated Snow Water Equivalent (mm)
<= 0
0 - 50
50 - 100
100 - 200
200 - 300
300 - 400
400 - 500
500 - 700
700 - 900
900 - 1100
1100 - 1300
> 1300

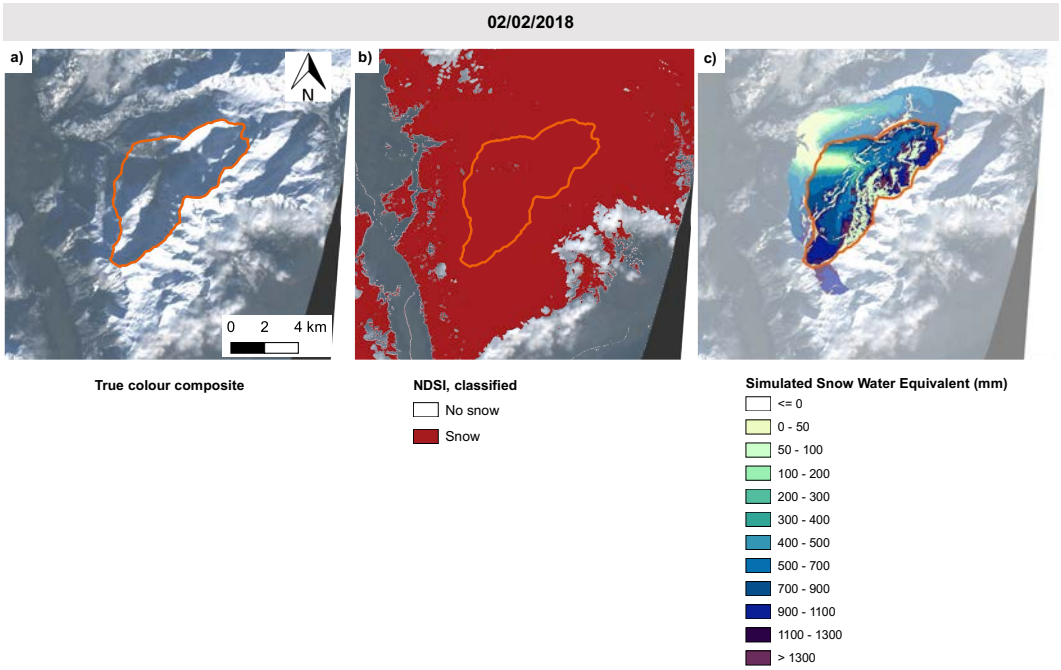
02/02/2018
a)
b)
c)
N
0 2 4 km
True colour composite
NDSI, classified
No snow
Snow
Simulated Snow Water Equivalent (mm)
<= 0
0 - 50
50 - 100
100 - 200
200 - 300
300 - 400
400 - 500
500 - 700
700 - 900
900 - 1100
1100 - 1300
> 1300

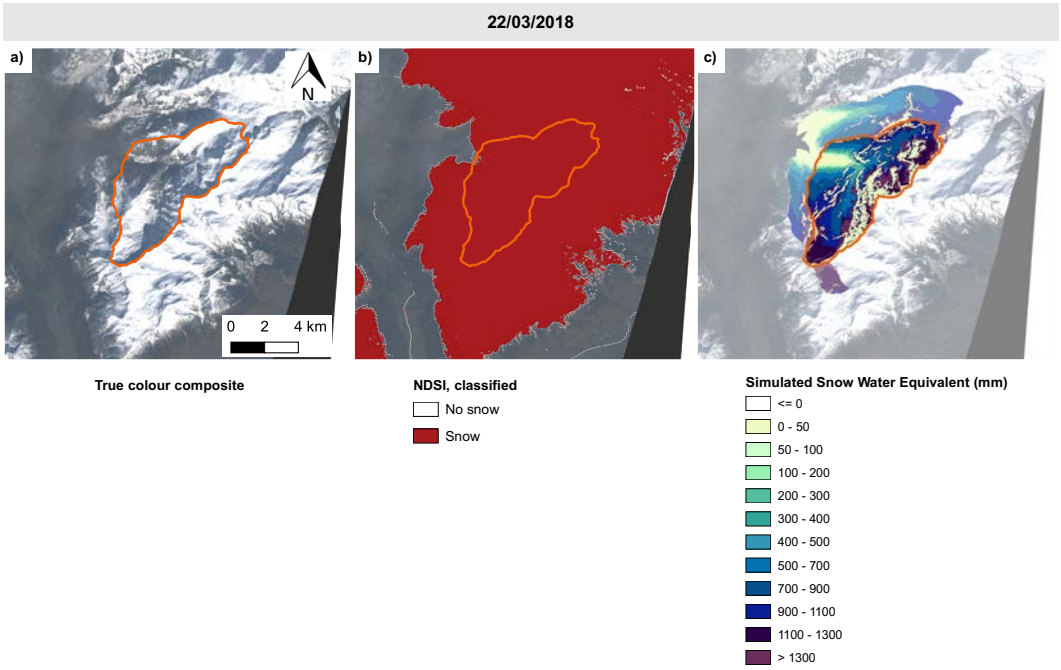
22/03/2018
a)
b)
c)
N
0 2 4 km
True colour composite
NDSI, classified
No snow
Snow
Simulated Snow Water Equivalent (mm)
<= 0
0 - 50
50 - 100
100 - 200
200 - 300
300 - 400
400 - 500
500 - 700
700 - 900
900 - 1100
1100 - 1300
> 1300

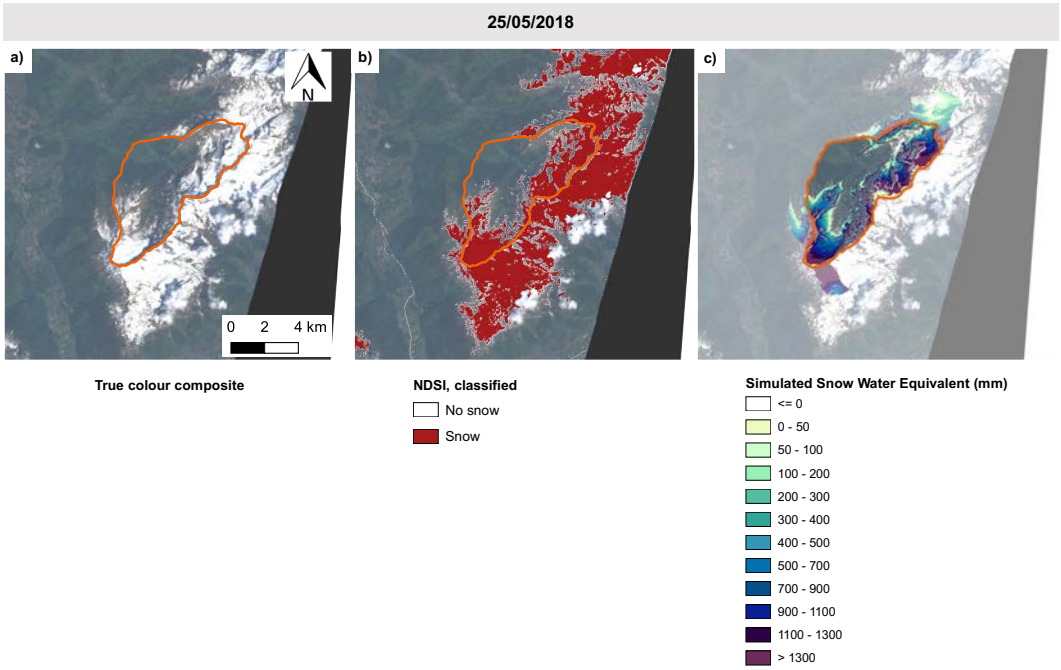
25/05/2018
a)
b)
c)
N
0 2 4 km
True colour composite
NDSI, classified
No snow
Snow
Simulated Snow Water Equivalent (mm)
<= 0
0 - 50
50 - 100
100 - 200
200 - 300
300 - 400
400 - 500
500 - 700
700 - 900
900 - 1100
1100 - 1300
> 1300

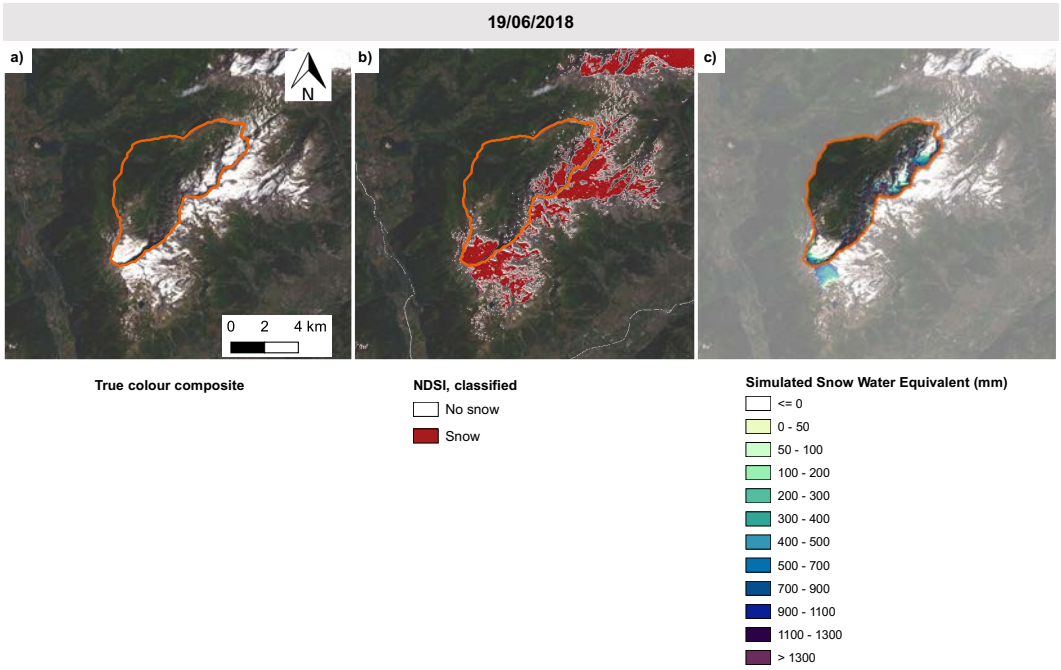

Figure B.4: (a) Landsat 8 true colour composite (TCC) images, (b) binary snow extents derived using the Normalised Difference Snow Index (NDSI), and (c) simulated Snow Water Equivalent (SWE) for each of the 17 days that formed the spatial component of the WaSiM model calibration dataset. The threshold chosen to generate each of the binary observed snow cover is indicated as t.

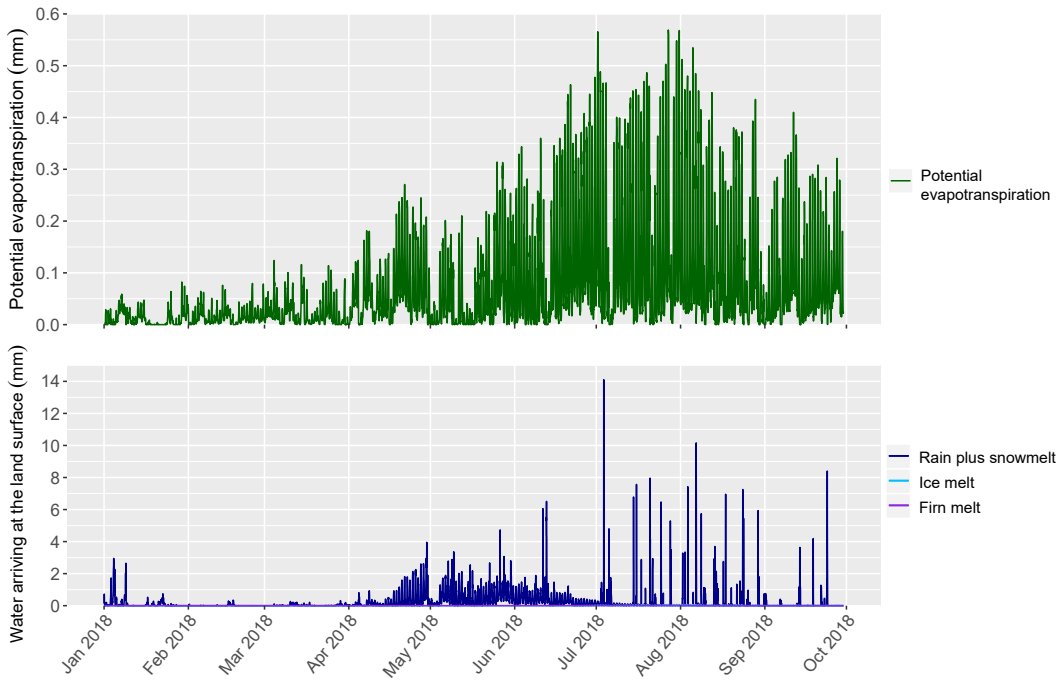

Figure B.5: Hourly simulated estimates of potential evapotranspiration (upper) and the four components of "surface water input" (i.e. liquid precipitation plus snowmelt, ice melt, and firn melt) (lower), averaged across the study catchment. Note the different scales. Only a subset of the full simulation period is shown. The figure illustrates the extremely dynamic nature of the meteorological forcing in the system, with diurnal cycles in melt and potential evaporation apparent, in addition to extremely intense, short lived convective precipitation events during summer. Small volumes of melt from ice and firn are also generated during the late summer, but given the low glaciated proportion of the study catchment are barely discernible when averaged across the catchment and plotted on the same axis as rain plus snowmelt.

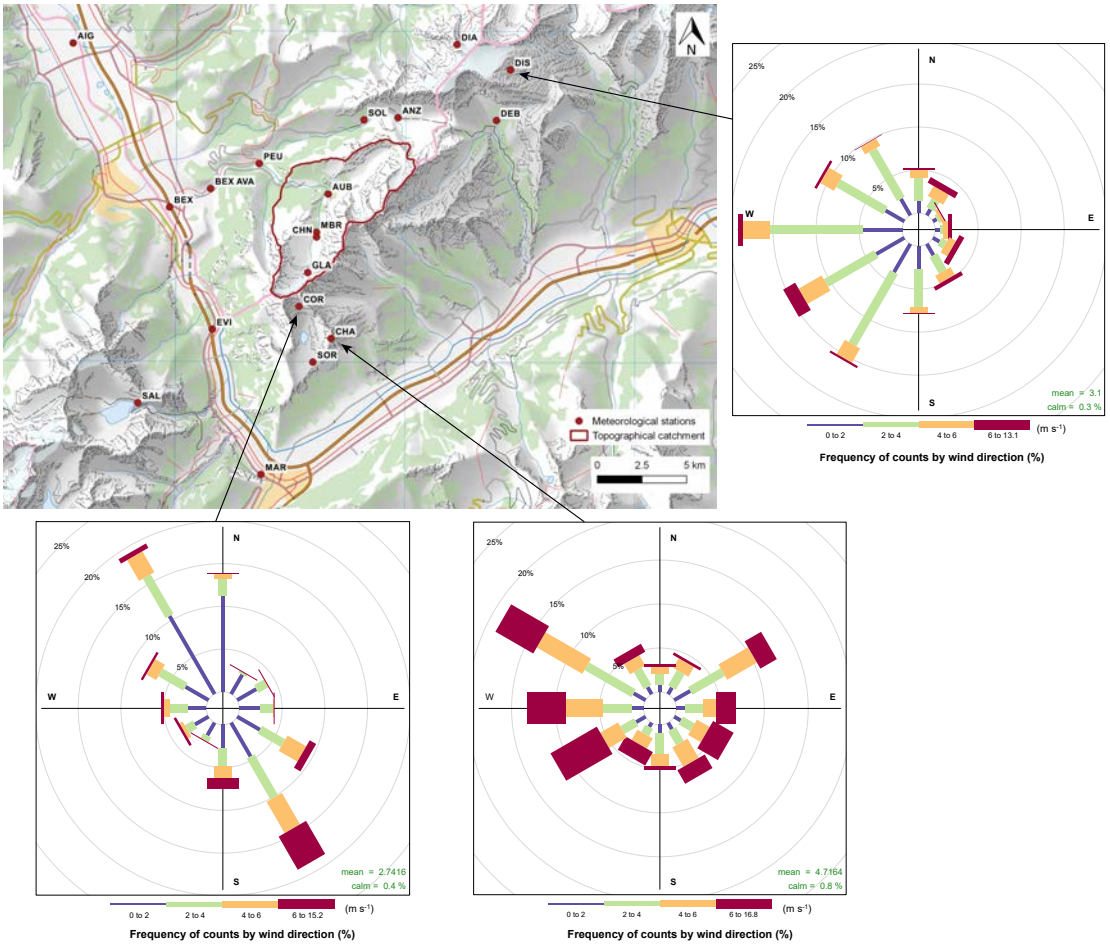

Figure B.6: Wind roses illustrating the relationship between winter (November–April inclusive) wind speed and direction at three high-elevation meteorological stations in the vicinity of the study region. The underlying data are hourly means, and span the period from 2015-2017 at the station CHA, and the period 2015-2018 at the stations DIS and COR. Such high-elevation locations are of most relevance to the consideration of potential redistribution of snow by wind since any such redistribution is expected to be most pronounced in the immediate surroundings of high-elevation ridges. From these data, it is clear that no clear prevailing wind direction could be identified for the region as a whole. This is probably due to a pronounced topographic influence on local wind fields. In the context of the present study, this prevented the successful application of the wind redistribution algorithm in WaSiM, which can presently only be parameterised with a single average prevailing wind direction.

C | Supplementary material for Chapter 4

Figures and an animation

The supplementary figures for Chapter 4 are presented below. After a period of embargo has passed (approximately 1 year from the date of defence), Animation C.1 will become available from the following online repository https://doi.org/10.6084/m9.figshare.12389756.v1.

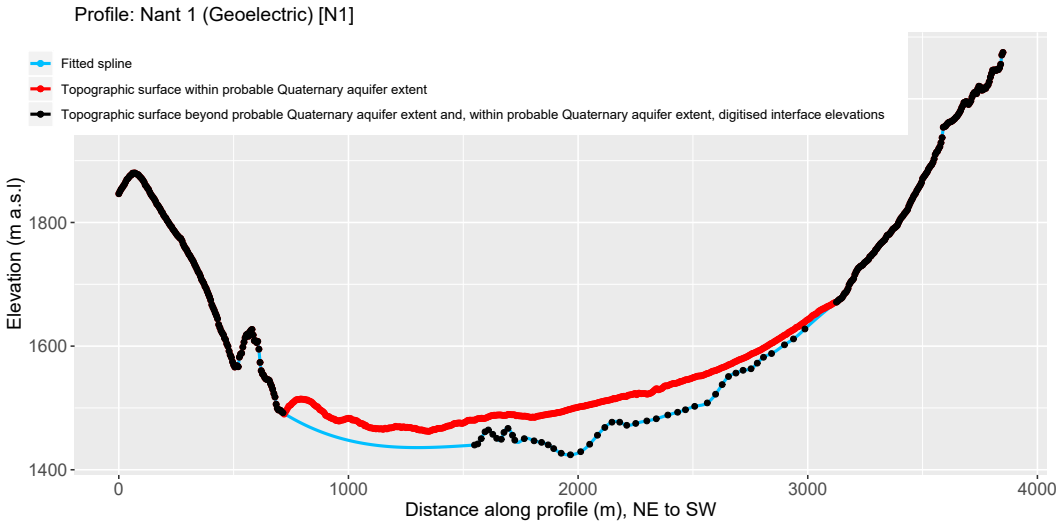
Profile: Nant 1 (Geoelectric) [N1]
Fitted spline
Topographic surface within probable Quaternary aquifer extent
Topographic surface beyond probable Quaternary aquifer extent and, within probable Quaternary aquifer extent, digitised interface elevations
Elevation (m a.s.l)
1800
1600
1400
0
1000
2000
3000
4000
Distance along profile (m), NE to SW

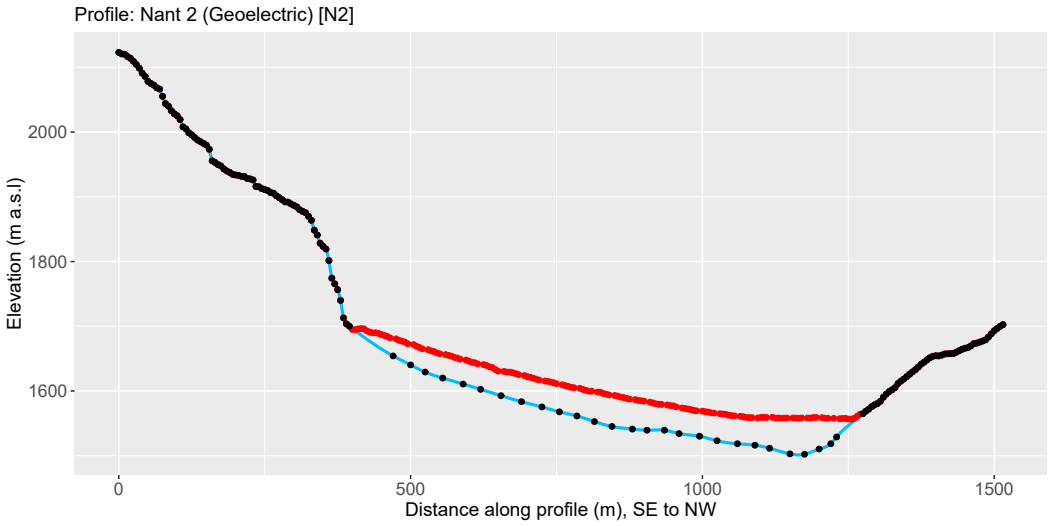
Profile: Nant 2 (Geoelectric) [N2]
Elevation (m a.s.l)
2000
1800
1600
0
500
1000
1500
Distance along profile (m), SE to NW

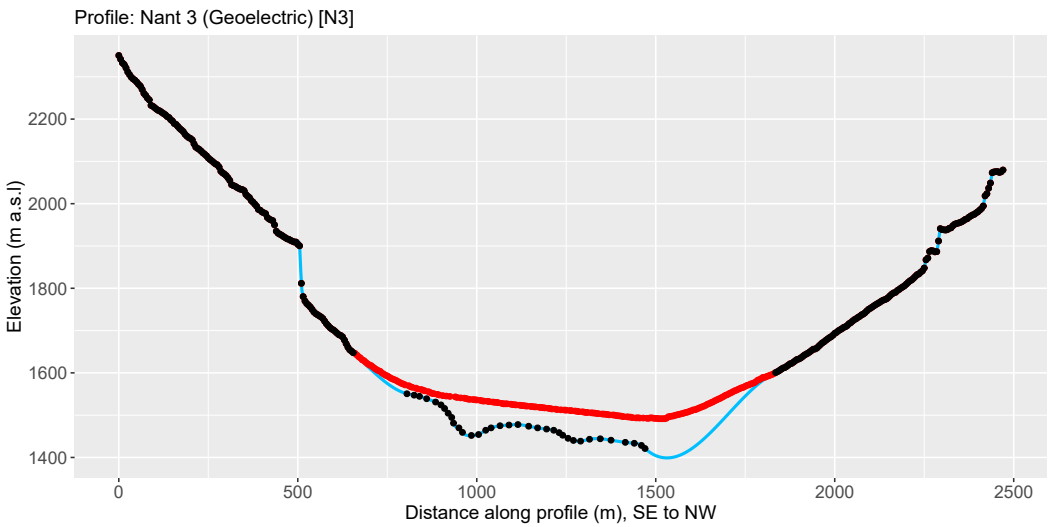
Profile: Nant 3 (Geoelectric) [N3]
Elevation (m a.s.l)
2200
2000
1800
1600
1400
0
500
1000
1500
2000
2500
Distance along profile (m), SE to NW

Appendix C

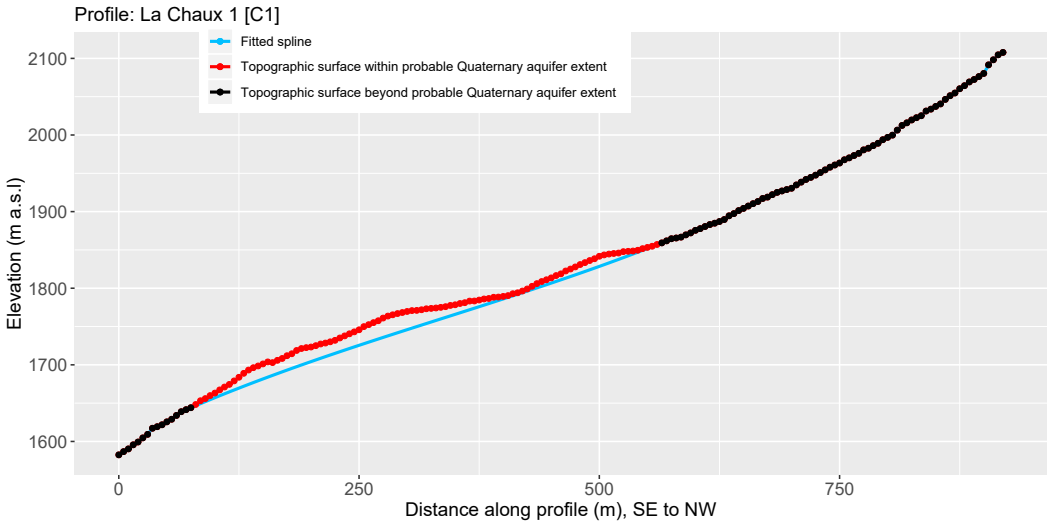
Profile: La Chaux 1 [C1]
Fitted spline
Topographic surface within probable Quaternary aquifer extent
Topographic surface beyond probable Quaternary aquifer extent
Elevation (m a.s.l)
2100
2000
1900
1800
1700
1600
0
250
500
750
Distance along profile (m), SE to NW

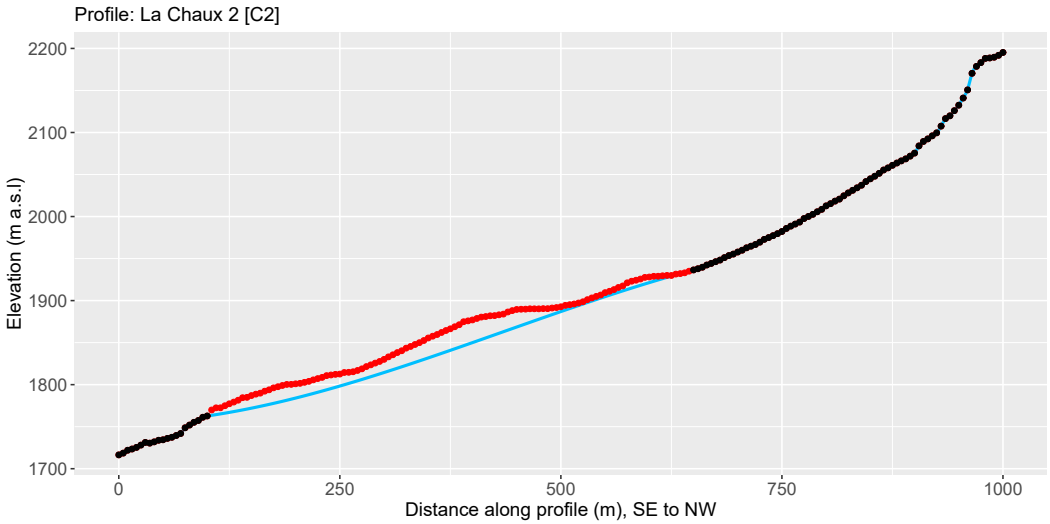
Profile: La Chaux 2 [C2]
Elevation (m a.s.l)
2200
2100
2000
1900
1800
1700
0
250
500
750
1000
Distance along profile (m), SE to NW

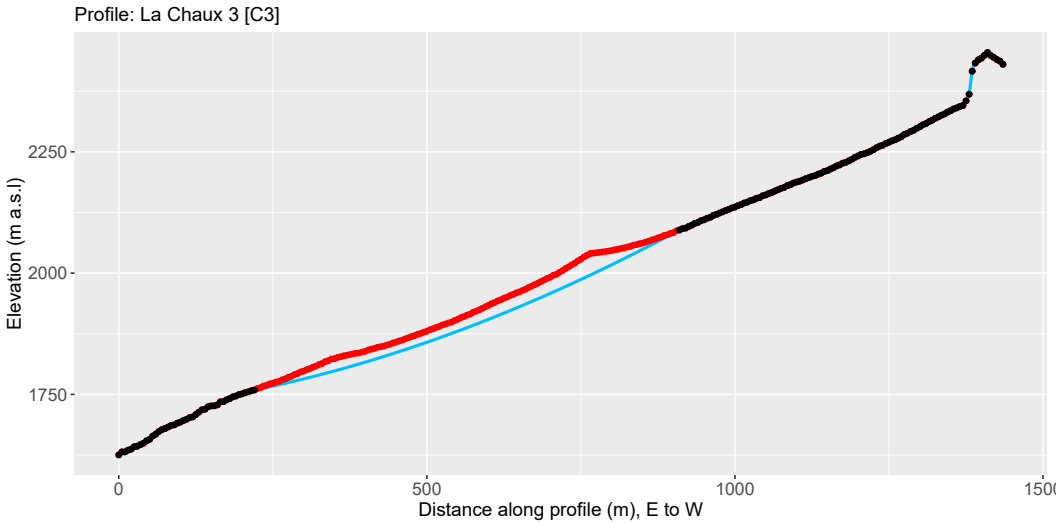
Profile: La Chaux 3 [C3]
Elevation (m a.s.l)
2250
2000
1750
0
500
1000
Distance along profile (m), E to W

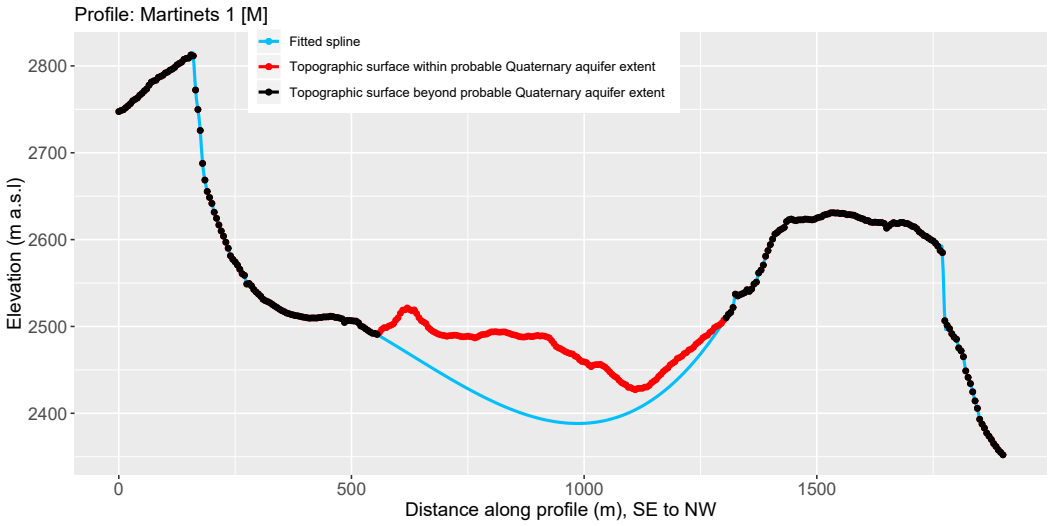
Profile: Martinets 1 [M]
Fitted spline
Topographic surface within probable Quaternary aquifer extent
Topographic surface beyond probable Quaternary aquifer extent
Elevation (m a.s.l)
2800
2700
2600
2500
2400
0
500
1000
1500
Distance along profile (m), SE to NW

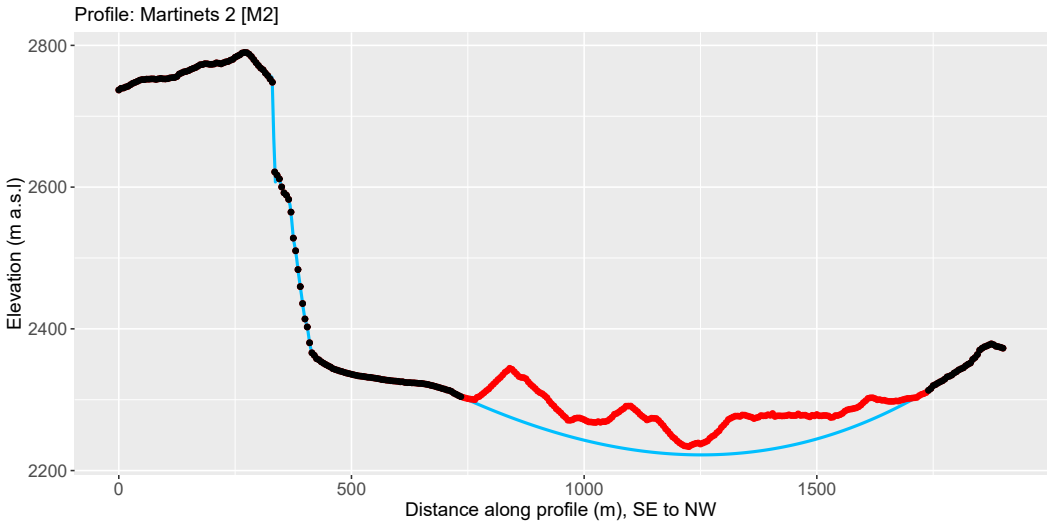
Profile: Martinets 2 [M2]
Elevation (m a.s.l)
2800
2600
2400
2200
0
500
1000
1500
Distance along profile (m), SE to NW

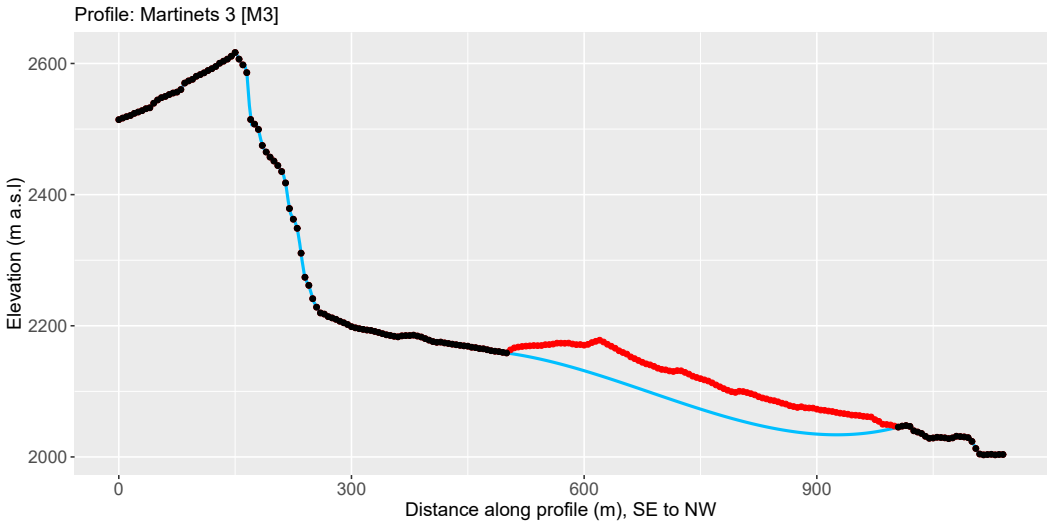
Profile: Martinets 3 [M3]
Elevation (m a.s.l)
2600
2400
2200
2000
0
300
600
900
Distance along profile (m), SE to NW

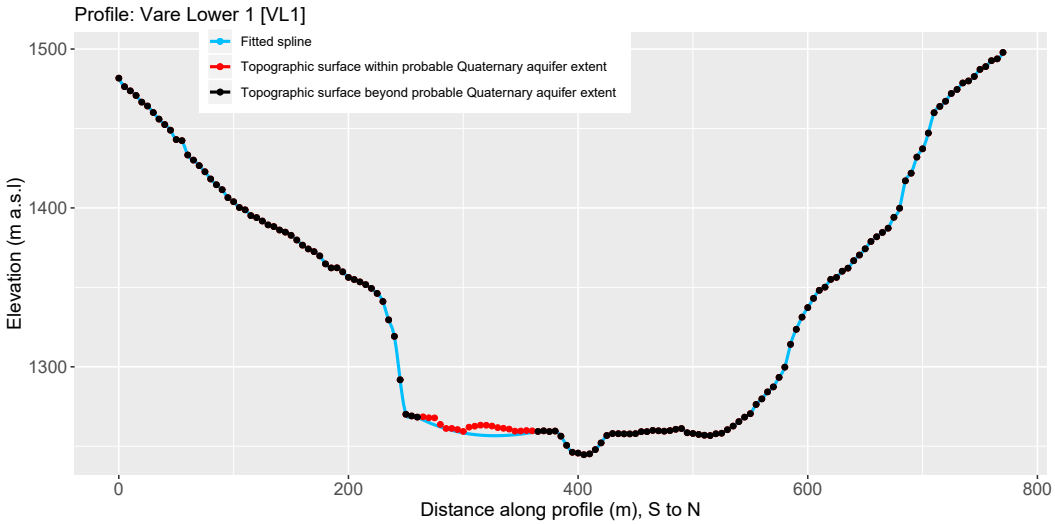
Profile: Vare Lower 1 [VL1]
Fitted spline
Topographic surface within probable Quaternary aquifer extent
Topographic surface beyond probable Quaternary aquifer extent
Elevation (m a.s.l)
1500
1400
1300
0
200
400
600
800
Distance along profile (m), S to N

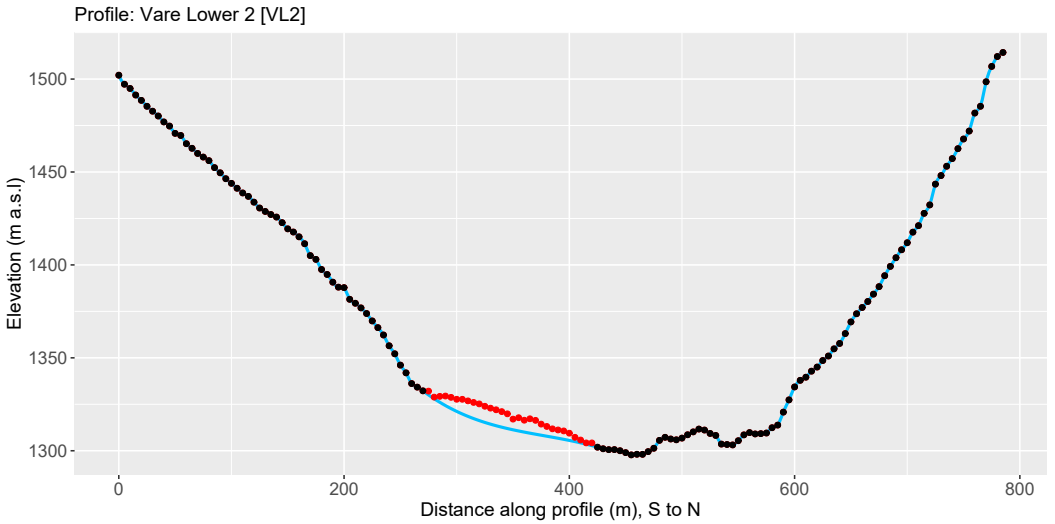
Profile: Vare Lower 2 [VL2]
Elevation (m a.s.l)
1500
1450
1400
1350
1300
0
200
400
600
800
Distance along profile (m), S to N

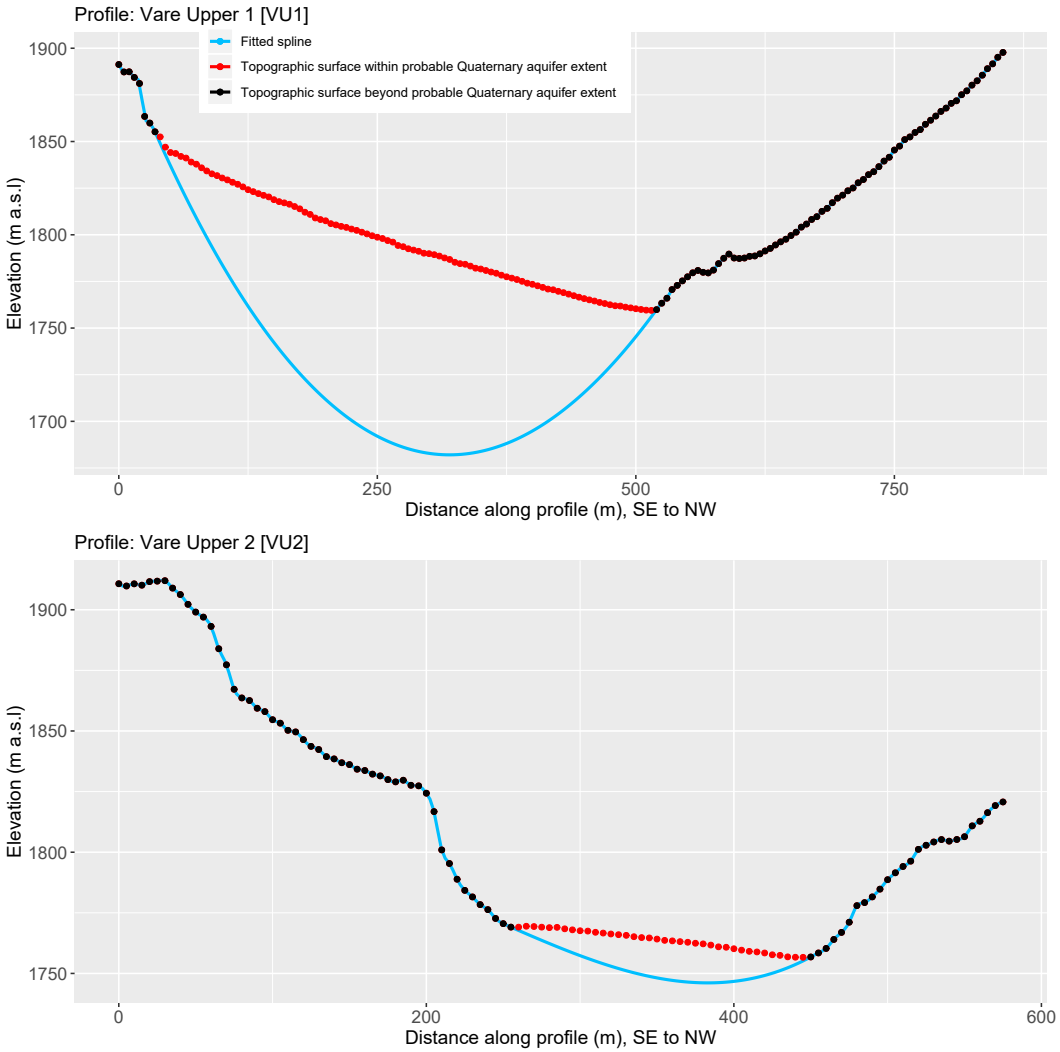

Figure C.1: Interpolated 2D cross-sections for each of the 13 topographical transects. For the three profiles pertaining to *Nant*, interfaces derived from the geophysical surveys were included in addition to the topographic points immediately outside the sedimentary features in order to constrain the estimated 2D bedrock interface. Elsewhere, the 2D interpolations were informed solely by the bedrock gradients immediately beyond the sedimentary feature in question.

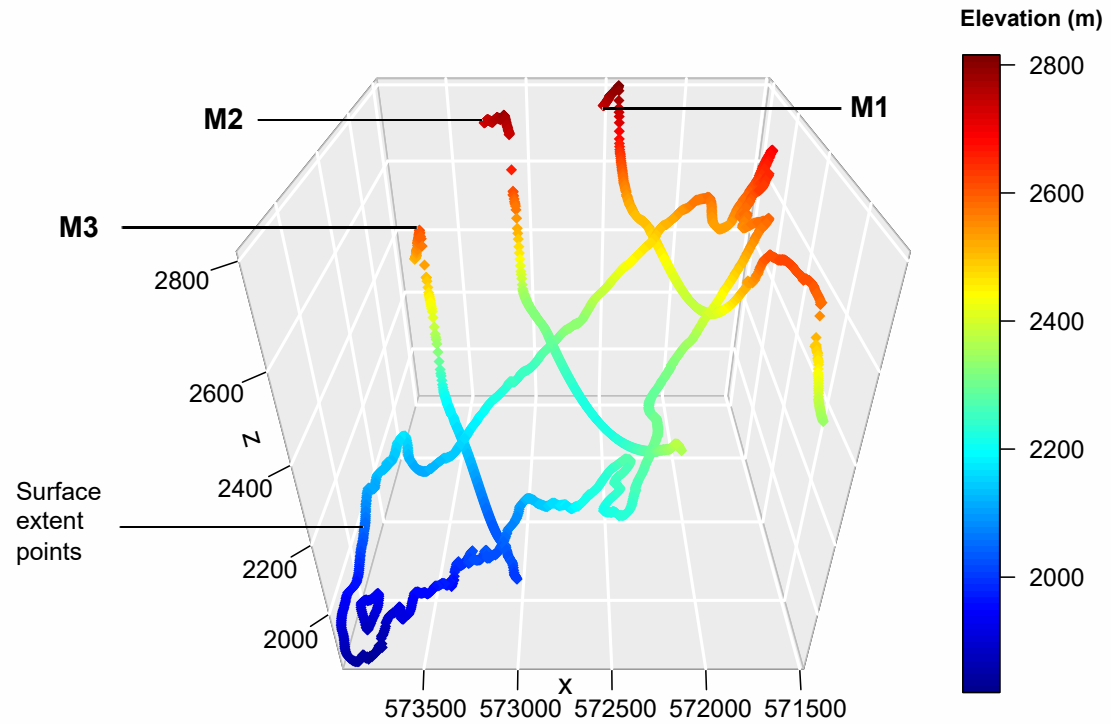

Figure C.2: 3D points forming the input to the Thin Plate Spline (TPS) interpolation of the bedrock interface beneath the moraines of *Les Martinets*, looking due south.

D | Supplementary material for Chapter 5

Figures and animations

The supplementary figures for Chapter 5 are presented below. After a period of embargo has passed (approximately 1 year from the date of defence), Animations D.1 and D.2 will become available from the following online repository: https://doi.org/10.6084/m9.figshare.12389756.v1.

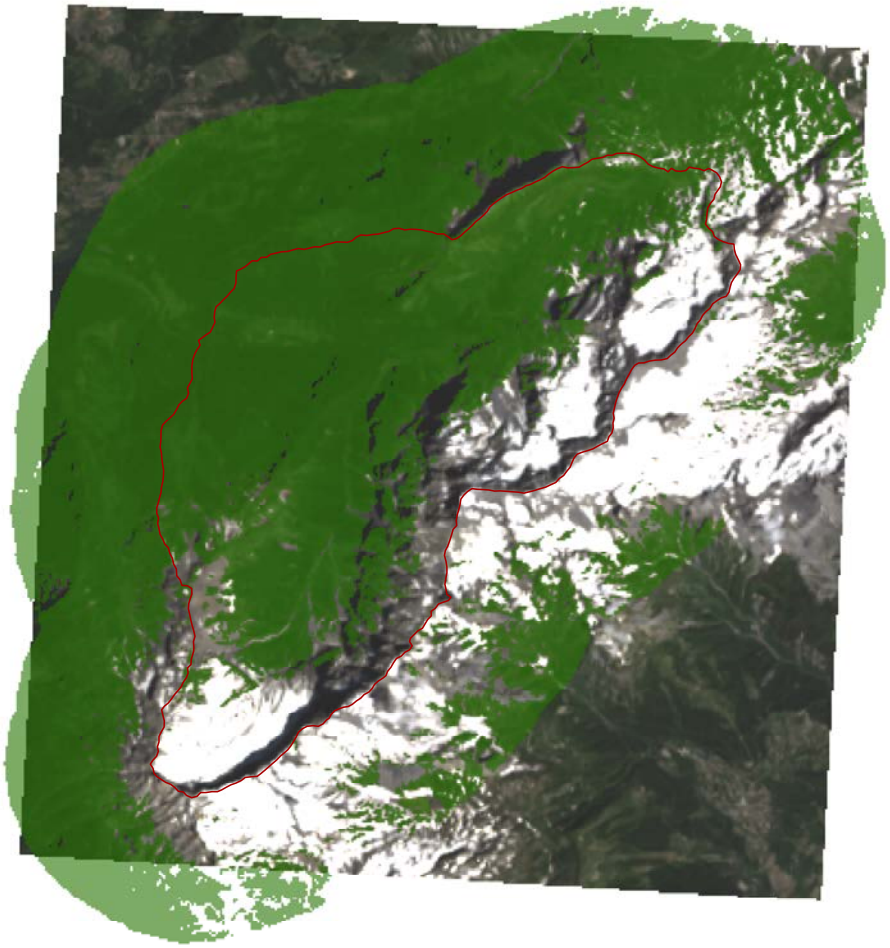

Figure D.1: Region with a present-day normalised difference vegetation index (NDVI) indicative of vegetation (in green), beyond which simulated future forest development was not excluded in order to represent the geomorphological and soil controls on forest expansion, these factors not being explicitly considered by TreeMig.

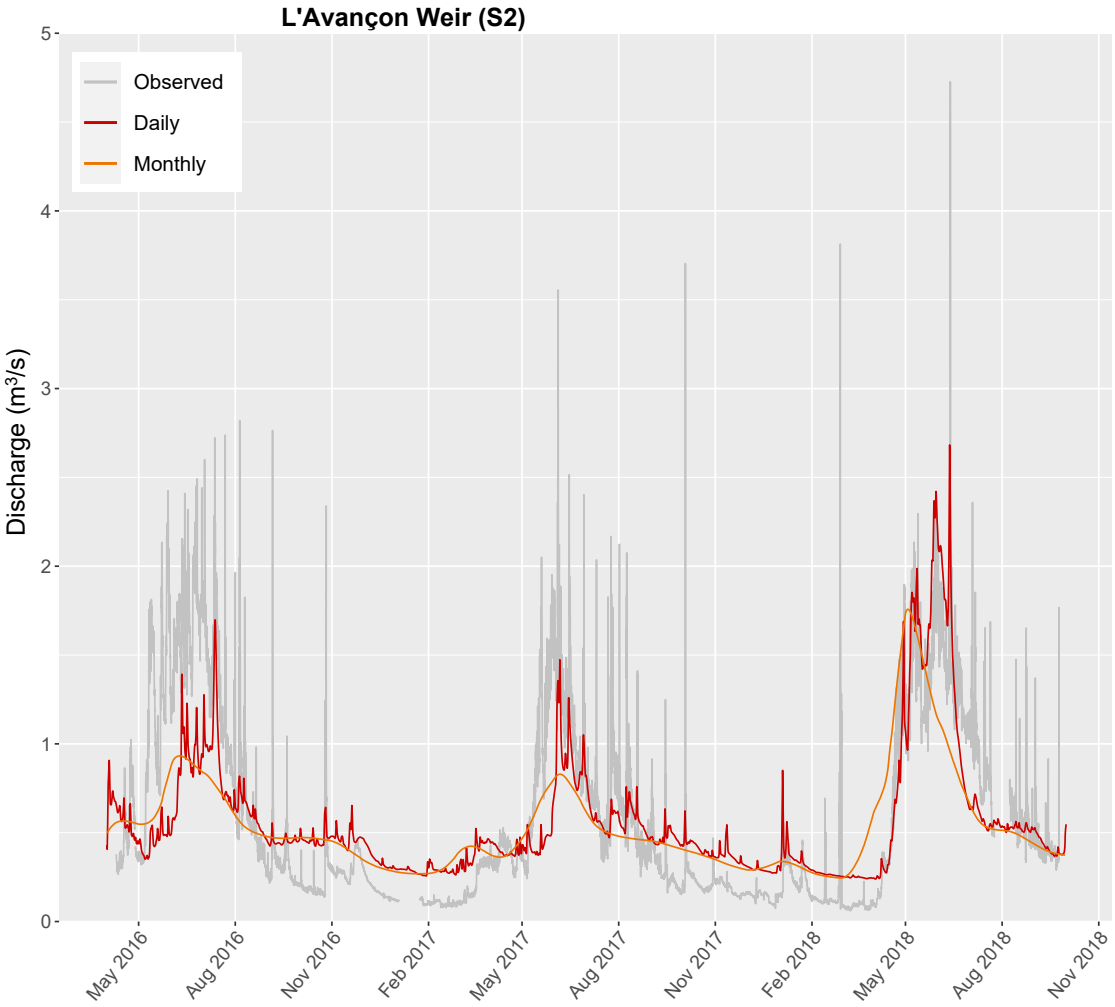

Figure D.2: Streamflow simulated at S2 using the integrated model after two calibration rounds with monthly vs. daily frequency (25 m resolution) forcing. The observed data are also plotted.

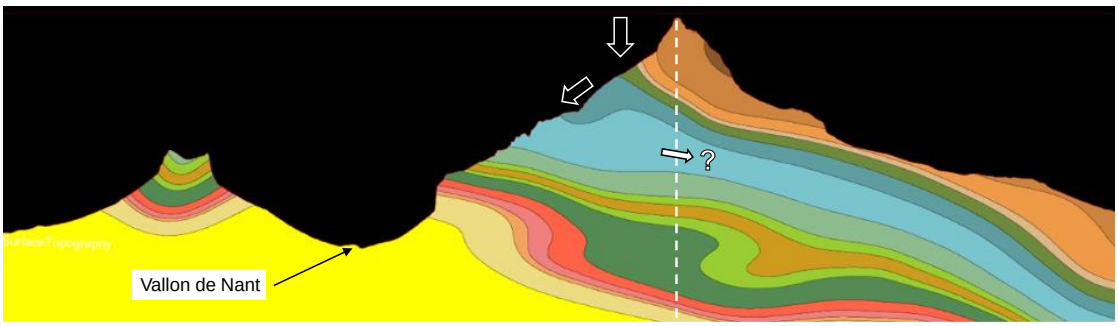

Figure D.3: Cross-section through the 3D bedrock geological model showing the possibility for groundwater exportation across the topographic divide on the eastern flank of the Vallon de Nant, which is illustrated using the dashed white line (i.e. across the no-flow boundary in the model).